To the Graduate Council:

We are submitting herewith a dissertation written by Ravindra Menon entitled "Effect of Microstructure, Inclusion Morphology and Composition on the Hydrogen-Induced HAZ Cracking Susceptibility of Cast and Wrought C-Mn-Si Steels." We have examined the final copy of this dissertation for form and content and recommend that it be accepted in partial fulfillment of the requirements for the degree of Doctor of Philosophy, with a major in Metallurgical Engineering.

Carl D. Lundin, Major Professor

E.E. Stansbury, Major Professor

We have read this dissertation
and recommend its acceptance:

C R Brooks

J E. Spruiell

Archie Mathews

Accepted for the Council:

The Graduate School

EFFECT OF MICROSTRUCTURE, INCLUSION MORPHOLOGY AND COMPOSITION ON THE HYDROGEN-INDUCED HAZ CRACKING SUSCEPTIBILITY OF CAST AND WROUGHT C-Mn-Si STEELS

A Dissertation

Presented for the

Doctor of Philosophy

Degree

The University of Tennessee, Knoxville

Ravindra Menon

June 1984

ACKNOWLEDGMENTS

The author would like to acknowledge the financial and technical support of the Steel Founders' Society of America which made this research effort possible. Extensive material contributions were made by the organizations listed below.

ESCO Inc.

Larson Consolidated

Sterling Castings

Atlas Foundry

Chicago Bridge and Iron

Rockwell International

Lukens Steel Co.

Appreciation is extended to the machine shop for help in sample preparation. The author would also like to thank his advisor, Dr. Carl D. Lundin, for providing technical guidance throughout the course of this work; and as a final word, the untiring efforts of Phyllis Davis to convert the manuscript to the present form are deeply appreciated.

ABSTRACT

The research program was undertaken to provide both basic and pragmatic information on the hydrogen-induced cracking (HIC) susceptibilities of cast steels and to determine the metallurgical conditions which govern the HIC behavior of welded cast components. The principal effort was coupled with a study of the mechanisms responsible for HIC and work to contrast the reported differences in behavior between cast and wrought steels of essentially identical composition. The work was extended into determinations of the effect of inclusion morphology, deoxidation practice, residual elements and the effect of very low sulfur contents (0.001%S) in wrought steels.

The test methods were varied to investigate the effect of composition, metallurgical structure in the HAZ and restraint (both inherent in welding and externally applied). The tests included the self-restraint rapidly cooled HAZ Battelle Underbead Cracking Test (UBCT), the applied-restraint Implant Test and a composition/hydrogen method, the UT-Modified Hydrogen Sensitivity Test (UT-Mod.HST). The samples generated provided test data as well as specimens for evaluation by optical and electron optic (SEM) techniques to define microstructure and inclusion morphology effects.

The pragmatic data provides a basis for selection of suitable welding conditions as well as the ranking of the steels to HIC. The basic metallurgical information formed a basis for determining the underlying mechanisms responsible for HIC. Further, the relationship

of metallurgical characteristics and steel processing parameters made clear the reasons for the relative behavior of the different materials.

The Literature Review provides the reader with a concise historical review and basis for theories involving HIC in both cast and wrought steels. The work in this program has answered many of the questions posed by previous researchers.

The results of the baseline underbead cracking tests indicate that the susceptibility to HIC of cast and normalized (C&N) C-Mn-Si and 8630 steels can be related to composition using a carbon equivalent formula of the type, C.E. = %C + %Mn/6 + %Si/24 + %Cr/12 + %Mo/10. C&N C-Mn-Si steels with C.E.'s up to 0.47 and total residual contents (%Cr + %Mo + %Ni + %V + %Cu) up to 0.59% require a preheat of only 100°F to avoid HIC in the UBCT using high-hydrogen (E 6010) electrodes. Wrought C-Mn-Si steels when test welded in the rolling direction in the underbead cracking and implant tests were found to be more susceptible to HIC when compared to cast steels of equivalent composition (C.E.). The greater susceptibility of wrought steels when tested in the rolling direction is related to the presence of elongated sulfide inclusions which act as more potent sites for the initiation of HIC compared to the globular inclusions in cast steels. In addition, banding (ingotism) in wrought steels presents a continuous path for crack propagation. When the wrought steels were tested with the weld normal to the rolling direction (inclusions and banding oriented perpendicular to the fusion line),

the susceptibility to HIC of cast and equivalent wrought steels was similar. The initial results indicating differences between the HIC susceptibilities of cast and wrought steels were further confirmed by testing remelted wrought materials and comparing the results to those for the "parent" wrought materials. The reasons for the literature reported differences as well as those obtained in this study were confirmed to be as a result of the differences in inclusion morphology and ingotism that arise from differences in solidification and thermo-mechanical treatments between cast and wrought steels.

For cast steels, Type II inclusions (eutectic sulfides) located on primary solidification boundaries were found to exacerbate susceptibility to HIC. Increasing the extent of deoxidation (higher total and residual aluminum contents) which leads to the formation of Type III inclusions (angular sulfides) in preference to Type II's, was found to decrease HIC susceptibility in cast steels.

A mechanism of HIC has been suggested to explain the HIC behavior of both cast and wrought steels. Trapping of hydrogen at inclusion/matrix interfaces leading to the accumulation of hydrogen sufficient to initiate and propagate a crack is suggested as a primary mechanism. The deleterious influence of Type II inclusions on HIC in cast steels and that of elongated sulfides in wrought steels is explained using this mechanism. Fracture morphologies observed in hydrogen-embrittled HAZ's are explained using the

mechanism in concert with Beachem's model of hydrogen-assisted cracking. The observance of a predominantly intergranular mode of HIC in low sulfur steels is explained using the above model.

TABLE OF CONTENTS

CHAPTER		PAGE
I.	INTRODUCTION	1
II.	LITERATURE REVIEW	5
	1. Weldability	5
	2. Hydrogen-Induced Cracking (HIC)	8
	3. Factors Affecting HIC	15
	4. Theories of Hydrogen Embrittlement	37
	5. Preheating and Post Weld Heat Treatment	41
	6. Effect of Sulfur and Inclusions	46
	7. Effect of Aluminum on HIC	61
	8. Weldability of Cast Steels	66
	9. Comparative Weldabilities of Cast and Wrought Steels	80
	10. Closure	83
III.	MATERIALS AND EXPERIMENTAL PROCEDURES	84
	1. Experimental Materials	84
	2. Weldability (HIC) Tests	96
	3. Serviceability Evaluation--Response of HAZ's to PWHT	109
	4. Determination of Diffusible Hydrogen	111
	5. Jominy End Quench Hardenability	115
	6. Optical Metallography	116
	7. Scanning Electron Microscopy	116

CHAPTER PAGE

IV. RESULTS AND DISCUSSION 117

1. Introduction 117

2. Underbead Cracking Tests--Cast Steels 122

3. Underbead Cracking Tests on Wrought C-Mn-Si Steels 137

4. UT-Modified Hydrogen Sensitivity Test 166

5. Tests on Foundry-Run Cast Steels 179

6. Remelted and Recast Wrought Steels 192

7. Effect of Inclusion Morphology/Deoxidation Practice 205

8. Tests on Low Sulfur Steels 230

9. Two Pass Implant Tests 253

10. Serviceability Requirements--Response to PWHT 256

11. Suggested Mechanism of HIC 267

12. Fundamental Significance of this Work 281

13. Engineering Significance of this Work 282

14. Future Work 284

V. CONCLUSIONS 286

LIST OF REFERENCES 296

VITA 305

LIST OF TABLES

TABLE		PAGE
1.	Hydrogen concentrations in arc atmosphere and weld metal deposited by various processes	33
2.	Preheat temperatures related to carbon equivalent . .	43
3.	Composition of cast steels used in the fabrication of dragline and dipper buckets	76
4.	Compositions of cast and normalized (C&N) and wrought C-Mn-Si steels tested in Phase I	87
5.	Compositions of cast and normalized (C&N) and wrought 8630 tested in Phase I	88
6.	Compositions of acid and basic melted A216-WCB and WCC tested in Phase II	89
7.	Compositions of acid melted 8630 steels tested in Phase II	91
8.	Composition of wrought and remelted A516-70 and 8630 steels	92
9.	Compositions of A216-WCB steels utilized in inclusion morphology/deoxidation practice studies	93
10.	Compositions of wrought low sulfur A537 and low sulfur cast steels	95
11.	Average worst-field inclusion ratings for cast and normalized and wrought C-Mn-Si and 8630 steels tested in Phase I	159
12.	Hardnesses (DPH) of charpy samples from DEOX-1, 2 and 3--as-thermal cycled and PWHT	225

LIST OF FIGURES

FIGURE		PAGE
1.	Factors affecting hydrogen-induced cracking	9
2.	Hydrogen-induced cracks in HAZ's of a) fillet and b) butt welds	11
3.	Thermal cycles experienced by indicated locations in the heat affected zone of an arc weld made with 100,000 joules/in for 1/2 in. steel plate at room temperature	12
4.	Solubility and diffusivity of hydrogen in iron as a function of temperature	14
5.	Influence of carbon content on the maximum hardness of as-quenched steel	16
6.	Interrelation of hydrogen level and underbead hardness determining cracking	20
7.	Steels divided into three categories according to their hardenability	21
8.	Comparison of thermal cycles experienced in the heat affected zone when welding with different processes	25
9.	CCT diagram for continuous cooling transformation showing critical points, critical cooling curves and critical cooling times	26
10.	Dilatometer cooling curves, for both slow and rapid thermal cycles	29
11.	Effect of homogenizing treatment on the crack sensitivity of a high strength structural steel . .	31
12.	Effect of hydrogen on the mechanical properties of steel	35
13.	Hydrogen in synthetic arc atmosphere vs. underbead cracking	36
14.	Dependence of hydrogen content on the duration and temperature of prior treatment	45

FIGURE PAGE

15. Diffusivity of hydrogen in ferritic materials as a function of temperature 49

16. Relation between pressure and hydrogen content . . . 52

17. Effect of cold reduction on the apparent diffusivity of hydrogen 53

18. Apparent diffusivity at 23°C against true void volume 55

19. Apparent diffusivity of hydrogen vs. sulfur content . 56

20. Relation between sulfur content and absorbed energy of heat affected zone 60

21. The effect of aluminum content upon underbead weld cracking sensitivity 62

22. Effect of aluminum on the HAZ transition temperature 65

23. Comparative hardness surveys showing the effect of preheat and stress relief on welds in manganese-molybdenum castings 68

24. Effect of preheat on the maximum hardness obtained in the heat-affected zone of manganese-molybdenum steel castings 70

25. Underbead cracking vs. carbon equivalent (room temperature) 71

26. Typical impact transition curves for 1Cr-1Mo-1V cast material 73

27. Typical tempering parameter curve for a 1.25%Cr-0.5%Mo casting HAZ 81

28. Underbead cracking test specimen showing cut section and location of underbead cracks 98

29. UT-Modified Hydrogen Sensitivity Test procedure . . . 101

30. Autogenous gas tungsten arc weld being made on the UT-Mod.HST sample 103

31. Schematic of original implant test developed by Granjon 105

FIGURE PAGE

32. Implant Test--sample and test method used 107

33. Semi-automatic welding set up for implant samples 108

34. Final machined dimensions of Charpy sample heat treated in the Gleeble 112

35. RPI silicone oil apparatus used to determine diffusible hydrogen 114

36. Extent of HIC at 32°F in cast and normalized (C&N) C-Mn-Si and 8630 steels 124

37. Extent of HIC at 100°F in cast and normalized (C&N) C-Mn-Si and 8630 steels 125

38. Microstructure of coarse grained HAZ in C&N C-Mn-Si steel, C.E. = 0.37 127

39. SEM micrograph of coarse grained HAZ in C&N C-Mn-Si steel, C.E. = 0.37 129

40. Microstructure of coarse grained HAZ in C&N C-Mn-Si steel, C.E. = 0.47 130

41. SEM micrograph of coarse grained HAZ in C&N C-Mn-Si steel, C.E. = 0.47 131

42. Microstructure of coarse grained HAZ in C&N C-Mn-Si steel, C.E. = 0.58 132

43. SEM micrograph of coarse grained HAZ in C&N C-Mn-Si steel, C.E. = 0.58 133

44. Preheat temperature (UBCT) required to prevent HIC related to Jominy hardenability for cast and normalized (C&N) C-Mn-Si steels 135

45. Schematic diagram showing orientation of specimens and welds in wrought plate UBCT samples 136

46. Extent of HIC at 32°F in wrought (WR) C-Mn-Si and 8630 steels compared to that in equivalent cast and normalized (C&N) C-Mn-Si steels (average line) 138

FIGURE PAGE

47. Extent of HIC at 100°F in wrought (WR) C-Mn-Si and 8630 steels compared to that in equivalent cast and normalized (C&N) C-Mn-Si steels (average line) 139

48. Preheat temperatures required to prevent HIC in cast and normalized C-Mn-Si and wrought C-Mn-Si (PRD) steels as determined in the UBCT 141

49. Preheat temperature required to prevent HIC in cast and normalized C-Mn-Si and wrought C-Mn-Si (TTD) steels as determined in the UBCT 142

50. Maximum hardness of coarse grained HAZ in C-Mn-Si and 8630 steels tested in the UBCT 144

51. Macrographs of wrought C-Mn-Si steel, A516-70, C.E. = 0.43 tested a) PRD and b) TTD in the UBCT 146

52. Microstructure of coarse grained HAZ in wrought C-Mn-Si steel, A516-70, C.E. = 0.43 147

53. Coarse grained HAZ in wrought C-Mn-Si steel, A516-70, C.E. = 0.43, showing HIC association with MnS inclusions 148

54. HIC association with inclusions and banding in wrought C-Mn-Si steel, A516-70, C.E. = 0.43 149

55. HIC association with inclusions in coarse grained HAZ of wrought C-Mn-Si steel, A299, C.E. = 0.68 . . 151

56. HIC associated with Type III inclusions in coarse grained HAZ of C&N C-Mn-Si steel, C.E. = 0.55 . . . 152

57. Fracture morphology of HIC in wrought C-Mn-Si steel, A516-70, C.E. = 0.43 153

58. Fracture morphology of HIC in C&N C-Mn-Si steel, C.E. = 0.58 154

59. Schematic representation of residual stress distribution in a bead-on-plate weld 156

60. Typical inclusions in C-Mn-Si steels 161

FIGURE PAGE

61. Evaluation of the effect of a post weld hold (PWH 100°F/2 hrs) in addition to a preheat (PH 100°F) on the HIC susceptibility of cast and normalized (C&N) and wrought (WR) C-Mn-Si steels 164

62. Evaluation of the effect of a post weld hold (PWH 150°F/2 hrs) in addition to a preheat (PH 100°F) on the HIC susceptibility of cast and normalized (C&N) and wrought (WR) C-Mn-Si steels 165

63. Preheat temperature required to prevent HIC in cast and normalized (C&N) C-Mn-Si and wrought C-Mn-Si steels as determined in the UT-Mod.HST 167

64. Weld metal hardness in UT-Mod.HST samples tested at a preheat of 75°F 169

65. Macrograph of UT-Mod.HST sample of C&N C-Mn-Si steel, C.E. = 0.37 170

66. Microstructure of fusion zone and HAZ in C&N C-Mn-Si steel, C.E. = 0.37 171

67. Microstructure of fusion zone in C&N C-Mn-Si steel, C.E. = 0.37 173

68. Macrographs of UT-Mod.HST sample from C&N C-Mn-Si steel, C.E. = 0.47 174

69. Microstructure of fusion zone and HAZ in C&N C-Mn-Si steel, C.E. = 0.47 175

70. Macrograph of UT-Mod.HST sample from C&N C-Mn-Si steel, C.E. = 0.58 176

71. Microstructures of the fusion zone in C&N C-Mn-Si steel, C.E. = 0.58 177

72. SEM micrographs of the fusion zone in C&N C-Mn-Si steel, C.E. = 0.58 178

73. Preheat temperature to prevent HIC correlation between results of the UBCT and the UT-Mod.HST for cast and normalized C-Mn-Si steels 180

74. UBCT preheat results for acid-melted A216-WCB and WCC cast steels 182

FIGURE PAGE

75. Inclusion morphology and associated HIC in acid-melted as-cast BA-1, A216-WCB, C-Mn-Si steel . . . 184

76. HIC association with Type II inclusions in the partially refined HAZ, as-cast BA-1, acid-melted A216-WCB 185

77. Typical Type III inclusions in acid-melted A216-WCB steel BA-3 186

78. UBCT preheat results for basic melted A216-WCB and WCC cast steels 188

79. UBCT preheat results for acid melted 8630 steels . . 190

80. Maximum hardness in the coarse grained HAZ of foundry grade A216 and 8630 cast steels 191

81. UBCT preheat results for remelted (R) and wrought (W) 8630 steels 194

82. Microstructure of as-cast remelted 8630 195

83. Typical inclusions in wrought and remelted 8630 . . . 196

84. UBCT preheat results for remelted (R) and wrought (W) A516-70 steels 198

85. Typical morphology of Type II inclusions in remelted as-cast A516 and associated HIC 199

86. Implant test results for wrought (W) and remelted (R) A516-70 200

87. HIC in coarse grained HAZ of implant tested as-cast remelted A516 showing association of IG cracks with Type II inclusions 201

88. Fracture morphology of implant specimen of W516 tested PRD, C.E. = 0.43 203

89. Fracture morphology of implant specimen of W516 tested TTD, C.E. = 0.43 204

90. Typical Type I inclusions in DEOX-1 cast A516-WCB steel 207

91. Typical Type II inclusions in DEOX-1 cast A216-WCB steel 208

FIGURE PAGE

92. Typical Type II and Type III inclusions in DEOX-2 cast A216-WCB steel 210

93. Typical Type III inclusions in DEOX-3 cast A216-WCB steel 211

94. UBCT preheat results for DEOX-1,2,3 tested in the as-cast (AC) condition 212

95. UBCT preheat results for DEOX-1,2,3 tested in the cast and normalized (C&N) condition 214

96. Microhardness distribution in the HAZ of DEOX-1,2,3 UBCT samples tested in the as-cast (AC) condition . 215

97. Microhardness distribution in the HAZ of DEOX-1,2,3 UBCT samples tested in the cast and normalized (C&N) condition 216

98. Implant test results for steels DEOX-1,2,3 tested in the as-cast (AC) condition 218

99. Microhardness distribution in the HAZ of steels DEOX-1,2,3 implant tested in the as-cast (AC) condition 219

100. Microstructure at fracture interface in implant specimen of DEOX-1-AC, C.E. = 0.45 220

101. Microstructure at fracture interface in implant specimen of DEOX-2-AC, C.E. = 0.42 221

102. Impact test results for DEOX-1,2,3 in the as-cast (AC), as-welded (T) and PWHT conditions 223

103. Microstructures in simulated coarse grained HAZ's of charpy specimens from DEOX-1, DEOX-2 and DEOX-3 226

104. Microstructures in simulated post weld heat treated coarse grained HAZ's of charpy specimens from DEOX-1, DEOX-2 and DEOX-3 227

105. Fracture morphology of charpy samples of DEOX-1, DEOX-2 and DEOX-3, AC, impact tested at 100°F . . . 229

106. UBCT preheat results for low sulfur A537 wrought steels tested PRD 232

FIGURE		PAGE
107.	Inclusion morphology in A537-7 and A537-12 steels . .	233
108.	Inclusion morphology in A537-1 and A537-8 steels . .	235
109.	Macrographs of UBCT samples of A537-1 and A537-8 showing HIC in the coarse grained HAZ and banding in base metal	236
110.	Macrographs of UBCT samples of A537-7 and A537-12 showing quenched and tempered base metal and HIC in coarse grained HAZ of A537-12	237
111.	Implant test results for low sulfur steels A537-1,7,8, 12 tested TTD	238
112.	Implant test results for low sulfur steels A537-1 and A537-8, tested PRD and TTD	240
113.	Fracture morphologies in implant specimens of A537 low sulfur steels tested TTD	242
114.	Typical fracture interface sections of implant specimens of A537 low sulfur steels tested TTD . .	243
115.	Fracture morphology of implant specimen of A537-1 . .	244
116.	Fracture morphology of implant specimen of A537-7 . .	246
117.	Fracture morphology of A537-1 implant specimen tested PRD	247
118.	Fracture morphology of A537-8 implant specimen tested PRD	248
119.	Microstructure in coarse grained HAZ of implant sample of low sulfur cast steel (LSC)	250
120.	Ruptured cross-section of implant sample of low sulfur cast steel (LSC)	251
121.	Fracture morphology of rupture in E 6010 weld metal in implant tested low sulfur cast steel (LSC) (See Figure 120b)	252
122.	Fracture morphology of HIC in two pass implant sample (E 6010 + E 6010) of A537-1, TTD, preheat 75°F, Stress 20 Ksi, time to rupture 11 minutes . .	255

FIGURE PAGE

123. Cross-section of two-pass (E 7018 + E 6010) implant sample of A537-1 257

124. Microstructural details of crack shown in Figure 123 258

125. Impact toughness at room temperature (75°F) of simulated coarse grained HAZ's in cast and normalized and 8630 steels 260

126. Impact toughness at -25°F of simulated coarse grained HAZ's in cast and normalized C-Mn-Si and 8630 steels 261

127. Microstructures of simulated coarse grained HAZ charpy samples of C&N C-Mn-Si steels, C.E. = 0.37 . 263

128. Microstructures of simulated coarse grained HAZ charpy samples of C&N C-Mn-Si steel, C.E. = 0.47 . 264

129. Microstructures of simulated coarse grained HAZ charpy samples of C&N C-Mn-Si steel, C.E. = 0.58 . 265

130. Schematic representation of fracture modes in martensite during HIC 271

131. Schematic representation of HAZ in cast steels illustrating location of microstructure and inclusions with respect to diffusing hydrogen front (from the weld metal into the HAZ) 273

132. Schematic representation of HAZ in wrought steels showing location of microstructure and inclusions with respect to diffusing hydrogen front 275

CHAPTER I

INTRODUCTION

In recent years, the performance requirements of steel castings have increased considerably, and this has led to the need for castings which have fewer internal flaws, and thus for more rigorous methods of inspection in the foundry. Considerable time and effort has been spent to eliminate the possibility of producing defective castings due to the difficulty in feeding different cross sections. Such a situation is typical, for example, in the case of castings for nuclear applications. Here, specifications for quality control of materials and workmanship are far more rigid than what foundries have encountered in the past. The complexity of component parts for nuclear power plants has further involved the casting industry as a major supplier of these components. The use of welding in the foundry has evolved from a repair standpoint to the use for the manufacture of composite cast/cast and cast/wrought components enabling the manufacture of a higher quality product.

During the welding of cast as well as wrought components a problem commonly encountered in the heat affected zone (HAZ) is hydrogen-induced cracking (HIC). The three most important factors affecting the HIC susceptibility of a steel are:

1. The composition, hence the hardenability;
2. The presence of hydrogen;
3. Restraint.

Initial work pointing to differences in HIC susceptibility between cast and similarly constituted wrought steels was reported by Williams et al.[1] The conclusions of this study were that at similar carbon contents and for similar carbon equivalents, the cast materials were less sensitive to HIC than the wrought materials. These reportings, while extensive in the testing realm, did not indicate any significant microstructural analysis of the materials. Other investigators[2,3] have also reported higher susceptibilities to HIC in wrought materials when compared to equivalent cast steels, but here again, no reasons for this behavior have been expounded. On the other hand, Linnert[11] has indicated that cast steels may be more susceptible to HIC than wrought steels.

It is recognized that the HAZ microstructure governs to a considerable extent, the susceptibility to HIC. In general, the harder the microstructure, the greater the susceptibility, with twinned martensitic structures being the most susceptible.[25] Other factors that have a bearing on the HIC susceptibility of the HAZ are known to be the hydrogen content of the weldment, and the stresses (restraint or applied) acting on the weldment. Considering the situation where all the above factors are identical for equivalent cast and wrought steels, the reasons for possible HIC differences between cast and wrought materials may arise from the intrinsic differences between the two types of materials. Cast steels are in general coarse grained, and exhibit relatively isotropic properties compared to their wrought counterparts. Inclusion morphologies in cast

steels are generally "globular" compared to the elongated stringered inclusions found in wrought steels. Further, as-cast steels may have regions of segregation or have regions of porosity or inter-dendritic shrinkage.

Compositional effects on HIC are usually summarized by using carbon equivalents to normalize the chemical composition. However, the carbon equivalent formulae commonly used do not take into account the effects of factors such as prior microstructure[29] or sulfur content[23,47] which have been reported to affect the HIC susceptibility of steels. Japanese researchers[17] have attempted to include the hydrogen content into the formulae; however, this entails the precise knowledge of "diffusible hydrogen" contents for each type of welding process employed. Other elements, such as the aluminum (acid soluble and total) and sulfur do no fall in the category of those that can be included to calculate the carbon equivalent, since they do not have a significant direct influence on hardenability. The aluminum content, however, has been reported to influence the HIC[64,66] as well as HAZ toughness[68] due to its influence on grain coarsening characteristics and nucleation/precipitation reactions in the HAZ. Further, the aluminum content together with the sulfur content influences the inclusion morphology and distribution. The sulfur content can be taken to be as a rough guide to the volume fraction of inclusions present, however, the morphology is determined by the deoxidation practice used prior to casting the ingot, and by the subsequent thermo-mechanical treatment.

From an overall "weldability" standpoint, the response of coarse grained HAZ's to post-weld heat treatment (PWHT) is an important factor to be considered. Microstructures which are less susceptible to HIC may not attain suitable toughnesses upon tempering during PWHT, i.e., steels with low carbon equivalents may have low HAZ toughnesses upon PWHT.

The purpose of the research program was to investigate the weldability of cast steels both from a fabricability and serviceability viewpoint. Specifically, the response of cast steels to HIC conditions was evaluated using self-restraint as well as applied-restraint tests. Identical tests were conducted on wrought steels to obtain comparative data. Testing was extended to a wide range of cast steels representing typical foundry practice (acid and basic melting) and to cast steels subjected to various degrees of deoxidation. The Gleeble was utilized to document the response of simulated coarse grained HAZ's to PWHT. To more clearly define the influence of inclusion content and morphology, additional testing was performed on low sulfur ($S < 0.01\%$) steels. The results of this research effect bring into focus the weldability concepts, the effects of composition, sensitivity to hydrogen and the techniques necessary to ensure adequate weldability of cast steels with a contrast to wrought products.

CHAPTER II

LITERATURE REVIEW

1. Weldability

The definition of weldability requires a careful consideration of the large number of variables[4] involved in welding including composition and mechanical properties of base metal, electrode type and diameter, energy input, welding sequence and joint design and constraint of the structure. Laboratory testing always seeks to simplify these conditions to but one or two variables at a time which in turn creates confusion in the interpretation of weldability tests. As Kinzel[7] points out, weldability "to the fabricator of thin walled containers made of rimmed steel it means one thing, to the builder of ships it means another, and to those concerned with gun mounts it has still different significance." A perfect weld could be defined as one in which two pieces of steel are joined by fusion into a continuous member which is equal in every respect to a similar piece of steel containing no welds. This may be achieved with several steels, but the degree of difficulty to achieve this type of joint may be different. Seferin and Leroy[4] have divided the weldability field into three parts, namely i) Constructional weldability, ii) Operative weldability and iii) Metallurgical weldability. A complete definition of weldability should be related to service requirements. This school of thought has led to the definition of weldability by Naval Research Laboratory as the property which permits localized consolidation of

metals by a welding process without an undesirable change in the base material. Herres[5] has defined it as the property of a steel to be fabricated by welding without detriment to its service properties. Reeve[6] stresses the importance of metallurgical factors controlling weldability of which hardenability is the most important.

These wide ranges of definitions gives rise to the need to select an adequate weldability test to determine proper welding procedure. The choice of a test depends on various factors but by far the most important one is that it should be designed to approach the service requirements of the structure as far as rigidity, rate of loading and temperature are concerned.

It is clear that in approaching the subject of weldability a marked dichotomy of views exist. Much of the confusion could be avoided if one were able to answer the simple question, "Will the materials crack after welding?" Despite the wealth of knowledge gained over the years as regards compositional and other effects on cracking, this is a difficult question to answer. This is because the seemingly simple operation of welding causes the following phenomena[12] to occur:

1. Introduction of rapidly cooled weld metal into the joint;
2. Rapid heating and cooling of surrounding base metal;
3. Plastic straining of the material surrounding the joint during both heating and cooling, and of the weld metal during cooling;
4. The presence of residual stresses in the weld after welding is completed.

These effects due to welding may lead to cracking which occur either during or immediately following welding or in service. According to Coe[9] the former may be divided into the following five types:

1. Solidification cracking (hot cracking) in weld metal;
2. Liquation Cracking (heat affected zone (HAZ) hot tearing);
3. Reheat cracking (heat treatment or stress relief cracking);
4. Lamellar Tearing;
5. Hydrogen-induced cracking (HAZ cold cracking, delayed cracking).

The first type of cracking, solidification cracking, occurs as the weld pool cools and grains grow from the fusion boundary towards the central region of the pool. Alloying elements and impurities are rejected ahead of the growing interface which lowers the melting point of the last liquid to freeze. As these intergranular films of liquid are not able to support contractional stresses, cracks are formed. These cracks are called hot cracks as they are formed when the weld metal is still hot.

Liquation cracking in the HAZ results due to the formation of liquated regions around second phase particles which are intersected by grain boundaries during grain growth.

Reheat cracking is a type of intergranular failure observed in the HAZ of certain austenitic stainless steels and low alloy steels. Precipitation of carbides during stress relief or in service, is responsible for this mode of cracking.

In all the above types of cracking the cracking mechanism has been postulated and confirmed by actual experimental observations. Once the mechanism has been defined, a major step towards establishing safe welding procedures can be taken.

The same cannot be said in the case of hydrogen induced cracking (HAZ, delayed or cold cracking). No single convincing theory has been given to explain the presence of cracks in one instance and the absence of them in the other. It is for this reason that this review is primarily concerned with "cold" cracking; its occurrence, factors governing it, and the precautions necessary to avoid the occurrence of such cracking.

2. Hydrogen-Induced Cracking (HIC)

Hydrogen-induced cracking in the HAZ's of steels is generally found to occur after the weld has cooled to room temperature, hence it is also referred to as "cold" cracking. Cold cracks need not occur immediately after welding; their formation may be delayed for even up to a week after welding has been completed, hence these types of cracks are sometimes referred to as "delayed" cracks. To avoid confusion, the term "hydrogen-induced cracking" (HIC) will be adopted throughout in the literature review to refer to cold, as well as delayed cracking.

The factors affecting the HIC tendency of a steel are shown schematically in Figure 1. Of these factors, three are most important; i) the composition and hence, the hardenability of the steel; ii) welding process (low hydrogen or non low hydrogen) and

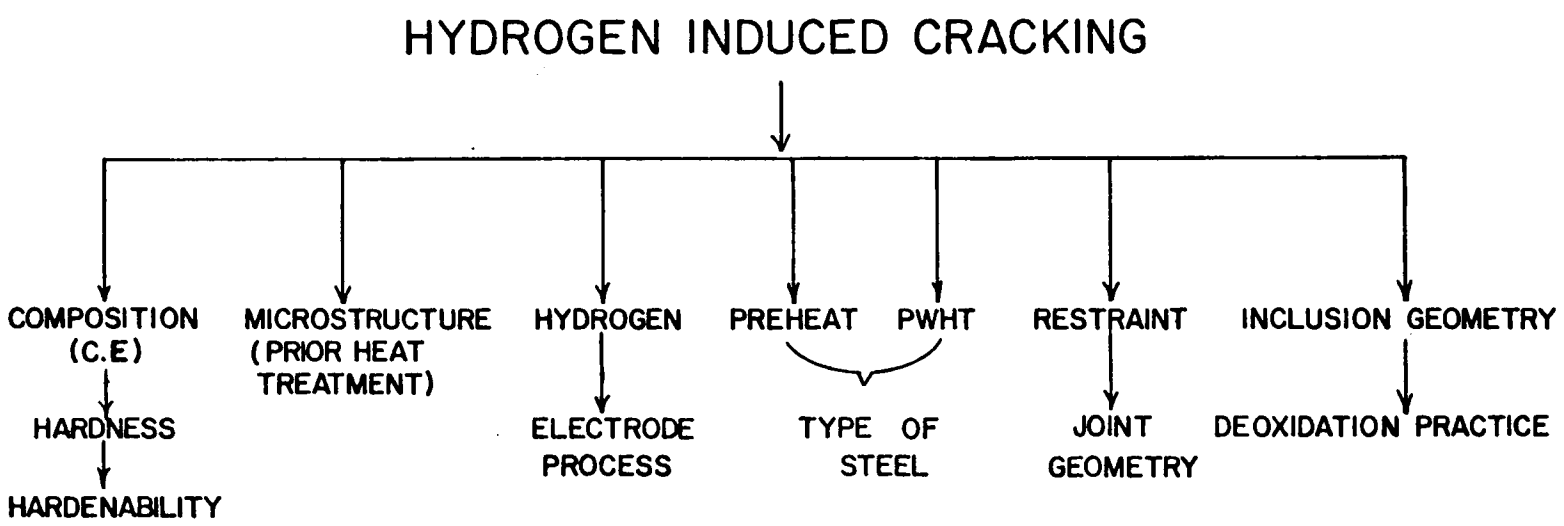


Figure 1. Factors affecting hydrogen-induced cracking.

iii) restraint (stresses associated with welding). All the factors shown in Figure 1 will be individually discussed in regard to their effects on cracking susceptibility.

Hydrogen-induced cracks can be observed either in the weld metal or the HAZ. These cracks could be longitudinal or transverse in relation to the weld (Figure 2). Longitudinal cracks in the HAZ of the base metal which occur just a short distance away from the weld fusion line are called underbead cracks. Toe cracks originate from the toe of the weld. The toe is a discontinuity in the cross section and therefore acts as stress concentrator for crack initiation.

Mechanism of HIC. The parent material adjacent to the weld known as the heat affected zone (HAZ) is raised to a high temperature, well above the A_3, during a weld thermal cycle. Typical weld thermal cycles are shown in Figure 3. The cooler surrounding base metal causes a rapid cooling of the HAZ, leading to hardening in the coarse grained region near the fusion line. The maximum hardness obtained in the coarse grained HAZ will be a function of the carbon content of the steel whereas the alloying elements will determine the hardenability of this region. The coarse grained HAZ will therefore possess a lower toughness when compared to that of either the base metal or other regions in the HAZ. If the welding process is one where hydrogen is evolved in the arc, the hydrogen dissociates into H atoms or H^+ protons which dissolve in the liquid metal. During subsequent cooling, supersaturation

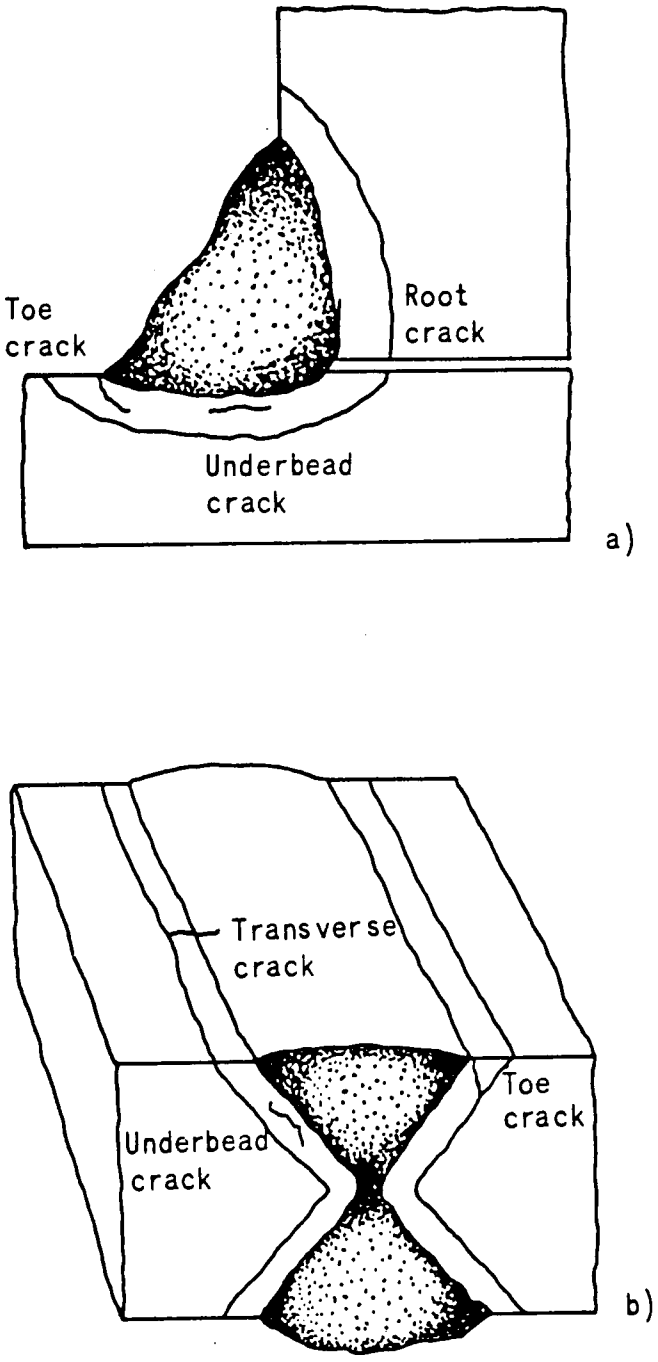


Figure 2. Hydrogen-induced cracks in HAZ's of a) fillet and b) butt welds.

Source: Coe, F.R., "Welding Steels Without Hydrogen Cracking," The Welding Institute (1973).

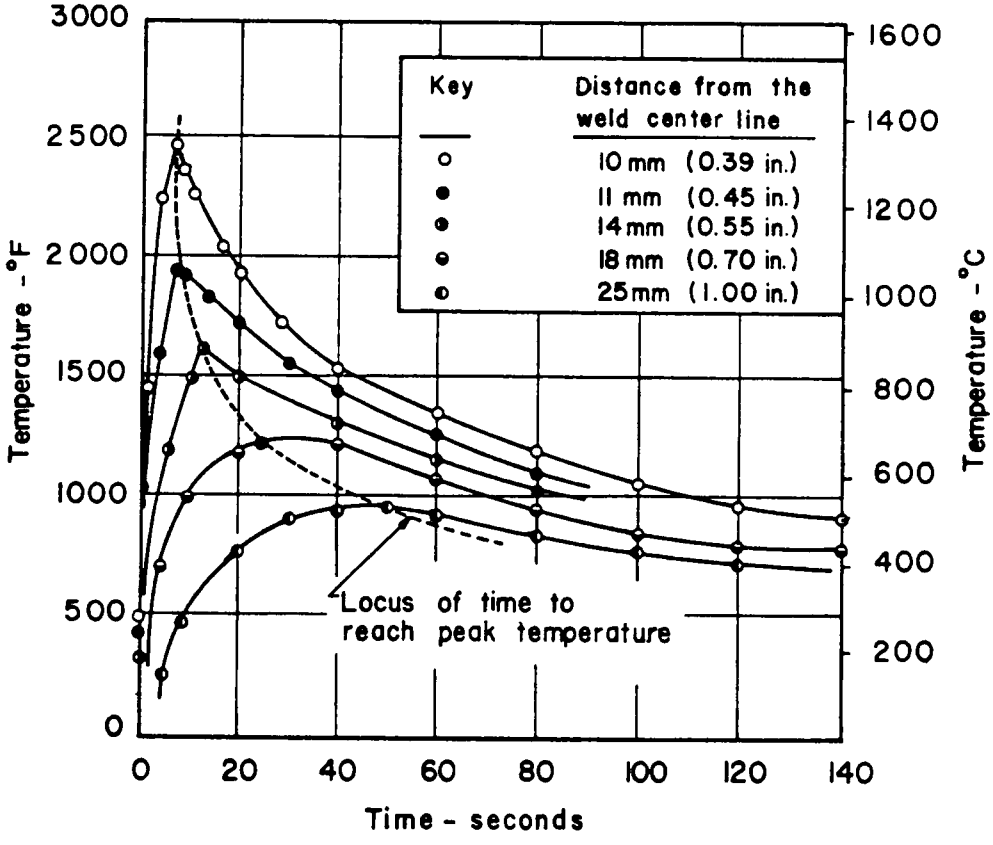


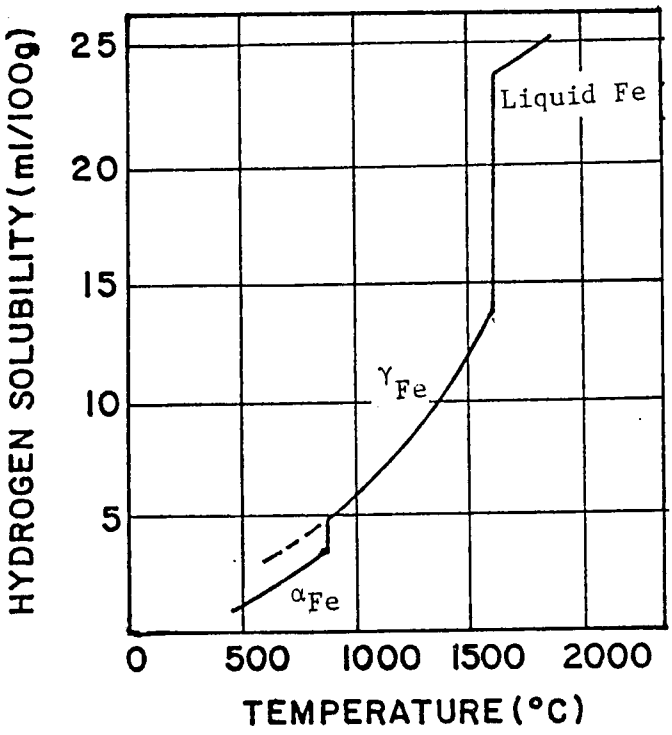
Figure 3. Thermal cycles experienced by indicated locations in the heat affected zone of an arc weld made with 100,000 joules/in for 1/2 in. steel plate at room temperature.

Source: AWS Handbook, Vol. 1, Seventh Edition (1976).

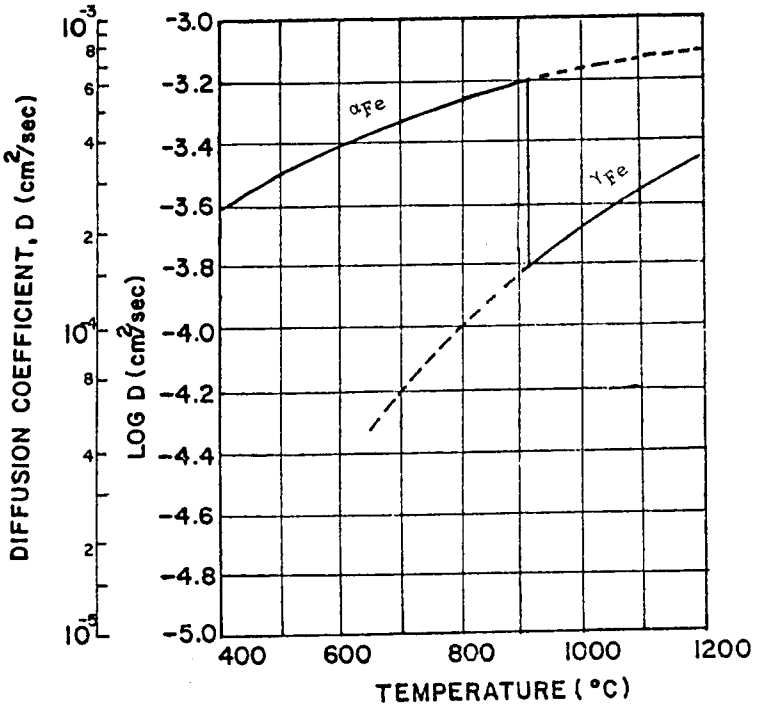
results because the solubility of hydrogen in iron decreases sharply at the freezing temperature and at the austenite to ferrite transformation temperature. The solubility of hydrogen in iron decreases during the austenite to ferrite transformation but at the same time its diffusivity is higher in the ferrite than in the austenite (Figure 4). Further, during a weld thermal cycle, the austenite can transform to martensite if the cooling rate is fast enough. This transformation is accompanied by a volume expansion, and hence transformation stresses. Thus, inherently we have a martensitic structure low in toughness and saturated with hydrogen and have stresses present. Cracking may occur spontaneously in those areas where hardening has taken place and the metal can no longer plastically deform to accommodate the stresses. Presence of stress raisers (e.g. inclusions) may act as initiation sites for crack formation.

The cooling rates in the HAZ depend upon several factors such as the heat input, plate thickness, preheat conditions, and hence, a variety of microstructures could result, depending upon the cooling rate. Linnert[11] has listed the propensity for cold cracking of microstructures in the following order:

1. Ferrite and carbides (in Pearlite);
2. Bainite;
3. Bainite mixed with martensite;
4. Martensite;
5. Martensite with some ferrite and bainite;
6. Martensite with internal twinning.



a)



b)

Figure 4. Solubility and diffusivity of hydrogen in iron as a function of temperature.

Source: (a) Coe, F.R., "Welding Steels Without Hydrogen Cracking," The Welding Institute (1973).

(b) Smialowski, M., "Hydrogen in Steels," Pergamon Press (1962).

It is clear that composition, microstructure, hydrogen and stresses are the most important factors concerned with cold cracking. Each of these and the other factors shown in Figure 1 will now be considered in detail.

3. Factors Affecting HIC

Composition. The type of microstructure formed in the HAZ of a welded joint will be dependent[13] upon composition of the steel, the maximum temperature attained, the time at this maximum temperature, the cooling rate, and any subsequent reheating due to additional passes. The carbon content will determine the maximum hardness obtained in the HAZ (Figure 5), whereas, the other alloying elements will determine the hardenability. Maximum hardness generally occurs immediately adjacent to the fusion line since the peak temperature is the highest and grain coarsening and dissolution of carbides occurs most readily. HIC increases with the formation of martensite and other hard structures in the heat affected zone, thus, the effect of each alloying element on hardenability has to be considered. The carbon equivalent (C.E.) concept is a convenient method to normalize chemical compositions (hardenability/hardness) to a single number to indicate how compositions affect hardenability, and hence the HIC susceptibility of a steel. One of the earliest[14] formulas used is $C.E. = \%C + \frac{\%Mn}{6}$. Over the years, a host of C.E. formulae have been developed to correlate results of cracking tests or maximum hardnesses in the HAZ with composition. Researchers at Battelle[1] used the formula

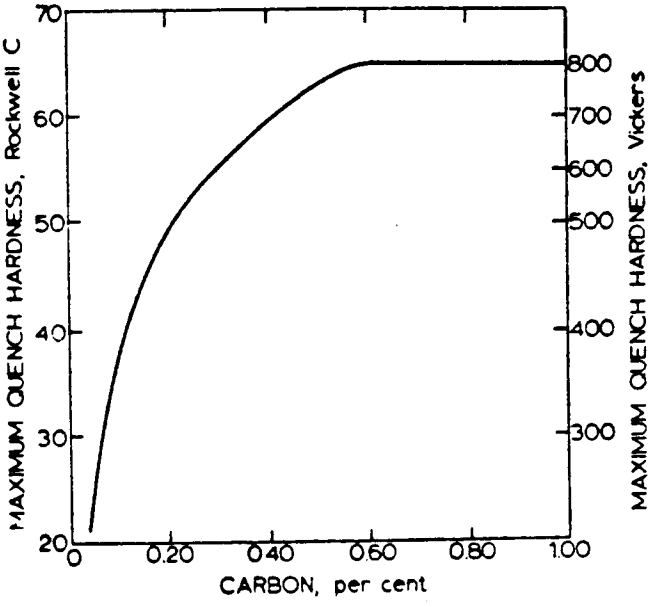


Figure 5. Influence of carbon content on the maximum hardness of as-quenched steel.

Source: Stout, R.D., "Hardness as an Index of the Weldability and Service Performance of Steel Weldments," WRC Bulletin 189, Nov. (1973).

C.E. = %C + $\frac{\%Mn}{4}$ + $\frac{\%Si}{4}$ to correlate with their results in the under-bead cracking test. The formula log DPN = 1.957 + 1.41 %C + 0.193 %Mn + 0.086 %Ni + 0.16 %Cr + 0.03 %Cu was suggested by Edson[15] to predict HAZ hardnesses. The formulae suggested by various workers differ essentially in the weight given to each of the elements present in the steel to represent its influence on hardenability and hence, susceptibility to cracking. Winterton[14] has suggested the following modified formula for the calculation of carbon equivalent:

$$C.E. = \%C + \frac{\%Mn}{6} + \frac{\%Ni}{20} + \frac{\%Cr}{10} - \frac{\%Mo}{50} + \frac{\%V}{10} + \frac{\%Cu}{40} \quad .$$

Since cold cracking susceptibility is also affected by the presence of hydrogen and by the plate thickness, Japanese workers[17] have incorporated these into the formula as:

$$P_c = \%C + \frac{\%Si}{30} + \frac{\%Mn}{20} + \frac{\%Cu}{20} + Ni/60 + \frac{\%Cr}{20} + \frac{\%Mo}{15} + \frac{\%V}{10} + 5\% B$$

$$+t/600 + H/60 \quad ,$$

where 't' is the thickness of the plate in millimeters and 'H' is the amount of diffusible hydrogen in cc/100g of weld metal. Pc is designated as a cracking parameter. The IIW Commission XIV, Sub-Commission G has proposed the following formula:

$$C.E. = \%C + \frac{\%Mn}{6} + \frac{\%Cr+\%Mo+\%V}{5} + \frac{\%Ni+\%Cu}{15} \quad .$$

Kihara et al.[17] proposed the carbon equivalent to be expressed as

$$C.E. = \%C + \frac{\%Si}{24} + \frac{\%Mn}{6} + \frac{\%Ni}{40} + \frac{\%Cr}{5} + \frac{\%Mo}{4} \quad .$$

The maximum HAZ hardness can be calculated by using the following formula base on the above C.E.

$$H_{max} \text{ (DPH)} = (666 \text{ C.E.} + 40) \pm 40 \quad .$$

It has to be borne in mind that not only do alloying elements have an effect on the hardenability of a steel, they also affect M_s and M_f temperatures. Bradstreet[18] has suggested the following formula based on observed M_f temperatures in fifty experimental steels.

$$\text{C.E.} = C + \frac{\%Mn}{20} + \frac{\%Ni}{15} + \frac{\%Cr + \%Mo + \%V}{10} \quad .$$

According to Winterton[14] hydrogen itself can be treated as an alloying constituent. Quoting Cottrell's data[16] he notes that the presence of 14cc/100g of hydrogen, which is typical of deposits from rutile coated electrodes, the M_f temperature is depressed by 108°F for a Manganese-Molybdenum steel and 144°F for a Boron-Molybdenum steel. In general, the majority of the alloying elements commonly used e.g. Mn, Si, Cr, Ni, Mo, V decrease the critical cooling rate. This implies that as a weldment cools, slower cooling rates can give rise to fully martensitic structures in the HAZ. As indicated earlier, such structures will inherit higher hardnesses and hence, will be more susceptible to HIC. Further, except for cobalt and aluminum all other alloying elements commonly used in steels lower the M_s temperature. A lower transformation temperature is also known to increase the susceptibility to HIC. The susceptibility of a steel to HIC has been correlated to the maximum

underbead hardness and the hydrogen content as shown in Figure 6; as the HAZ hardness increases, less hydrogen can be tolerated before HIC occurs. In the study of a wide range of steels, Rothwell[19] found that his steels could be divided into three groups depending on their carbon and alloy contents. His results are shown in Figure 7. In his words,

> Zone I steels have a low carbon content with a fairly flat hardening curve and even the hardest microstructure that can be produced during welding is not very susceptible to cracking. Zone II steels have a higher carbon content but a low alloy content and display steep hardening curves with a wide range of hardnesses. Zone III steels have both a high carbon as well as alloy content and will produce susceptible microstructures under all conditions of welding.

The effect of some of the most common alloying elements on the HIC susceptibility of a steel can be summarized as follows. Carbon is the element most deleterious, manganese, molybdenum, vanadium and nickel follow in that order towards rendering a steel more susceptible to HIC.

The effect of silicon has not been reported with any certainty in literature. Luther et al.[21] observed that their experimental manganese-silicon steels had a less tendency for HIC than commercial carbon-manganese steels. These results agree with those of Jackson, et al.[22] who concluded that "the use of silicon as a strengthener of normalized steels for welding is to be preferred to that of carbon or manganese as lower weld hardening and higher weld ductility results in the silicon steels." However, if present in excessive amounts, silicon can degrade weldability by lowering the notch toughness.

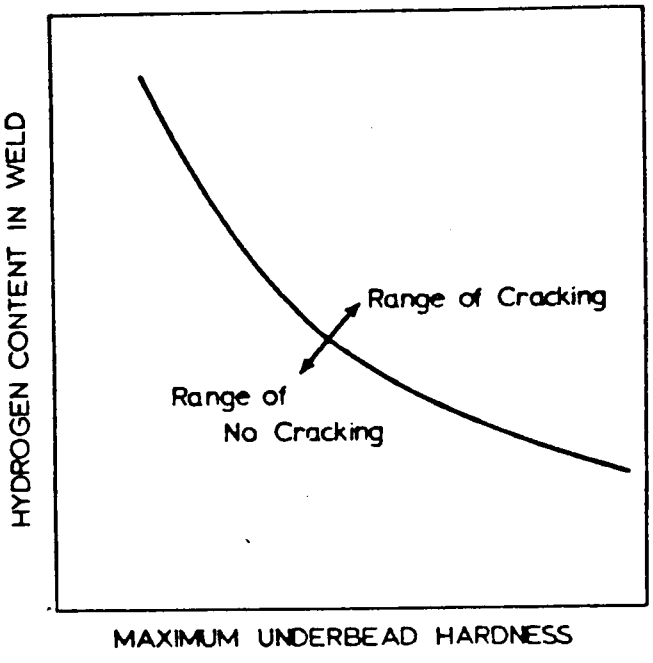


Figure 6. Interrelation of hydrogen level and underbead hardness determining cracking.

Source: Stout, R.D., "Hardness as an Index of the Weldability and Service Performance of Steel Weldments," WRC Bulletin 189, Nov. (1973).

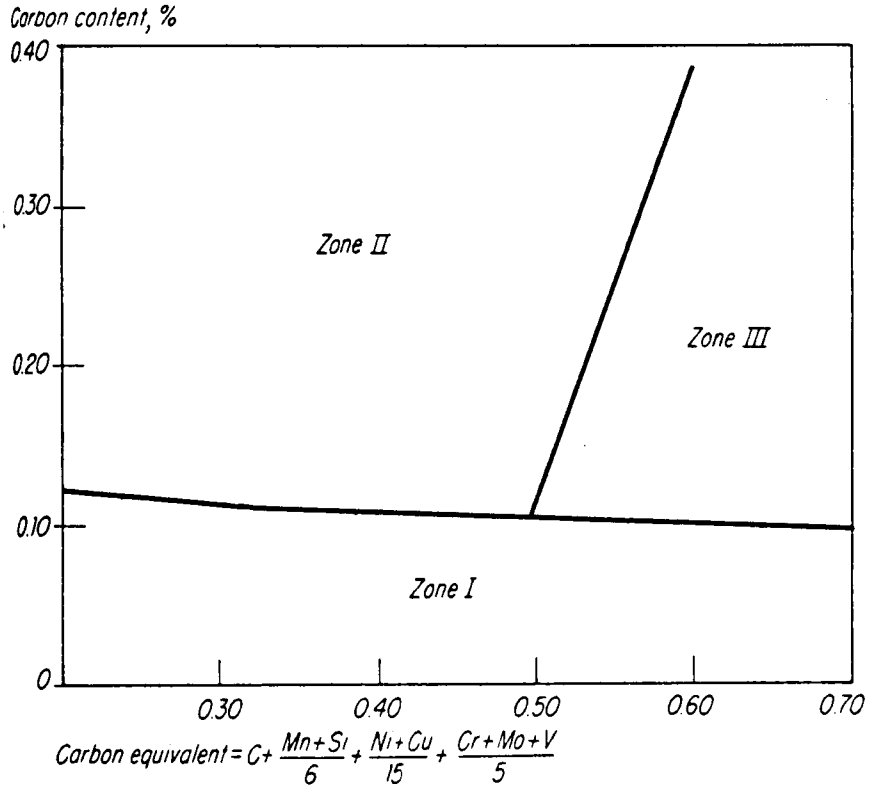


Figure 7. Steels divided into three categories according to their hardenability.

Source: Rothwell, A.B., "Weldability of HSLA Structural Steels," Metal Progress, June, 43-50 (1977).

Sulfur, which is considered a main culprit as far as hot cracking is concerned, has been found to have an opposite effect when HIC of wrought steels is considered. Such steels with sulfur less than 0.010% have been reported[23] to be exceptionally susceptible to HIC. The explanation offered[47] is that lowered sulfur contents reduce the volume of voids associated with manganese sulfide inclusions where hydrogen can accumulate, which in turn increases the pressures built up in the lattice due to hydrogen. The susceptibility to HIC of low sulfur cast steels is different, and will be discussed later.

As far as effects of rare earths on cold cracking are concerned, Rothwell[19] quotes the results of Banks and Gunn as,

> With the exception of CO_2 welding, it has been found that the weldability of REM treated C/Mn/Cb steel is identical to that of a REM free steel. When weldability is considered in relationship to resistance to lamellar tearing, the weldability of the REM treated steel is improved.

REM treated steels possess essentially globular inclusions which do not get rolled out into flat laminations. This significantly improves resistance to lamellar tearing.

From the discussion until now, it is clear that the susceptibility of a steel to HIC is governed by hardenability. Doan et al.[24] used this concept to devise a weldability evaluation technique which is briefly outlined below. The technique utilizes the Jominy end quench hardenability test to correlate hardnesses with cooling rates. Since every point on the Jominy Bar experiences a certain known cooling rate, known cooling rates

in the HAZ can simply be expressed as locations on an end quench bar. Thus, the hardness of the HAZ can be determined. In addition to hardness, the ductility of the HAZ can be specified as the important criterion to evaluate weldability. A slow notchbend specimen is used to determine the ductility of the steels. The ductility that accompanies each hardness level is found by quenching specimens of a steel to different hardnesses so as to encompass the entire range of hardnesses of the Jominy bar. These specimens are then bent to failure and the angle of cracking is taken as a measure of ductility. Once the hardnesses have been correlated with ductility, actual welds are made on the steel using various heat inputs, and the maximum hardness in the heat affected zone is related to the heat input. With the help of all the above data, one could suggest welding procedures once the ductility needed was specified.

Though the above method proposed by Doan et al. showed the importance of controlling heat input to control properties of the HAZ, it has a serious deficiency in that the results of the Jominy test, which is conducted through a slow austenitization and long soaking times will differ from the rapid austenitization, brief soaking times and higher peak temperatures experienced by the HAZ during an arc weld. Moreover, the method also requires extensive testing to be carried out for each grade of steel. In the welding of cast steels, the effects of segregation will have to be taken into account, as the composition in the region where welding is carried out will be a function of the casting process used as well as the casting thickness.

Microstructure. As has been indicated earlier, regions near the fusion line are raised to temperatures well above the grain coarsening temperature and cooled rapidly due to the mass of surrounding metal which acts as an excellent heat sink. The microstructure will depend upon the cooling rate and the composition and hardenability of the steel. A comparison of thermal cycles experienced by the HAZ as a function of the welding process is shown in Figure 8. It is clear that as the heat input is increased, slower cooling rates result in the HAZ. The continuous cooling transformation (CCT) diagram has to be referred to in order to predict the microstructure that will be obtained as the result of a particular cooling rate. A typical CCT diagram is shown in Figure 9. Referring to the figure, it can be seen that cooling rates such as 'Z' which result from low heat inputs, will give rise to fully martensitic heat affected zones. Heat inputs for two processes, shielded metal arc welding (SMAW) and gas metal arc welding (GMAW) are shown in the figure. Cooling rates lying between Z and F will give rise to martensite and intermediate structures in the heat affected zone. If the heat input is such that cooling rates are slower than E, fully ferritic-pearlitic HAZ structures will be obtained. Since a fully martensitic structure may have a low toughness, heat inputs should be controlled so as to obtain cooling rates slower than Z. It was found[11] that steels with cooling rates slow enough to produce some transformation to proeutectoid ferrite ordinarily did not crack spontaneously and exhibited reasonable ductility and toughness. It is

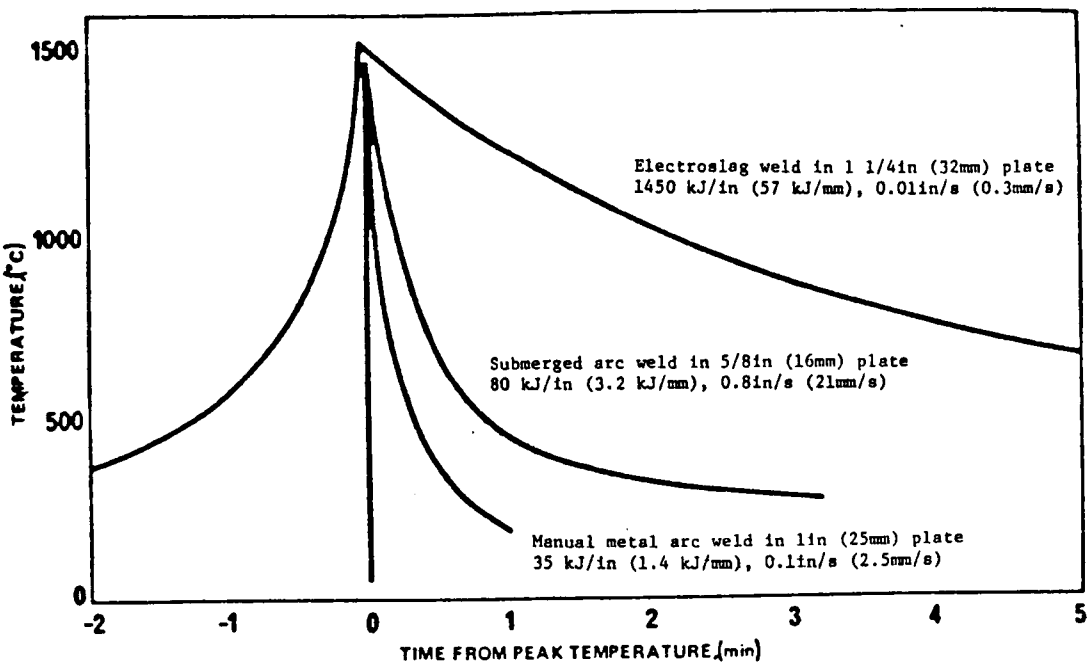


Figure 8. Comparison of thermal cycles experienced in the heat affected zone when welding with different processes.

Source: Ridal, E.J., "Metallurgical Factors Involved in Welding Carbon and Low Alloy Steel Castings," AFS International Cast Metals J., 2 (2), 47-56 (1977).

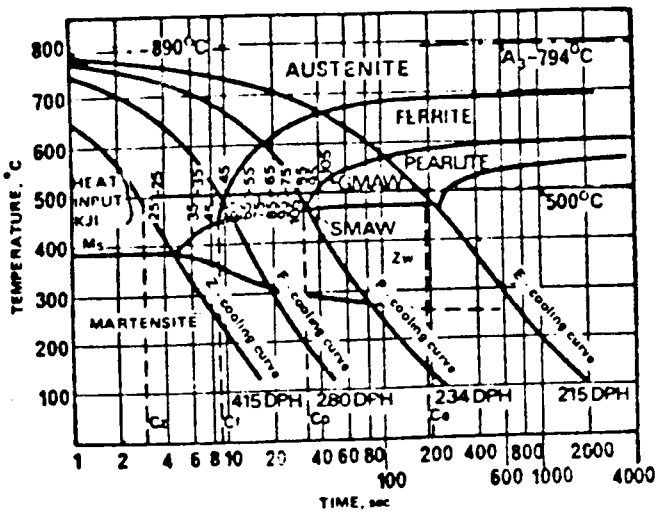


Figure 9. CCT diagram for continuous cooling transformation showing critical points, critical cooling curves and critical cooling times.

Source: Inagaki, M., and Sekiguchi, H., "Continuous Cooling Transformation Diagrams of Steels for Welding and Their Applications," Trans. of the National Research Institute for Metals (Japan), 2 (2), 102-125 (1960).

therefore clear from the above that various heat affected-zone microstructures can be produced depending upon the heat input which in combination with the plate thickness, determine the cooling rates.

The occurrence of HIC has been associated with the presence of martensitic structures although the proportion of martensite and other structures may play a decisive role. Fully martensitic structures are known to exhibit[25] appreciable susceptibility to embrittlement in the presence of hydrogen. Mixed martensitic-bainitic and fully bainitic structures have been found to be less susceptible, in that order. Medium carbon martensite containing an appreciable portion of internally twinned grains have been reported to be the more susceptible than low carbon martensites where no internal twinning exists. Further, Bonizewski et al.[26] report that low carbon martensite is less embrittled than mixtures of low carbon martensites and bainite, the inferior properties of the low carbon bainitic structures appear to be related to the susceptibility of the bainitic colonies to transcrystalline cracking. Investigation[27] of the HAZ's in 9% Nickel steel has also shown the greater susceptibility of twinned martensitic structures to embrittlement compared to low carbon auto-tempered martensitic structures. In general, it may be summarized that the higher the hardness of the microstructural composite, the greater is its susceptibility to hydrogen embrittlement and consequently HIC.

Prior microstructure. As early as in 1945, Hoyt et al.[28] reported widely differing crack sensitivities of two lots of SAE 4130 steel despite the fact that both lots were almost identical in composition. End quench tests had shown these two steels to possess similar hardenabilities. One of the results (Figure 10) of their work showed that the crack sensitive steel had a higher Ar_3 temperature than the less crack sensitive steel in a slow heating and cooling cycle. However, when a rapid heating and cooling cycle was employed to simulate welding conditions, the situation was reversed. The crack sensitive steel now showed an apparent Ar_3 temperature which was lower than that for the less crack sensitive steel. The above result was explained by arguing that the finer carbides in the crack sensitive steel go into solution more completely, thus yielding austenite which is enriched in carbon which when quenched, rendered the steel more susceptible to HIC. On the other hand, the coarser carbides in the less crack sensitive steel would result in austenite of lower carbon and alloy content, thus decreasing the crack susceptibility. An observation made[29] was that a spheroidization treatment reduced crack sensitivity, but if a spheroidized steel was normalized the crack sensitivity did not revert to the original high level. This was attributed to the presence of chromium and molybdenum carbides in SAE 4130 steels. These carbides are known to dissolve more slowly than iron carbide. Thus it was concluded that the type and morphology of carbides had a strong influence on

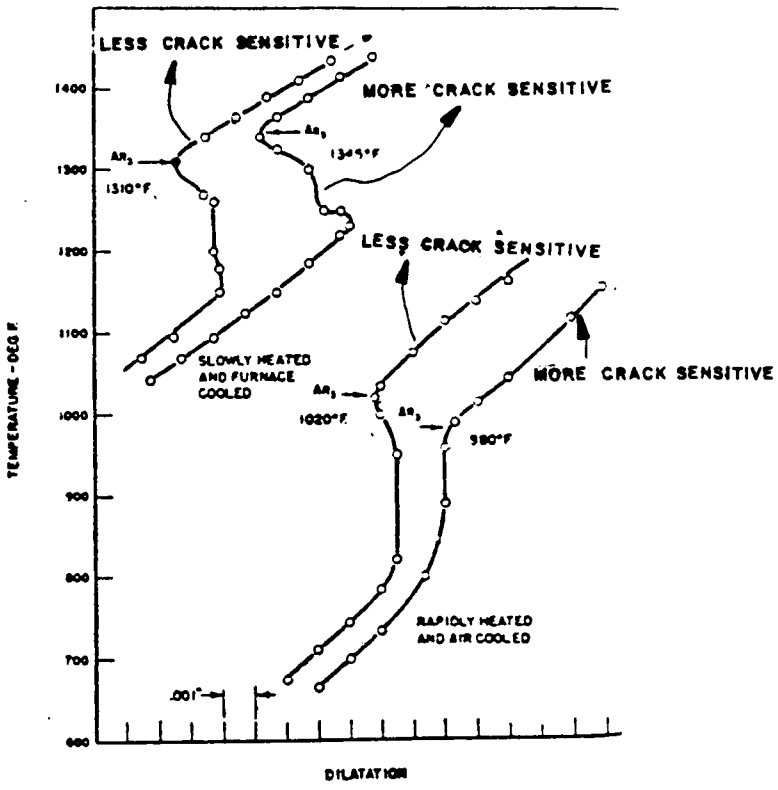


Figure 10. Dilatometer cooling curves, for both slow and rapid thermal cycles.

Source: Hoyt, S.L., Sims, C.E., and Banta, H.M., "Metallurgical Factors of Underbead Cracking," Welding J., 24 (9), 433s-445s (1945).

the cracking behavior of a steel. The influence of inclusion distribution and morphology was not considered.

A recent Russian evaluation[30] of a high strength steel shows that the cold cracking resistance of the HAZ is improved considerably by heat treatments producing globular pearlite. The carbides in this steel are reported to be of the type Cr_7C_3 and alloyed cementite type $(MFe)_3C$, the kinetics of dissolution of which are very slow. This affects the hardening of HAZ and hence the HIC sensitivity as indicated earlier.

Sims and Banta[29] also conducted extensive testing on a carbon manganese structural steel obtained in various heat treated conditions. Using the underbead cracking test, they correlated the average underbead cracking to the carbon equivalent, %C + %Mn/6. But here again, Sims and Banta observed as for the SAE 4130 steel, anomalous cases of cracking. They concluded that these were the results of manganese segregation which persisted from the ingot through the usual soaking pit and hot working practice. A homogenization treatment which diffused the manganese, was found to reduce the crack sensitivity considerably. These results are shown in Figure 11. Sims and Banta also found that the crack sensitivity could not be related to the maximum hardness in the heat affected zone i.e., steels having almost the same maximum HAZ hardness were found to show widely differing crack sensitivities. Similar conclusions were drawn from hardness surveys conducted on a steel in two heat treated conditions. The maximum hardness and the hardness

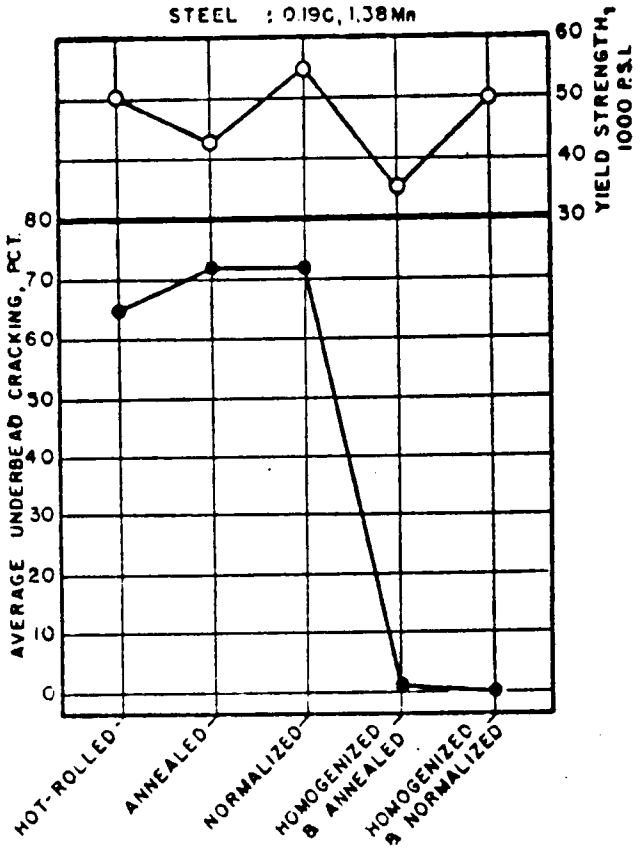


Figure 11. Effect of homogenizing treatment on the crack sensitivity of a high strength structural steel.

Source: Voldrich, C.B., "Cold Cracking in the Heat Affected Zone," Welding J., 26 (3), 153s-169s (1947).

gradient were seen to be the same, despite the fact that these two heat treated conditions show widely differing crack sensitivities. This is in agreement with Stout's[13] conclusions that the HAZ hardness is not a good criteria to base weldability upon unless the degree of segregation and hydrogen levels are specified.

Hydrogen. The introduction of hydrogen into a weldment can be caused by several factors, some of which are,[31] i) Organic chemicals, chemically bonded water and absorbed (and adsorbed) water in the covering of electrodes for shielded metal arc welding, and flux for submerged arc welding, ii) Hydrogen containing contaminants such as residual wire draw compounds, iii) Moisture in shielding gas for gas metal arc welding and iv) Surface contaminants.

The hydrogen concentrations in the arc atmosphere and weld metal deposited by various processes are shown in Table 1. The hydrogen "potential" varies[10] from "high" in shielded metal coated electrodes to "low" in gas metal arc and gas tungsten arc processes. The higher the hydrogen content in the arc atmosphere, the higher the content in the weld metal.

The mechanism by which hydrogen affects the cracking tendency of a steel has been reviewed earlier. A number of experimental methods have been used to evaluate the embrittling effects of hydrogen on steel. The most popular one is to electrolytically charge specimens (usually tensile) with known amounts of hydrogen, and study subsequent effects upon the strength and ductility of the steel. The literature concerning these types of studies is

Table 1. Hydrogen concentrations in arc atmosphere and weld metal deposited by various processes.

Process and electrode	Approximate Values for Low-Carbon Steel Weld Metal Hydrogen--ml/100g[b]				
	Hydrogen[a] in arc atmosphere % by volume	Present in liquid weld metal	Diffusible hydrogen liberated during first 24 hours	Diffusible hydrogen liberated during subsequent 20 days	Residual hydrogen remaining in as-welded deposit
Metal-arc, E6010	40	28	10	3	15
Metal-arc, E6012	35	15	6	2	7
Metal-arc, E6015	5	8	2	1	5
Gas tungsten-arc, (argon)	0	4[a]	1	0	3

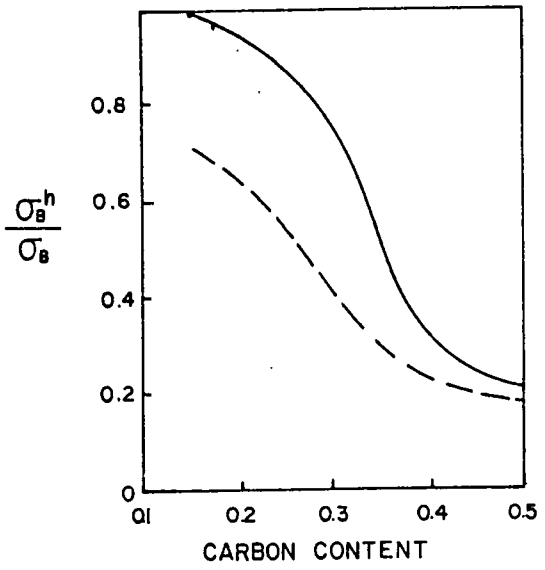
[a]Presumably hydrogen contained in filler metal and covering if present.

[b]Hydrogen content in % by weight can be calculated by multiplying ml/100g by 0.00009: For example, 28 ml/100g equals 0.0025% by weight, or 25 ppm (parts per million by weight).

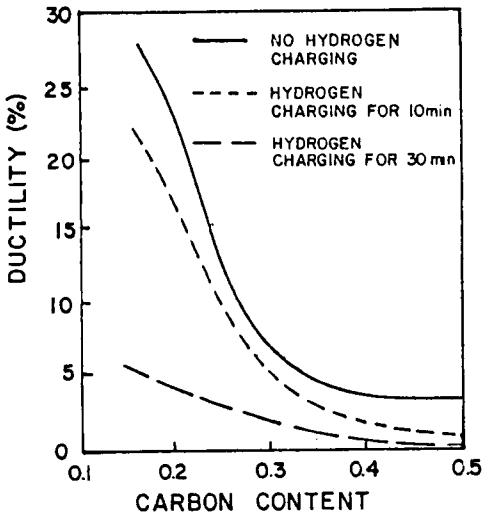
Source: Linnert, G.E., "Welding Metallurgy," Vol. 2, AWS (1967).

voluminous, and hence, the results of only one typical study will be discussed here. In this study by Mnuskin and Petrov,[32] steels of carbon contents varying from 0.16 to 0.50% were subjected to simulated weld thermal cycles having peak temperatures of 1330° - 1350°C (2425° - 2460°F). The specimens were then electrolytically charged with hydrogen for 2 - 3 days in 4% H_2SO_4 at a current density of $5A/dm^2$. The hydrogen charging time was varied to obtain varying hydrogen concentrations. The embrittling effect of hydrogen was assessed from the ratio of the tensile strength of the charged specimen (σ_B^h) to that of the uncharged specimen (σ_B) and from ductility measurements. These results are shown in Figures 12a and b. It can clearly be seen that an increase in hydrogen content resulting from an increase in charging time, reduces strength and ductility. Further, the deterioration in strength and ductility is more pronounced for the higher carbon steels.

A factor which is most important and which is extremely difficult to specify for a general welding situation is how much hydrogen will cause embrittlement that will lead to cracking. The difficulty arises from the fact that the quantitative determination of hydrogen content in iron or steel is a very difficult task, especially in localized areas like the weld metal or the heat affected zone. But one fact is confirmed, and that is, the greater amount of hydrogen, the greater will be the probability of embrittlement and the possibility of cracking. Mallett and Rieppel[33] found a direct correlation between the hydrogen content of the weld deposit and the extent of underbead cracking (Figure 13).



a) Effect of hydrogen-charging on the relative strength of steels in relation to carbon content.



b) The dependence of ductility on carbon content for steels charged with hydrogen for various periods of time.

Figure 12. Effect of hydrogen on the mechanical properties of steel.

Source: Mnushkin, O.S., and Petrov, V.P., "The Effect of Hydrogen on the Properties of the Heat Affected Zone in Low and Medium Alloy Steels," Welding Research Abroad, 25 (1), 20-22 (1979).

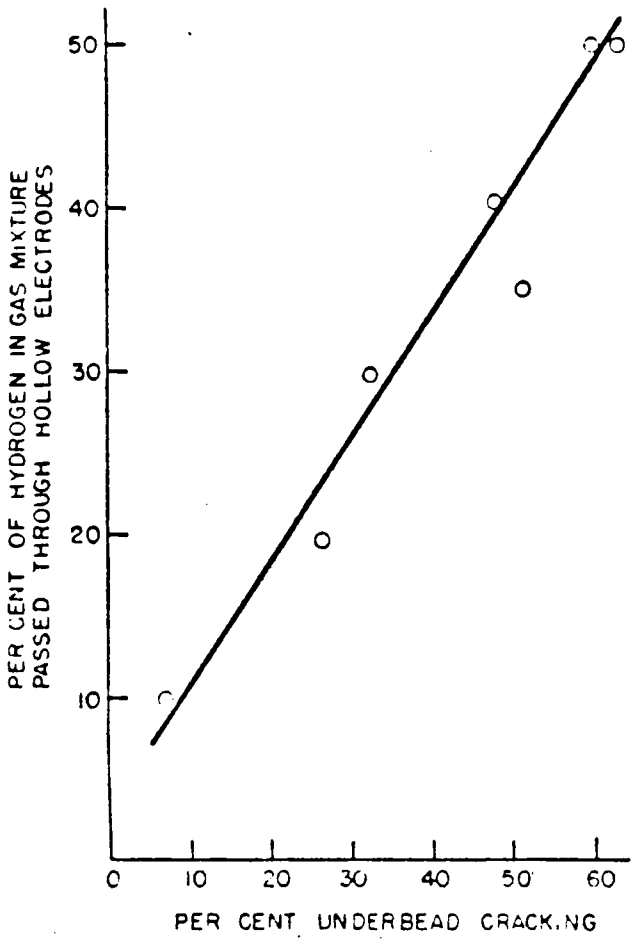


Figure 13. Hydrogen in synthetic arc atmosphere vs. underbead cracking.

Source: Mallett, M.W., and Rieppel, P.J., "Arc Atmospheres and Underbead Cracking," Welding J., 25 (1) 748s-759s (1946).

It is fairly well understood that HIC in the HAZ's of weldments is the result of hydrogen embrittlement. The necessity therefore now arises to examine the various theories of hydrogen embrittlement that have been advanced, and to analyze them with respect to the problem of HIC in weldments.

4. Theories of Hydrogen Embrittlement

The phenomenon of hydrogen embrittlement has been investigated for a considerable time span by researchers both in the basic and applied sciences. However, despite the enormous amount of work that has been done in this area in the past century, no single convincing theory has been put forward that can explain all the observations that accompany this phenomenon. Experimental observations have revealed that hydrogen embrittlement occurs under the following conditions:

1. Temperatures close to ambient;
2. Low strain rates (as in a tensile test) as opposed to high strain rates (as in an impact test).

These two observations immediately suggest that the diffusion of hydrogen may be an important contributing mechanism. The practical significance is that hydrogen can possibly be driven out (of a weldment) before it can cause any embrittlement. The current state of understanding was arrived at through numerous hypothesis and experimentations and hence an understanding of the early work is called for.

One of the earliest theories was proposed by Zappfe and Sims.[34] In this "planar pressure" theory, hydrogen is supposed to enter metals in the atomic form. In a typical welding situation, hydrogen picked up by the weld metal would have a high solubility in the liquid steel and as the temperature dropped, the solubility would decrease sharply, first at the freezing point and then at the austenite-ferrite transformation temperature, thus causing a saturation of hydrogen in the weldment. According to Zappfe, hydrogen would then diffuse into sites (in the weld metal and HAZ) such as voids or "rifts" in the matrix where the atomic hydrogen could combine to form molecular hydrogen. Zappfe proposed that this action partitions the gas into an atomic portion that is dissolved in the lattice, and a much greater remainder portion to be occluded physically under high stress as molecular or "quasi-molecular" hydrogen. The pockets of gas under high pressure in the "planar openings" within a grain are then supposed to immobilize surfaces to slip, causing embrittlement. However, Kazinczy[35] refuted the above theory based on the fact that the hardness is not increased by hydrogen as should have been the case if slip was restricted. Further, he argued that the yield point should be raised, which has not been seen in hydrogen embrittled specimens. The ultimate tensile strength is found to be decreased which consequently leads to a decrease in ductility. Kazinczy proposed that both shear strength and cleavage strength are lowered by hydrogen. As cracks (which are supposed to preexist in the material) grow,

the occluded gas expands and supplies part of the energy required for crack propagation, thus reducing the applied stress for fracture. Bastien and Azou[36] suggested that hydrogen tends to concentrate in zones of maximum free energy e.g. as Cottrell clouds around dislocations. The application of stress is supposed to cause these clouds to migrate and reach cavities created by plastic deformation where hydrogen is discharged into the cavities and then can give rise to a state of triaxial stress. This state reduces the ultimate tensile strength, causing embrittlement. Smialowski[37] in his review of hydrogen embrittlement theories concludes that the "pressure" theories do not explain experimental results. Specifically, he contends that the "precipitating" hydrogen is itself not embrittling and that embrittlement precedes the development of voids. Petch and Stables[38] also argued against the "pressure" theories, and suggested that hydrogen reduces the energy required to cause fracture by adsorption on the propagating crack surfaces and lowering the surface free energy. This theory implies that hydrogen has to diffuse from the lattice to a clean crack surface, thus explaining the temperature dependence of hydrogen embrittlement. However, as Kazinczy[35] points out, the adsorption theory does not explain why different hydrogen contents give rise to different values of cleavage strength. Troiano[39] postulated that a critical combination of stress state and hydrogen concentration must be attained to initiate a crack. An incubation period was initiated which was the time required for hydrogen to

accumulate, the driving force for hydrogen diffusion being the activity gradient resulting from a non-uniform stress state. Crack propagation was therefore implied to be discontinuous because sufficient hydrogen has to diffuse to the crack tip for crack propagation to occur, i.e., crack propagation was thought to be nothing but a series of crack initiations. Crack initiation was thought to occur at an area of local stress concentration where fracture embryos are created in the form of blocked dislocation arrays. The dependence of the diffusion of hydrogen on the stress state explains the dependence of embrittlement on the strain rate. Oriani[40] on calculating the maximum hydrogen attainable at yield stress levels, concluded that this concentration would be so low that the occurrence of embrittlement would not be able to be explained by any known mechanism. He, however, utilized Troaino's ideas together with Troaino's suggestion that hydrogen lowers the cohesive strength of the lattice, and proposed a model for a lattice decohesion theory of hydrogen embrittlement. In contrast to Troaino's ideas, the model postulates that crack propagation in a homogeneous material is intrinsically a continuous non-intermittent phenomenon caused by the penetration of hydrogen into an elastically stressed region and the consequent lowering of cohesive forces between atoms. Beachem[41] furnished a new model of hydrogen-assisted cracking (HAC) based on the hypothesis that hydrogen diffuses into the lattice just ahead of the crack tip and aids whatever deformation processes the matrix will allow. The type of

fracture is related to the stress intensity factor and concentration of hydrogen at the crack tip. The model differs from earlier theories in that instead of hindering the motion of dislocations, hydrogen is hypothesized to simply allow normal fracture to take place at unusually low microscopic strains. The existence of intergranular (IG), quasi-cleavage (QC) and microvoid coalescence (MVC) fracture features has been explained using the concentration of hydrogen at the crack tip and the stress intensity factor. The fracture features depicted by HAC observed in stress corrosion[41] as well as weldability tests[42] have been found to have good correlation with Beachem's theory of HAC.

In summary, theories which utilize the "diffusive" part of hydrogen in explaining characteristics of HIC, have gained more favor with researchers involved in investigating both the basic and applied mechanistics of this problem.

Since the diffusivity of hydrogen depends on temperature, preheating and post weld heat treating procedures can be used to diffuse hydrogen out of the weldment before it can cause any embrittlement. This forms the basis of two powerful techniques to prevent HIC, which are discussed in detail in the next section.

5. Preheating and Post Weld Heat Treatment

Temperature has a strong effect on hydrogen embrittlement. In ferritic steels embrittlement occurs only at low temperatures, close to the ambient. Hence, cracking can be avoided by maintaining the steel at a high temperature before and/or after welding.

The effects of preheating can be summarized[11] as follows: i) reduces cooling rate in the heat affected zone, ii) slows cooling and hence allows any martensite that has been formed to be "self" tempered, and iii) promotes the escape of hydrogen present in the HAZ after welding. Even preheats as low as 100°F can be very effective in preventing HIC. Postheating can further aid the diffusion of hydrogen out of the HAZ as well as temper any martensite that may be formed. This will further aid in reducing the stresses that are associated with the transformation. Preheat temperatures are generally specified based on the composition of the steel. A convenient way of doing this is by relating them to the carbon equivalent. A typical preheating schedule based on carbon equivalent is shown in Table 2. Welding Research Council Bulletin 191 lists preheat and post weld heat treatment required for an extensive range of wrought and cast steels. The requirements have been specified for both low hydrogen and non-low hydrogen procedures. The British Standard, BS4520: Part 2, "Fabrication Welding," also gives preheat and post treatment requirements, special considerations such as maintaining preheat between the finish of welding and stress relieving, etc. Preheat requirements can also be established if the maximum hardness that can be tolerated in the HAZ is decided upon. From the Jominy hardenability curve of the steel (which can be calculated from its composition), the cooling rate required to produce this maximum hardness can be found. Use then can be made of the tables generated by Hess et al.[43] which

Table 2. Preheat temperatures related to carbon equivalent.

Equivalent Carbon Content (C.E.)	Suggested Preheat Temperature
Up to 0.45%	Optional
0.45 to 0.60%	200 - 400°F
Above 0.60%	400 - 700°F

$$C.E. = \%C + \frac{\%Mn}{6} + \frac{\%Ni}{15} + \frac{\%Cr}{5} + \frac{\%Cu}{13} + \frac{\%Mo}{4}$$

Source: Linnert, G.E., "Welding Metallurgy," Vol. 2, AWS (1967).

provide cooling rate data as a function of plate thickness, heat inputs and preheat temperatures. If the plate thickness and heat input are known, preheat temperatures can be determined from the table which will result in a cooling rate in the HAZ slower than that are needed to obtain the specified maximum hardness. The postheat temperature and the time for which it is to be maintained will be a function[10] of the hydrogen concentration at the end of welding, the composition of the steel and the level of restraint. The higher the carbon content and the restraint, the higher will be the required preheat, interpass and post heat temperature. To evaluate post heating times, one needs to know some critical level of hydrogen below which cracking will not occur. Post heating durations will also vary[46] depending upon the thickness and shape of the joint. Critical concentrations of hydrogen have to be estimated which can be used to determine post heating times. Longer times are needed to diffuse out hydrogen as the plate thickness increases. A considerable amount of research has been done to evaluate post heating times needed to diffuse hydrogen out of the weldments. Results of Flanigan and Lee[44] (Figure 14) obtained from E 6010 welds on ASTM - A285C plate indicate that complete removal of hydrogen was achieved at 1200, 750 and 425°F. However, at 270° and 100°F the hydrogen content was found to stabilize itself at around 1cc/100g and this level of hydrogen was found to be maintained even in specimens which had been aged for up to ten years. This gives credence to the theory that at low temperatures

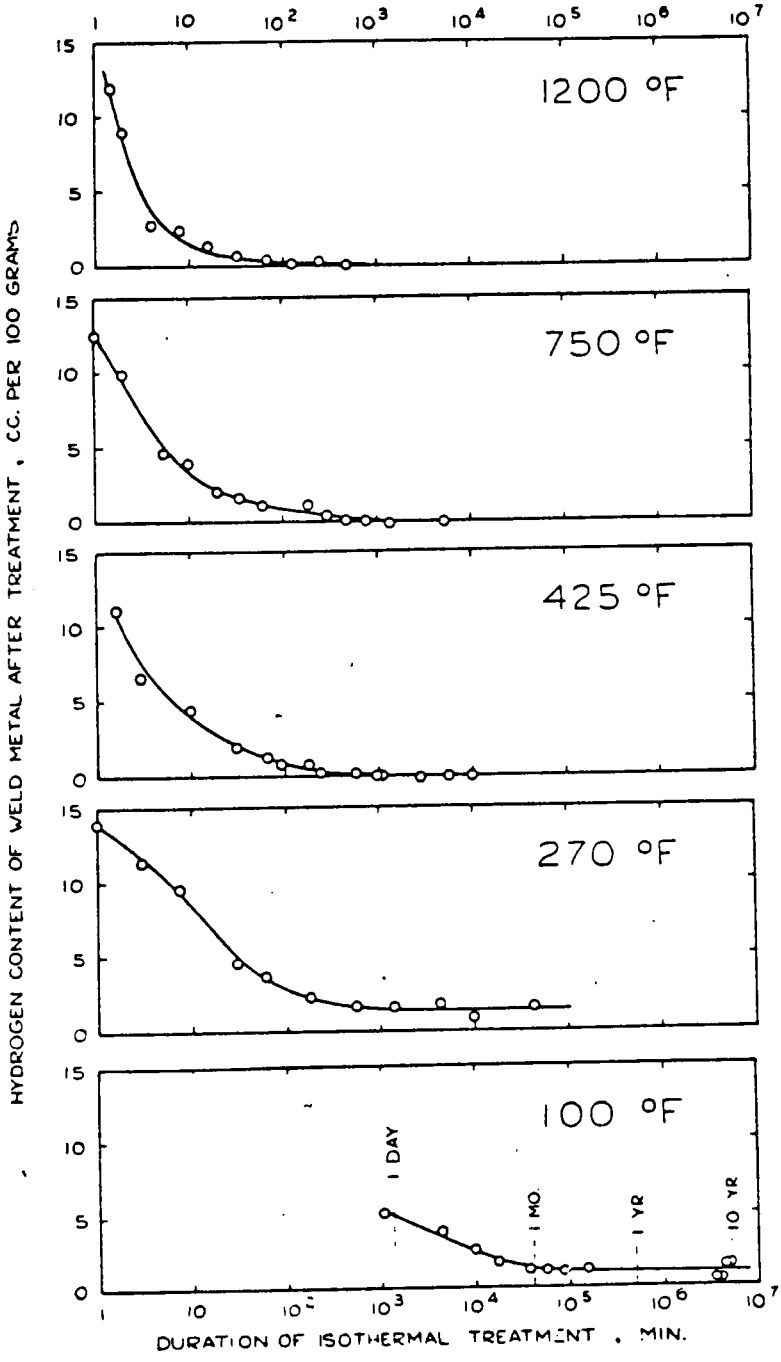


Figure 14. Dependence of hydrogen content on the duration and temperature of prior treatment.

Source: Flanigan, A.E., and Lee, E.U., "On the Escape of Dissolved Hydrogen from Weld Metal," Welding J., 45 (10), 477s-480s (1966).

there exists a hydrogen fraction which is trapped and therefore non-diffusible. Graville[45] found that the notch tensile strength of H_2 charged specimens tested at temperatures ranging from 23°C (74°F) to 158°C (316°F) coincided at a hydrogen level of 0.5cc/100g. The existence of a "trapped" fraction of hydrogen will be further taken up in detail in the next section.

6. Effect of Sulfur and Inclusions

The effect of inclusion morphology, type and distribution has largely been neglected in cold cracking evaluation studies. The elongated non-metallics in wrought steel impart directional properties to the section. Cast steels on the other hand, are not worked and hence, the inclusions are not elongated. This makes the cast steels less anisotropic. In this regard, the effect of manganese sulfide inclusions on hydrogen embrittlement, and hence HIC becomes an important factor to be considered.

Smith and Bagnall[47] found forged header materials with low sulfur contents (<0.01%) to be susceptible to hydrogen-induced cold cracking. At the same point in time, Hewitt and Murray[23] also reported a high susceptibility to cracking for a low sulfur forged steel and an extensive study of 120 lots indicated to them that an increase of 0.010% sulfur decreased cracking by 15%. They attributed the increased cracking susceptibility of low sulfur steels to the fewer number of MnS inclusions (and the voids associated with them) which act as hydrogen sinks. Evans et al.[48] however, report that in implant tests conducted on steels with

sulfur compositions ranging from 0.005 to 0.033%, the cold cracking susceptibility was more related to the orientation of the implant specimens; in the longitudinal direction susceptibility decreased as sulfur content increased, whereas in short transverse direction susceptibility increased as sulfur content increased. In contrast, Hart and Brooks[49] report that in their longitudinal implant specimens, low sulfur steels were found to be more susceptible to HIC than steels with higher sulfur content. This, they attributed to the increased hardenability resulting from an effective increase in Mn content, since less of it is tied up as MnS. Gondoh et al.[50] however, found that sulfur contents in the range of 0.002 to 0.01% did not influence their CTS test results. Hirai et al.[51] using y-groove restraint tests report that higher preheat temperatures were required to prevent cracking in low sulfur steels when compared to those required in steels of higher sulfur contents. It is therefore clear that a marked difference of opinion exists in the manner in which sulfur affects the HIC susceptibility of steels. The effect of inclusions per se' has not been definitively determined.

The methodology adopted in this review was to understand how the presence of sulfur and inclusions influence the factors responsible for hydrogen induced cracking, these factors being: i) hydrogen content and diffusivity, ii) hardenability and toughness of the HAZ and iii) influence as stress raisers (crack initiators) in the HAZ.

Hydrogen diffusion. The diffusivity of hydrogen in steel is influenced by factors such as the composition, temperature and the thermal history of the steel. Sykes et al.[52] using solubility and permeability data derived the diffusivity in ferrite,

$$D_\alpha = 7.6 \times 10^{-4} \, e^{-1150/T} \ cm^2/sec. \quad (1)$$

whereas the diffusivity in austenite,

$$D_\gamma = 1.5 \times 10^{-2} \, e^{-6000/T} \ cm^2/sec. \quad (2)$$

This shows that the diffusivity in ferrite is higher than in austenite. However, as HIC is usually encountered at temperatures close to room temperature, the diffusivity in ferrite, D_α, is of greater consequence. The diffusivity of hydrogen in ferrite as predicted by equation (1) together with diffusivities actually measured in a host of ferritic materials is shown in Figure 15 (from Reference 9). It is clear that at temperatures above 300°C, diffusion follows classical diffusion laws. However, at lower temperatures the measured diffusivities are lower than those predicted by the Sykes et al. equation. This phenomenon has been attributed to the presence of 'traps' in steels. The physical nature of the traps has not been clearly defined. According to Coe and Moreton,[53] traps exert their most potent effect at temperatures below 80°C. Trapping can occur[53] at crystal imperfections, lattice vacancies, dislocations, microvoids associated with non-metallic inclusions, microcracks, etc. Hence, the diffusivity measured at temperatures below 300°C is not strictly the interstitial lattice

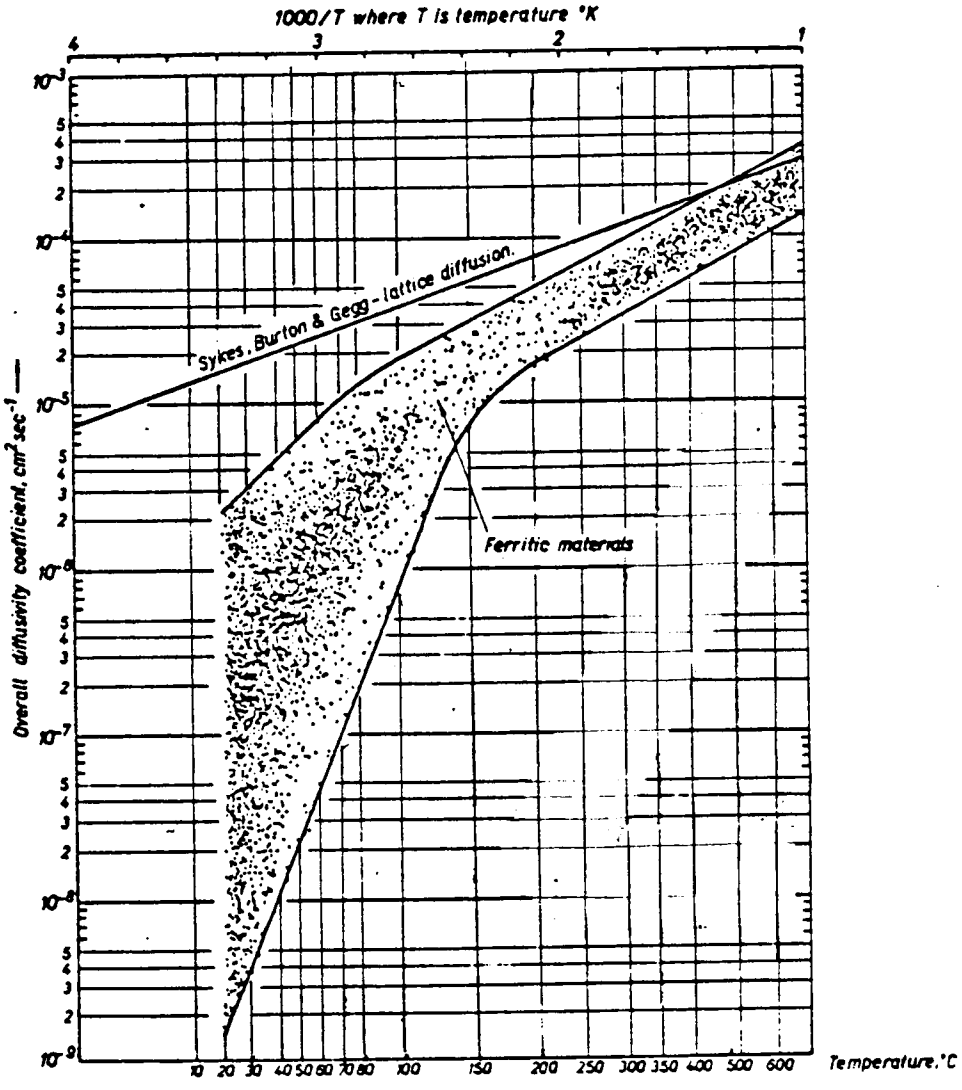


Figure 15. Diffusivity of hydrogen in ferritic materials as a function of temperature.

Source: Coe, F.R., "The Avoidance of Hydrogen Cracking in Welding," The Welding Institute (1973).

diffusivity, but is that which is modified by the presence of these traps. Coe and Moreton[53] therefore classify this as the "overall" or "apparent" diffusivity i.e., the diffusivity modified by the existence of traps. Having established the significance of traps, it now becomes essential to find out how the sulfur and the inclusion content can influence the apparent diffusivity (D_{app}) of hydrogen and consequently affect the hydrogen induced cracking susceptibility of a steel.

Here again, a wide variety of results and opinions are available from different investigators. Bonizewski and Moreton[54] conducted extensive studies on the influence of MnS inclusions on D_{app} and came to the conclusion that inclusions retard hydrogen evolution but do not retain the hydrogen permanently. Diffusivities in a free cutting steel with sulfur contents of 0.25% were found to be about an order of magnitude lower than in a steel with a sulfur content of 0.018%. They concluded that MnS inclusions have a mitigating effect on the hydrogen embrittlement of steel when the inclusions are stringer-like and when the inclusion-metal interface is undamaged by hot working. However, micro-voids associated with MnS inclusions were thought to act as sites for hydrogen accumulation which could lead to subsequent hydrogen adsorption and lattice decohesion. That microvoids could result at MnS inclusions during thermal treatment, was demonstrated by Brooksbank and Andrews[55] who experimentally determined the coefficient of thermal expansion (ρ) for a number of inclusions. Using an ρ value

of 14.79×10^{-6}/°C for ferritic steels and an experimentally determined value of ρ_{MnS} of 18.1×10^{-6}/°C they showed that a substantial volume of voids (10 to 20% of the total void volume in 0.01%S steels) can be created due to differential thermal contraction. As the sulfur content decreases, the total volume of such voids created will decrease and for a given volume of hydrogen, the internal pressures built up in the existing voids will increase. Hewitt and Murray[23] utilized this argument to explain the higher cracking susceptibilities encountered in their low sulfur steels. A relation between pressure and hydrogen content as affected by the sulfur content is shown in Figure 16. Evans and Rollason[56] agree with Bonizewski and Moreton's contention that non-metallic inclusions of the oxide and sulfide type do not have any affinity for hydrogen, but serve as sites for the introduction of microvoids. These microvoids retard the evolution rate of hydrogen but do not fix the gas permanently. In a related paper,[57] they report that the apparent diffusivity of hydrogen in a free cutting steel (S=0.26%) decreased after cold rolling; however, after swaging the diffusivity increased indicating the effect of the production and elimination of microvoids depending on the process (cold rolling or swaging) used. These results are shown in Figure 17. They refute Hewitt and Murray's theory of microvoid formation based on thermal contraction and attribute the overall microvoid volume to the presence of gas and shrinkage pores and microcracks at inclusions/matrix interfaces. A relation between apparent diffusivity and void volume

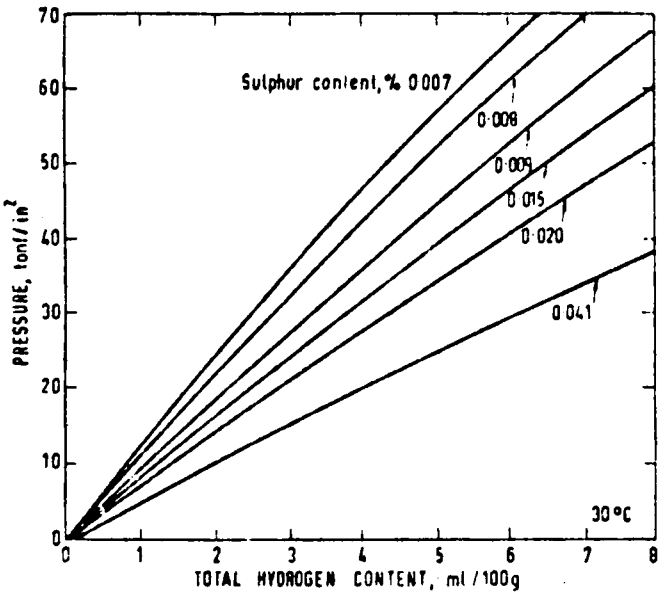


Figure 16. Relation between pressure and hydrogen content.

Source: Hewitt, J., and Murray, J.D., "Effect of Sulphur on the Production and Fabrication of Carbon-Manganese Steel Forgings," Metal Construction and British Welding J., Feb., 24-31 (1969).

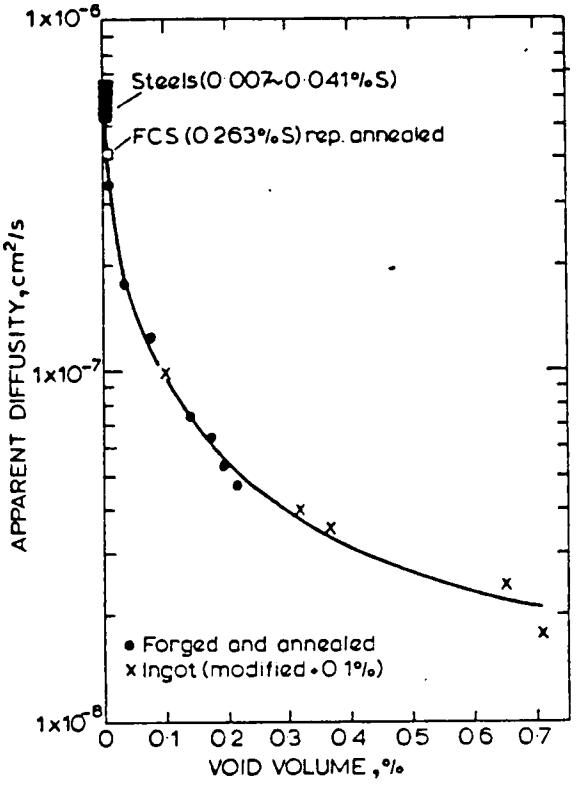


Figure 17. Effect of cold reduction on the apparent diffusivity of hydrogen.

Source: Evans, G.M., and Rollason, E.C., "Influence of Microvoids on the Apparent Diffusion of Hydrogen," J. of the Iron and Steel Inst., Dec., 1591-1598 (1969).

obtained by them is shown in Figure 18. Chew and Fabling[58] studied the diffusivity of hydrogen in 2 1/4Cr-1Mo steels of sulfur contents varying from 0.01 to 0.02%. Their results showed that sulfur contents alone could not be correlated to hydrogen diffusivity in these steels. They also recommend that the void volume be related to the entire thermo-mechanical history of the material. On a similar note, Evans et al.[48] found insignificant differences in the diffusivity of hydrogen in rolled C-Mn steels of sulfur contents varying from 0.005% to 0.033%. Figure 19 shows their results as apparent diffusivity vs. sulfur content. The lowest diffusivity was found in the steel having a sulfur content of 0.018%. Hart and Brooks[49] also found no significant differences in diffusivity of hydrogen in Al treated and non-Al treated low and high sulfur steels. They concluded that the total inclusion content governs the apparent diffusivity. Hirai et al.[51] found in hydrogen permeation experiments that the apparent diffusivity of hydrogen in carbon manganese steels depends upon the sulfur and total inclusion content. Non-metallic inclusions such as sulfides and aluminates are regarded to act as trap sites for hydrogen. Thus with increasing inclusion content, the apparent diffusivity was found to be reduced. Hirai et al. found the presence of intergranular root cracks in the low sulfur steels. It was hypothesized that the lowered inclusion content in these steels may have caused the hydrogen concentration to build up at the coarsened heat affected zone grain boundaries, causing embrittlement and cracking.

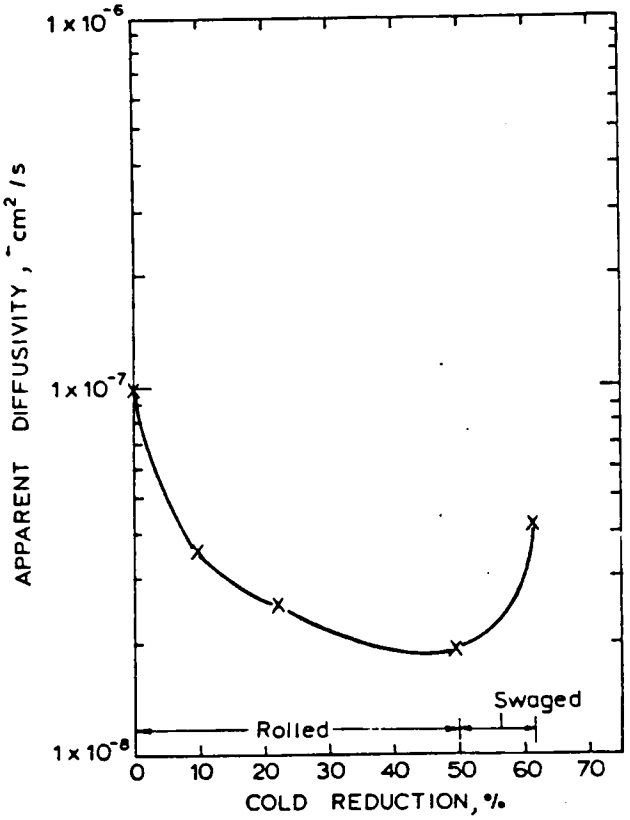


Figure 18. Apparent diffusivity at 23°C against true void volume.

Source: Evans, G.M., and Rollason, E.C., "Influence of Microvoids on the Apparent Diffusion of Hydrogen," J. of the Iron and Steel Inst., Dec., 1591-1598 (1969).

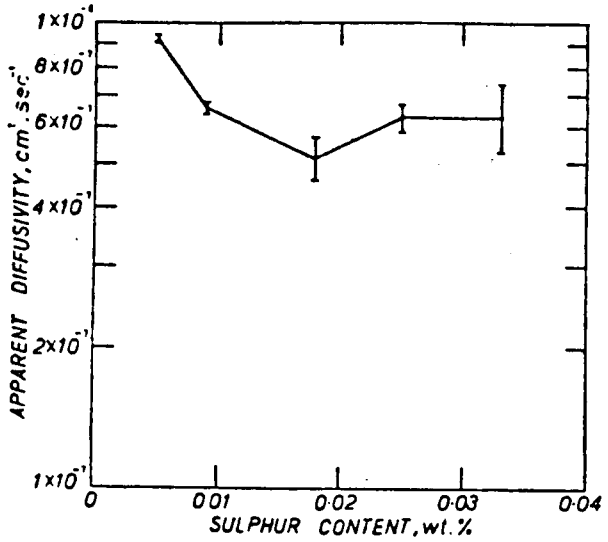


Figure 19. Apparent diffusivity of hydrogen vs. sulfur content.

Source: Evans, G.M., Wintermark, C., and Christensen, N., "Effect of Sulfur on the Weldability of Rolled C-Mn Steels," Scand. J. of Metallurgy, Vol. 2, 228-232 (1973).

Therefore, the results presented in literature indicate that the diffusivity of hydrogen is not affected in any consistent manner by the sulfur content. Correlations could perhaps be drawn in regard to the total inclusion content and the total void volume of the steel. In such a case, the apparent diffusivity has generally been found to be reduced with increasing inclusion content and void volume, both of which act as traps for hydrogen at temperatures below 800°C.

HAZ transformation behavior. The susceptibility of any HAZ to hydrogen induced cracking depends in addition to the presence of H_2 and stresses, on the transformation products that result from the weld thermal cycle. Hard transformation products such as internally twinned martensite have the greatest susceptibility whereas softer microstructures such as low carbon martensite, which possess good toughness, are less susceptible. Very little work has been reported regarding the effect of sulfur and inclusions on the toughness of the heat affected zone. However, some information is available about their affects on weld metals, from which certain conclusions can be drawn. Steel[59] using charpy and COD testing found that sulfur decreased the upper shelf toughness and increased the transition temperature of mild steel weld metal. Further, the best toughness properties were associated with fine acicular structures in the as-deposited condition. The volume fraction of inclusions was found to increase with increasing sulfur in the weld metal and Steel found this to be the best parameter to relate to

weld metal properties. Abson et al.[60] report that the nucleation of ferrite in weld metals is influenced to a considerable extent by inclusions. A decrease in oxygen content to 0.011% virtually eliminated the nucleation of acicular ferrite and produced a predominantly bainitic structure. They concluded that inclusion type and size distribution was substantially more important than the total inclusion volume fraction in influencing ferrite nucleation. Hart and Brooks[49] report similar phenomena in the HAZ of C-Mn steels. They found that a higher proportion of upper temperature transformation products (pro-eutectoid ferrite, upper bainite) in the HAZ's of high sulfur steels than in those of low sulfur steels. These products were found in association with MnS and Mn-silicate inclusions. They attributed the lower hardenability of the high sulfur steels to the fact that a high sulfur content would lead to a higher proportion of MnS inclusions which in turn would increase the proportion of the softer high temperature transformation products in the HAZ. Hart and Brooks[49] therefore recommend that the total inclusion count is more appropriate in correlating with the HAZ hardenability and hence the susceptibility to hydrogen-induced cold cracking. However they found that cracking at a HAZ hardness below 375 HV was due to microvoid coalescence and this observation explained the increased susceptibility of the high sulfur steels at low HAZ hardness levels (less than 375 HV). Gondoh and Nakasagi,[50] however, report that the HAZ toughness decreased as the sulfur content increased from 0.002 to 0.01% in their pipe steels. Their results are shown in

Figure 20. Hirai et al.[51] concluded that sulfur and inclusion contents have little or no effect on HAZ hardenability. They inferred that Hart and Brooks' results differed from their results because of the difference in inclusion sizes involved. Hart and Brooks used laboratory scale ingots which gave rise to smaller inclusions whereas Hirai et al. used production scale ingots which had larger inclusions. Hirai et al. contend that it is the extra fine inclusions less than 1 μm in diameter, that play an important role in the austenite to ferrite transformation.

Evans et al.[48] report a direct increase in the amount of martensite in the simulated coarse grained heat affected zone of a 0.005% S steel compared to that of a 0.033% S steel. This observation is consistent with the fact that sulfur has a negative contribution to hardenability. However, the increased fraction of martensite in 0.005% S steels did not cause it to be more susceptible to cold cracking than the higher sulfur steels. The overall susceptibility was thought to be controlled by numerous other factors such as microvoids, microstructure, and banding in the steel.

In summary, the effect of sulfur and inclusions on the transformation characteristics of heat affected zones in carbon-manganese steels has not been resolved in any definitive manner. The limited information available indicates that softer transformation products may result from fine inclusions, and that HAZ toughness decreases as the sulfur content increases. No consistent trends of behavior can be surmised.

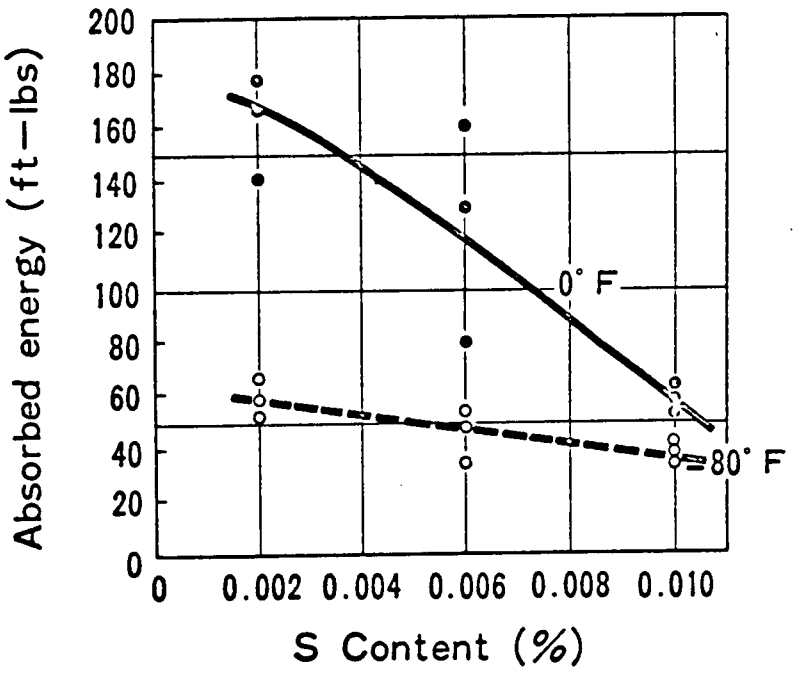


Figure 20. Relation between sulfur content and absorbed energy of heat affected zone.

Source: Gondoh, H., and Nakasagi, H., "Welding of Extremely Low Sulfur Steels for Large Diameter Pipe," Nippon Steel Corporation Report.

Stress raisers (crack initiation). The roll of elongated sulfide inclusions as crack initiators has been reported by Baillie[61] during his investigation of cold cracks in the HAZ. Savage et al.[62] also report cracks in the HAZ of HY-80 weldments to be nucleated at elongated sulfide inclusions. Evans et al.[48] make use of a similar argument to explain the greater susceptibility of their steels implant tested in the short transverse direction. The fracture surface of these specimens were observed to become more step-like with increasing sulfur level exhibiting a woody fracture type normally associated with lamellar tearing. However, if elongated MnS inclusions alone indeed contributed to increased susceptibility, then low sulfur steels should have proven to be less susceptible to cracking. This has not been found true by several researchers.

In conclusion, it may be stated that the effect of sulfur and inclusions on cold cracking susceptibility remains an enigma[63] and that extensive tests taking into account the overall factors responsible for such cracking will have to be conducted to gain further understanding into this interesting but perplexing problem.

7. Effect of Aluminum on HIC

Since deoxidation of cast steels usually involves the use of aluminum, it is relevant to consider the role of aluminum in HIC. As for other sections of this review, the literature data available is for wrought steels. Sims and Banta[64] were the earliest to report the influence of aluminum on the HIC susceptibility of steels. Their results shown in Figure 21 indicate that aluminum

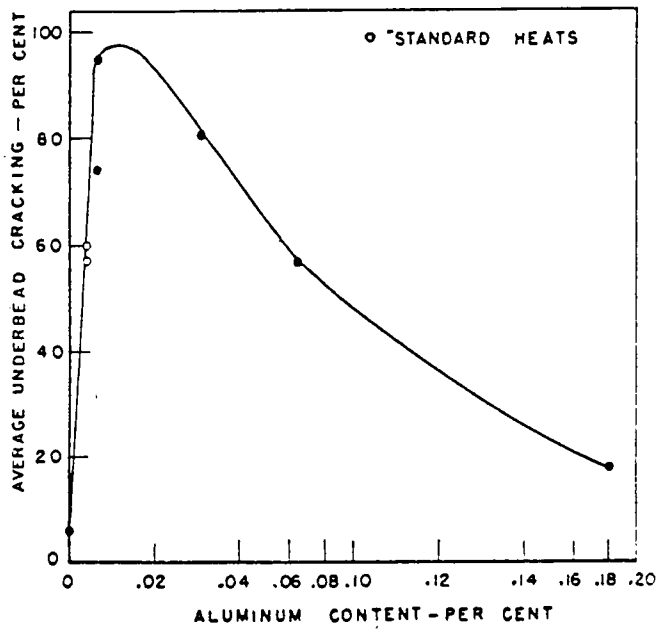


Figure 21. The effect of aluminum content upon underbead weld cracking sensitivity.

Source: Sims, C.E., and Banta, H.M., "Development of Weldable High Strength Steels," Welding J., 28 (4), 178s-192s (1949).

contents up to 0.01% increase HIC susceptibility, and for higher aluminum contents cracking susceptibility decreased. Sims and Banta therefore recommended that aluminum should either be omitted or added in large amounts to minimize HIC. Confirmatory tests conducted by them[64] showed that steels with aluminum contents of 0.005% were considerably more susceptible than equivalent steels without any aluminum. No reasons for this behavior were given. In contrast to the above results, Campbell[65] reported that no consistent effect of aluminum on HIC could be deciphered in his steels. Campbell attributed the differences between his results and those of Sims and Banta[64] to the differences in experimental procedures (type of electrode, method of preheat, etc.) adopted by them. Campbell concluded that there was no justification in limiting aluminum for deoxidation purposes. On the other hand Hasebe[66] found a similar trend in results as those of Sims and Banta, with cracking susceptibilities increasing with acid soluble aluminum contents up to 0.01% and then dropping rapidly as acid soluble aluminum contents approached 0.10%. In addition, Hasebe also observed that for identical aluminum contents, higher nitrogen contents reduced the cracking susceptibility. No explanations for this behavior were given. A possible reason could be the presence of sufficient AlN to enable the nucleation of upper temperature transformation products (pro-eutectoid ferrite, upper bainite), which are known to be less susceptible to HIC.

The beneficial effect of nitrides has been utilized by Japanese steelmakers[67] to substantially improve the impact

properties of HAZ's, created especially during high heat input welding. Their technique capitalizes on the high affinity of aluminum for nitrogen and the fact that reduced levels of free nitrogen improves the impact toughness of steel. The acid soluble aluminum level is kept high (0.04 to 0.07%) and their results (Figure 22) show that lower transition temperatures were obtained in synthetically created HAZ's with increasing acid soluble aluminum contents. Use of titanium was also reported to achieve similar results; however, titanium in excess of 0.01% is not recommended since the formation of TiC leads to deterioration in toughness. A Ship Structure Committee report[68] which includes a comprehensive literature review of nitrogen and aluminum effects, indicates that grain coarsening is prevented to a considerable extent with the presence of aluminum nitrides and nitrides and carbides of colombium, vanadium and titanium. Literature references quoted therein indicate that grain coarsening can be prevented up to a temperature of 1830 to 1920°F with AlN, columbium carbo-nitride and vanadium nitride; however, with TiN resistance to grain coarsening up to about 2190 to 2370°F can be obtained. Some other positive contributions of aluminum are reported[69] to minimize strain aging embrittlement in the sub-critical HAZ. Aluminum aids in more complete deoxidation of the steel and provides for a higher recovery of reactive elements such as Ti, Ca and REM which can then perform their allotted functions.

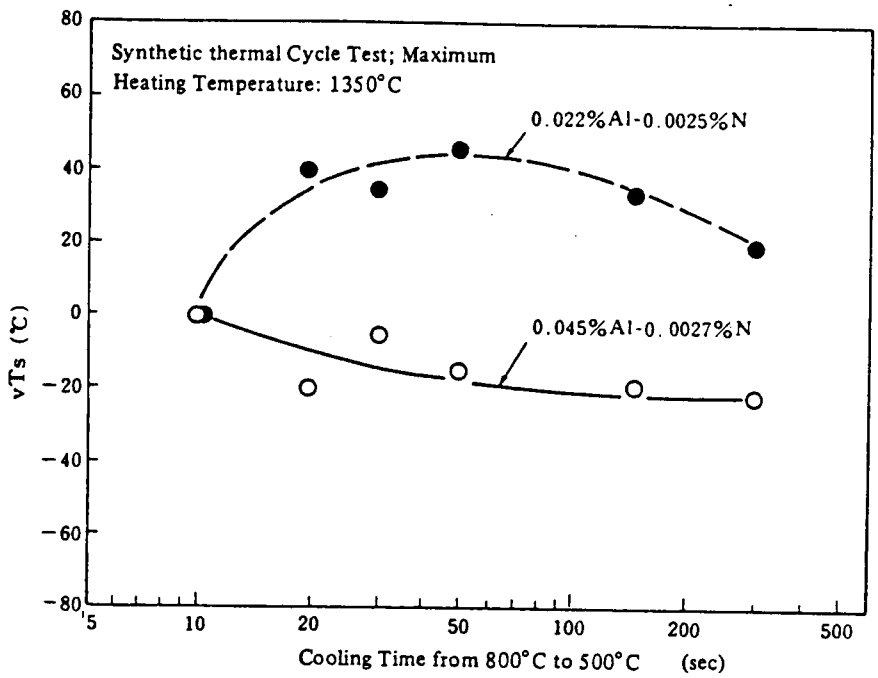


Figure 22. Effect of aluminum on the HAZ transition temperature.

Source: NKK Technical Report," Newly Developed Steel Suitable for High Heat Input Welding--"NK-HIWEL"."

In summary, aluminum has been regarded as a positive factor as far as the influence on base metal as well as HAZ toughness is concerned. The beneficial effects of aluminum are presumably due to the role of AlN in restricting in grain coarsening and aiding the nucleation of high temperature transformation products.

8. Weldability of Cast Steels

The use of welding in foundries came about slowly through a long period of transition from fully cast components to cast-cast and cast-wrought components. Therefore, the literature available on the weldability of cast steels is meager. The review has been focused mainly on those situations where the weldability of a cast steel could be compared to that of an equivalent wrought steel for which welding procedures have already been established. The review has been confined to the weldability of cast C-Mn-Si steels and low alloy steels with regard mainly to their susceptibility to heat affected zone HIC.

An early study of welded structures in cast and wrought steels was performed by Bolton and Smith.[70] They grouped the cast and wrought steels tested according to their relative tendencies for martensite formation. Use of preheat prior to welding was found to give rise to coarser grains in the heat affected zone of all the steels. However, an interesting conclusion they drew from their limited tests was that their wrought steels were more susceptible to grain coarsening than their cast ones; the addition of molybdenum was found to reduce this tendency. The weldability of the steels

was evaluated based on this grain coarsening tendency from which it was concluded that cast carbon steel with carbon contents up to 0.24% could be safely welded without any preheat. Preheating at temperatures greater than 600°F was not recommended because excessive grain growth could occur. The minimum preheat temperatures needed to avoid formation of hard structures (martensite) in the HAZ were evaluated, although no hardness values were given. Smith and Bolton[71] concluded that fears regarding the weldability of aluminum deoxidized cast steels were unwarranted, and that these steels showed as good, and in many cases better weldability than comparable wrought steels, the "weldability" being related to the tendency to form martensite in the HAZ.

Mueller et al.[72] reported that for satisfactory welding of plain carbon steel castings having a maximum carbon content of 0.35% associated with 0.60 manganese, no preheat need be used. However, they specified a subsequent stress relief or full anneal. Preheat was specified for the welding of a Mn-Mo cast steel having a carbon content of 0.35 to 0.40% associated with 1.25 to 1.50% manganese and 0.20% molybdenum. To completely prevent cracking in the Mn-Mo steels a preheat ranging from 300 to 600°F together with a post weld heat treatment (PWHT) at 1200°F was specified. Hardness surveys across the welds in the Mn-Mo cast steels are shown in Figure 23. In the figure, electrodes "73" and "100" are heavy mineral coated types yielding weld metal strengths of 76 and 100 Ksi respectively. In the figure shown, the maximum hardness in the HAZ is seen to drop from 300 to 200 HB, as preheat and stress

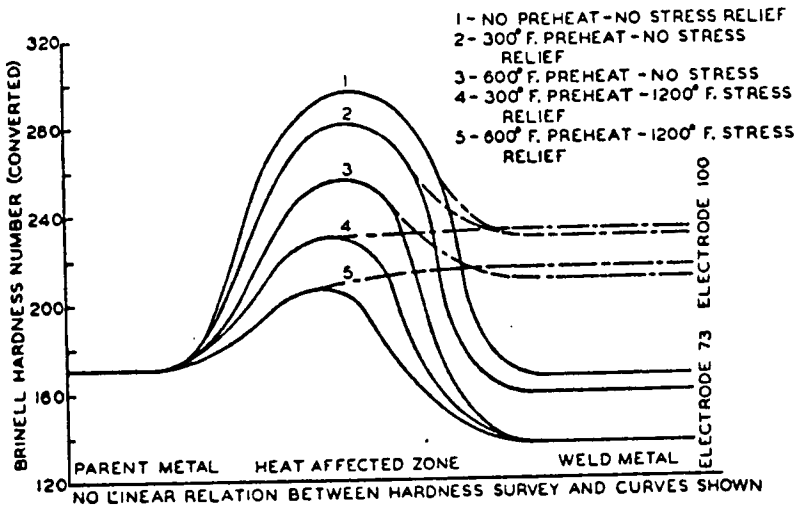


Figure 23. Comparative hardness surveys showing the effect of preheat and stress relief on welds in manganese-molybdenum castings.

Source: Mueller, S.E., Smith, A.B., and Oersterle, J.F., "Welding of Medium Carbon Steel Castings by the Metal Arc Process," Trans. AFS, Vol. 50, 995-1031 (1942).

relief are used. The lowest hardness was obtained with a preheat of 600°F and a 1200°F stress relief. In Figure 24 the maximum hardness in the HAZ for a single pass and a multipass weld is shown as a function of preheat temperature. The multipass weld as opposed to the single pass weld has a beneficial effect in that it partially refines and tempers preceding passes. Hence, preheats were seen not to have any major effect on the maximum hardness during multipass welding. Mueller et al. also concluded that casting stresses and segregation have no detrimental effects on weldability. It is interesting to note that no mention of hydrogen was made in connection with the cracking observed.

Williams et al.[1] at Battelle conducted an extensive weldability study of cast and wrought carbon-manganese steels. In the underbead cracking test, they observed that the cast steels were less susceptible to HIC than the rolled steels of similar composition. Typical underbead cracking test results are shown in Figure 25. From the results of their tests, which plots average underbead cracking versus carbon equivalent as given by $\%C + \frac{\%Mn + \%Si}{4}$, it is clear that the cast steels (2x, 3x, 4x) were less susceptible to cracking than wrought steels of similar carbon equivalent. This observation was made at all preheat temperatures used. The reasons for this behavior were not explained. Furthermore, cast steels unexpectedly exhibited a higher underbead hardness and a lower bend angle than wrought steels of the same carbon equivalent, thus illustrating the danger of using hardness alone

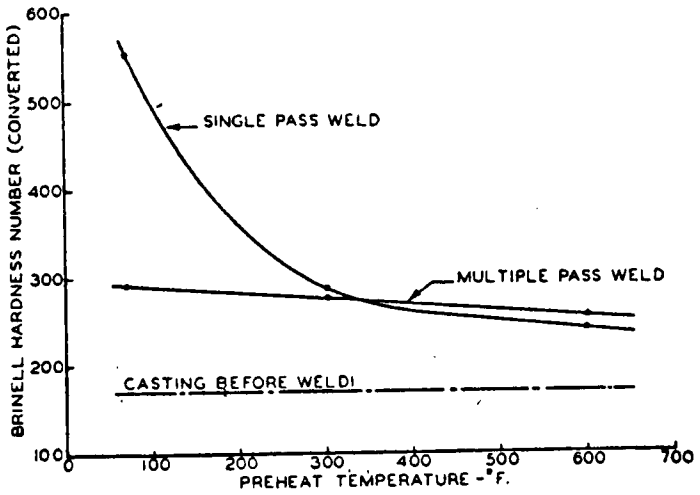


Figure 24. Effect of preheat on the maximum hardness obtained in the heat-affected zone of manganese-molybdenum steel castings.

Source: Mueller, S.E., Smith, A.B., and Oersterle, J.F., "Welding of Medium Carbon Steel Castings by the Metal Arc Process," Trans. AFS, Vol. 50, 995-1031 (1942).

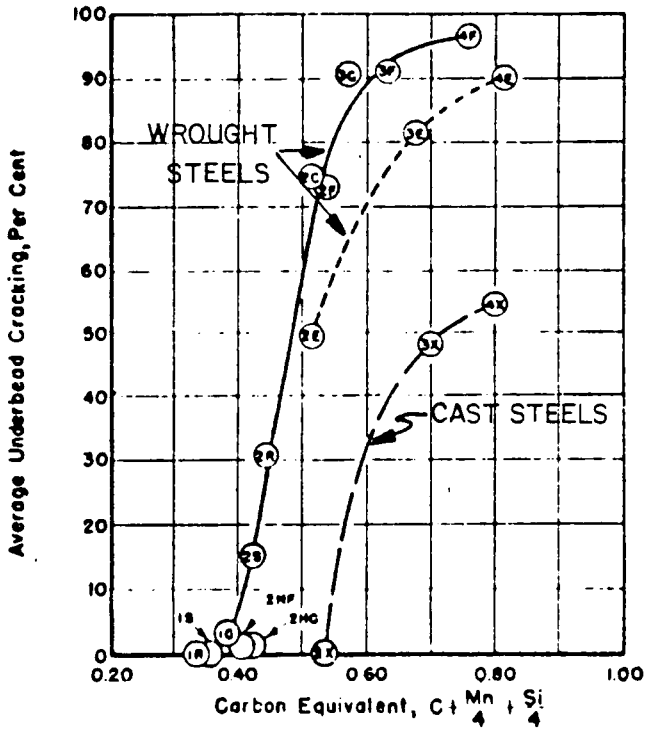


Figure 25. Underbead cracking vs. carbon equivalent (room temperature).

Source: Williams, R.D., Roach, D.B., Martin, D.C., and Voldrich, C.B., "The Weldability of Carbon-Manganese Steels," Welding J., 28 (7), 311s-325s (1949).

to predict crack sensitivity. The results of Williams et al. were not explained using any microstructural evidence.

The beneficial effects of preheat and postheat treatments were utilized by Bland et al.[73] in welding 2%Cr-1/2Mo alloy Steel (ASTM-A157, Grade C-3A) in the shape of a tee fitting, for use with 5 in Schedule 160 piping (ASTM-A-355, Grade P36). The welding was done by using 2 1/4Cr-1Mo low hydrogen electrodes. Residual stress measurements showed that preheat was effective in reducing residual stresses in the weld deposit. Another interesting result obtained by them was that the heat affected zone hardnesses of the cast alloy materials were higher than those of similar (nominal) analysis of wrought pipe materials. This agrees with the observations made by Williams et al.[1] However, hardnesses in wrought or cast base metals were relatively unaffected by a 300°F preheat. This is because that preheat level probably had a small effect upon the cooling rate.

Chapin et al.[74] have described fabrication and repair welding of large alloy steel castings for use in steam turbines. To select preheat temperatures for welding 1Cr-1Mo-1/4V cast material, they made use of the impact energy curves given in Figure 26. The minimum preheat chosen was 450°F, which corresponds to impact energies in the upper shelf region for this steel. This was done because Chapin et al. state that repair welds in large sections can have high triaxial residual stresses. However, they seemed to have overlooked one aspect, and that is that the HAZ will

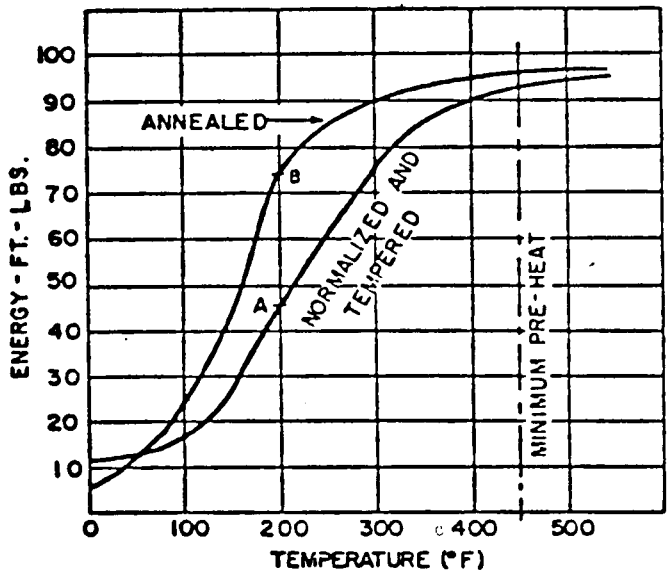


Figure 26. Typical impact transition curves for 1Cr-1Mo-1V cast material.

Source: Chapin, N.A., Soldan, C.H., and Songer, L.W., "Welding Low Alloy Steels for High Pressure and High Temperature," Welding J., 37 (10), 979-987 (1958).

possess a structure which will be considerably coarser than that of the base metal. The coarse grained region of the HAZ will possess a lower notch toughness, and hence preheat temperatures based on this toughness would be higher. Chapin et al. also report the use of intermediate subcritical stress relief to minimize high residual stresses in hard affected zones.

Ridal[75] has given results of extensive tests carried out on a plain carbon cast steel (B.S.592Gr A - C-0.2%, Si-0,33%, Mn-0.73%) and a 1 1/2 Ni-Cr-Mo steel (B.S. 1459). Though the results are mainly concerned with the mechanical properties of the welds, some useful information regarding the preheats required to weld these steels is also given. The recommended procedure for welding BS 592 GrA given by the B.S.C.R.A. specifies no preheat but a post weld heat treatment (PWHT) at 600 - 650°C (1100 - 1200°F) and with a note that this PWHT is not always essential. For B.S. 1459 a minimum preheat of 200°C (392°F) is recommended; also PWHT is specified. For certain hardened and tempered castings, the PWHT temperature is suggested to be kept low to maintain specific tensile strengths. However, Ridal informs that even without using the recommended minimum preheat temperature of 200°C (392°F) for B.S. 1459, underbead cracking was not observed in his tests. He cautions that as restraint was absent in his test, the results do not represent actual conditions. In any case, the situation where a preheat of 200°C (392°F) is recommended, although the absence of preheat in testing resulted in no cracking, indicates that welding specifications for castings are probably conservative.

Ridal has also given the precautions used for welding steam chests. The casting is made from a 1%Cr-1/4% V type of steel. The casting is stress relieved at 400°C (750°F) and the feeder heads are removed while they are hot. A full annealing treatment is then given at 1000 - 1025°C (1830 - 1880°F), subsequent to which fettling and ultrasonic testing is carried out. Preheating is carried out at 250°C (480°F) and care is taken to see that the casting temperature does not fall below this temperature. Welding is then carried out. Grinding, crack detection and final heat treatment then follow. Finally, radiographic and ultrasonic inspection are carried out to evaluate the quality of the weld.

Hipkins[76] has stressed that some form of post weld heat treatment should be given to all steel castings on which welding has been carried out. He reports the use of a 50°C - 150°C (110 - 300°F) preheat during the welding of BS592 Grade A cast steel. Stress relief was carried out at 600 - 650°C (1100 - 1200°F) for 1 hour per inch of thickness. Thus, even though the B.S.C.R.A. codes do not require a preheat or post heat schedule for this steel, cast weldment fabricators have preferred to remain conservative and use all the precautions that may be available to them. Bower[77] has given weldability test results of cast steels used in the fabrication of dragline and dipper buckets. The designations and compositions of these steels are given in Table 3. The 12M alloy (C-0.31, Mn-1.41, Mo-0.31) when evaluated with the controlled thermal severity (C.T.S.) test was found to exhibit underbead

Table 3. Composition of cast steels used in the fabrication of dragline and dipper buckets.

Material	C%	Si%	Mn%	Mo%	Ni%
Alloy 12 M	0.30	0.5	1.4	0.3	- + small amounts of V and B
Austenitic Mn	1.2	0.75	12.5	-	-
Austenitic Mn-Ni	0.75	0.75	12.5	-	3.5

Source: Bower, C.W., "Fabrication of Dragline Buckets for Earth Moving Equipment," Proceedings SCRATA, Paper 3:1-3:19 (1968).

cracking without any preheating. Even the use of controlled hydrogen electrodes did not eliminate cracking. Preheat temperatures up to 350°C (660°F) were used in combination with controlled hydrogen electrodes to prevent cracking. For the austenitic manganese steel, interpass temperatures were held below 200°C (390°F) and other precautions such as stringer bead welding, pre-buttering joint faces and skip welding were used to prevent carbide precipitation embrittlement. The 12M alloy showed a high level of notch toughness in HAZ when welded using correct procedures and precautions.

New high strength low alloy cast steels (yield strength 70 Ksi, tensile strength 100 Ksi) have been developed[78] which are reported to be resistant to HIC in the underbead cracking test. Heat affected zone toughnesses up to 70 ft. lb. at room temperature have been reported for this steel. (LN-866 of the International Nickel Company C-.08/.12%, Mn-1/4/2.0%, Si-0.2/0.4%, Ni-0.8/1.3%, Mo-0.15/.25%, Cr-0.4/.8%).

As has been mentioned earlier, the power industry has adopted cast weldment fabrication in a big way. Whitley[79] points out that as operating temperatures increased turbine castings changed from C-Mo steels to the 2 1/4Cr-1Mo type for service up to 565°C (1050°F). A switch then took place (in Britain) to the 1%Cr-1Mo-V, as this was thought to have a superior creep strength. However, this was done at the cost of weldability and increased susceptibility to HAZ cracking during stress relief treatment after welding. The aluminum

content of the steel was found to affect its stress-relief cracking tendency. This led to an aluminum restriction of 0.03% maximum soluble content.

For the 1/2-1Cr-1/2%Mo-1/4%V cast steel, Whitley reports the results of research aimed at studying the effect of trace elements on hot strength and ductility of HAZ material. The results led to copper, tin and aluminum to be further restricted to 0.25%, 0.20% and 0.025%, respectively. Use of zirconium and titanium as deoxidation elements was encouraged.

Wallett[80] has given typical examples of cast weldments encountered in the power industry. Details of joint preparation, preheat, post heat treatments are given for interceptor valve chests, reheat steam chest assembly, low pressure casings and astern cylinders.

Wu[81] conducted synthetic HAZ studies on centrifugally cast 5% chromium steel. He found that this steel possesses good weldability. However, charpy specimens thermally cycled using 1800 and 2000°F as peak temperatures showed low impact strength. This was attributed to the presence of retained austenite and high carbon martensite resulting from these thermal cycles. A post weld tempering treatment was suggested to improve the toughness of the martensite and to decompose the austenite.

In conclusion, a review of the comments and suggestions of Mellili and Biron[82] regarding postheating and stress relief of castings is in order. They recommend that large and extensive welds

in low alloy steel castings be partially welded so that in intermediate sub-critical tempering heat treatment can be employed. This would help to reduce the buildup of stresses. Mellili and Biron[82] also stress the importance of avoiding notches due to undercutting and overlapping prior to post weld heat treatment. The avoidance of notches is important especially when an intermediate, sub-critical tempering PWHT is employed. This type of PWHT is to be employed especially on heavy section welds of large castings which are highly restrained.

The factors which decide[82] whether or not a casting is to be cooled from the preheat temperature prior to PWHT are:

1. Base metal heat treatment before welding;
2. Transition temperature of base metal;
3. Impact strength of base metal;
4. HAZ properties;
5. Geometry and section size of the casting;
6. Volume and extent of process welding;
7. Characteristics of the alloy steel.

Mellili and Biron identify stress relief treatments as those treatments which are usually conducted at sub-critical temperatures to reduce residual stresses. They also alter HAZ hardness and toughness.

The removal of residual stresses is very important as far as the dimensional stability of a casting is concerned. If such an operation is not performed, stress relaxation can occur during

service which may alter the dimensions of a casting. Stress relieving also improves brittle fracture characteristics for service at low temperatures.

Sub-critical treatments that combine stress relief and a reduction of HAZ hardnesses are called tempering. One way of establishing a tempering schedule is to generate data[82] of the type shown in Figure 27. Hardness measurements have been taken in the base metal and HAZ of a 1.25/Cr-0.5%Mo casting as a function of holding temperature at a constant time (8 hours). It can be seen that at 1275°F the HAZ hardness was reduced to that of the base metal. This type of data is especially useful for alloys where secondary hardening can take place. Hence, Mellili and Biron[82] emphasize that rules of thumb regarding PWHT in such cases would be hazardous, and should be avoided.

Finally, the importance of using a qualified welding procedure should not be overlooked. As Gross[83] suggests, use of a qualification procedure which has been proven by years of experience minimizes the possibility of missing essential elements in a repair or fabrication procedure. He recommends the use of ASME Boiler and Pressure Vessel Code Section IX or other standards such as ASTM A488.

9. Comparative Weldabilities of Cast and Wrought Steels

The earliest differences in weldability between cast and wrought steels were reported by Williams et al.[1] and have been described earlier. They found that cast steels were less susceptible to HIC than wrought steels in the underbead cracking test. Linnert[11]

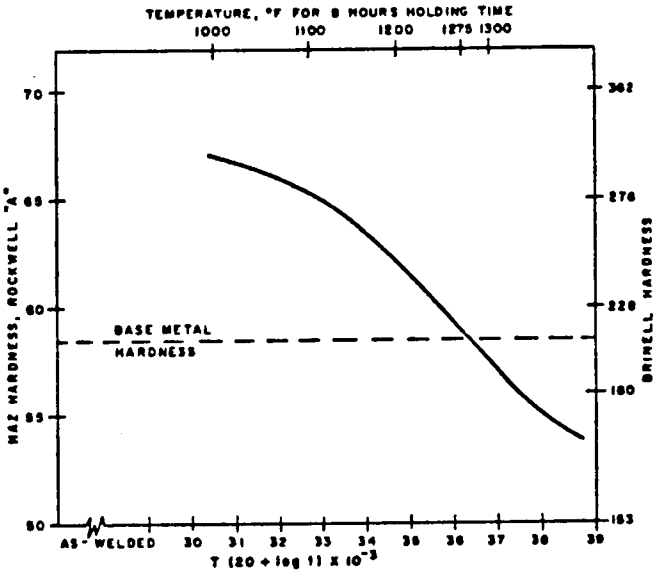


Figure 27. Typical tempering parameter curve for a 1.25%Cr - 0.5%Mo casting HAZ.

Source: Mellili, A.S., and Biron, R.H., "Preparation, Preheat and Postheat Considerations for the Welding of Steel Castings," Trans. AFS, 429-436 (1975).

however, quotes generally that cast steels are more susceptible to cracking than wrought steels. Again CTS tests[84] on cast and wrought steels of low sulfur contents (S<0.01%) have shown that cast steels are more crack resistant. This has been attributed to presence of voids and interdendritic shrinkage areas in cast steels to which hydrogen can diffuse and avoid building up of high pressures. The superior resistance of cast steels to HAZ cracking has also been reported by Short[2] and Granjon.[3] However, an implant test (an externally applied restraint test) result of Aymard and Nectoux[85] may indicate that the weldabilities of cast and equivalent wrought steels may be the same.

In the entire extent of literature reviewed, few investigations were found to be reported which compared the relative weldabilities of cast and wrought steels. Only the work of Williams et al.[1] gave some definite results in that they found cast steels were less susceptible to cracking than equivalent wrought steels. The reasons why this difference of weldability exists may be attributed to:

1. Porosity and microshrinkage associated with cast steels may provide 'sinks' for hydrogen;
2. The transformation behavior in the heat affected zone may be affected by localized variations in elemental concentration which result from segregation;
3. The globular inclusion morphology in cast steels differs from that in wrought steels in which the inclusions are

elongated. The elongated inclusions could act as crack initiators.

10. Closure

It is clear from the review of the literature presented that no systematic studies have been conducted to evaluate the HIC susceptibility of cast steels. Most of the data available suggests an empirical use of techniques based on experience. This research work is aimed at providing comprehensive experimental data with regard to the susceptibility of cast C-Mn-Si steels to heat affected zone HIC. Further, it is aimed to study HIC susceptibility differences between cast and equivalent wrought steels. The primary emphasis is to obtain microstructural evidence to correlate with test results. Synergistic elemental effects will be evaluated by comparing the results of tests on controlled composition cast steels and "foundry-run" castings. Some of the other objectives of the program are to:

1. Evaluate the HIC susceptibility of remelted wrought steels;
2. Study the effect of the extent of deoxidation on HIC of cast steels;
3. To document the response of coarse grained HAZ's in cast steels to PWHT;
4. To resolve the enigma of the role of sulfur in affecting the HIC of steels.

CHAPTER III

MATERIALS AND EXPERIMENTAL PROCEDURES

1. Experimental Materials

This research program comprised of a wide range of cast and wrought steels. As indicated in the Literature Review, very little data has been reported which could serve as baseline data for the weldability (HIC) evaluation of cast steels. The program therefore evolved in two phases; Phase I established the necessary baseline data utilizing cast steels whose composition limits were rigidly controlled whereas Phase II was involved with the testing of cast and wrought steels where the evaluation of certain compositional or processing effects was desired. These included the effect of higher residuals (compared to Phase I materials), heat treatment, melting practice, deoxidation practice, inclusion morphology and sulfur content.

The cast steels tested in Phase II generally conform to the ASTM A216 specification (carbon steel castings suitable for fusion welding for high temperature service). For the study of residual element effects, A216 steels manufactured by both, acid and basic melting practices were obtained in the as-cast condition. The composition limits were as for typical "foundry-run" materials (however, within those specified by A216). The effect of inclusion morphology (as affected by deoxidation practice) on HIC was evaluated by testing A216-WCB steels which had been deoxidized to achieve

three types of inclusion morphologies; Type I (globular sulfides), Type II (eutectic sulfides) and Type III (angular sulfides). The influence of inclusion morphology differences between cast and equivalent wrought steels was directly studied by testing "dead-melted" wrought steels. Finally, Phase II also tested the susceptibility to HIC of low sulfur (<0.01%S) steels, which, as described in the Literature Review, have been reported to be extraordinarily susceptible to HIC.

The materials evaluated in Phase I of the program consist of eight grades of cast and normalized (C&N) carbon-manganese-silicon (C-Mn-Si) steels and equivalent wrought steels. The choice of cast materials provided for a variation in three major elements; C, Mn and Si with comparable wrought steels only at the low Si levels. The residual elements in the cast C-Mn-Si steels were restricted as follows: Ni<0.15%, Cr<0.15%, Mo<0.07%, Cu<0.10%, P<0.02% and S<0.02%. All cast C-Mn-Si steels were obtained from a master melt produced by melting mild steel and pig iron in an induction furnace. Iron ore was used to lower the carbon content when necessary. Deoxidation was accomplished using calsibar, ferro-aluminum and zirconium-silicon. All the cast C-Mn-Si steels were normalized at 1800°F after the risers were removed. For ease of identification, the compositions of the cast and normalized C-Mn-Si steels as well as the wrought steels have been normalized into carbon equivalents using the carbon equivalent formula,

$$C.E. = \%C + \frac{\%Mn}{6} + \frac{\%Si}{24} + \frac{\%Cr}{12} + \frac{\%Mo}{10} + \frac{\%Ni}{40} \quad .$$

This formula is a modification of the C.E. formula proposed by Kihara[17] for wrought C-Mn-Si steels. The modifications were effected in the coefficients for the compositions of Cr and Mo in order to enable better correlation with the results of the under-bead cracking tests. The C&N C-Mn-Si steels ranged in C.E. from 0.37 to 0.58 whereas the wrought C-Mn-Si steels ranged from 0.40 to 0.68. The "residuals" as described by ASTM A216 comprise of Cu, Ni, Cr, Mo and V. The sum of these "residuals" for the C&N C-Mn-Si steels amounts to 0.19% maximum whereas for the wrought C-Mn-Si steels the maximum residual content is 0.49%. Thus for both the cast and wrought materials, the total residual content is well below the 1% maximum allowed by ASTM A216. The compositions of the C&N C-Mn-Si as well as the wrought C-Mn-Si steels and their Brinell hardnesses are given in Table 4. In addition to the C-Mn-Si steels described above, a C&N 8630 was also tested and contrasted with its wrought equivalent. The compositions of the 8630 materials are given in Table 5.

The second phase of the research program involved testing a series of cast steels corresponding to A216 with the residuals ranging up to 0.59% maximum. The C.E.'s for these steels range from 0.38 to 0.48. These "foundry-grade" steels were produced by both acid and basic melting practices. The compositions and designations of these steels are given in Table 6. In the designation the first letter "B" or "C" refer to whether the steel is A216-WCB or A216-WCC (WCC is specified to have a higher yield

Table 4. Compositions of cast and normalized (C&N) and wrought C-Mn-Si steels tested in Phase I.

STEEL	C	Mn	Si	P	S	Ni	Cr	Mo	Cu	Ti	V	Al	Residuals	C.E.	HB
C&N C-Mn-Si	0.25	0.69	0.20	0.009	0.015	0.00	0.00	0.00	0.04	0.00	0.00	0.037	0.04	0.37	128
	0.25	0.73	0.66	0.009	0.020	0.05	0.09	0.00	0.05	0.00	0.00	0.041	0.19	0.41	146
	0.32	0.69	0.23	0.008	0.015	0.00	0.00	0.00	0.04	0.00	0.00	0.050	0.04	0.45	141
	0.25	1.26	0.20	0.009	0.019	0.02	0.04	0.00	0.05	0.00	0.00	0.056	0.11	0.47	144
	0.34	0.74	0.75	0.010	0.017	0.02	0.01	0.00	0.04	0.00	0.00	0.083	0.07	0.50	169
	0.24	1.40	0.69	0.010	0.018	0.02	0.05	0.00	0.05	0.00	0.00	0.068	0.12	0.51	166
	0.33	1.22	0.26	0.010	0.019	0.02	0.04	0.00	0.04	0.00	0.00	0.052	0.10	0.55	168
	0.34	1.26	0.71	0.008	0.016	0.01	0.01	0.00	0.04	0.00	0.00	0.049	0.06	0.58	183
Wrought C-Mn-Si	0.26	0.68	0.21	0.010	0.014	0.14	0.16	0.02	0.17	0.00	0.000	0.006	0.49	0.40	156
	0.24	1.09	0.27	0.007	0.016	0.00	0.02	0.01	0.01	0.00	0.004	0.039	0.03	0.43	143
	0.36	0.83	0.24	0.001	0.018	0.03	0.01	0.00	0.02	0.00	0.000	0.001	0.06	0.51	167
	0.42	1.35	0.23	0.010	0.017	0.02	0.20	0.11	0.02	0.00	0.003	0.011	0.35	0.68	194

$$C.E. = \%C + \frac{\%Mn}{6} + \frac{\%Si}{24} + \frac{\%Cr}{12} + \frac{\%Mo}{10} + \frac{\%Ni}{40}$$

Residuals = %Cr + %Mo + %Ni + %V + %Cu

HB = Brinell Hardness

Table 5. Compositions of cast and normalized (C&N) and wrought 8630 tested in Phase I.

STEEL	C	Mn	Si	P	S	Ni	Cr	Mo	Cu	Ti	V	Al	C.E.	HB
C&N 8630	0.30	0.78	0.20	0.010	0.016	0.77	0.45	0.22	0.05	0.000	0.000	0.001	0.52	223
Wrought 8630	0.32	0.83	0.27	0.015	0.022	0.53	0.46	0.20	0.18	0.001	0.002	0.030	0.53	209

$$C.E. = \%C + \frac{\%Mn}{6} + \frac{\%Si}{24} + \frac{\%Cr}{12} + \frac{\%Mo}{10} + \frac{\%Ni}{40}$$

HB = Brinell Hardness

Table 6. Compositions of acid and basic melted A216-WCB and WCC tested in Phase II.

STEEL	IDENTIFICATION	C	Mn	Si	P	S	Ni	Cr	Mo	Cu	Ti	V	Al	C.E.	Residuals	HB	
																AC	C&N
A216-WCB	BA-1	0.25	0.82	0.54	0.019	0.024	0.06	0.07	0.03	0.07	0.007	0.005	0.070	0.42	0.24	159	161
A216-WCB	BA-2	0.24	0.65	0.42	0.024	0.023	0.08	0.09	0.03	0.06	0.003	0.010	0.070	0.38	0.27	159	161
A216-WCB	BA-3	0.27	0.67	0.41	0.021	0.032	0.12	0.14	0.04	0.13	0.007	0.003	0.073	0.42	0.44	160	167
A216-WCB	BA-4	0.22	0.76	0.46	0.014	0.021	0.17	0.21	0.05	0.08	0.006	0.001	0.022	0.39	0.51	184	172
A216-WCB	BB-1	0.29	0.85	0.52	0.016	0.020	0.13	0.12	0.06	0.14	0.002	0.005	0.045	0.48	0.46	173	173
A216-WCB	CB-1	0.21	1.11	0.44	0.012	0.010	0.11	0.16	0.11	0.13	0.002	0.005	0.048	0.44	0.52	152	170
A216-WCB	BB-2	0.23	0.88	0.45	0.011	0.002	0.17	0.31	0.04	0.07	0.000	0.000	0.010	0.43	0.59	161	165
A216-WCB	CA-1	0.24	0.92	0.50	0.015	0.019	0.19	0.16	0.09	0.13	0.000	0.002	0.058	0.44	0.57	165	170

$$\text{C.E.} = \%C + \frac{\%Mn}{6} + \frac{\%Si}{24} + \frac{\%Cr}{12} + \frac{\%Mo}{10} + \frac{\%Ni}{40}$$

$$\text{Residuals} = \%Cr + \%Mo + \%Ni + \%V + \%Cu$$

HB = Brinell Hardness

AC = As-cast

C&N = Cast and normalized

strength than WCB) and the second letter, "A" or "B" signifies whether the melting practice utilized was "acid" or "basic" respectively. All the above steels were obtained in the as-cast condition. Tests were conducted on these steels in the as-cast as well as cast and normalized conditions. The normalization was performed at 1800°F.

Two lots of acid melted 8630 steels were also tested in the as-cast as well as cast and normalized (1650°F) conditions. The compositions of these steels are given in Table 7.

The effects of the differences in inclusion morphology between cast and equivalent wrought steels on HIC were studied directly by testing remelted wrought steels A516-70 and 8630. The compositions of these steels together with those of the "parent" wrought materials are given in Table 8. The compositions of the remelted steels are quite similar to those of the "parent" steels, excepting for the higher chromium content of the remelted A516. The increased level of chromium may have resulted due to chromium contamination from the furnace refractories. However, the resulting difference in C.E.'s between the wrought and remelted A516 is only 0.01, which is not very significant.

The compositions of steels utilized to study the effects of inclusion morphology and extents of deoxidation on the HIC susceptibility of cast steels are detailed in Table 9. The original aim of this experiment was to split one master heat of cast A216-WCB to obtain three separate heats possessing Type I, Type II and Type III inclusion morphologies. The above could be achieved by

Table 7. Compositions of acid melted 8630 steels tested in Phase II.

IDENTIFICATION	C	Mn	Si	P	S	Ni	Cr	Mo	Cu	Ti	V	Al	C.E.	HB	
														AC	C&N
8630-1	0.28	0.81	0.54	0.017	0.023	0.56	0.47	0.20	0.09	0.001	0.010	0.083	0.51	244	245
8630-2	0.31	0.85	0.54	0.019	0.034	0.57	0.44	0.18	0.03	0.010	0.003	0.069	0.54	208	218

$$C.E. = \%C + \frac{\%Mn}{6} + \frac{\%Si}{24} + \frac{\%Cr}{12} + \frac{\%Mo}{10} + \frac{\%Ni}{40}$$

HB = Brinell Hardness
AC = As-cast
C&N = Cast and normalized

Table 8. Compositions of wrought and remelted A516-70 and 8630 steels.

STEEL	IDENTIFICATION	C	Mn	Si	P	S	Ni	Cr	Mo	Cu	Ti	V	Al	C.E.	HB
Wrought A516-70	W516-70	0.24	1.09	0.27	0.007	0.016	0.00	0.02	0.01	0.01	0.000	0.004	0.039	0.44	143
Remelted A516-70	R516-70	0.24	1.04	0.22	0.006	0.021	0.13	0.32	0.02	0.02	0.000	0.005	0.002	0.45	153 (AC) 160 (C&N)
Wrought 8630	W8630	0.31	0.84	0.26	0.015	0.022	0.53	0.46	0.20	0.18	0.001	0.006	0.030	0.53	209
Remelted 8630	R8630	0.33	0.78	0.35	0.014	0.021	0.54	0.46	0.20	0.17	0.000	0.001	0.020	0.55	241 (AC) 240 (C&N)

$$C.E. = \%C + \frac{\%Mn}{6} + \frac{\%Si}{24} + \frac{\%Cr}{12} + \frac{\%Mo}{10} + \frac{\%Ni}{40}$$

HB = Brinell Hardness

AC = As-cast

C&N = Cast and normalized

Table 9. Compositions of A216-WCB steels utilized in inclusion morphology/deoxidation practice studies.

IDENTIFICATION	C	Mn	Si	P	S	Ni	Cr	Mo	Cu	Ti	Al (Total)	Al (Acid Soluble)	N	O	C.E.	HB AC	HB C&N
DEOX-1	0.25	0.80	0.49	0.009	0.023	0.32	0.40	0.06	0.24	0.001	0.015	0.007	0.0063	0.0078	0.45	176	194
DEOX-2	0.25	0.60	0.33	0.011	0.031	0.34	0.47	0.00	0.21	0.000	0.030	0.019	0.0094	0.0076	0.42	152	167
DEOX-3	0.25	0.80	0.61	0.009	0.023	0.32	0.40	0.06	0.24	0.002	0.071	0.064	0.0097	0.0105	0.46	177	179

$$C.E. = \%C + \frac{\%Mn}{6} + \frac{\%Si}{24} + \frac{\%Cr}{12} + \frac{\%Mo}{10} + \frac{\%Ni}{40}$$

HB = Brinell Hardness

AC = As-cast

C&N = Cast and normalized

simply increasing the extents of deoxidation. However, casting problems led to the Type II heat being improperly poured. The Type II heat was therefore remelted and recast separate from the Type I and Type III heats. Metallographic examination revealed that the "Type I" heat also possessed Type II inclusions whereas the "Type II" heat contained Type II and Type III inclusions. Only the "Type III" heat possessed exclusively Type III inclusions. Hence, the intended Type I, Type II and Type III heats have been designated as DEOX-1, DEOX-2 and DEOX-3 to reflect only the extent of deoxidation as indicated by the acid-soluble/total aluminum contents. In Table 9, DEOX-1 and DEOX-3 heats are split heats from a master melt, whereas, DEOX-2 was cast separately. The oxygen contents, do not reflect the extent of deoxidation, with DEOX-3 having a higher oxygen content than DEOX-1 or DEOX-2. The higher oxygen content may have resulted from the DEOX-3 melt being held in the ladle for a longer time than DEOX-1 or DEOX-2 before pouring. However, the acid soluble as well as the total aluminum contents clearly indicate that increasing aluminum contents were added to DEOX-1 through to DEOX-3 to effect more deoxidation. Further, inclusion morphologies existing in the three heats enabled a qualitative evaluation of the extent of deoxidation. Details are elaborated upon in the next chapter.

The effect of sulfur content on the HIC susceptibility of wrought steels, was investigated using four A537 grade steels, the compositions of which are listed in Table 10. The sulfur contents in these steels vary from 0.001 to 0.012% whereas the C.E.

Table 10. Compositions of wrought low sulfur A537 and low sulfur cast steels.

IDENTIFICATION	C	Mn	Si	P	S	Ni	Cr	Mo	Cu	Ti	V	Al	C.E.	HB
A537-1	0.24	1.39	0.22	0.007	0.001	0.19	0.17	0.08	0.24	0.000	0.000	0.026	0.51	168
A537-7	0.21	1.43	0.23	0.007	0.007	0.13	0.11	0.04	0.17	0.000	0.004	0.013	0.47	187
A537-8	0.22	1.39	0.24	0.009	0.008	0.27	0.21	0.06	0.21	0.000	0.000	0.030	0.49	186
A537-12	0.21	1.30	0.30	0.010	0.012	0.19	0.17	0.06	0.18	0.000	0.004	0.022	0.46	188
Cast LSC	0.19	0.89	0.37	0.020	0.001	0.06	0.19	0.06	0.11	0.000	0.000	0.035	0.38	142

$$C.E. = \%C + \frac{\%Mn}{6} + \frac{\%Si}{24} + \frac{\%Cr}{12} + \frac{\%Mo}{10} + \frac{\%Ni}{40}$$

H.B. = Brinell Hardness

values vary from 0.46 to 0.51. In addition, a cast low sulfur steel (0.001%S) was also included in the testing schedule. The carbon equivalent of this steel is only 0.38, and hence its behavior in HIC tests could not be directly compared to that of the low sulfur wrought steels.

2. Weldability (HIC) Tests

As has been indicated earlier, the only positive evidence of differences in HIC susceptibilities between cast and equivalent wrought steels was given by Williams et al.[1] These differences were deciphered using the Underbead Cracking Test developed at Battelle, hereby referred to as the UBCT. The UBCT was therefore adopted to serve as a major test method in this evaluation. The UBCT requires a relatively small amount of material per individual test and hence for the extensive amount of testing envisaged, was ideally suited for quick comparative evaluations.

In the introduction to hydrogen-induced cracking, it was mentioned that three factors are responsible for the occurrence of HIC, these being, a susceptible microstructure such as martensite, the presence of hydrogen and the existence of stresses acting upon the weld. All HIC tests essentially differ in the manner in which these three factors are controlled. In this research program three different HIC tests were employed. The UBCT was used extensively for reasons aforementioned. The UT-Modified Hydrogen Sensitivity Test (UT-Mod. HST) was used to confirm relative evaluations

observed in the UBCT. Finally, implant tests were performed on those materials where confirmatory data was needed and where the nature of HIC could be deciphered completely only if an external restraint was needed to be applied. The three tests are now described in detail.

The Battelle Underbead Cracking Test (UBCT). This test, developed at Battelle, is a simple bead-on-plate test, and involves the deposition of a weld bead on a block of the test material, the dimensions of the block being 3" x 2" x 1" (Figure 28). The weld bead is approximately 1 1/4" long and is generally deposited using a 1/8" E 6010 (high-hydrogen) electrode. Low-hydrogen electrodes of the type E 7018 can also be used. The welding parameters used are a current of approximately 100 amps at 24 to 26 volts and a travel speed of 10 inches per minute. These parameters result in a heat input* of 15,000 Joules/in (15 KJ/in). The cooling rates attained in the coarse grained HAZ's of plain carbon steels with the use of this heat input are usually sufficient to enable the formation of martensite. Hydrogen is introduced into the weldment through the arc; the amount of hydrogen introduced can be low or high, depending on whether low or high hydrogen electrodes are used. The strain developed in this test is only that due to the self restraint of the

---

*Heat input (KJ/in) = $\frac{VxI}{S}$ x 60/1000

V - voltage in volts
I - welding current in amperes
S - welding speed in inches per minute

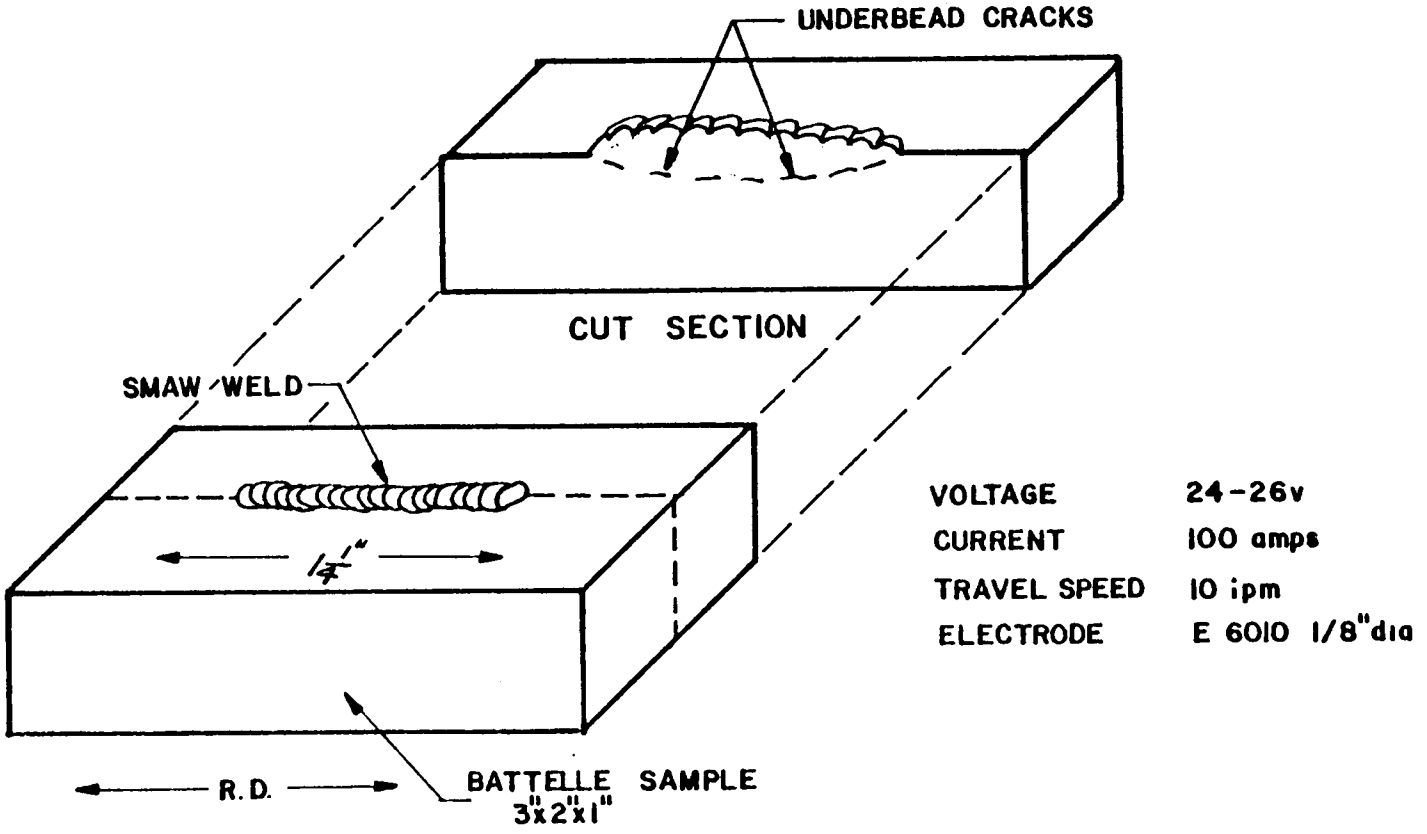


Figure 28. Underbead cracking test specimen showing cut section and location of underbead cracks.

block. After welding, the block is held at room temperature (70-75°F) for 24 hours to allow the underbead cracks to develop. The block is then tempered at 1100°F for 1 hour to soften the HAZ microstructure and thereby avoid the formation of cracks during the subsequent sectioning and grinding. This tempering cycle is not carried out when HAZ hardnesses are to be determined. The underbead cracks are exposed for examination by a longitudinal section such as the one shown in Figure 28. The cut section is then polished to 1 micron, etched and then examined metallographically to detect the underbead cracks. The extent of cracking is reported as the ratio of the sum of the length of the underbead cracks (overlapping cracks counted as one) to the length of the weld, expressed in percent.

From the description given above, it is clear that the UBCT is an extremely simple test to evaluate the HIC susceptibility of steels. The test because of its small sample dimensions is amenable to be conducted at any desired preheat temperature. In this research effort, tests were initially carried out at 32°F, (samples in ice water) and then at increasing preheat temperatures in steps of approximately 50°F, starting at 100°F, until no underbead cracking was observed in the polished and etched samples. The preheat temperatures required to prevent cracking obtained from this test are quite representative of those used in practice for C-Mn-Si steels. The effect of holding the preheat temperature after welding (post-weld hold)

was also studied as a solution to the necessity for high preheat temperatures.

The University of Tennessee Modified Hydrogen Sensitivity Test (UT-Mod. HST). The hydrogen sensitivity test utilized at The University of Tennessee is a modified version (hereby referred to as the UT-Mod. HST) of that developed at RPI by Savage et al.[88] to study hydrogen-induced cracking in HY-80 steel weldments. During the development of the test, which involves straining a bead-on-plate welded sample, Savage et al.[88] recognized that no macroscopic cracking would result unless sufficient diffusible hydrogen was present and the applied stress exceeded the yield strength of the specimen. The diffusible hydrogen in their tests was obtained by intentionally contaminating the electrode coating with moisture and a constant plastic strain was achieved by using a fixture similar to the one shown in Figure 29b. An approximate value of the augmented (or plastic) strain on the top surface of the weld is given by,

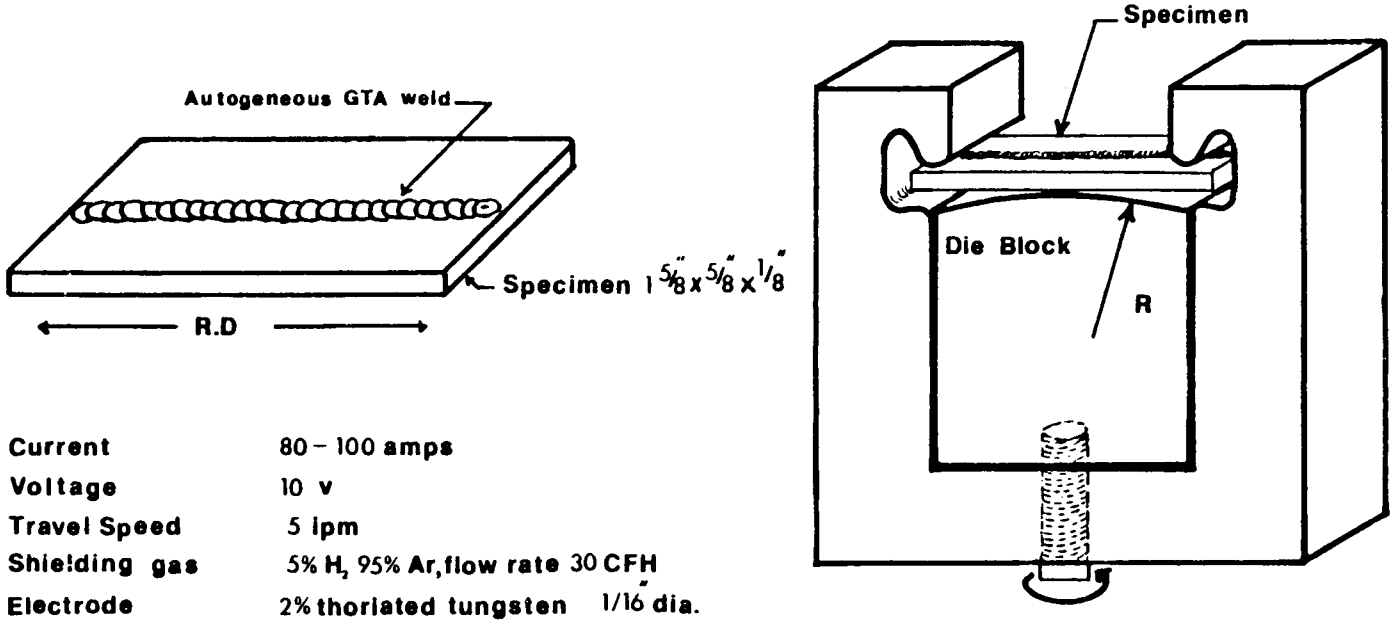
$$\varepsilon = t/2R$$

where ε = augmented strain

t = specimen thickness

R = bend radius.

The UT-Mod. HST essentially uses the same principle, however, instead of using shielded metal arc electrodes on samples 1/2" thick (as in the RPI test), the UT-Mod. HST utilizes autogenous gas tungsten arc (GTA) welds deposited on samples 1/8" thick, as shown in



Current	80 – 100 amps
Voltage	10 v
Travel Speed	5 ipm
Shielding gas	5% H_2 95% Ar, flow rate 30 CFH
Electrode	2% thoriated tungsten 1/16" dia.

Figure 29. UT-Modified Hydrogen Sensitivity Test procedure. a) Specimen, b) Straining apparatus.

Figure 29a. During the deposition of the welds, hydrogen is added to the shielding gas (Ar + 5% H_2) to saturate the weld fusion zone with hydrogen. A typical autogenous weld being made is shown in Figure 30. The welding parameters used are: current-70 amperes, voltage-10 volts and a travel speed of 5 inches/min. After welding, the samples are cooled to room temperature and strained in the fixture shown in Figure 29b. Using a specimen thickness of 1/8" and a bend radius of 1 1/2" yielded a strain of approximately 4.1%. This augmented strain was kept constant for all the tests. Susceptibility to cracking was determined by noting whether the samples cracked on the face strained in tension. Preheat temperatures were raised in steps of 100°F until cracking was prevented.

The UT-Mod. HST has been used with considerable success in the evaluation[89,90] of the hydrogen cracking sensitivity of wrought low alloy as well as 9Cr-1Mo steels. The advantage of this test is in its ability to quickly rank the weldability of steels with respect to preheat temperature and restraint. An added advantage that can be incorporated into the test is that the strain can be applied at temperatures below the ductile-brittle transition temperature of the material being evaluated. This factor becomes especially important in the evaluation[90] of the hydrogen cracking sensitivity of 9Cr-1Mo steels.

The Implant Test. In many of the weldability tests, utilized to evaluate the HIC susceptibility of steels, the microstructure

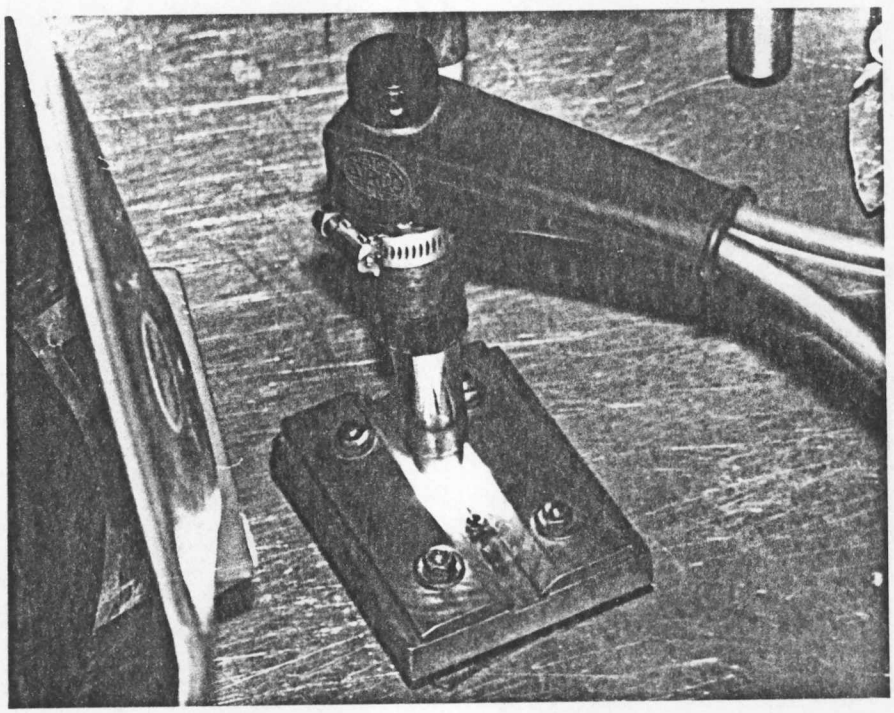


Figure 30. Autogenous gas tungsten arc weld being made on the UT-Mod.HST sample.

and the hydrogen content in the HAZ can be controlled by choosing an appropriate heat input and welding process. However, the third factor responsible for HIC (i.e., stress), cannot be strictly controlled or measured. This is because many of the HIC tests involve the use of fairly large samples in which the strain developed is primarily due to the self restraint of the test sample. Cracking can occur at any location in the coarse grained HAZ where the state of stress may not be known or may be difficult to determine.

The "implants" method developed by Granjon[91] enables the application of a known stress to an isolated HAZ of the material to be tested. In the original test developed by Granjon, a small cylindrical test specimen having a circumferential notch at one end is introduced into a hole drilled in a base plate (Figure 31). A weld is then deposited on the plate to fuse in the end of the specimen, and after a predetermined time, the specimen is loaded in tension to a desired stress level based on the nominal or notched diameter of the specimen. The time to rupture is noted as a function of the stress level. As the stress levels decrease, the times to rupture increase, and eventually at a particular stress value, no rupture will occur in 24 hours of loading. This stress is termed as the "critical stress" and it represents the HIC characteristic of the material for that particular set of heat input and hydrogen level condition. Hence, for the same heat input/hydrogen level, steels of different compositions can be compared as regards their susceptibility to HIC, based on their critical stresses. The effect of

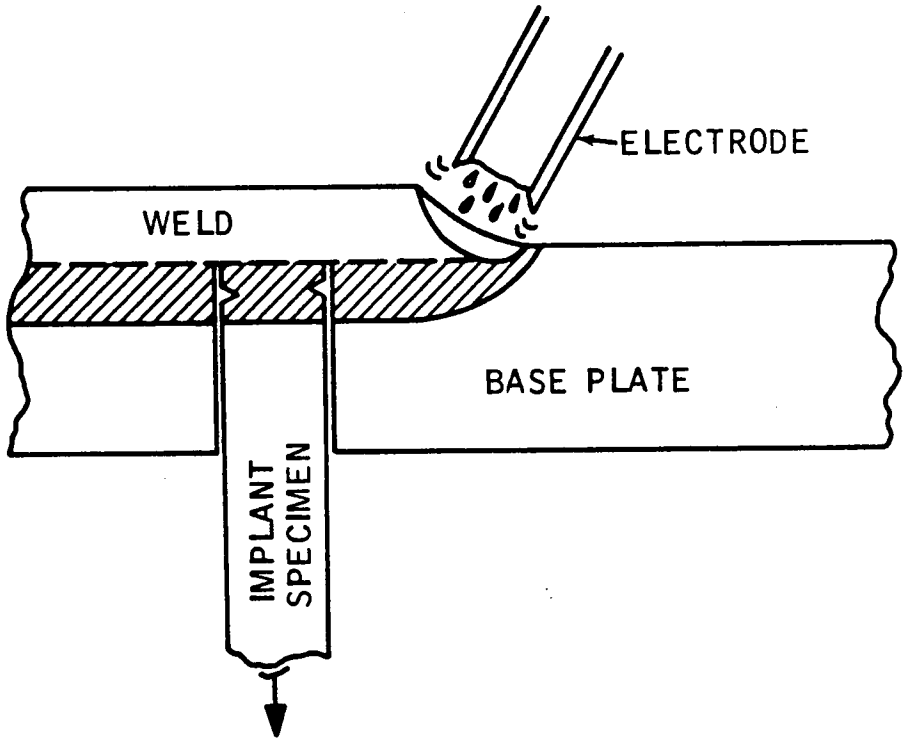


Figure 31. Schematic of original implant test developed by Granjon.

other variables such as preheat, post-weld hold and PWHT can also be evaluated since each of the three factors responsible for HIC can be controlled independently. The original implant test has a major difficulty in the location of the notch in the same microstructure of the HAZ for a series of tests. This difficulty was circumvented by Sawhill et al.[92] by utilizing a helical notch instead of a single circumferential notch. They contended that the helical notch would traverse the entire region of the HAZ and therefore failure would occur at the most susceptible microstructure in the HAZ.

The sample and the set up used in this research program is shown in Figure 32. The sample essentially conforms to that developed by Sawhill; further, the base plate utilized has the same dimension (3" x 2" x 1") as the UBCT sample. The purpose of this was to obtain identical cooling rates in the coarse grained HAZ of the implant sample as would be in that of the UBCT sample, for the same heat input condition. The implant samples were welded using a semi-automatic technique, utilizing a submerged arc welder which could be modified to perform semi-automatic shielded metal arc welding. The semi-automatic facility shown in Figure 33, helped to achieve consistent quality welds. Further, the welding parameters were adjusted to give approximately the same heat input as in the UBCT (15 KJ/in). Since a relative idea of susceptibility to HIC was to be evaluated, high-hydrogen E 6010 electrodes were utilized. All the implant tests were conducted at room temperature

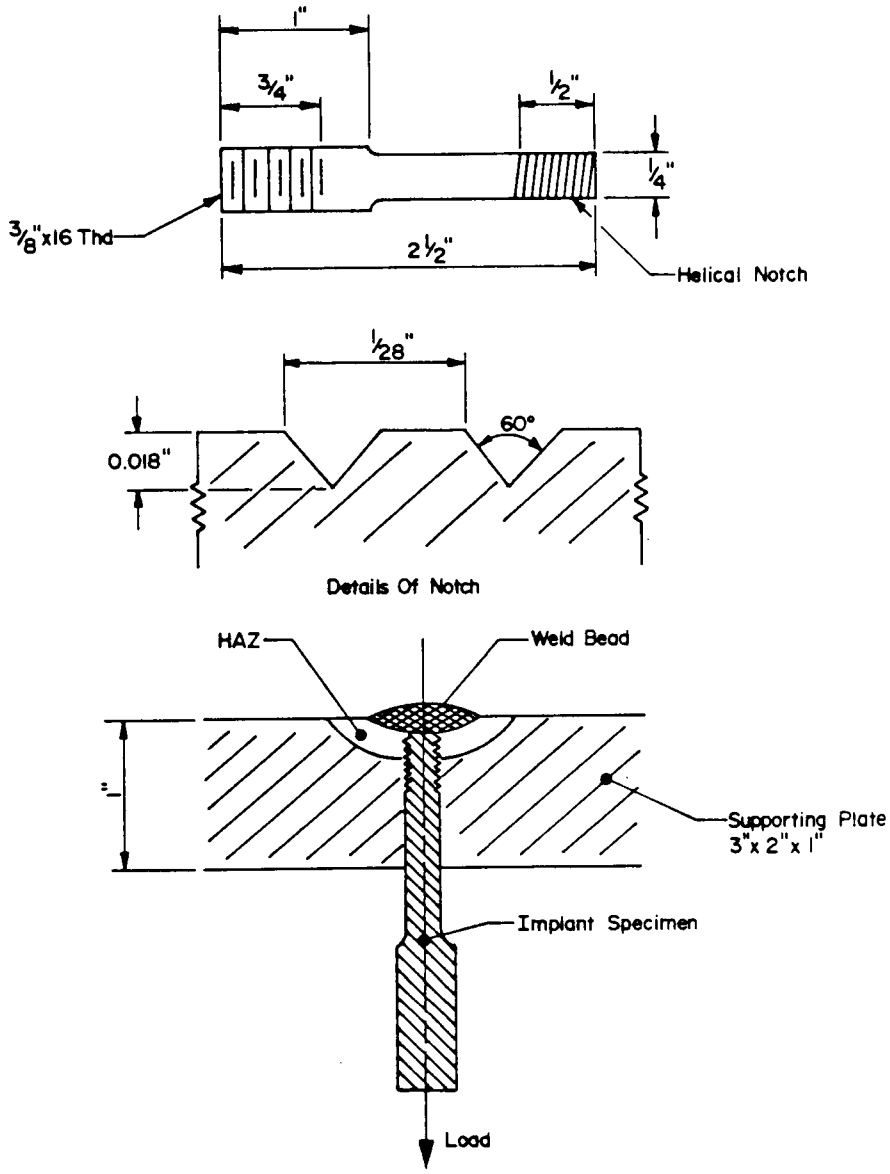


Figure 32. Implant Test--sample and test method used.

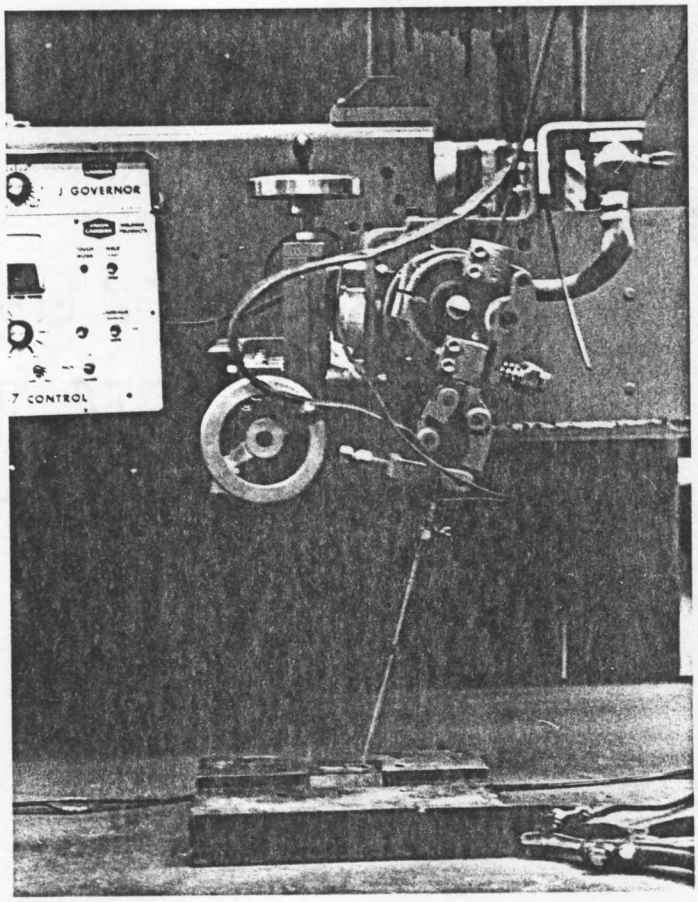


Figure 33. Semi-automatic welding set up for implant samples.

(74-80°F) and a relative grading of the susceptibility to HIC was obtained by simply evaluating the critical stress for each material in question. All unfailed test assemblies (implant sample and the base plate) were examined metallographically by taking a single transverse section along the center of the implant sample and mounting and polishing the cut faces. Metallographic examination was also conducted on selected ruptured assemblies, the corresponding ruptured implant samples were examined in the SEM to record distinctive fracture features.

As an additional study, two-pass weld implant tests were conducted on selected steels utilizing high as well as low hydrogen electrodes. These tests enabled the study of the response of tempered HAZ's to HIC conditions. Specifics regarding this test procedure are detailed in the next chapter.

3. Serviceability Evaluation--Response of HAZ's to PWHT

The coarse grained HAZ in C-Mn-Si steels resulting from a weld thermal cycle, generally possesses an extremely poor toughness due to the nature of microconstituents, martensite and bainite, that are formed. Multi-pass welding does temper, to some extent, the HAZ's created due to previous passes, however, the last pass will always give rise to an untempered HAZ. Hence, it may be desireable to conduct a PWHT i.e., a tempering operation on the weldment to enable the HAZ to achieve reasonable impact properties. A convenient method of evaluating the toughness of the coarse grained HAZ is by using simulated HAZ charpy samples. The simulation is

achieved by using a "Gleeble" device, originally developed at RPI. The Gleeble can reproduce the exact thermal cycle found at a particular point of interest near an actual weld in a specimen of suitable size. This implies that the microstructure in the coarse grained HAZ can be duplicated in a charpy sample for a particular combination of peak temperature, heat input, preheat temperature and plate thickness.

Briefly, the apparatus (Gleeble) consists of a proportional, variable rate, on-off, time-temperature controller that has the ability to duplicate, in a specimen of convenient size, the thermal conditions existing at any point in the HAZ of an arc weld. In operation, a specimen is clamped between two water-cooled copper jaws, one fixed and one movable, which are connected to the secondary of a transformer. The specimen is thus heated by its resistance to the passage of an electric current and is cooled by extraction of heat longitudinally to the water cooled jaws. By use of a thermocouple welded to the specimen, the Gleeble compares a programmed reference signal to the specimen temperature 120 times per second and makes the necessary corrections. Any thermal cycle may be reproduced with heating rates up to 3000°F per second and cooling rates not exceeding approximately 200°F per second.

The Charpy blanks measured 0.42" x 0.42" x 2.196" in length. Chromel-alumel thermocouples were percussion welded exactly to the center of the sides of the specimen where the notch was to be located. For the cast steels, the notch was located perpendicular to a cast surface, whereas for the wrought steels the notch was

positioned perpendicular to a rolled surface as well as to the rolling direction. These procedures generally follow the recommendations of ASTM E 23 (standard method for notched bar impact testing of metallic materials).

The procedure used involved the subjecting of a number of specimens to a thermal cycle corresponding to a peak temperature of 2400°F using an energy input of 50 KJ/in., in a 1" steel plate, welded at 80°F. The thermally cycled Charpy blanks were then post weld heat treated at 1200°F for 1 hour. Although no specific post weld heat treatments procedures are given in the ASTM specification A216, which covers the grades of cast steels investigated, a post weld heat treatment has been specified for welds in castings one inch thick and greater. After the thermal cycle and PWHT were performed, the specimens were machined to the final Charpy dimensions shown in Figure 34. Impact testing was then carried out, at appropriate temperatures, using standard procedures outlined in ASTM E23. In addition to the evaluation of the toughness of the post weld heat treated samples, Charpy specimens as-thermal cycled as well as from the as-received plate were also impact tested. The broken Charpy bars were retained for metallographic and fractographic examination.

4. Determination of Diffusible Hydrogen

Since the presence of hydrogen is probably the most important factor in rendering a HAZ susceptible to HIC, it was relevant to have a quantitative idea of the amount of diffusible hydrogen that

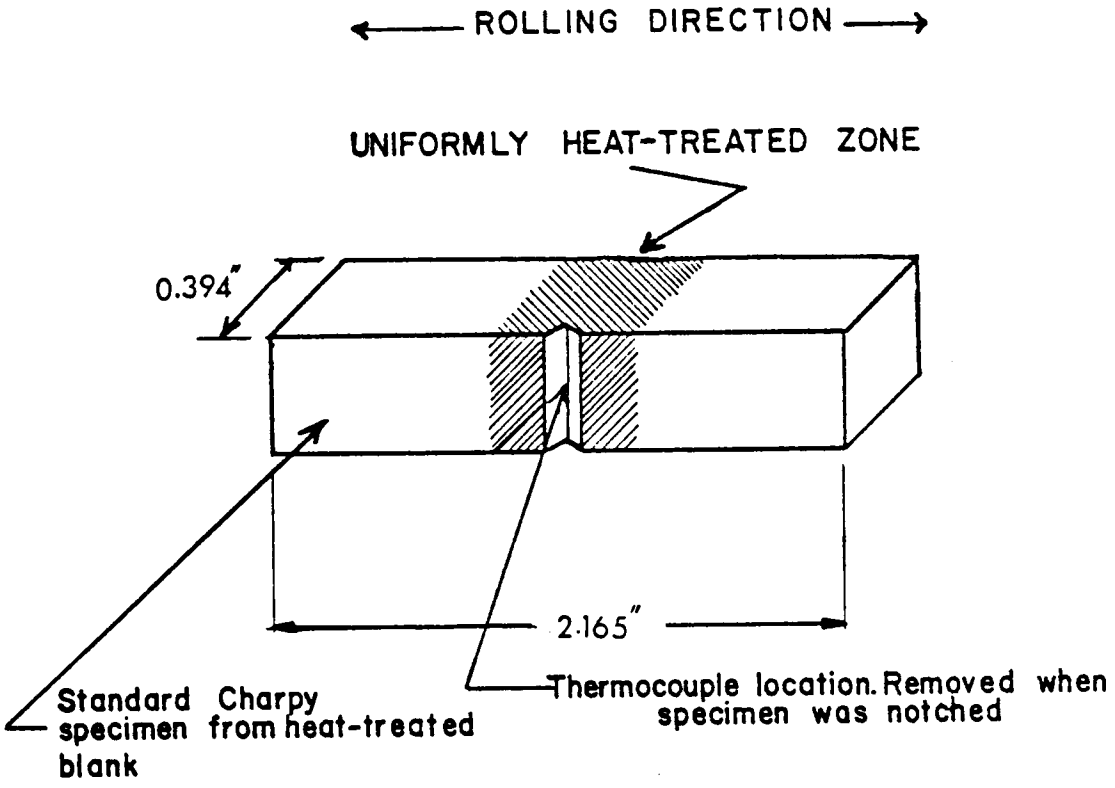


Figure 34. Final machined dimensions of Charpy sample heat treated in the Gleeble. (Rolling direction indicated for wrought steels.)

was generated in the welding process used. Although measurements were not made on each of the test samples, a representative idea of the diffusible hydrogen content was obtained for the welding processes utilized. The method used to determine the diffusible hydrogen was the silicone-oil method of Ball and Nippes.[93] The method basically involves the extraction of diffusible hydrogen from a sample placed in a silicone oil bath saturated with hydrogen and the collection of the evolved hydrogen in a burette. Figure 35 shows the general arrangement of the apparatus. Two pyrex beakers are used in a "double-boiler" configuration and are heated by a standard hot plate. Both beakers are filled with high-grade silicone oil. The inner bath is maintained at a constant temperature of 100 ± 10°C and is saturated with hydrogen by bubbling the gas into the oil through a fritted disc bubbler. After the sample is introduced into the inner bath, the hydrogen evolved is collected in a burette through a collection funnel attached to the burette. The temperature of the bath is maintained at 100 ± 10°C enabling the evolution of hydrogen to be completed in about two hours. The average of hydrogen evolutions from three samples was evaluated for each type of steel. Prior to welding, the samples were baked in an inert gas atmosphere muffle furnace at a temperature of 1200°F for one hour. The baking was performed to eliminate any occluded gases in the samples which may have interfered with the test results. The samples were ground on 180 grit paper to remove any scale that may have formed during baking, weighed and then

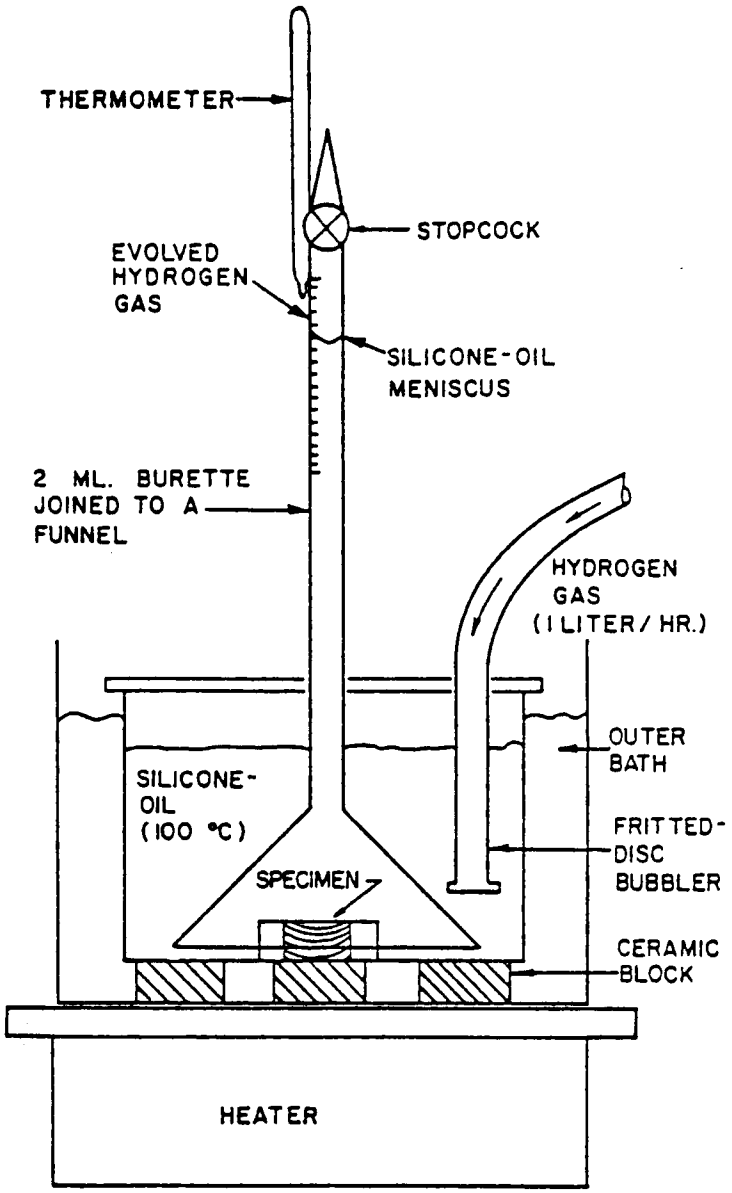


Figure 35. RPI silicone oil apparatus used to determine diffusible hydrogen.

Source: Ball, D.J., Gestal, W.J., Jr., and Nippes, E.F., "Determination of Diffusible Hydrogen in Weldments by the RPI Silicone-Oil Extraction Method," Welding J., 60 (3), 50s-56s (1981).

assembled for welding, with run-on and run-off tabs, on the semi-automatic device shown in Figure 33. A single bead of weld metal was deposited using welding parameters similar to those used in the underbead cracking and implant tests. Within ten seconds of the deposition of the weld, the assembly was introduced into liquid nitrogen and held there for 30 seconds. The assembly was then withdrawn from the liquid nitrogen and broken apart using a chisel and hammer. The samples were washed in 95% methanol for one minute, blown dry with IG-LO® brand refrigerant and analyzed individually for diffusible hydrogen. After analysis, the samples were cleaned in methanol and reweighed to establish the average amount of diffusible hydrogen (in milliliters) obtained per 100 grams of deposited weld metal.

5. Jominy End Quench Hardenability

Standard end-quench hardenability tests were conducted on selected lots of cast and wrought steels as per the ASTM standard A255. The hardnesses starting from the quenched end were recorded on the Rockwell C scale (HRC) and when the hardness fell below HRC 20, they were recorded on the Rockwell B (HRB) scale.

The hardenability tests were conducted to obtain the response of the steels to typical quench situations. Higher hardenability generally implies a greater susceptibility to HIC. Correlations between hardenability and HIC are very useful, since the hardenability is a property that can be determined easily by experimental or analytical procedures.

6. Optical Metallography

Selected samples from many of the tests described above were cut, cleaned and mounted using Buehler plastic epoxy. After mounting, the specimens were ground and polished to 1μ and if desired, to 0.06μ. Examination for non-metallic inclusions was conducted with the samples in the unetched condition. Microstructural details were evaluated after etching the samples with etchants such as 2% Nital, Picral or Vilella's reagent. Selected microstructures were photographed on a Leitz optical microscope using Polaroid Land Type 55 film.

7. Scanning Electron Microscopy

Selected samples polished and etched (as described above) as well as fracture surfaces from Charpy, implant and underbead cracking tests were examined in an AMR 900 Scanning Electron Microscope to obtain detailed microstructural and fractographic information. For the metallographic specimens, the epoxy area was coated with carbon paint to provide conduction with the stage of the microscope. The fracture surfaces were usually sputtered with gold or platinum to improve resolution at high magnifications. An ORTEC detector and energy dispersive multichannel analyzer were used for x-ray fluorescence analysis, typically those of inclusions.

CHAPTER IV

RESULTS AND DISCUSSION

1. Introduction

The earliest use of welding and cutting in the foundry was to effect repair or in the removal of runners and risers. The expanded use of welding processes in the foundry evolved in a slow transition from the manufacture of fully cast components to composite cast/cast and cast/wrought components. The production of complex castings requires intricate cross sections to be fed and this led to the use of welding to join complex components in preference to the casting of a single complex component. Complex high quality castings are required by the nuclear industry where sophisticated NDT techniques are utilized to detect flaws in castings as well as in weldments. The greater degree of inspection also led to enhanced casting quality and a higher degree of confidence in cast/welded components.

In the welding of castings, the range of "weldability" problems encountered are very similar to those that are evident in the welding of wrought materials. The problems include hot cracking, hydrogen-induced "cold" cracking (HIC) and reheat cracking which have been discussed in the earlier portions of this document. The current research effort was confined to the evaluation of the susceptibility of cast steels to HIC and the comparison of their behavior to that of equivalent wrought steels.

As has been indicated before, the factors necessary for HIC to occur are; i) the presence of a suceptible microstructure (martensite), ii) the presence of hydrogen, and iii) the existence of a tensile stress (restraint or applied) across the weld region. These factors interact with each other in a complex manner to give rise to the problem of HIC. The microstructure is primarily governed by the composition (hardenability) of the steel. The hydrogen level is controlled by the nature of the welding process, whereas the magnitude of the stress is related to the thickness and configuration of the weld and structure. Since the welding of castings has only recently gained momentum, most of the systematic evaluations of the weldability of steels are with reference to wrought steels. In the case where the composition of the cast steel is identical to that of the wrought steel, possible differences in weldability between these materials may arise due to their inherent physical properties e.g. cast steels possess more isotropic properties as compared to wrought steels since they are not subjected to any thermo-mechanical treatments. Inclusions in wrought steels are generally elongated (unless the steel has been specially treated), whereas in cast steels the inclusions possess morphologies which are governed primarily by the deoxidation practice used. The inclusion morphology in cast steels can be globular, angular or eutectic sulfide type depending on the extent of deoxidation carried out. In wrought steels hot working enables the closure of shrinkage cavities and voids that may have resulted during primary ingot

solidification; however, in cast steels, these voids and cavities will persist if they were created during initial solidification.

The earliest reporting of differences between the HIC susceptibilities of cast and equivalent wrought steels was by Williams, et al.[1] Using the Battelle underbead cracking test (UBCT), they found that cast steels were less susceptible to HIC than equivalent composition wrought steels. Other investigators[2,3] have also made similar observations, however, no one has produced sufficient documentation to put Williams et al.[1] results on a firm footing.

Three tests were chosen for use in this research program to evaluate the HIC susceptibility of cast and wrought steels (see Chapter III). The following paragraphs describe the philosophy behind the use of these tests and the implications of the results thus obtained.

In this investigation, the underbead cracking test (UBCT) has been used successfully to discriminate between the HIC susceptibilities of cast and wrought steels. The UBCT was the primary test used, since extensive testing was required to compare the numerous grades of steels evaluated and this test provided the requisite HIC information with relatively small samples and short testing periods. Further, the UBCT directly yields an assessment of the preheat temperature required to prevent cracking. The preheat temperatures determined from the test results for a wide range of compositions, are conservatively representative of those

employed in practice. One significant limitation of the test method is that the stress developed in the weld HAZ region is only that due to the self restraint of the small test block, whereas in general welding practice, the stress acting on the weldment can be higher, and hence the UBCT cannot adequately simulate situations where long range stresses due to applied stresses may act in concert with the restraint and transformation stresses. Another attribute is that the low energy input weld bead employed generally produces harder HAZ microstructures than those obtained in normal welded fabrication. It is possible that these two factors are offsetting in most cases and the test results are quite applicable to practice.

The University of Tennessee Modified Hydrogen Sensitivity Test (UT-Mod.HST) is a test where a known and variable strain can be applied to levels exceeding that corresponding to the yield strain of the material. The advantage of the test lies in its ability to rapidly evaluate the relative susceptibilities to HIC of the materials in question. The susceptibility is established on a go/no-go basis, thus unlike the UBCT, the UT-Mod.HST does not evaluate any "extent of cracking"; it evaluates only if the material will or will not crack under the particular test conditions. The test, in essence, evaluates the "unmixed fused zone" of the weldment i.e. the region of the weldment where the base material undergoes melting and solidification without any mixing with the weld metal. Since the region tested is the weld metal,

the influence of factors such as inclusion morphology and distribution in the base material will not be a part of the assessment. However, the UT-Mod.HST has been used with considerable success for the evaluation of the HIC susceptibility of Cr-Mo steels[89,90] and was therefore used as a confirmatory test to verify trends obtained in the UBCT.

As mentioned earlier, despite the simplicity of the UBCT, it suffers from disadvantages, in that the restraint developed does not fully represent actual weld situations, and the HAZ microstructure may not be representative of practice. In the UT-Mod.HST, though the influence of restraint to levels well above the yield can be evaluated, secondary influences of factors such as inclusion morphology and distribution cannot be studies, since the region evaluated is the fusion zone. The two tests are therefore complimentary in terms of the information obtained.

The third test used, the implant test, (the conduct of which is described in detail in Chapter III) is able to circumvent many of the problems, since a known stress can be applied to a "true" HAZ in the material of interest. The implant test is able to simulate long range stresses which may exist in weldments encountered in the welding of structures and vessels. In this investigation, the implant test was used primarily to determine the relative susceptibilities of steels to HIC; however, it has also the potential to be utilized to determine practical welding parameters such as preheat temperatures and post weld heat treatment (PWHT) schedules.

In this chapter, the results and discussions are arranged so as to gain an understanding of the compositional effects on the HIC susceptibility of cast and wrought steels and the discussion is then expanded to include special considerations such as deoxidation practice, inclusion morphology and sulfur content. As the end of the chapter, a mechanism of HIC is proposed which explains the results of the various test methods in relation to the fracture morphologies in the hydrogen embrittled HAZ's.

2. Underbead Cracking Tests--Cast Steels

The initial approach in this investigation was to obtain data to compare the HIC susceptibility of a variety of cast steels. The cast steels described in Tables 4 and 5 (pages 87 and 88) were utilized. These steels were tested in the cast and normalized condition so as to reduce the possible effects of micro-segregation existing in the as-cast condition and to provide a more uniform grain size. Underbead cracking tests (Battelle) were initially conducted at 32°F and then at preheat temperatures in intervals of 50°F starting at 100°F until a preheat temperature was reached where no underbead cracks were observed in the polished and etched samples. A minimum of three tests were conducted at each preheat temperature, with additional tests conducted in the temperature range where cracking was eliminated. The results shown in the subsequent figures are the average of at least three tests. Since the aim was to obtain a relative ranking of susceptibility, all results reported, unless otherwise stated, are for tests with high-hydrogen electrodes

(E 6010). (This is the standard electrode for conducting the Battelle UBCT).

UBCT results for cast and normalized (C&N) C-Mn-Si and 8630 steels are shown in Figure 36. These test data were obtained under the most severe condition with the initial temperature of the samples at 32°F. In Figure 36, the data points are the average of the spread in the extent of cracking for at least three tests. The data spread ranges from ±5% to a maximum of ±15% in terms of crack length. The average extent of cracking for the C&N C-Mn-Si steels is directly related to the C.E. For C.E. values up to 0.47, the extent of cracking is insignificant. At values greater than a C.E. of 0.47, cracking tendencies rise sharply. In the results shown in Figure 36, the C&N steel with a C.E. value of 0.50 cracked to a greater extent than one with a C.E. of 0.51, reflecting the effect of the higher carbon content of the C.E.= 0.50 steel (C=0.34%). Clearly, even though increasing C.E.'s imply greater extents of cracking, the strong influence of carbon content alone on HIC is evident. The C&N C-Mn-Si steels with carbon contents of 0.34, 0.33 and 0.34% all cracked to average extents of 60% or more. The C.E. formula used is a modified version of that proposed by Kihara, et al.[17] Using this modified formula, the extent of cracking for the C&N 8630 falls close to the average line drawn for the C&N C-Mn-Si steels drawn in Figure 36. The results of the UBCT tests conducted at 100°F on the C&N C-Mn-Si and 8630 steels are shown in Figure 37. Cracking is eliminated in steels with C.E. values up to 0.47 and the average extent of cracking for the remainder of the steels,

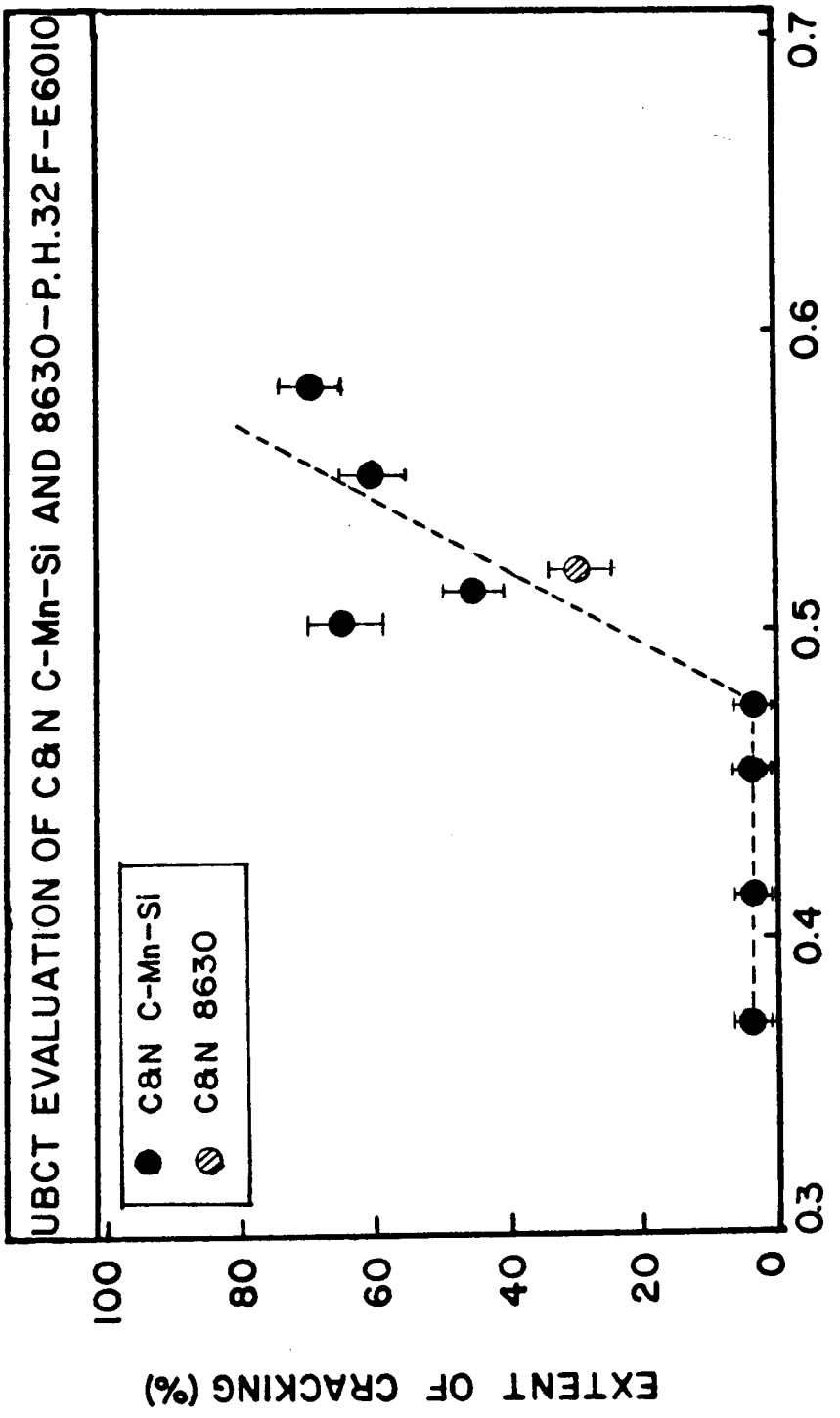


Figure 36. Extent of HIC at 32°F in cast and normalized (C&N) C-Mn-Si and 8630 steels. UBCT, E 6010.

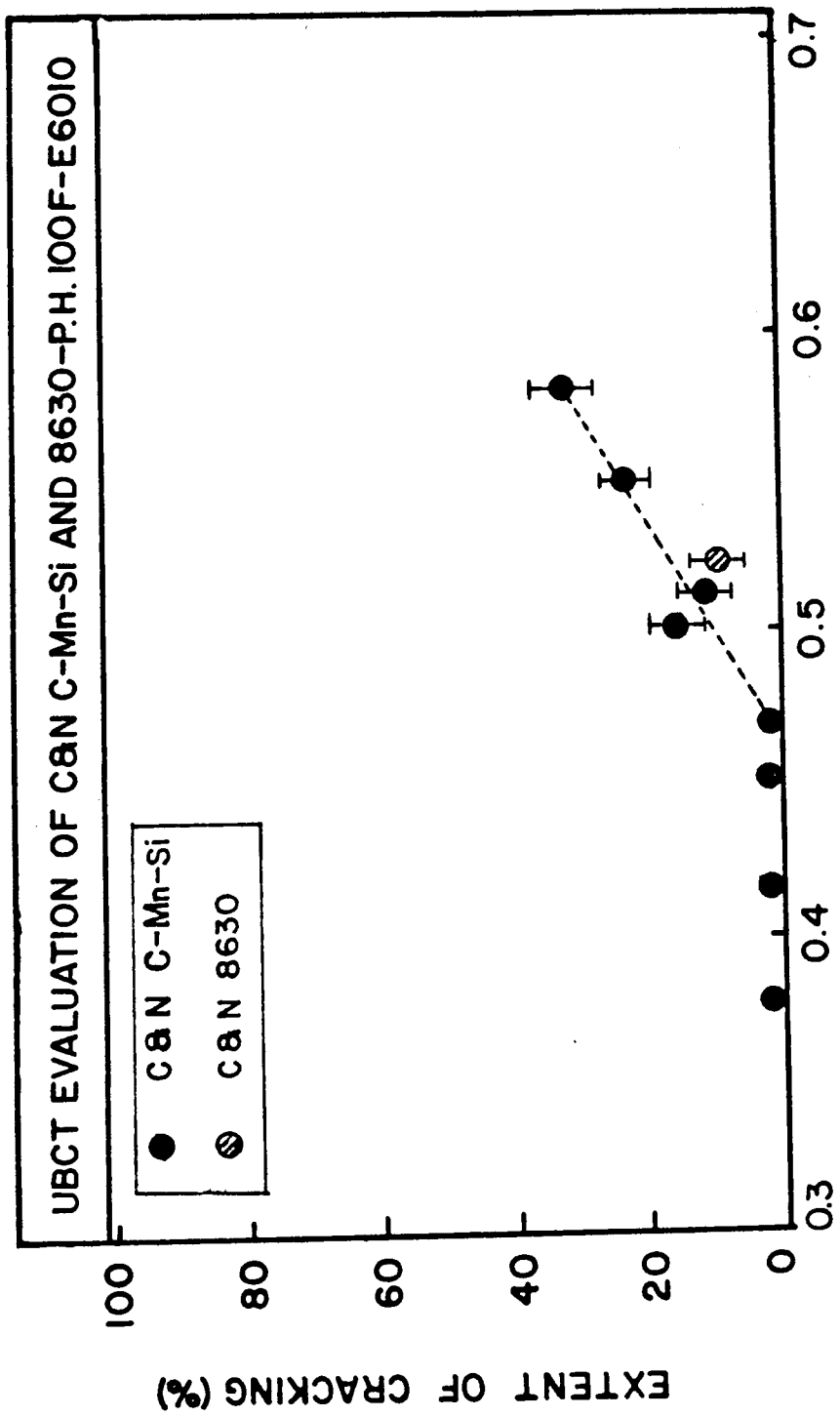


Figure 37. Extent of HIC at 100°F in cast and normalized (C&N) C-Mn-Si and 8630 steels. UBCT, E 6010.

including the 8630, shows a good correlation with the C.E. The steel with a C.E. of 0.58 has the maximum cracking tendency. When the preheat temperature was raised to 150°F, cracking was eliminated in all but the highest C.E. (0.58) C-Mn-Si steel. A preheat temperature of 200°F was not sufficient to prevent cracking in this steel and a preheat of 250°F had to be utilized to prevent cracking at this high C.E.

Therefore it is clear from these baseline test results (Figures 36 and 37) that the susceptibility to HIC of cast and normalized steels is a direct function of the C.E. The baseline test results also indicate that under the conditions of the tests employed, the variability in test results (extent of cracking) for a steel at a particular preheat temperature ranged between 5 and 15%. In subsequent figures concerning results of the UBCT, this data spread will not be indicated to retain clarity.

Since the HIC susceptibility is affected by the C.E. (the hardenability of the steel), metallographic examination was performed to evaluate the transformation products in the coarse grained HAZ where the cracks occur. In Figure 38, the coarse grained HAZ in the C&N C-Mn-Si steel having the lowest C.E. (0.37) is shown. The mixed nature of the transformation products in the HAZ is apparent. The grain boundaries appear to have nucleated the upper temperature transformation products, pearlite and Widmanstätten ferrite. The constituent within the prior-austenite grains is essentially martensite. Microhardness of the grain interiors yielded a hardness

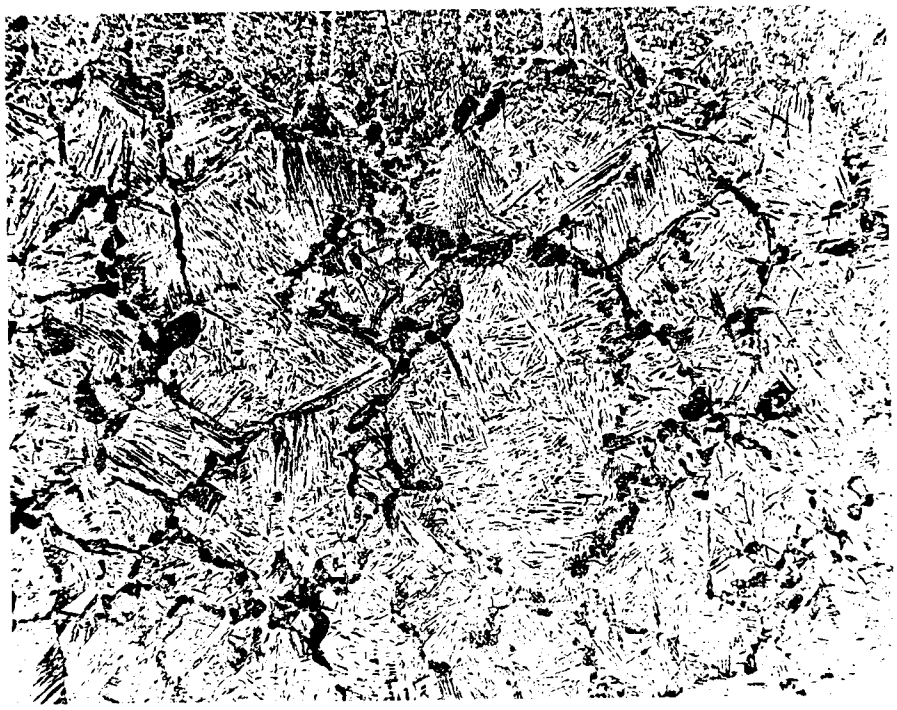


Figure 38. Microstructure of coarse grained HAZ in C&N C-Mn-Si steel, C.E. = 0.37. UBCT, preheat 100°F. Picral etch, OLM, 200X.

of HRC 47 which corresponds to that of 90+% martensite at a 0.24% carbon level. These microconstituents are clearly visible in the SEM photomicrographs shown in Figures 39a and b. In the C&N C-Mn-Si steel with a C.E.=0.47, the coarse grained HAZ is almost entirely composed of martensite with some bainite/Widmanstätten ferrite at the prior austenite grain boundaries close to the fusion line (Figure 40). The higher magnification SEM photomicrograph in Figure 41a details the region to be essentially martensitic and in Figure 41b, the plate-like morphology of the Widmanstätten ferrite is evident. For the C&N steel with the highest C.E. (0.58), the presence of a completely martensitic structure in the coarse grained HAZ is shown in Figure 42. The SEM photomicrographs in Figures 43a and b show the presence of a small fraction of a bainitic constituent on the prior austenite grain boundary. The microstructural studies show a change in microstructure from a "mixed" (martensite with other higher and lower temperature transformation products) to one composed almost entirely of martensite as the C.E. levels exceed 0.47. It may be recalled that the extent of cracking in tests at 32°F rose sharply for steels with C.E. values greater than 0.47. Further, in tests at 100°F, C&N C-Mn-Si steels with C.E.'s up to 0.47 did not exhibit any cracking. It is therefore apparent that the higher the percentage of martensite or low temperature transformation products in the microstructure, the greater is the susceptibility to HIC.

Since the extent of formation of martensite during welding is primarily a function of the hardenability of the steel, hardenability

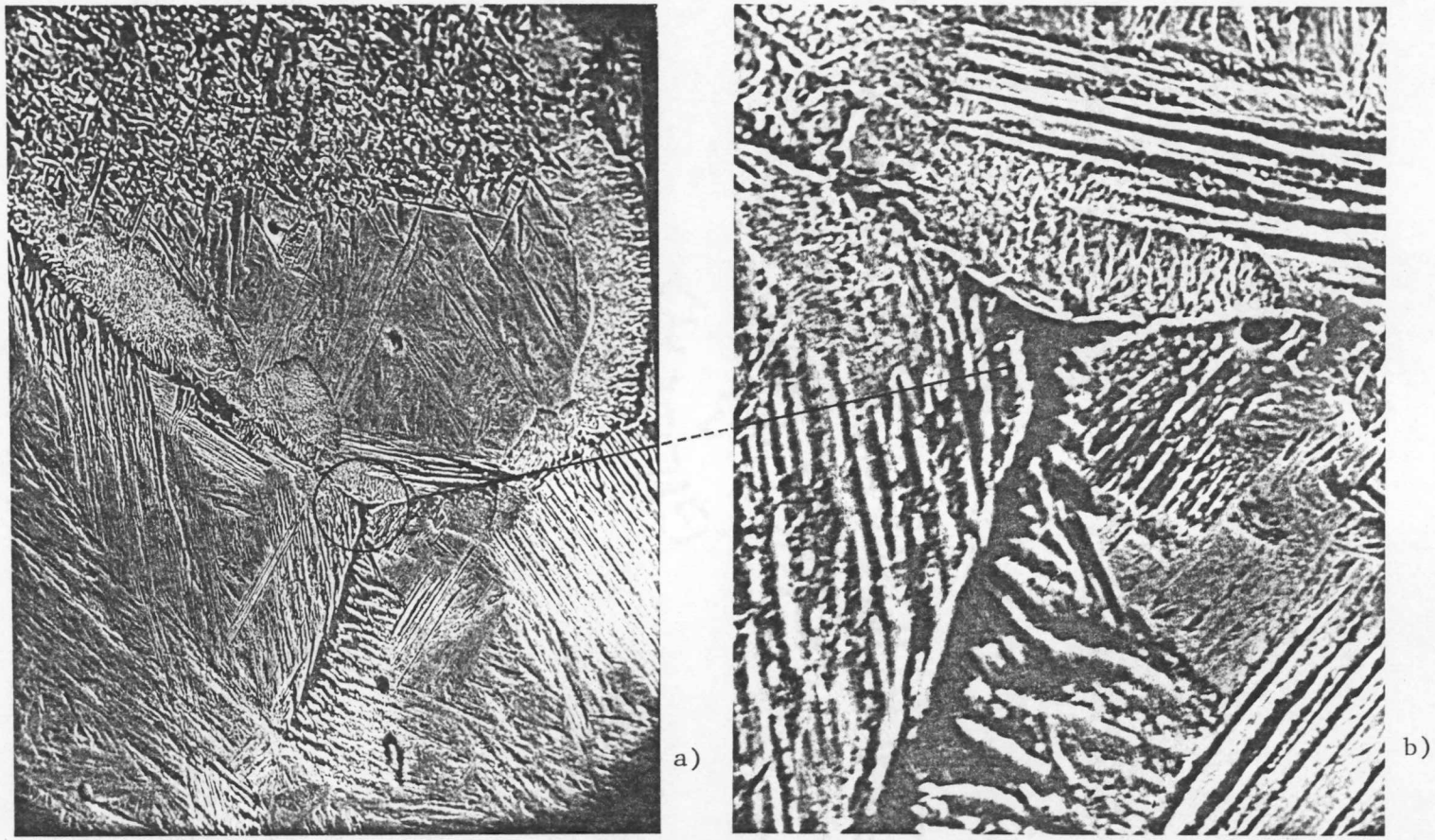


Figure 39. SEM micrograph of coarse grained HAZ in C&N C-Mn-Si steel, C.E. = 0.37. UBCT, preheat 100°F. 2% Nital etch, SEM, a) 1000X, b) 5000X. (See Figure 38)

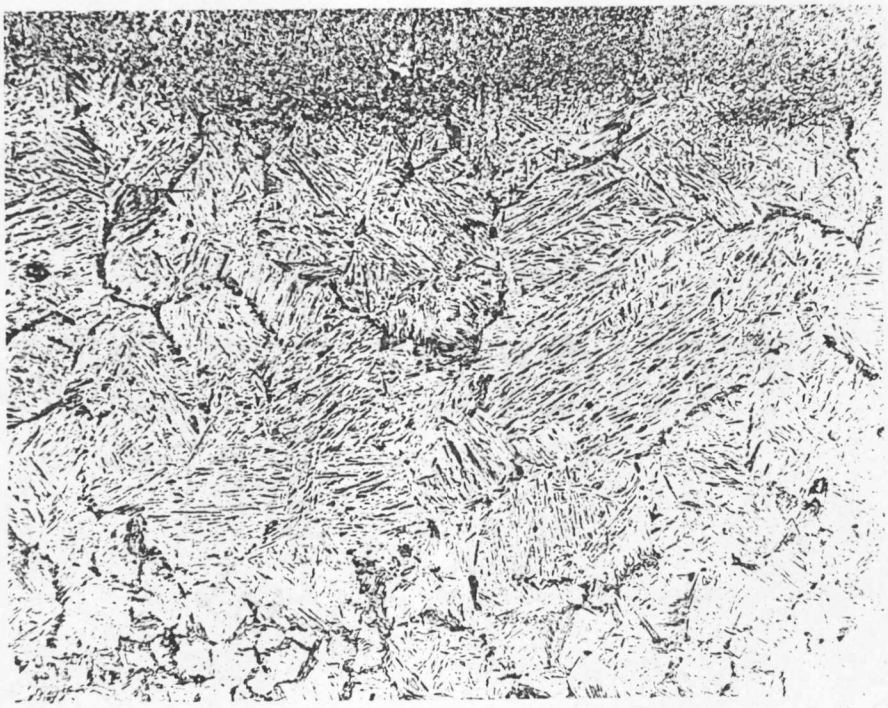


Figure 40. Microstructure of coarse grained HAZ in C&N C-Mn-Si steel, C.E. = 0.47. UBCT, preheat 100°F. Picral etch, OLM, 200X.

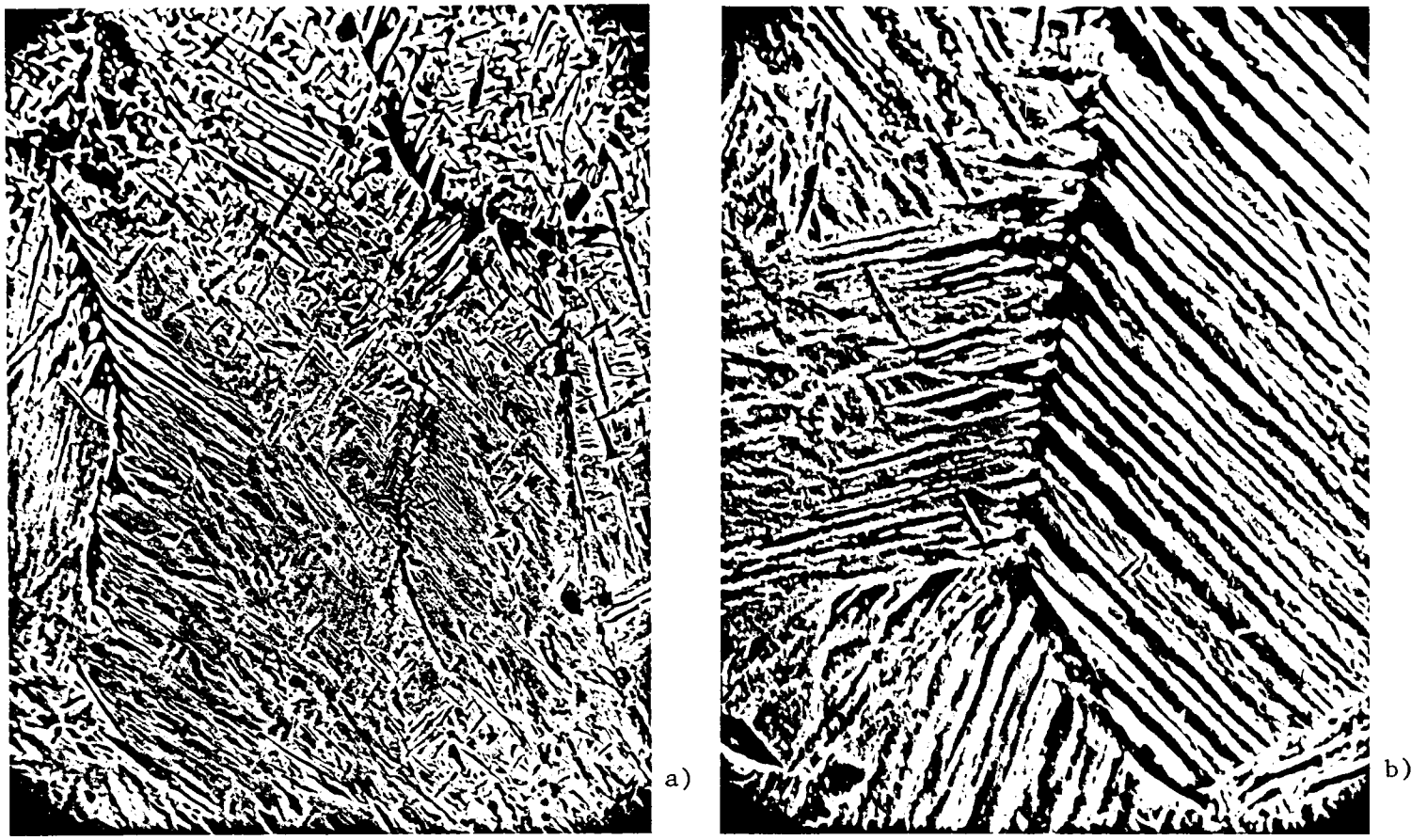


Figure 41. SEM micrograph of coarse grained HAZ in C&N C-Mn-Si steel, C.E. = 0.47. UBCT, preheat 100°F. 2% Nital etch, SEM, a) 1000X, b) 5000X. (See Figure 40)

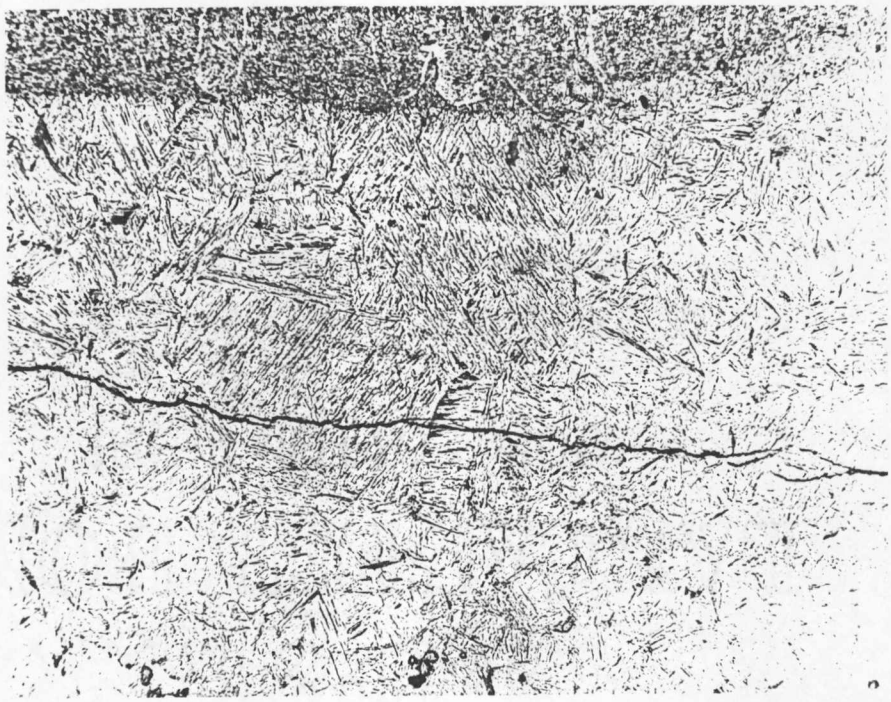
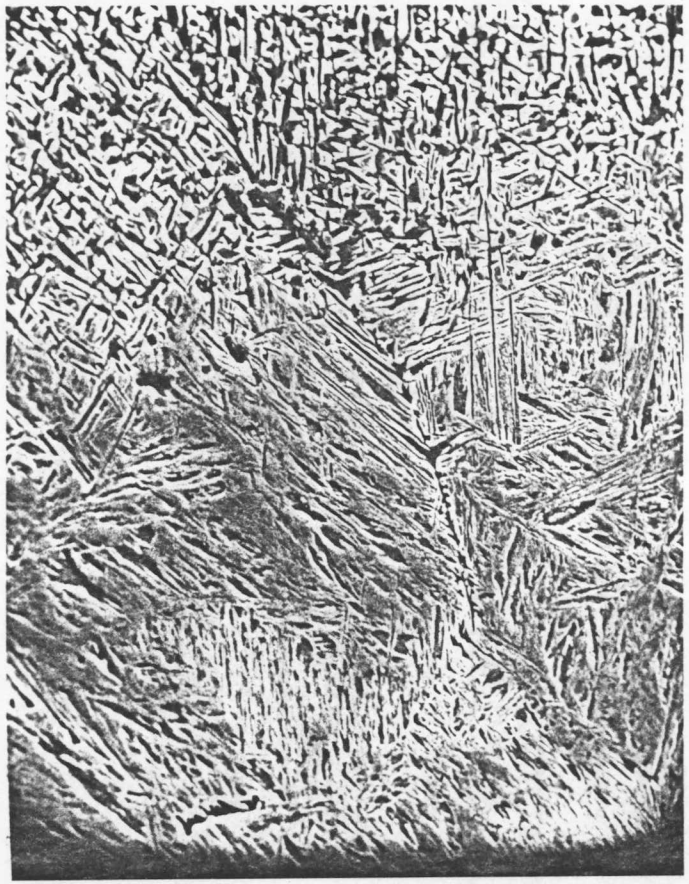


Figure 42. Microstructure of coarse grained HAZ in C&N C-Mn-Si steel, C.E. = 0.58. UBCT, preheat 100°F. Picral etch, OLM, 200X.



a)



b)

Figure 43. SEM micrograph of coarse grained HAZ in C&N C-Mn-Si steel, C.E. = 0.58. UBCT, preheat 100°F. 2% Nital etch, SEM, a) 1000X, b) 5000X. (See Figure 42)

comparisons were made between the steels just discussed. Standard Jominy end quench hardenabilities of the eight C&N C-Mn-Si steels (Table 4, page 87) are compared in Figure 44. These hardenabilities fall into bands which have been labeled with the appropriate preheats required to prevent cracking under high-hydrogen conditions (E 6010 electrodes). It is clear that standard hardenability test data can be reasonably utilized to evaluate relative HIC susceptibilities. This is not surprising, since the abscissa of a hardenability plot directly reflects cooling rate in the weld HAZ as a function of the energy input and preheat temperature. As has been mentioned earlier, the hardenability concept has been utilized by many[24,43] to select preheat temperatures to avoid HIC in the HAZ and has been a standard way of initially approaching weldability problems relating to HIC.

With the baseline HIC data for the C&N steels established, the wrought C-Mn-Si and wrought 8630 steels were tested to obtain comparative HIC susceptibilities. Since orientation is a possible variable in wrought steels, tests were conducted with the weld made parallel to a rolled surface in the rolling direction and parallel to the through-thickness direction with the sample thickness extending in the primary rolling direction. These weld orientations are shown in Figure 45 and are labeled as PRD and TTD respectively. The tests conducted by Williams et al.[1] on the wrought steels were only in rolling direction and hence it was necessary to conduct tests TTD to check if the results were influenced by orientation

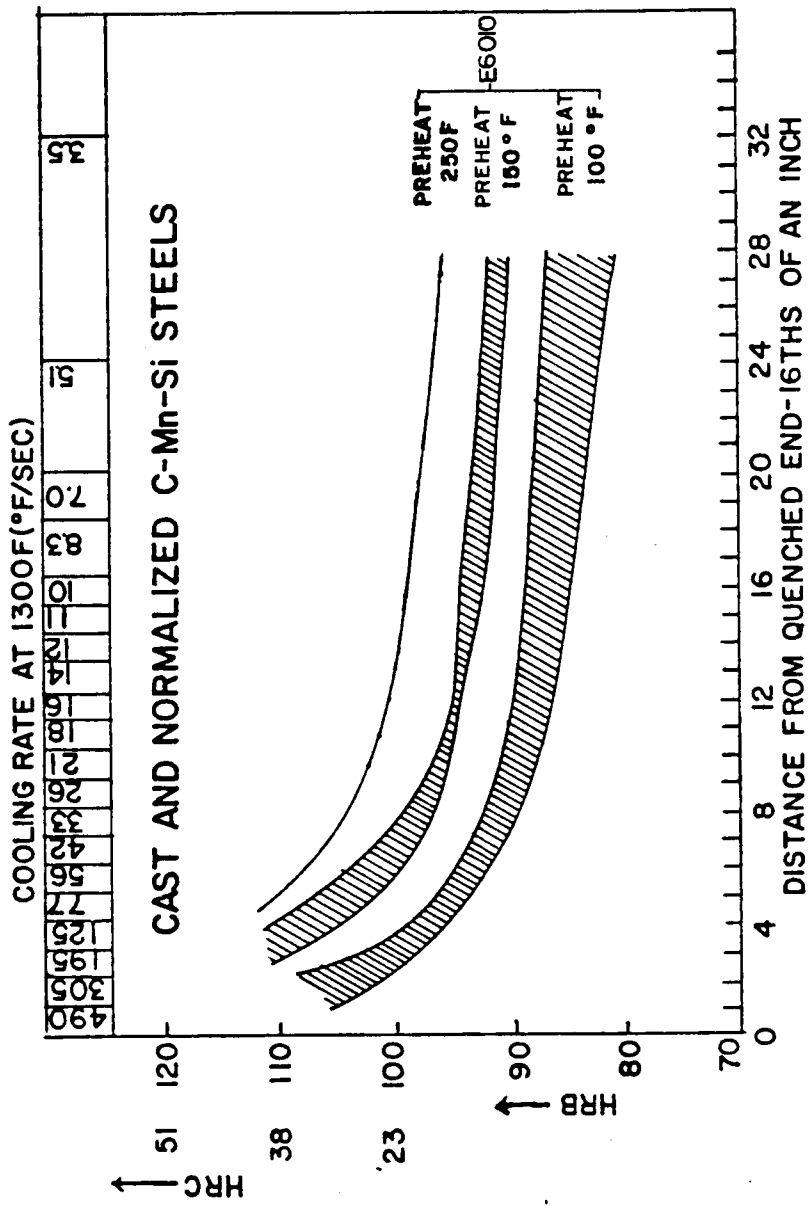


Figure 44. Preheat temperature (UBCT) required to prevent HIC related to Jominy hardenability for cast and normalized (C&N) C-Mn-Si steels. E 6010.

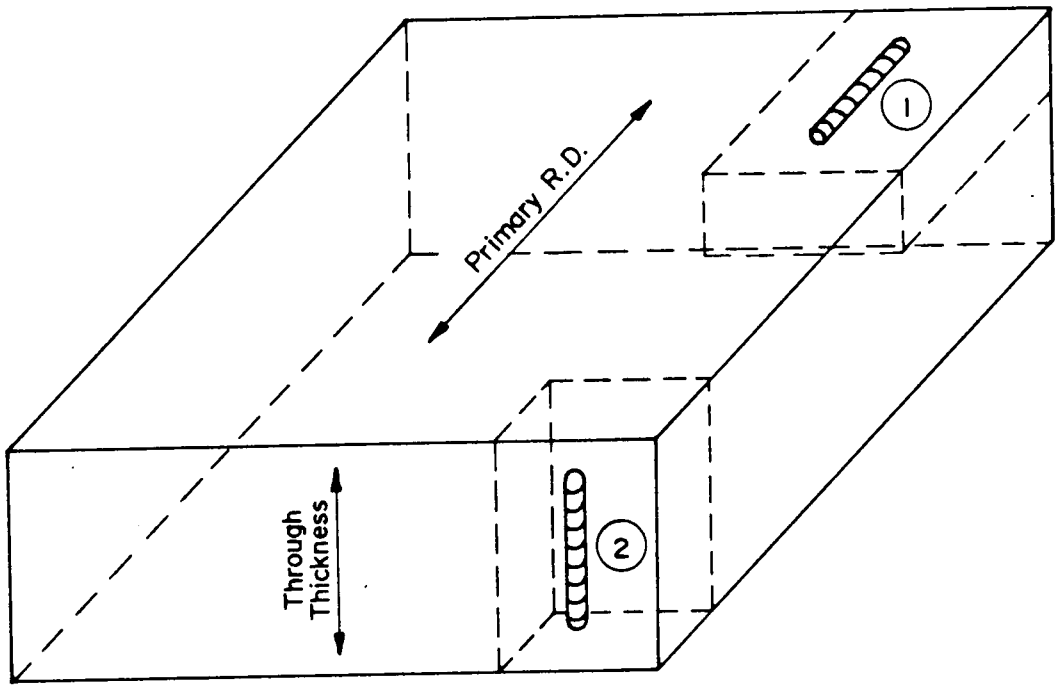


Figure 45. Schematic diagram showing orientation of specimens and welds in wrought plate UBCT samples. 1) PRD, 2) TTD.

effects. It was quickly noted that the orientation effects were very important and help to explain the results of earlier studies as well as this study.

3. Underbead Cracking Tests on Wrought C-Mn-Si Steels

In a manner similar to that for the cast steels, the wrought steels were tested using the UBCT method at 32°F and at preheat intervals of 50°F starting at 100°F, until cracking was eliminated. The results of the tests at 32°F are shown in Figure 46. The solid line in Figure 46 is the line derived from the analysis of the data in Figure 36 (page 124) for the C&N C-Mn-Si steels. It is clear that when the wrought C-Mn-Si and 8630 steels are tested with the weld made PRD, the extent of cracking in the wrought steels far exceeds that for equivalent C&N grades. However, when tested with a weld made TTD, the susceptibility to HIC is very nearly the same as that revealed for the C&N steels. These data clearly indicate an effect of orientation on HIC. Similar results were obtained when the tests were repeated using a preheat of 100°F. The solid line in Figure 47 represents the line drawn from the analysis of the data in Figure 37 (page 125) for C&N C-Mn-Si steels. The wrought steels tested PRD cracked to a greater extent than their C&N equivalents, whereas when these same steels were tested in the TTD, they cracked to an extent equivalent to the cast steels. At a preheat temperature of 150°F, cracking was prevented in all the wrought steels tested in the TTD excepting the wrought C-Mn-Si steel with the highest C.E. (0.68). At a 150°F preheat temperature, for the samples

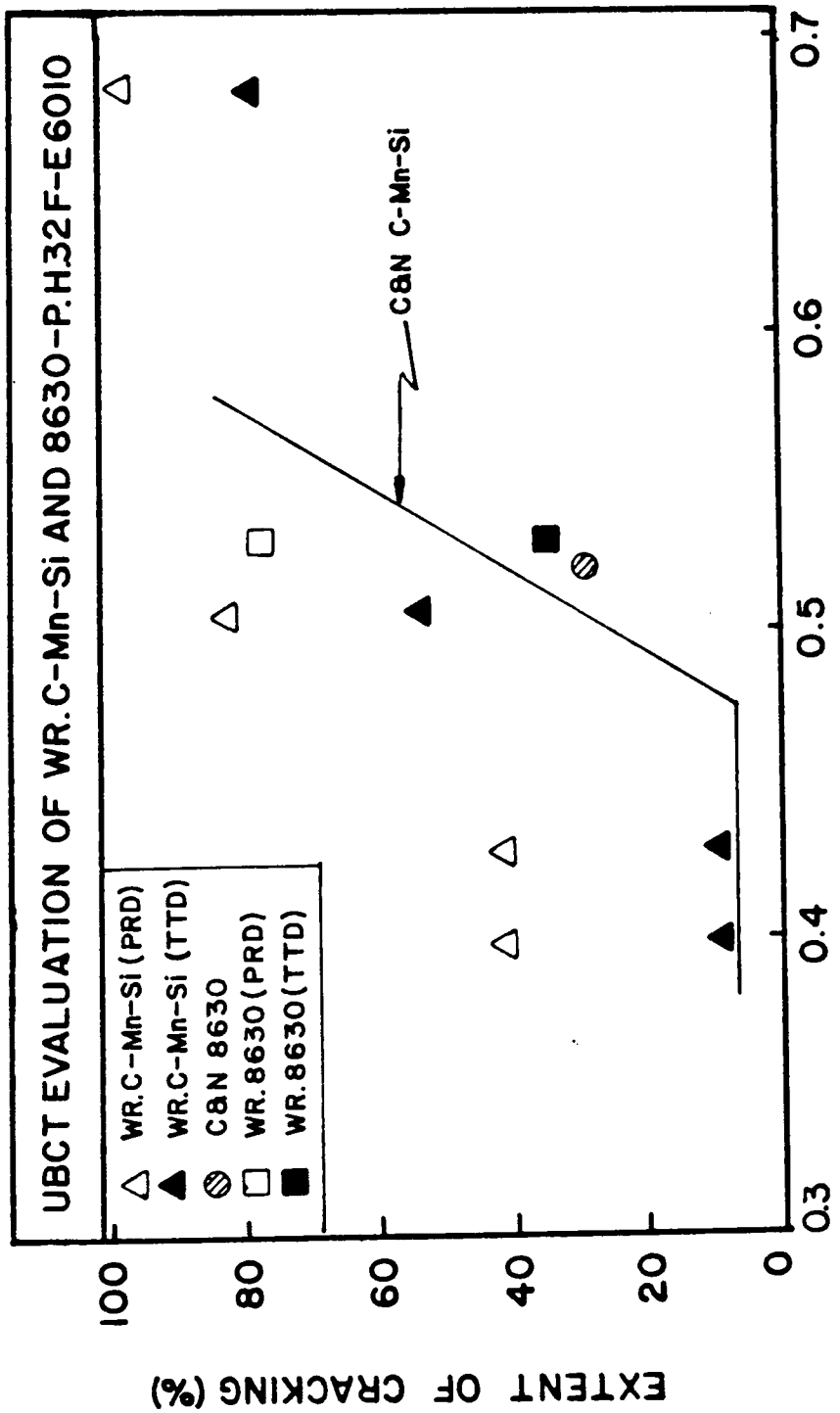


Figure 46. Extent of HIC at 32°F in wrought (WR) C-Mn-Si and 8630 steels compared to that in equivalent cast and normalized (C&N) C-Mn-Si steels (average line). UBCT, E 6010.

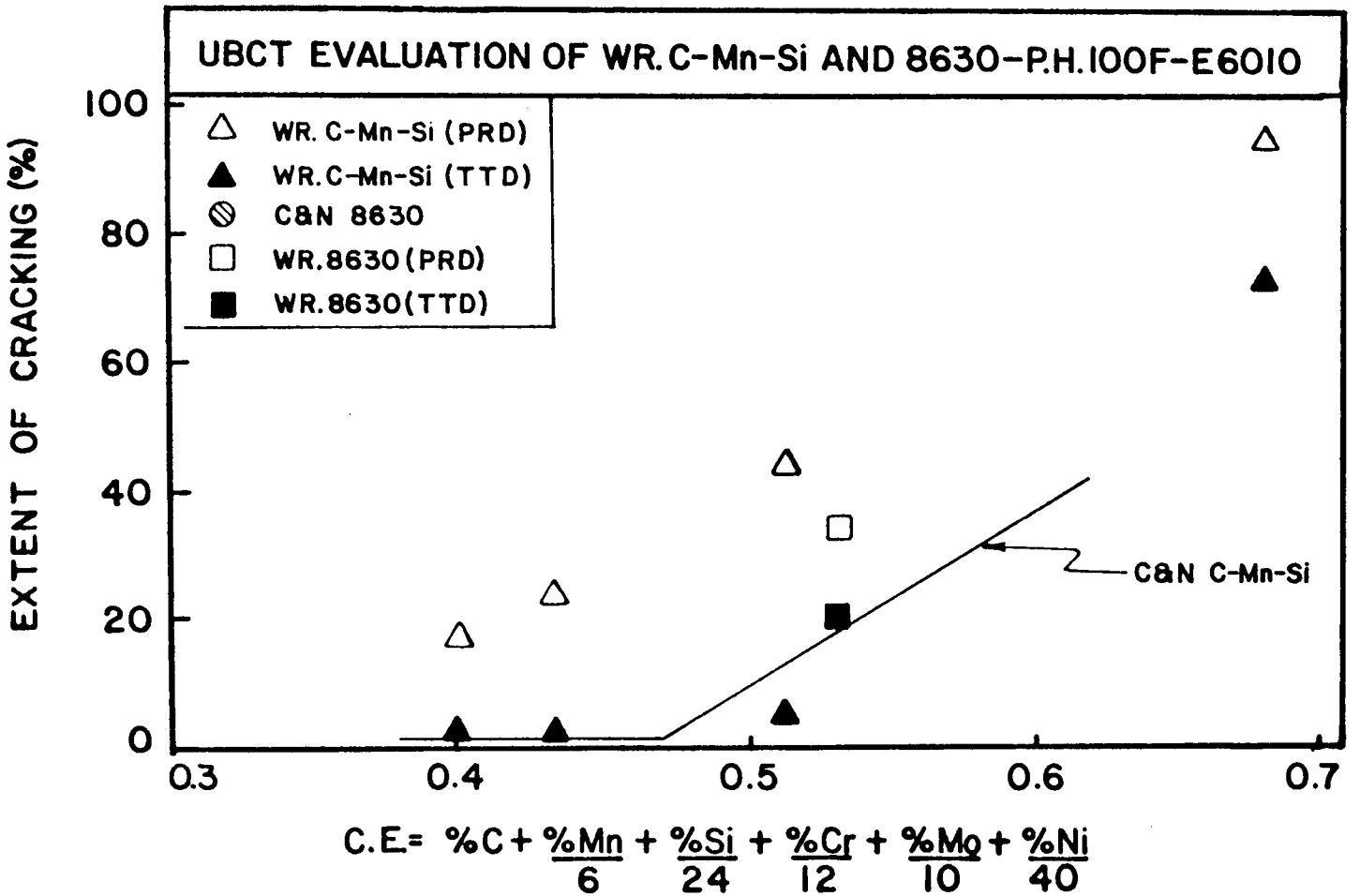


Figure 47. Extent of HIC at 100°F in wrought (WR) C-Mn-Si and 8630 steels compared to that in equivalent cast and normalized (C&N) C-Mn-Si steels (average line). UBCT, E 6010.

test welded PRD, cracking persisted in the wrought C-Mn-Si steels at C.E.'s of 0.51 and 0.68 as well as in the wrought 8630. Increasing the preheat temperature to 200°F eliminated cracking in the wrought C-Mn-Si steel (C.E.=0.51) tested with welds PRD and at a preheat of 250°F, cracking was eliminated in the wrought 8630 test welded PRD as well as the highest C.E. wrought C-Mn-Si steel test welded TTD. A preheat of 350°F was required to prevent cracking in the highest C.E. wrought steel test welded PRD. From these additional results, it is clear that wrought steels test welded PRD are more susceptible to HIC than equivalent C&N steels, whereas when test welded TTD, the susceptibilities of the wrought steels is nearly equivalent to that of their C&N counterparts. The results of the tests on the wrought steels with welds made in the PRD and TTD are compared to that for the C&N steels in Figures 48 and 49 respectively as the preheat temperature required to prevent cracking in the UBCT vs. the C.E. The lines drawn in the figures represent average trends for the C&N steels. The results indicate that wrought C-Mn-Si steels test welded PRD require higher preheat temperatures to avoid HIC when compared to equivalent composition C&N C-Mn-Si steels. When the same wrought steels are test welded TTD, the preheat temperatures required to prevent HIC for the wrought and equivalent C&N C-Mn-Si steels are comparable.

Correlation of HIC susceptibility with maximum HAZ hardness. Since the susceptibility to HIC is dependent to a large extent on the microstructure (amount of martensite) in the coarse grained

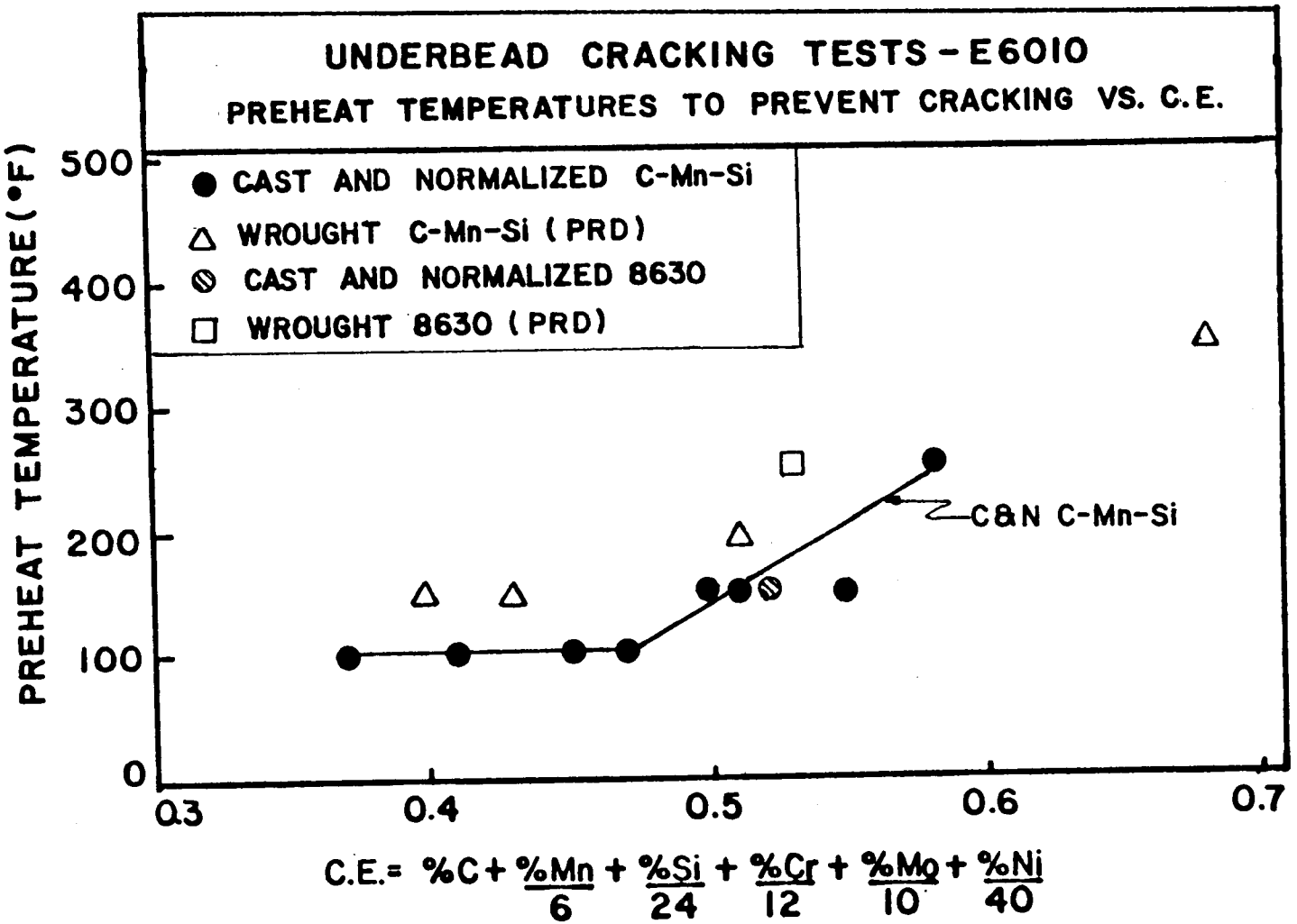


Figure 48. Preheat temperatures required to prevent HIC in cast and normalized C-Mn-Si and wrought C-Mn-Si (PRD) steels as determined in the UBCT. E 6010.

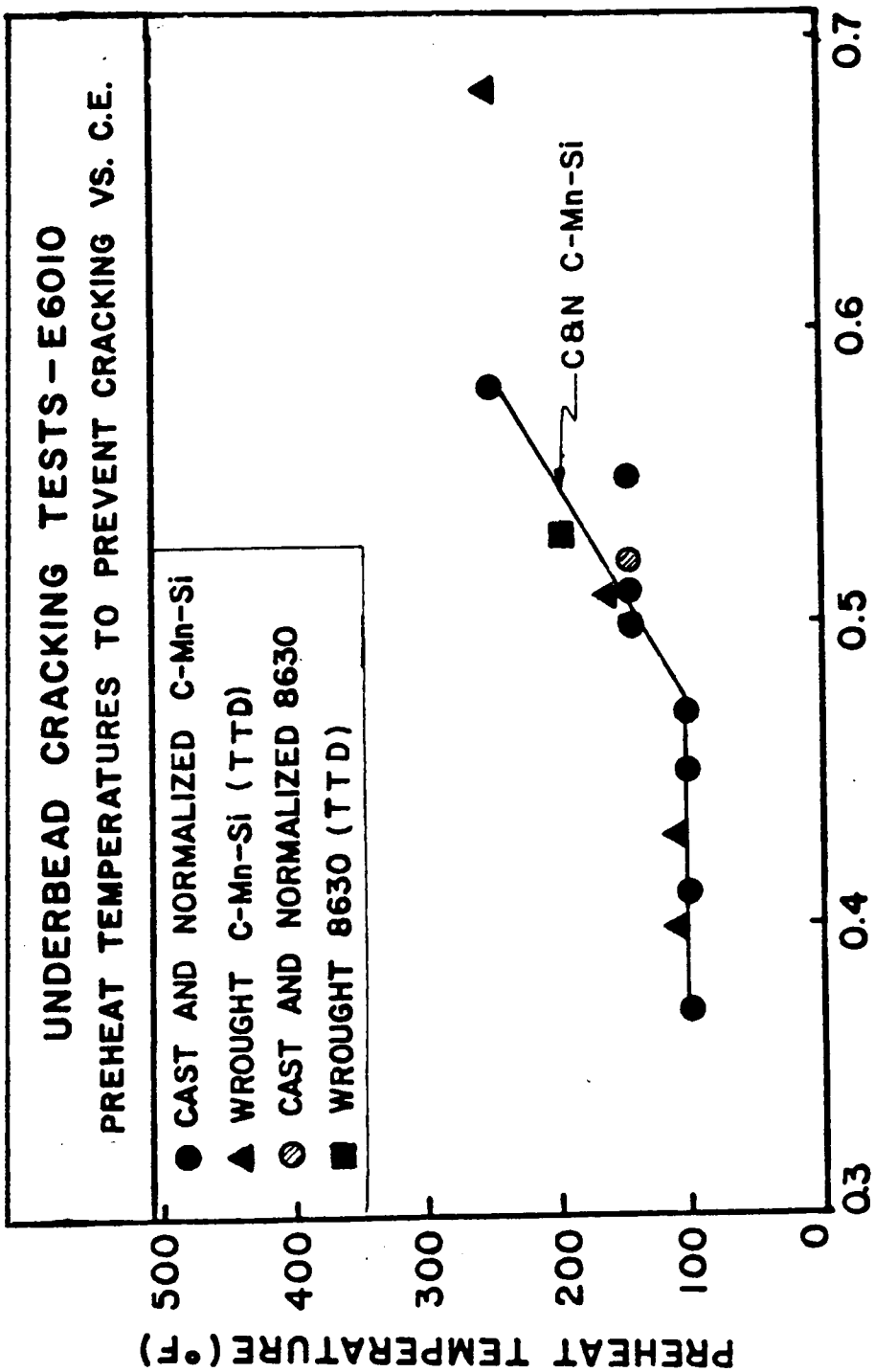


Figure 49. Preheat temperature required to prevent HIC in cast and normalized C-Mn-Si and wrought C-Mn-Si (TTD) steels as determined in the UBCT. E 6010.

HAZ, microhardness measurements were made in the HAZ of representative cast and wrought UBCT specimens. The microhardness tests were conducted in the HAZ of the UBCT samples tested at 32°F and 100°F. The hardness measurements utilized the DPH scale with a Tukon tester at a 5Kg load. The DPH values have been converted to the Rockwell C scale (HRC). The maximum HAZ hardness for the UBCT samples test welded at 32°F is shown in Figure 50. The maximum HAZ hardness corresponds with that predicted by the C.E. of the steels. Steels with higher susceptibilities to cracking had higher HAZ hardnesses. The maximum HAZ hardness of the C&N steels can be estimated from the equation which represents the line shown in Figure 50.

Maximum HAZ hardness: HRC = 60*(C.E.)+22

The maximum HAZ hardness attained in the HAZ of wrought C-Mn-Si steels is almost identical to that measured in the HAZ of C&N C-Mn-Si steels, at comparable C.E.'s. A similar observation was made for the C&N and wrought 8630. Hence, the maximum HAZ hardness cannot explain why wrought steels welded PRD are more susceptible to HIC than comparable C&N steels. Hardness surveys carried out in the HAZ of UBCT samples welded at 100°F showed that this modest preheat did not have any effect upon the maximum HAZ hardness. This is not surprising since the HAZ hardness is governed by the cooling rate which is not affected to a great extent with a preheat of 100°F. The data at 100°F also indicate a similar trend in that the maximum HAZ hardness was found to be a function of the C.E. and this hardness can be predicted by an equation of the type indicated earlier. It

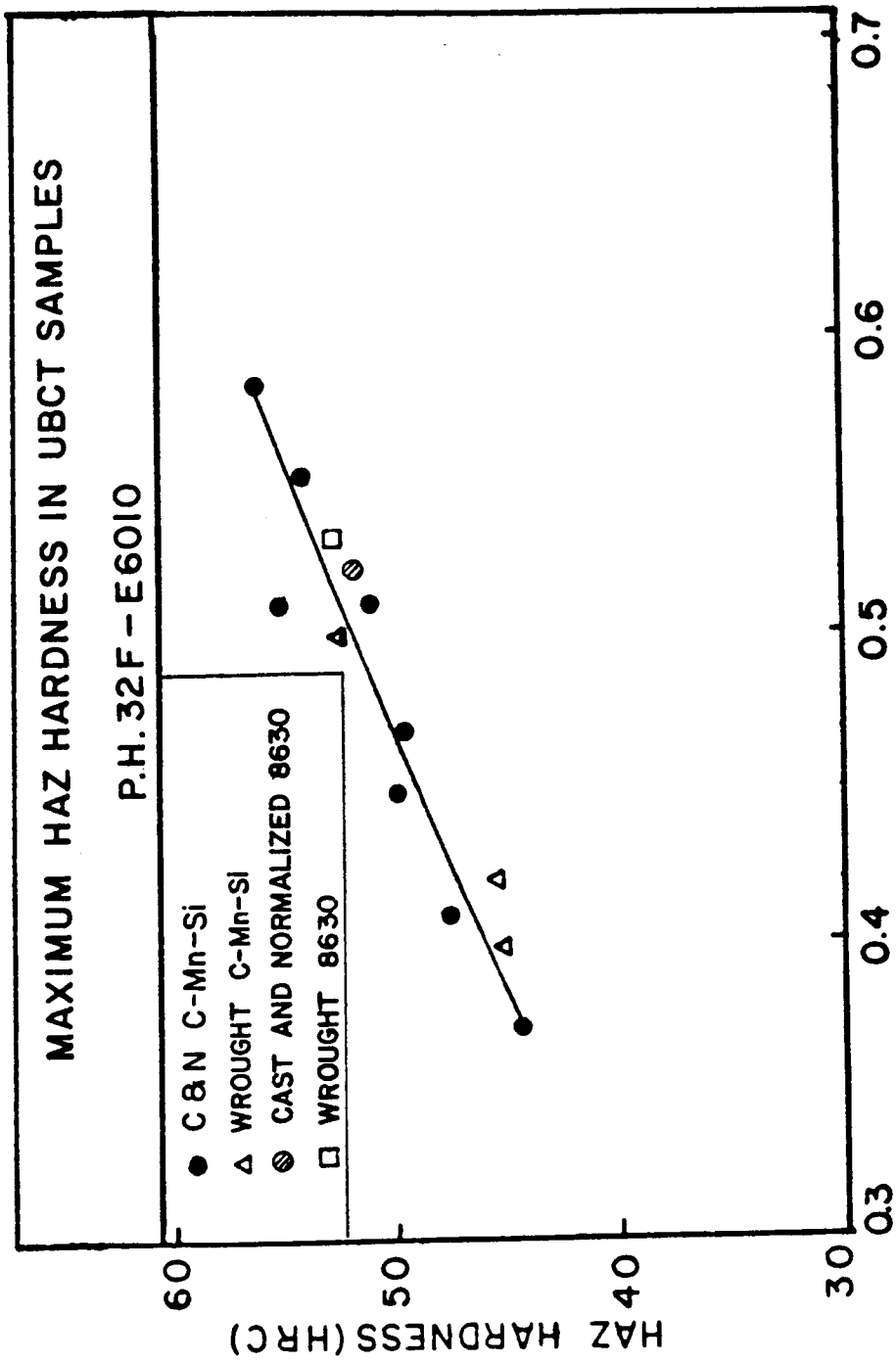


Figure 50. Maximum hardness of coarse grained HAZ in C-Mn-Si and 8630 steels tested in the UBCT. Preheat 32°F, E 6010.

is therefore clear that the higher susceptibilities of the wrought steels to HIC when tested PRD cannot be explained using a criterion involving the maximum hardness in the HAZ.

Metallographic examination. Metallographic examination was undertaken to define the association of the cracks with particular features of the microstructure. The SEM was employed to determine the fracture morphology of the crack interfaces broken open for evaluation. Micrographs of wrought C-Mn-Si steel (C.E.=0.43) test welded PRD and test welded in the TTD at a temperature of 100°F are shown in Figures 51a and b. It is clear that in the sample welded PRD, the cracks present run parallel to the fusion line, whereas for the sample test welded in the TTD, no cracks were found. At a higher magnification (Figure 52), the cracks in the sample welded PRD are clearly seen to be associated with the elongated non-metallic inclusions in the steel. At a still higher magnification, the SEM photomicrograph in Figure 53a shows the association of the underbead cracks to an inclusion. The EDAX analysis on the inclusion in Figure 53b shows it to be of the MnS type. In addition to the association of the underbead cracks with inclusions in the coarse grained HAZ, cracks were also found to be associated with inclusions/banding in other regions of the HAZ, such as in the partially refined region. An example typical of this morphology is shown in Figure 54a and at a higher magnification in the SEM micrograph in Figure 54b. The presence of extensive sulfide inclusions and the high hardenability of the wrought C-Mn-Si steel with a

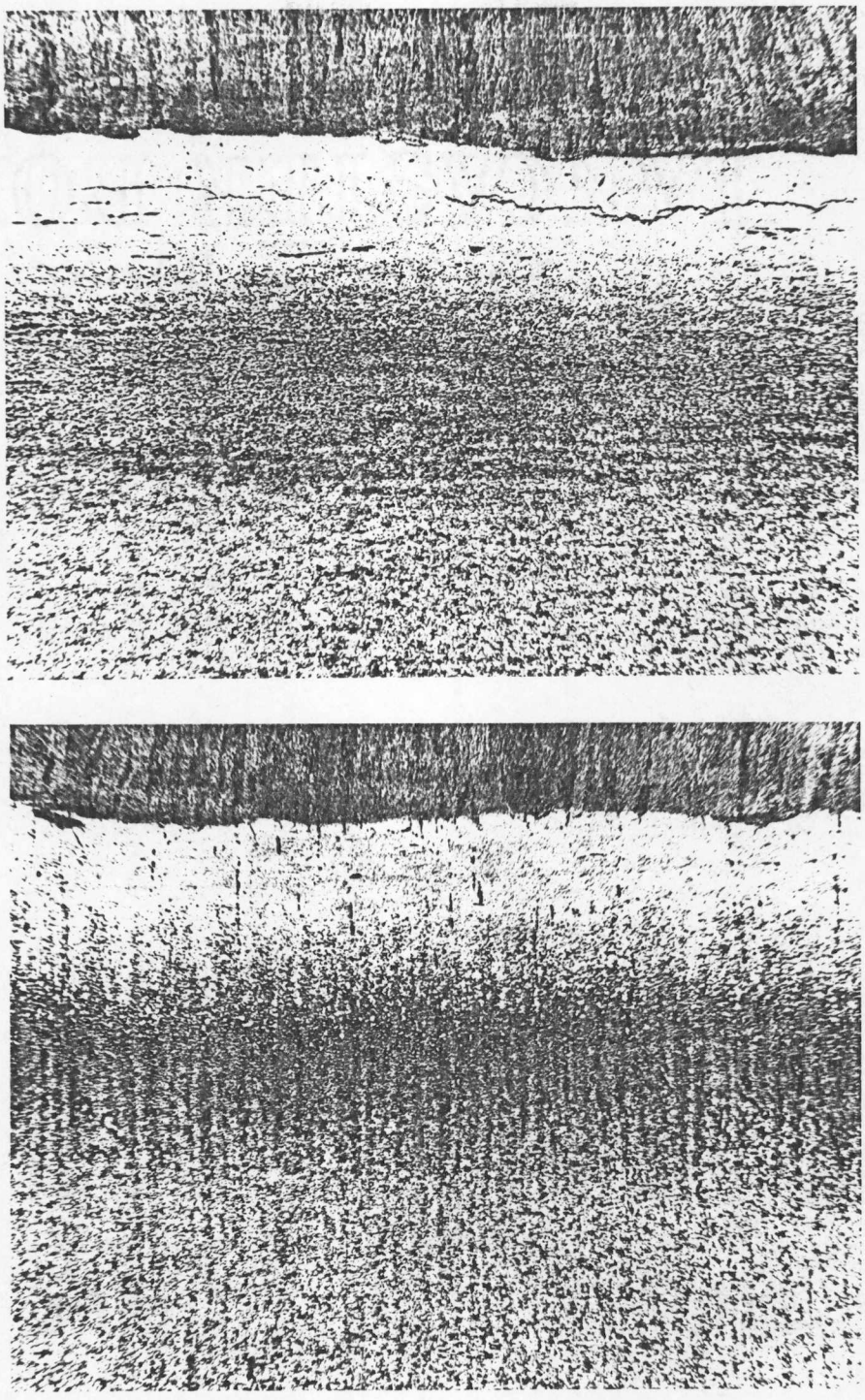


Figure 51. Macrographs of wrought C-Mn-Si steel, A516-70, C.E. = 0.43 tested a) PRD and b) TTD in the UBCT. Note HIC in the sample tested PRD. Preheat 100°F. Picral etch, OLM, 20X.

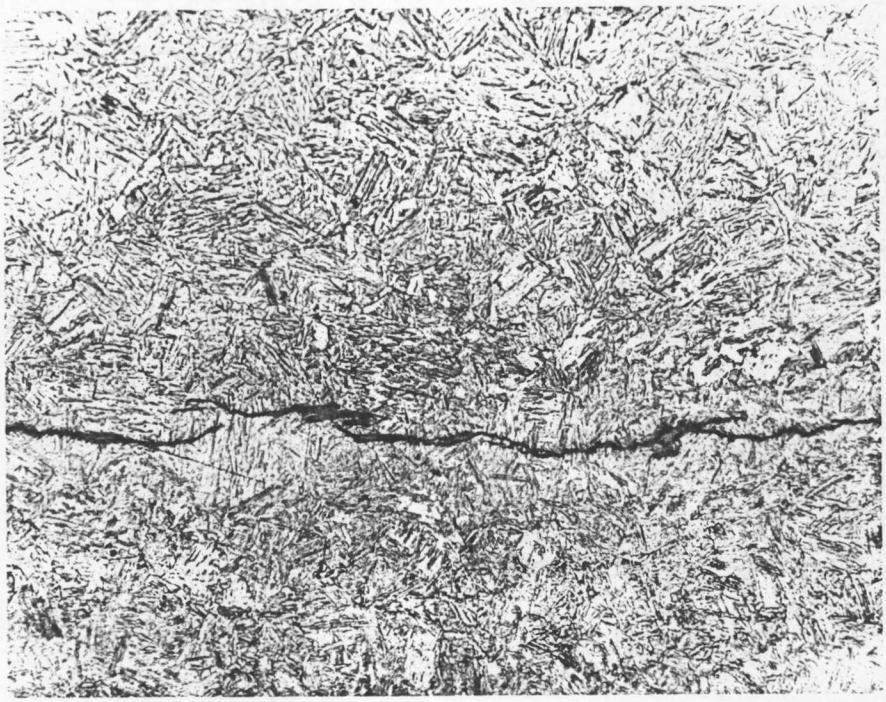
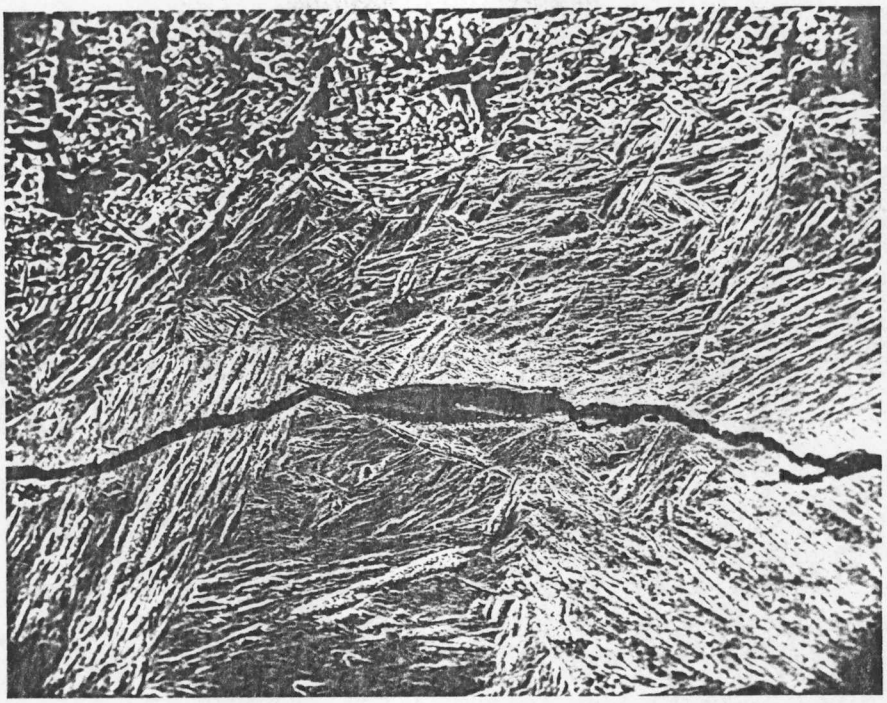
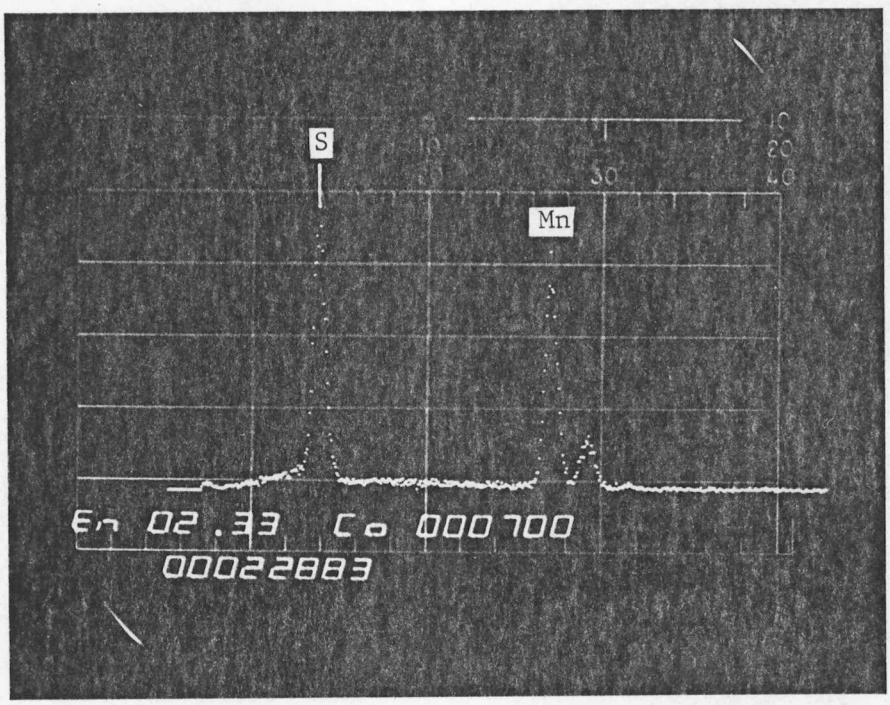


Figure 52. Microstructure of coarse grained HAZ in wrought C-Mn-Si steel, A516-70, C.E. = 0.43. Tested PRD in the UBCT, HIC association with MnS inclusion, preheat 100°F. Vilella's etch, OLM, 250X. (See Figure 51a)



a)



b)

Figure 53. Coarse grained HAZ in wrought C-Mn-Si steel, A516-70, C.E. = 0.43, showing HIC association with MnS inclusions. UBCT sample tested PRD. a) SEM, 1000X, b) EDAX of inclusion. (See Figures 51a and 52)

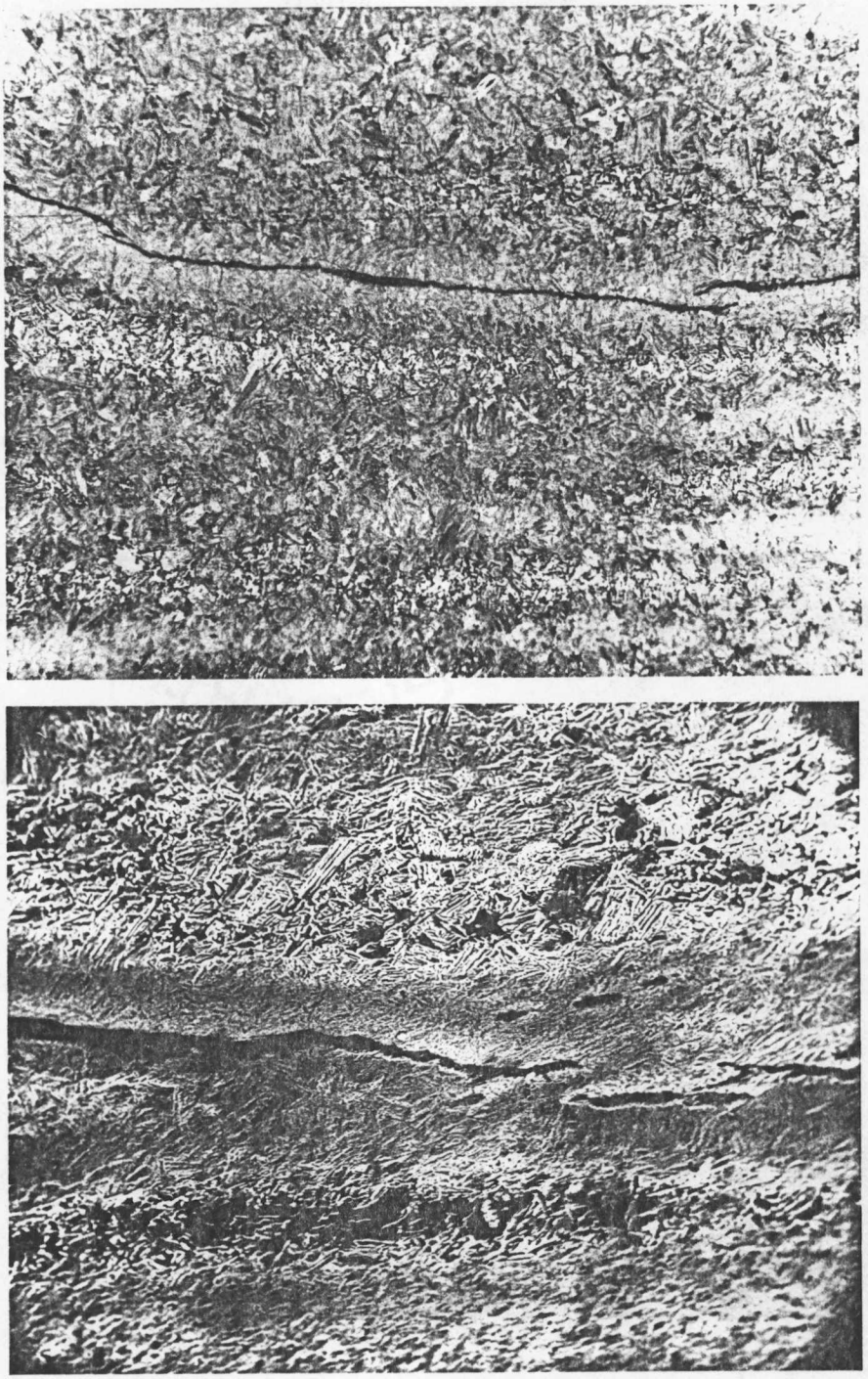


Figure 54. HIC association with inclusions and banding in wrought C-Mn-Si steel, A516-70, C.E. = 0.43. UBCT, PRD, preheat 100°F. a) Picral etch, OLM, 200X, b) Picral etch, SEM, 500X.

C.E.=0.68 make it extremely susceptible to underbead cracking. Cracking in this steel in a region where inclusions/laminations were present in the HAZ is shown in Figure 55. The inclusion/matrix interfaces are associated with the cracks and appear to have decohered and opened. The association of underbead cracks with inclusions was also noted in some instances for the cast steels, as shown in Figure 56. The inclusions are "globular" in morphology and hence are not as potent as crack initiators as are the elongated sulfides in the wrought steels. The SEM fractograph in Figure 57a reveals the presence of inclusion sites on the fracture surface of a UBCT sample of a wrought steel. The fracture morphology adjacent to the crack is quasi-cleavage indicating that cracking occurred in a semi-brittle fashion (Figure 57b). An example of a typical underbead crack surface exhibited in a cast steel is shown in Figure 58 and the fracture surface adjacent to the inclusion reveals both cleavage and quasi-cleavage morphologies.

The conclusion that can be drawn from the metallographic and fractographic examinations is that wrought steels are rendered more susceptible to HIC than equivalent C&N steels when welded PRD due to the elongated sulfide inclusions present in them. The inclusions act as sites for the buildup of hydrogen and when inclusions have sharp asperities, the probability for crack initiation is enhanced. In addition, banding also provides a continuous path for crack propagation. When welds are performed in the through-thickness direction, the inclusions traverse away from the fusion line, from

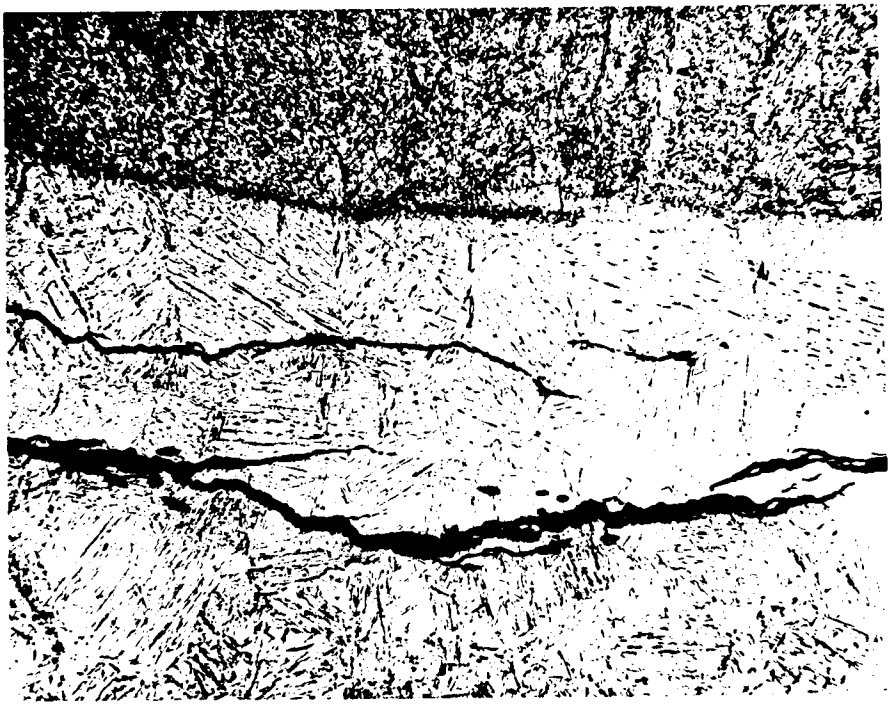


Figure 55. HIC association with inclusions in coarse grained HAZ of wrought C-Mn-Si steel, A299, C.E. = 0.68. UBCT, PRD, preheat 100°F. Picral etch, OLM, 200X.

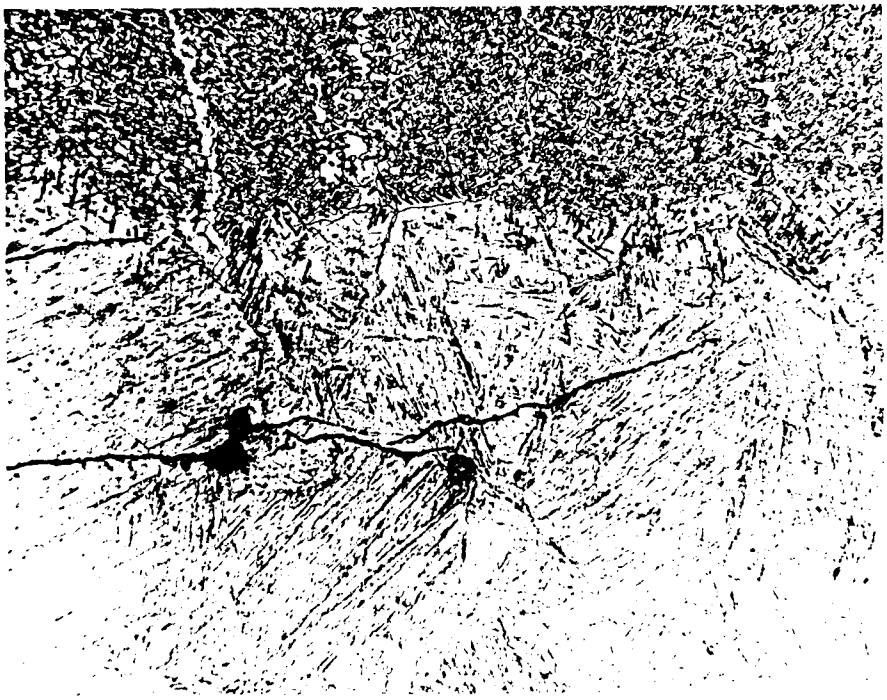


Figure 56. HIC associated with Type III inclusions in coarse grained HAZ of C&N C-Mn-Si steel, C.E. = 0.55. UBCT, preheat 100°F. Picral etch, OLM, 200X.

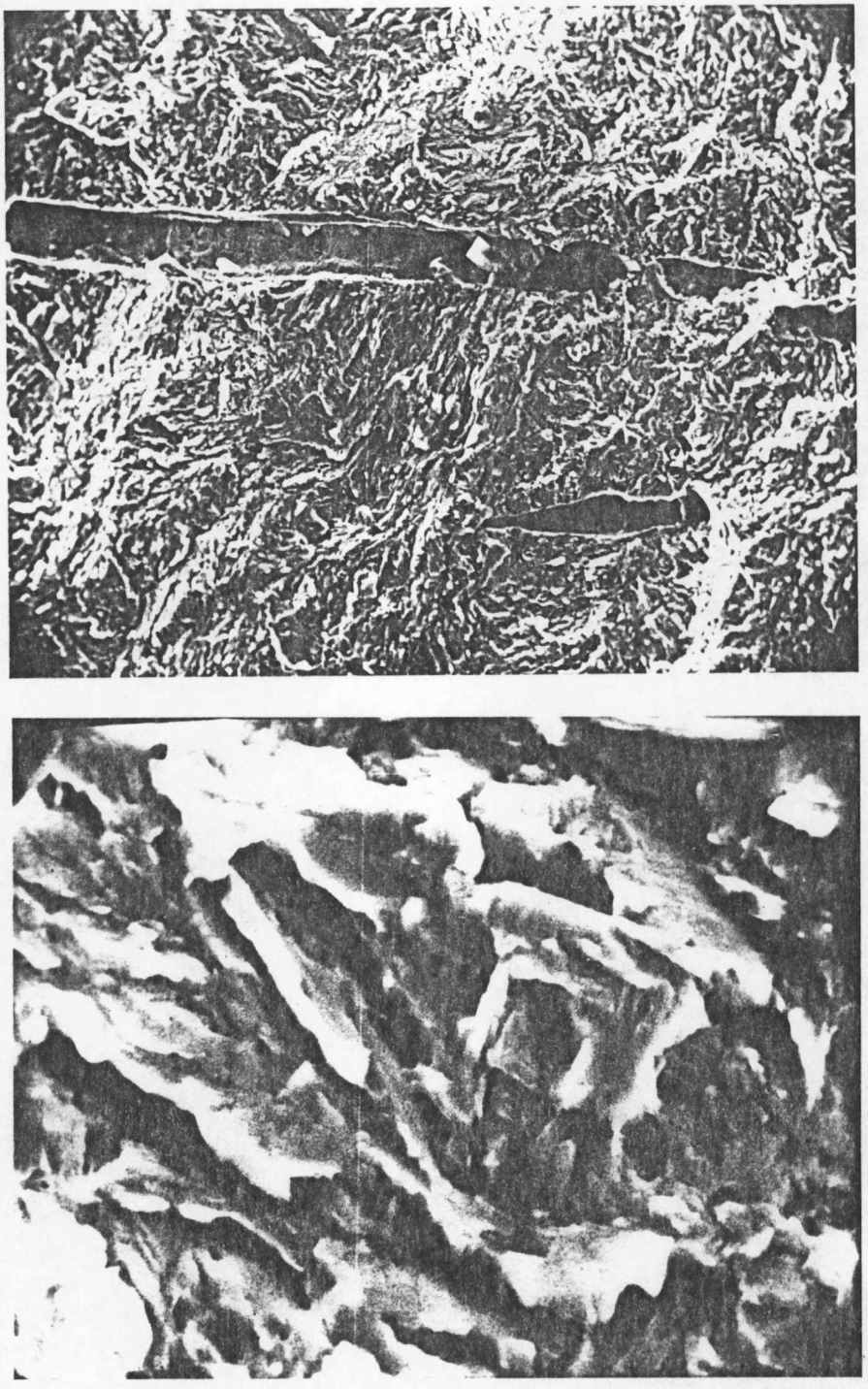


Figure 57. Fracture morphology of HIC in wrought C-Mn-Si steel, A516-70, C.E. = 0.43. UBCT, preheat 100°F. a) Inclusion sites on crack surface. b) Quasi-cleavage fracture morphology. SEM, 5000X.

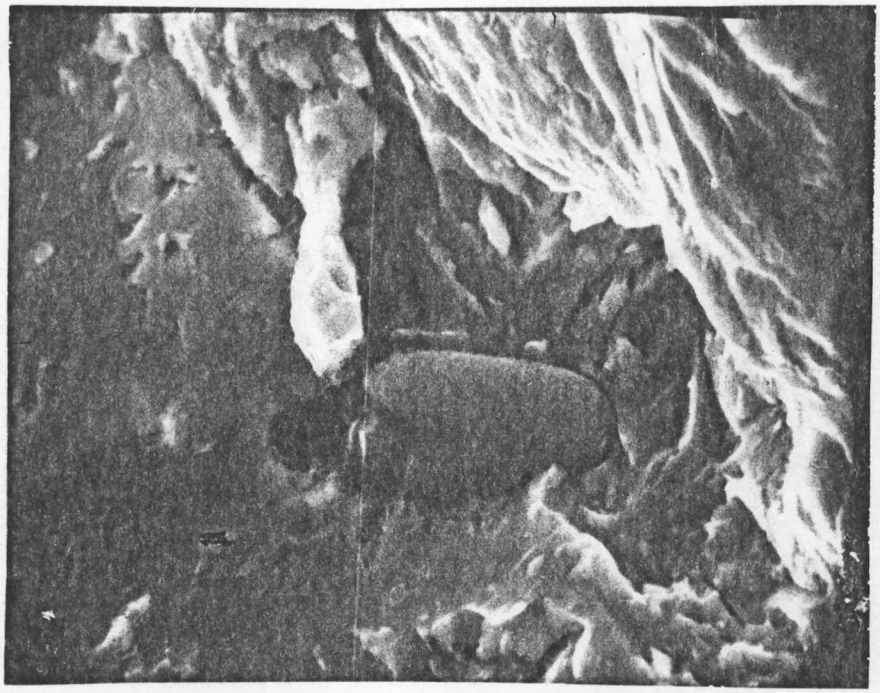


Figure 58. Fracture morphology of HIC in C&N C-Mn-Si steel, C.E. = 0.58. UBCT, preheat 100°F. SEM, 5000X.

the hard martensitic regions to softer non-martensitic regions. Further, the inclusions can act as short circuit diffusion paths for hydrogen, diffusing it away from the martensitic coarse grained HAZ, thus reducing the hydrogen concentration. Also banding does not provide an easy path for crack propagation. The reasons for orientation effects on HIC are also related to the state of residual stress developed in the HAZ of a UBCT sample and are detailed below.

State of stress in the UBCT sample. It has been mentioned that the presence of a stress acting on the HAZ is a necessary factor for HIC to occur. In an UBCT sample, the stress acting on the HAZ is that developed due to the self-restraint of the test block, which translates into residual stresses in the longitudinal, transverse and short-transverse directions. The residual stresses generated in a bead-on-plate weld can be approximated to those occurring in a butt weld. Schematic views of the longitudinal, transverse and short-transverse residual stresses in a butt weld are shown in Figures 59b, c and d respectively. The longitudinal stress (σ_x) possesses a high tensile magnitude in the region near the weld, and rapidly drops off and becomes compressive at a distance several times the width of the weld. The width of the tension zone 'b' and the maximum value of the tensile residual stress (σ_m) are parameters relevant to the hydrogen-induced cracking susceptibility of the coarse grained HAZ. The larger these quantities, the greater will be the probability of HIC. In welds performed on low carbon steel, the maximum residual stress, σ_m, is usually as high as the

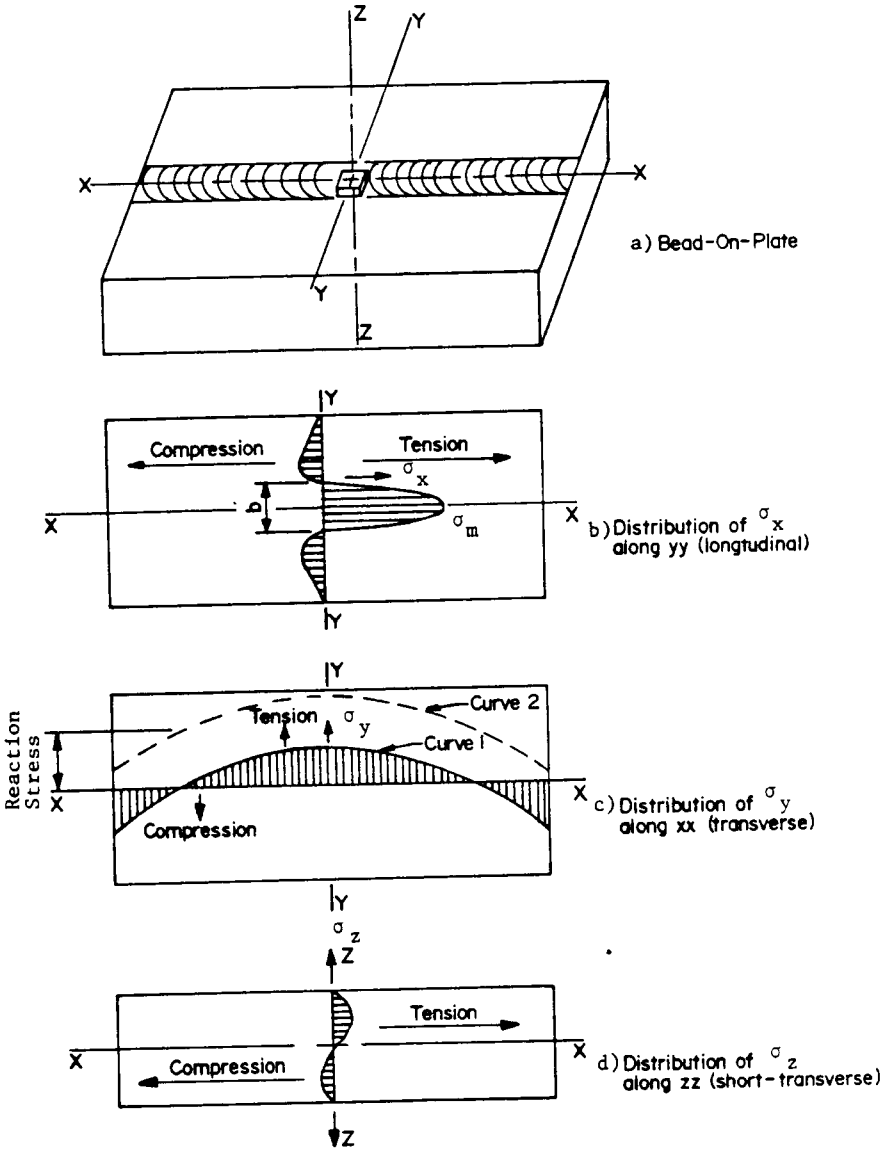


Figure 59. Schematic representation of residual stress distribution in a bead-on-plate weld. a) Bead-on-plate weld, b) longitudinal, c) transverse and d) short-transverse stress distributions.

Source: a), b), c) Welding Handbook, Vol. 1, Seventh Edition (1976). d) Private communication, Ed Rybicki, Dec. 1983.

yield stress of the weld metal.[86] The distribution of the transverse residual stress, σ_y, is shown in Figure 59c. Curve 1 shows the distribution of the transverse stress along the length of the weld. Tensile stresses of low magnitude develop at the middle of the joint and compressive stresses at the end of the joint. In the case where lateral contraction is restrained, curve 2 represents the state of stress with an addition of a reaction stress. A schematic representation of the short transverse stress, σ_z, (Figure 59d) shows that the residual stress in the short-transverse direction is tensile in the regions near the weld and is compressive near regions opposite to the face on which the weld is made. It is therefore clear that the residual stresses, σ_x, σ_y and σ_z are all tensile in nature close to the region encompassing the coarse grained HAZ. However, the short transverse stresses, σ_z, can be expected to have a predominant effect on the extent of cracking in the UBCT, since the longitudinal and transverse stresses and are confined to regions very close to the surface plane of the weld. The significance of inclusion and banding orientation can now be explained. When the UBCT samples are test welded PRD, σ_z acts normal to the plane of the inclusions and banding and therefore aids the nucleation and propagation of HIC. In the case when the welds are performed TTD, the inclusions and banding lie in the plane of σ_z and therefore are not oriented favorably to cause the nucleation and propagation of HIC.

The deleterious influence of elongated inclusions in influencing HIC in HAZ's has been reported by Baillie[61] and Savage[62] in weldability tests on wrought steels. An elongated inclusion may initiate a crack at a preheat temperature where a "globular" inclusion might be harmless. Asperities of elongated inclusions in wrought steels act as more potent stress concentrators than the "globular" inclusions in cast steels. In addition, a larger area of incoherent inclusion/matrix interface exists in the wrought steels compared to that in the cast steels, thus enabling the hydrogen concentration to build up to that required for HIC to occur.

Since these results emphasize the importance of inclusion distribution and morphology in affecting HIC, quantitative analysis of the inclusion content was carried out to take into account the effect of this variable. Direct volume/area fraction comparisons using line intercept or point count techniques were found to be unsuitable for a comparative evaluation of the inclusion content, since the morphologies in the cast and wrought steels are vastly different. It was therefore decided to use standard rating techniques outlined in the ASTM Standard E45 (recommended practice for determining inclusion content). Examination for non-metallic inclusions was carried out using Method A of the standard. The examination for inclusion content was carried out close to the region of cracking in the HAZ's and many of the metallographic samples for the inclusion analysis were extracted from the underbead cracking test coupons. The results obtained are detailed in Table 11. These results are based on an average of six specimens

Table 11. Average worst-field inclusion ratings for cast and normalized and wrought C-Mn-Si and 8630 steels tested in Phase I.

Steel	Type A		Type B		Type C		Type D	
	Thin	Heavy	Thin	Heavy	Thin	Heavy	Thin	Heavy
C&N C-Mn-Si								
C.E.=0.37	0	0	1	0	0	0	2	0
0.41	0	0	0	0	0	0	3	0
0.45	0	0	1	0	0	0	2	0
0.47	0	0	0	0	0	0	3	0
0.50	0	0	0	0	0	0	2	0
0.51	0	0	1	0	0	0	3	0
0.55	0	0	0	0	0	0	3	0
0.58	0	0	0	0	0	0	2	0
Wrought C-Mn-Si								
C.E.=0.40	2	1	0	0	1	0	0	0
0.43	2	0	0	0	2	0	0	0
0.51	2	2	0	0	0	2	0	0
0.68	2	0	2	0	0	0	0	0
C&N 8630	0	0	0	0	0	0	3	0
Wrought 8630	2	1	0	0	1	0	0	0

from each of the steels. It is clear that the inclusion ratings for the cast steels are quite similar with a Type D (globular) rating of 2 or 3. This similarity is not surprising since the sulfur contents of the cast steels are similar, ranging between 0.015 and 0.020%. Within the wrought steels, the inclusion ratings are almost similar with the ratings distributed between Type A (elongated sulfides) and Type C (elongated silicates). It is relevant to mention here that the Type D inclusion rating for the cast steels encompasses sulfides, oxides as well as silicates since it was not possible to distinguish between these types of inclusions at the magnification for which the evaluation is specified (100X). On the other hand, in the wrought steels, the silicates can be distinguished because of their larger length/width aspect ratio compared to that of the sulfides and their dark appearance compared to the dove grey appearance of the sulfide inclusions. Based on the inclusion ratings shown in Table 11, it can be qualitatively stated that the volume fraction of inclusions in the cast and wrought steels is equivalent (inclusion rating 2-3). Representative photomicrographs of the inclusions typical of the cast and wrought steels are shown in Figures 60a and b respectively.

The results of the inclusion studies indicate that for identical sulfur contents, the wrought steels possess elongated/stringered inclusion morphologies, whereas the cast steels have a "globular" inclusion morphology. The volume fractions were found to be equivalent. However, the elongated inclusions in the wrought steels render the wrought materials more susceptible to HIC when welded PRD

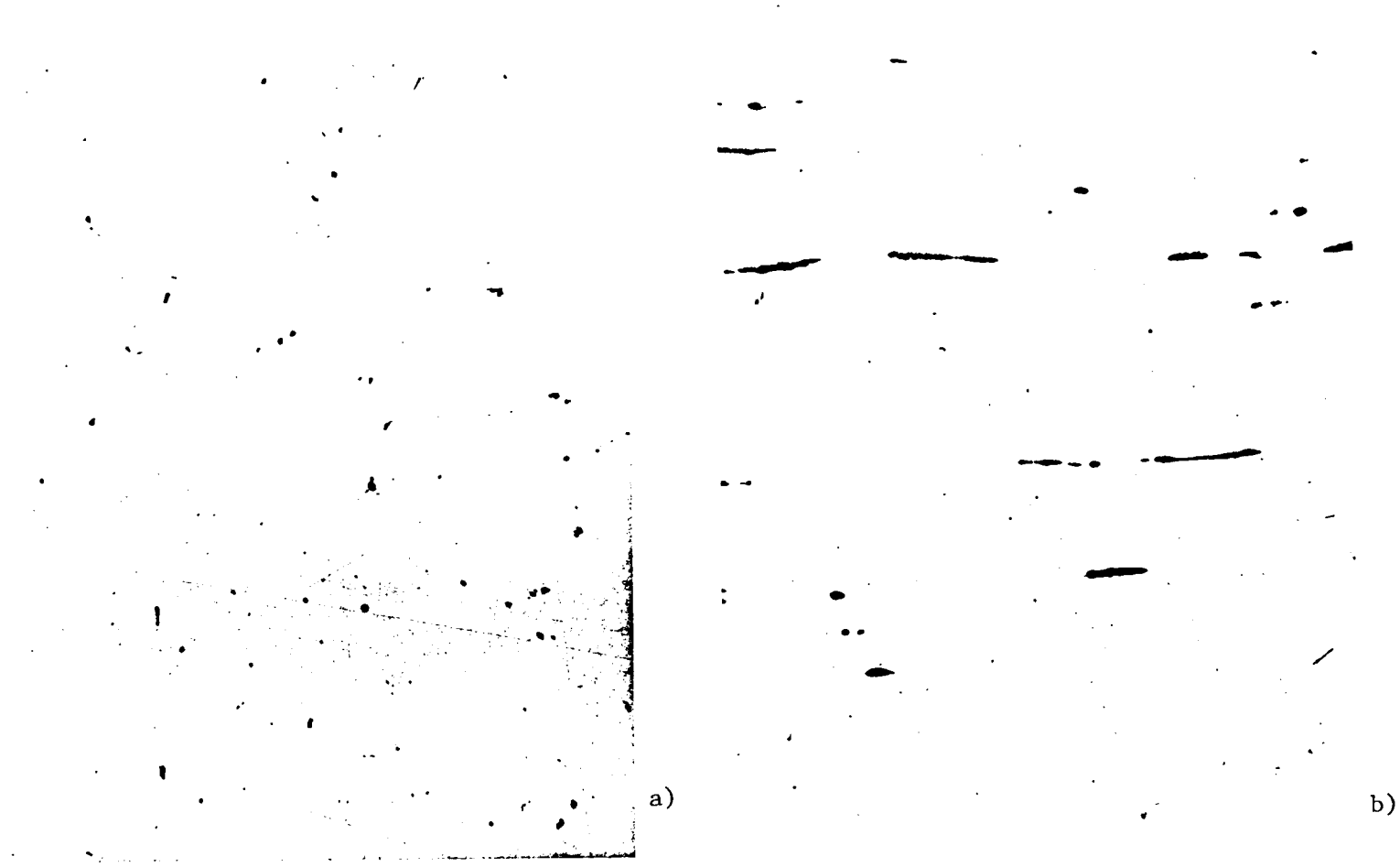


Figure 60. Typical inclusions in C-Mn-Si steels. a) C&N C-Mn-Si steels, b) wrought C-Mn-Si steels. Unetched, OLM, 1000X.

by acting as more potent crack initiators. The effect of banding is to provide a continuous path for crack propagation. The decrease in susceptibility to HIC of the wrought steels when they are test welded TTD, justifies the above conclusions since now the inclusions and banding traverse away from the coarse grained HAZ and under the stress state conditions developed in the UBCT sample, are not in a conducive orientation to aid the initiation and propagation of HIC.

Post weld hold treatments. The reasons why preheat is beneficial to the prevention of HIC have been detailed earlier. Preheating tends to reduce the cooling rate in the HAZ and thus maintains the weldment at an elevated temperature for longer times and hence enhances the diffusion of hydrogen. The higher the preheat temperature, the longer will be the time period for which the weld will be maintained at a higher temperature and therefore the lower the hydrogen content in the coarse grained HAZ. A post weld hold at the preheat temperature after welding has been completed can provide for a more complete diffusion of hydrogen out of the weldment. To show the potential for post weld holding, C&N C-Mn-Si steels in the higher range of C.E.'s (0.50, 0.51, 0.55 and 0.58) and wrought steels with C.E.'s of 0.43 and 0.51 were selected for the study. These C&N steels required preheat temperatures greater than 100°F to avoid underbead cracking. The wrought steels, when test welded PRD, also require preheat temperatures exceeding 100°F to remain crack free. Underbead cracking tests were made using a preheat of 100°F followed by a post weld

hold at 100°F after welding for two hours. The results of these tests are shown in Figure 61. Cracking was eliminated in C&N C-Mn-Si steels with C.E.'s of 0.50 and 0.51 and was reduced in the steels with C.E.'s of 0.55 and 0.58. The extent of cracking was also reduced in the wrought steels, however, cracking was not eliminated in the wrought steels even at a C.E. level of 0.43. When the post weld hold temperature was raised to 150°F, cracking was eliminated in the C&N steel with a C.E. of 0.55, however, cracking persisted in the highest C.E. (0.58) C&N C-Mn-Si steel. In the wrought steels, cracking was almost reduced to zero. However, microcracks were still found associated with inclusions. The results are shown in Figure 62. A post weld hold of 200°F for 2 hrs. was required to prevent cracking in the highest C.E. cast and normalized steel.

The post weld hold studies show that, i) cracking can be prevented with the use of lower preheat temperatures than those required without a post weld hold, and ii) wrought steels test welded PRD were again found to be more susceptible to HIC than comparable C.E. C&N steels. Cracks in the wrought steel were associated with inclusions. It is therefore conceivable that the larger inclusion/matrix areas available in the wrought steels form excellent trapping sites for hydrogen to accumulate and hence higher post weld hold schedules are required in the wrought steels than in the C&N steels to diffuse out the hydrogen from the coarse grained HAZ.

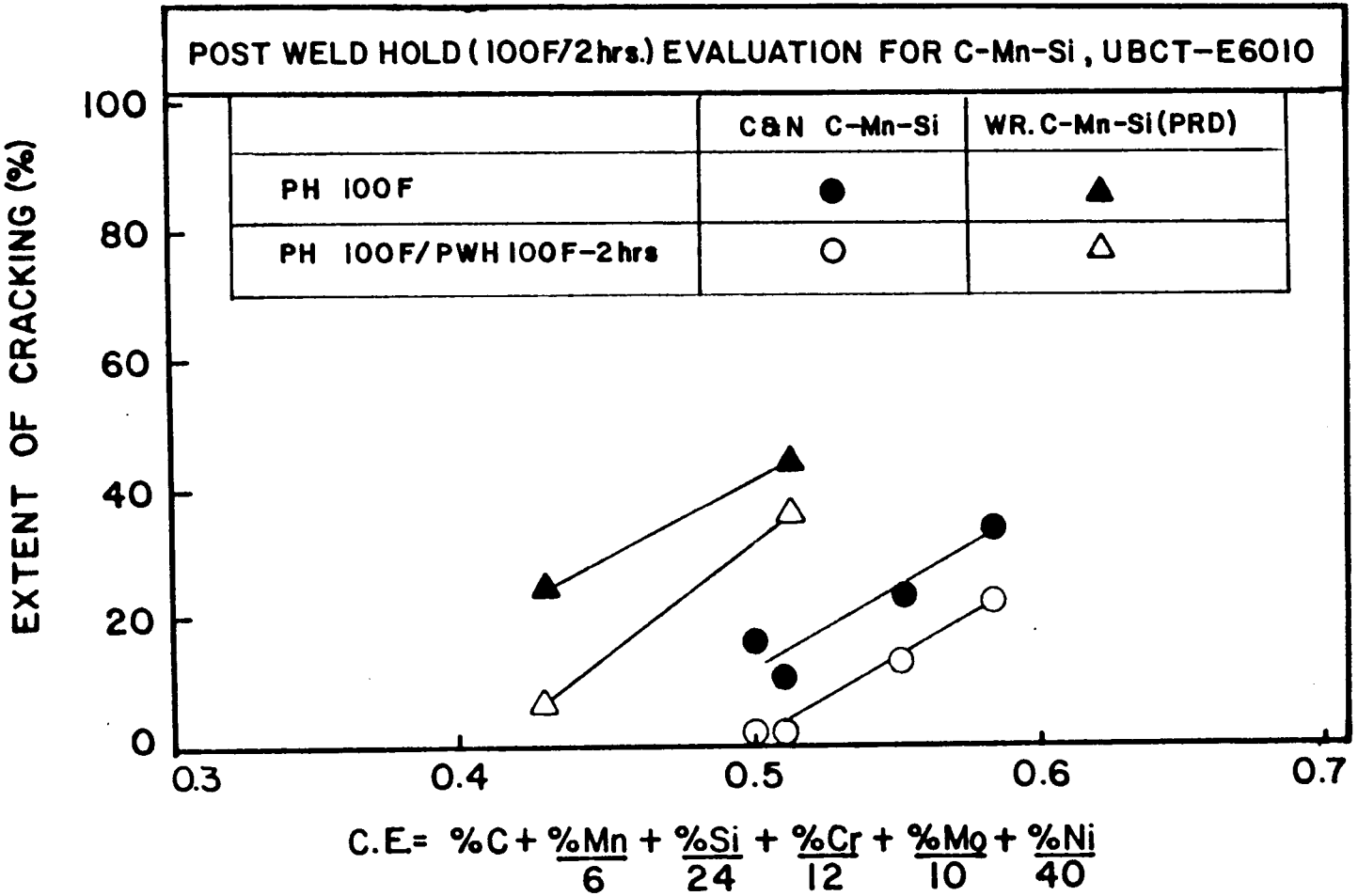


Figure 61. Evaluation of the effect of a post weld hold (PWH 100°F/2 hrs) in addition to a preheat (PH 100°F) on the HIC susceptibility of cast and normalized (C&N) and wrought (WR) C-Mn-Si steels. UBCT, E 6010.

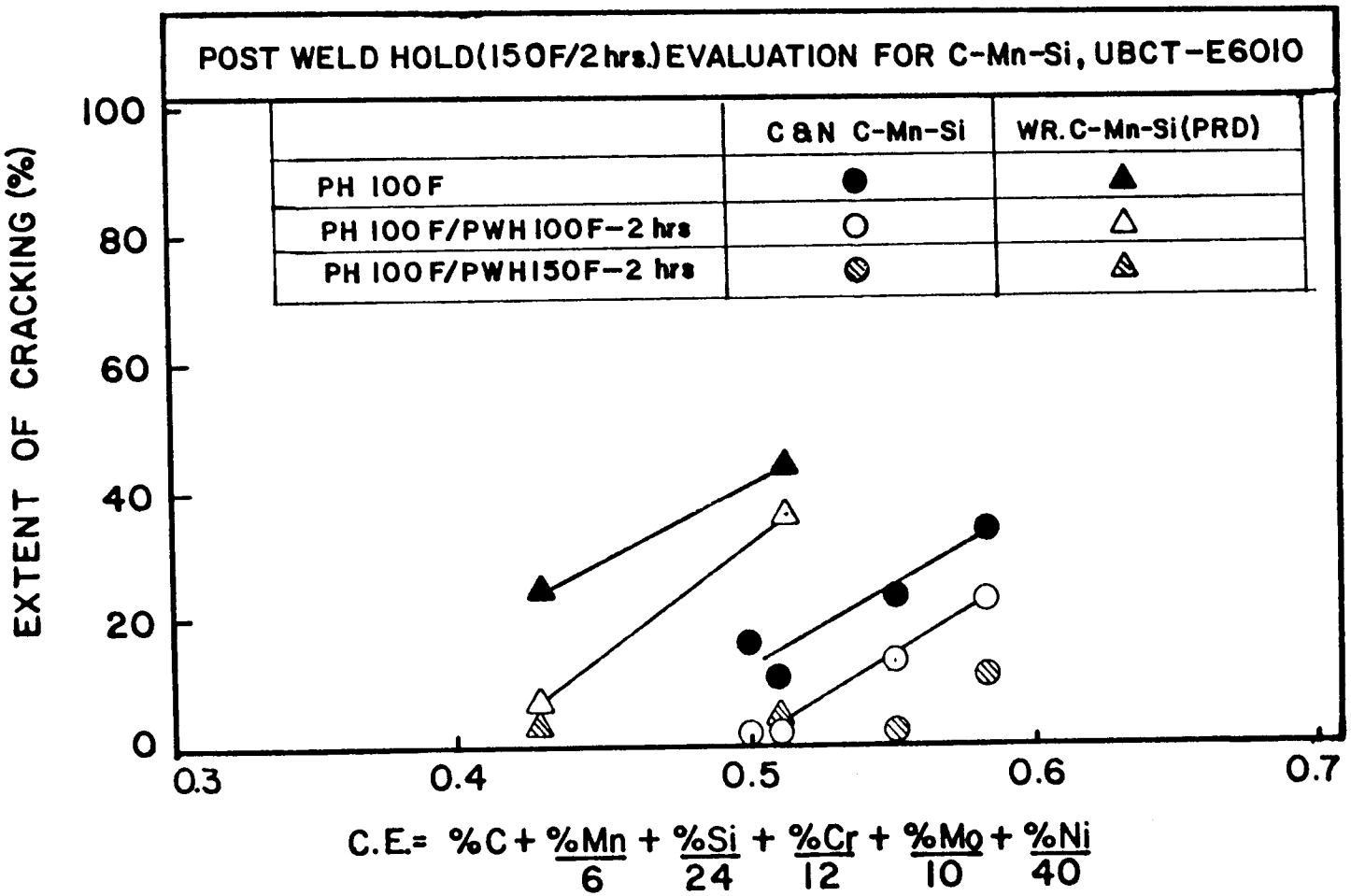


Figure 62. Evaluation of the effect of a post weld hold (PWH 150°F/2hrs) in addition to a preheat (PH 100°F) on the HIC susceptibility of cast and normalized (C&N) and wrought (WR) C-Mn-Si steels. UBCT, E 6010.

4. UT-Modified Hydrogen Sensitivity Test

The UBCT as has been described before, is a test where the strain developed is that due to the self restraint of the sample. In the UT-Modified Hydrogen Sensitivity Test (UT-Mod.HST), the response to HIC conditions of samples that have been strained plastically to various levels can be studied. Hence, the test was used to augment baseline data generated in the UBCT's. The results for the C&N and wrought C-Mn-Si steels are presented in Figure 63 as the preheat temperature to prevent cracking vs. the C.E. The results show that up to a C.E. of 0.45, an ambient temperature (75°F) preheat is sufficient to prevent cracking. An increase in C.E. beyond this level, necessitated the use of a preheat temperature of at least 300°F to prevent cracking (preheat temperatures were increased in steps of 100°F starting at 100°F). The transition in the UBCT (corresponding to a sudden increase in the extent of cracking) was at a C.E. of approximately 0.47, which is in close agreement to the C.E. level of 0.45 in the UT-Mod.HST beyond which a significant increase in preheat temperature was required to prevent HIC. The highest C.E. C&N steel required a preheat of 700°F to remain crack free. The figure also shows the results for the wrought steels. It is clear that wrought steels with C.E.'s of 0.40 and 0.51 required the same preheat as their C&N counterparts to remain crack insensitive. However, the wrought steel with a C.E. of 0.43 required a higher preheat (200°F) than that required (75°F) by its C&N equivalent. This result is due to a large grain size

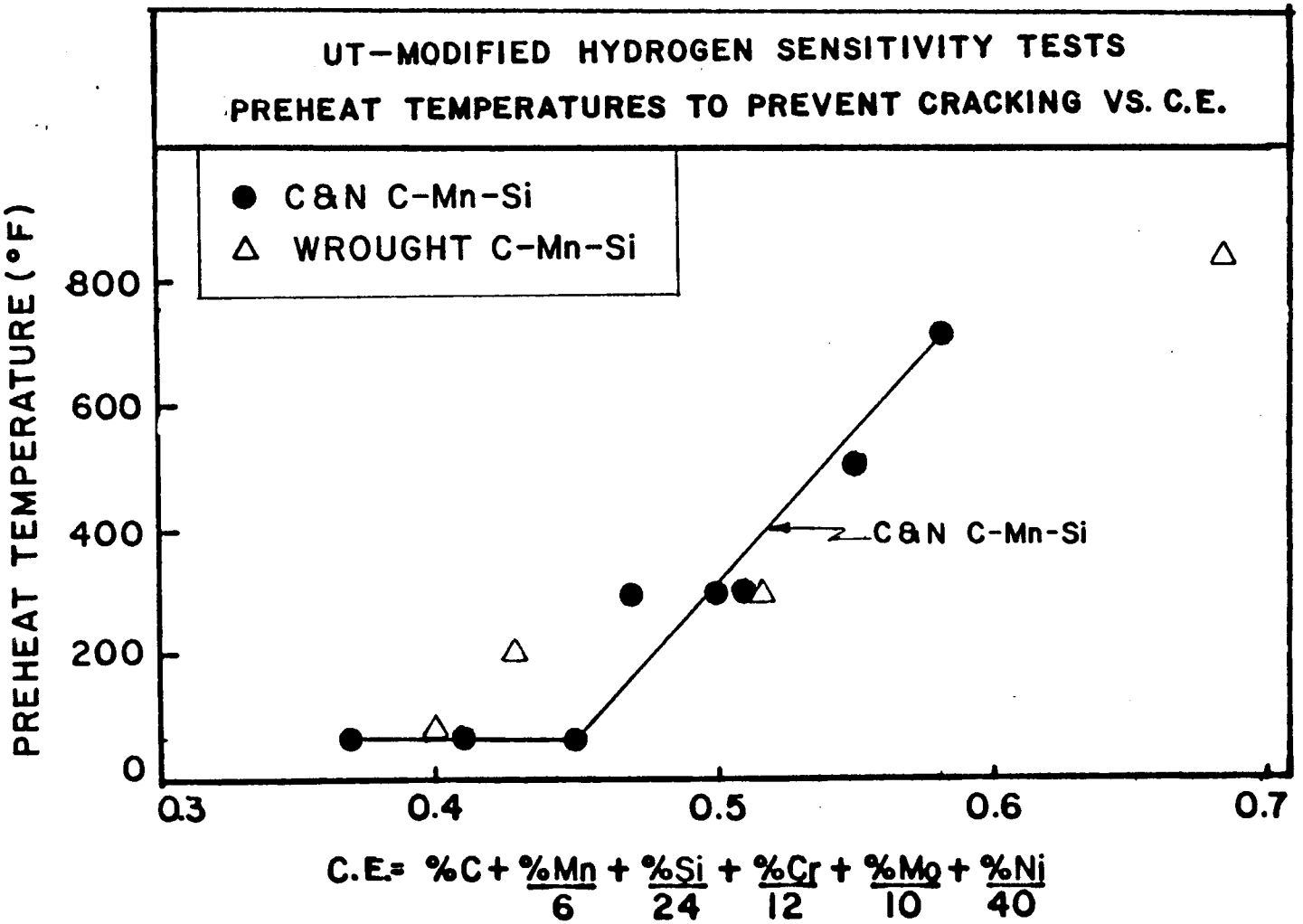


Figure 63. Preheat temperature required to prevent HIC in cast and normalized (C&N) C-Mn-Si and wrought C-Mn-Si steels as determined in the UT-Mod.HST. 5% H_2, 4.1% augmented strain.

attained in the fusion zone of this wrought steel due to epitaxial growth from the coarse grains in the HAZ. This steel was manufactured to a coarse grained practice and this gave rise to fact that the weld metal also exhibited large grains. The highest C.E. (0.68) wrought steel required a preheat of 800°F to avoid cracking, the excessively high carbon and alloy content of the steel rendered it very susceptible to HIC.

The absence of any definitive difference in response to HIC conditions imposed in the UT-Mod.HST between the C&N and wrought steels, can be explained in the following manner. The UT-Mod.HST tests the HIC susceptibility of the weld metal and hence, as such, the effects of inclusion density and morphology on the HIC susceptibility of the steels are not evident. The "weld metal" in this test is the autogenously remelted base material and corresponds to the "unmixed zone" that would exist close to the fusion line of an actual weld. Microhardness tests conducted on the test samples show that the weld metal hardness is comparable for the cast and the wrought steels (Figure 64). The microhardness test results follow a similar trend to that for the UBCT samples. The susceptibility of each individual steel depends upon the nature of transformation products in the fusion zone; the microhardness (5Kg load) gives an idea of the composite hardness of these microconstituents. Figure 65 shows a low magnification view of the weld in the C&N steel with a C.E. of 0.37. At a higher magnification, Figure 66 shows the existence of pro-eutectoid ferrite outlining the grain

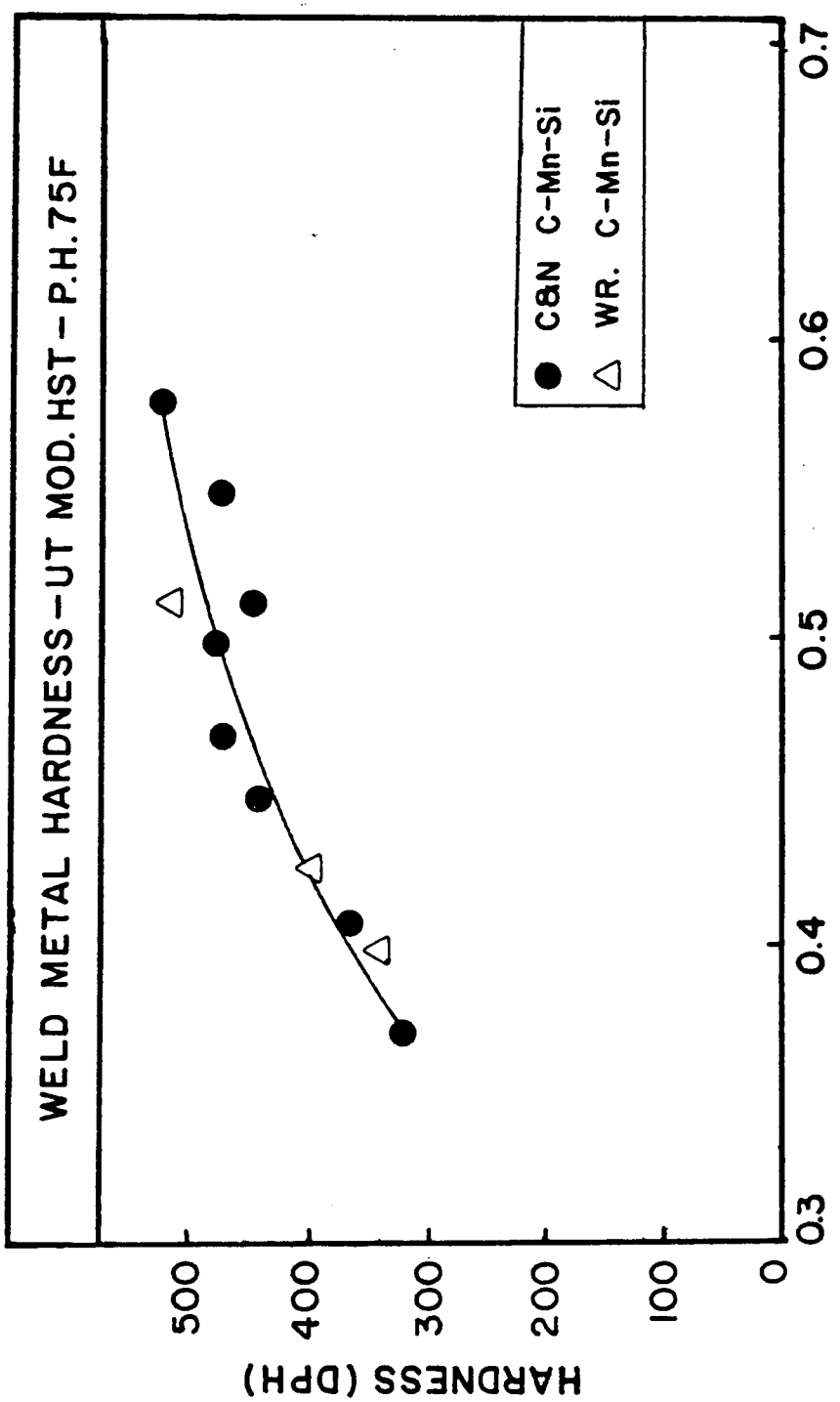


Figure 64. Weld metal hardness in UT-Mod.HST samples tested at a preheat of 75°F.

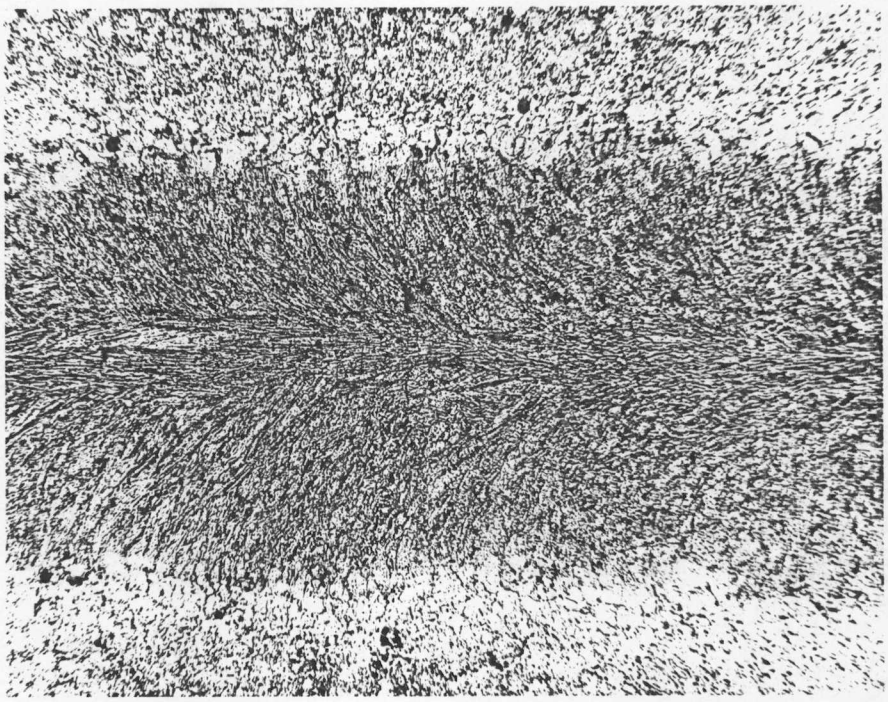


Figure 65. Macrograph of UT-Mod.HST sample of C&N C-Mn-Si steel, C.E. = 0.37. Preheat 75°F. Picral etch, OLM, 20X.

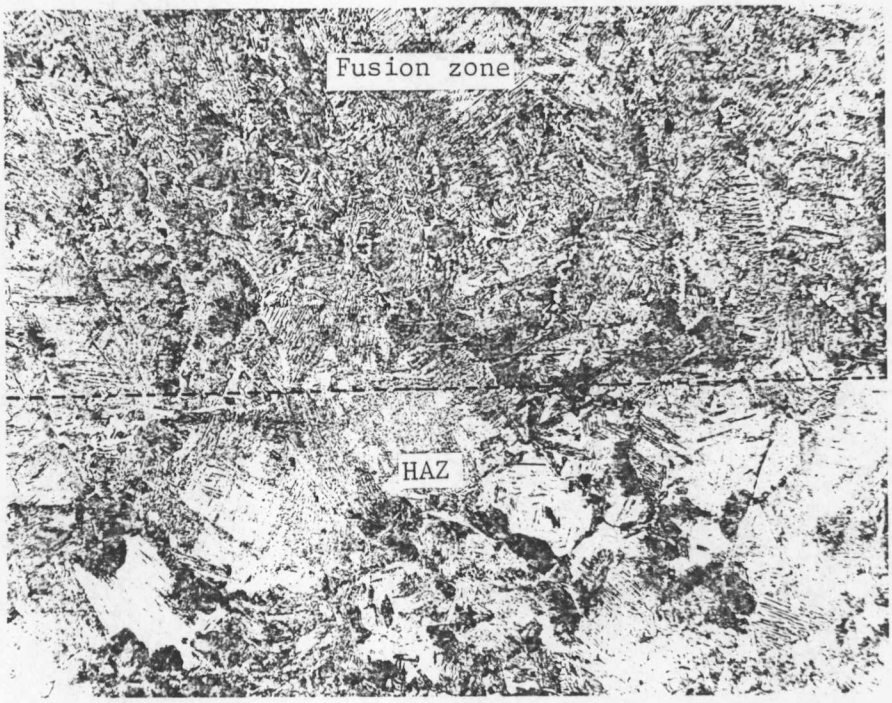


Figure 66. Microstructure of fusion zone and HAZ in C&N C-Mn-Si steel, C.E. = 0.37. UT-Mod.HST, preheat 75°F. Picral etch, OLM, 200X. (See Figure 65)

boundaries in the weld metal. Across the fusion boundary, in the HAZ, the microconstituents present appear to be martensite, bainite and fine pearlite. The SEM micrograph in Figure 67 shows the weld metal in this steel to be comprised of pearlite and bainite. The composite hardness of this microstructure was found to be 325DPH and this specimen did not crack when tested wtih an ambient temperature preheat. Examination of the C&N sample with a C.E. of 0.47 revealed the cracking in the fusion zone to be essentially transgranular. Figures 68a and b show longitudinal and transverse sections of the sample; the transverse section shown in Figure 68b shows the cracks to be essentially confined to the weld metal. Another feature that can be noted, is that the dendritic substructure is faintly revealed. At a higher magnification, in Figure 69, the fusion zone as well as the HAZ appears to be essentially martensite with some traces of bainite at the grain boundaries. Figure 70 shows a longitudinal view of the C&N UT-Mod.HST sample having the highest C.E. (0.58). The cellular dendritic substructure is clearly evident. The high alloy content permitted the substructure to be "frozen" upon solidification and be revealed clearly upon etching. In the longitudinal and transverse sections shown in Figures 71a and b respectively, the presence of bainite is also noted at the grain boundaries. SEM photomicrographs in Figures 72a and b show clearly the presence of bainite at the grain boundaries.

The UT-Mod.HST ranks the steels in the same order as the UBCT and as predicted by their C.E.'s. The relation between the preheat

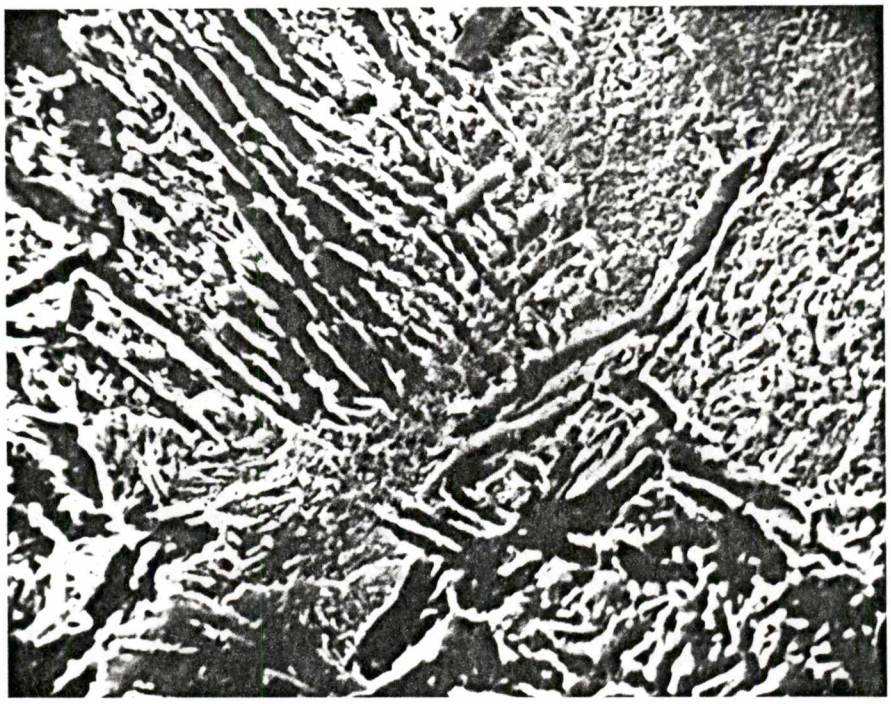


Figure 67. Microstructure of fusion zone in C&N C-Mn-Si steel, C.E. = 0.37. UT-Mod.HST, preheat 75°F. 2% Nital etch, SEM, 5000X. (See Figures 65 and 66)

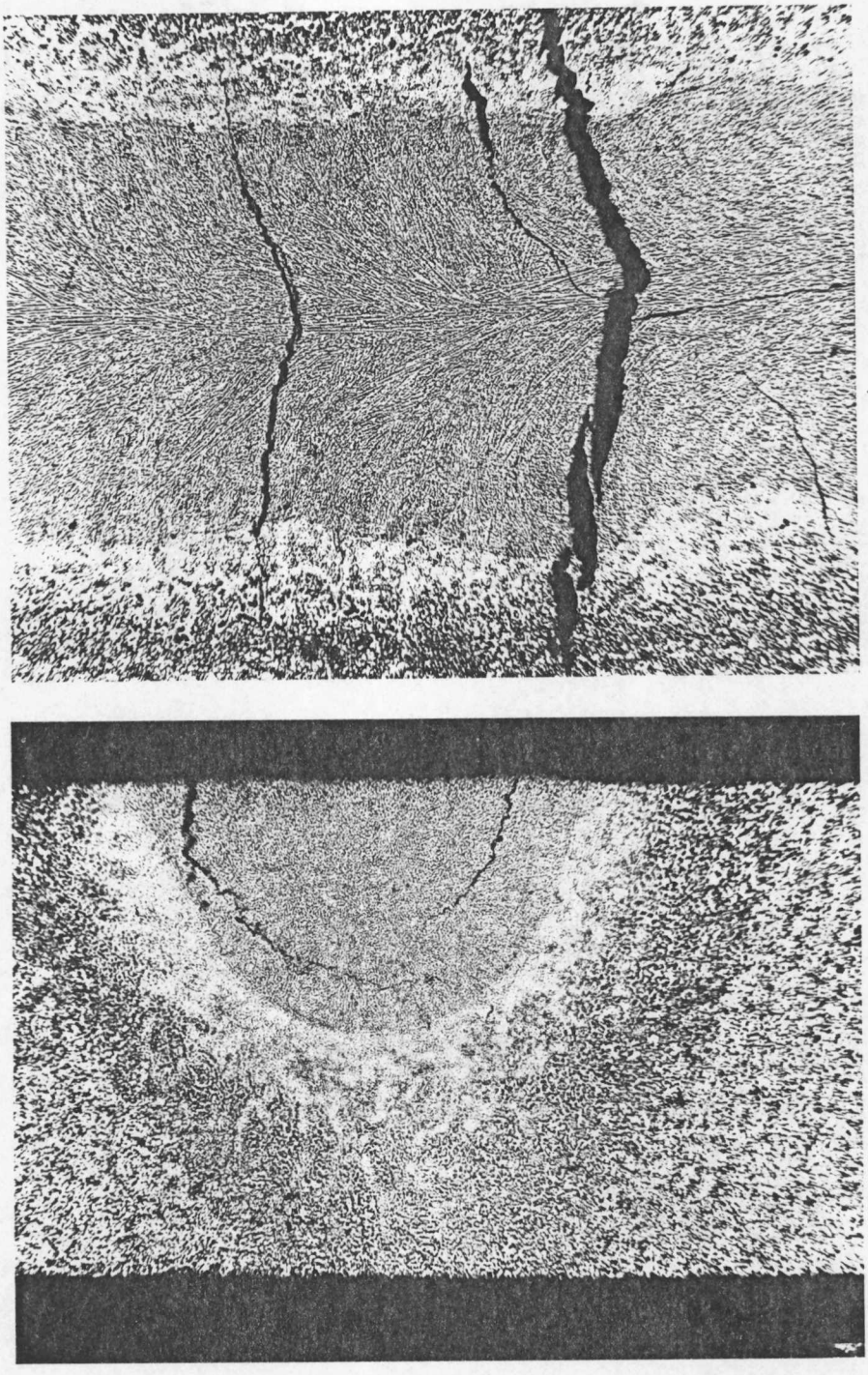


Figure 68. Macrographs of UT-Mod.HST sample from C&N C-Mn-Si steel, C.E. = 0.47. Preheat 75°F. a) Longitudinal, b) Transverse. Picral etch, OLM, 20X.

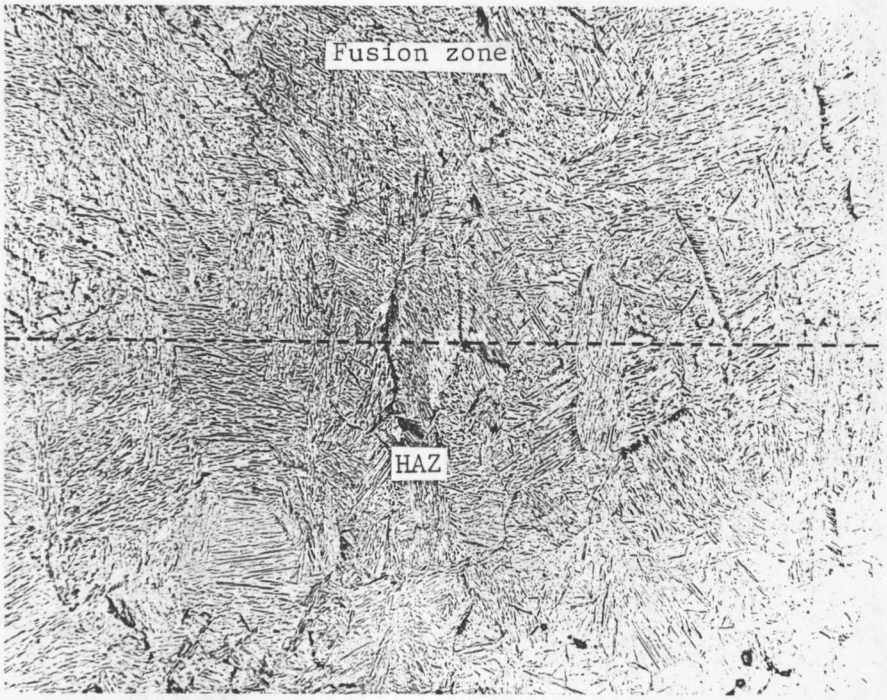


Figure 69. Microstructure of fusion zone and HAZ in C&N C-Mn-Si steel, C.E. = 0.47. UT-Mod.HST, preheat 75°F. Picral etch, OLM, 200X. (See Figure 68)

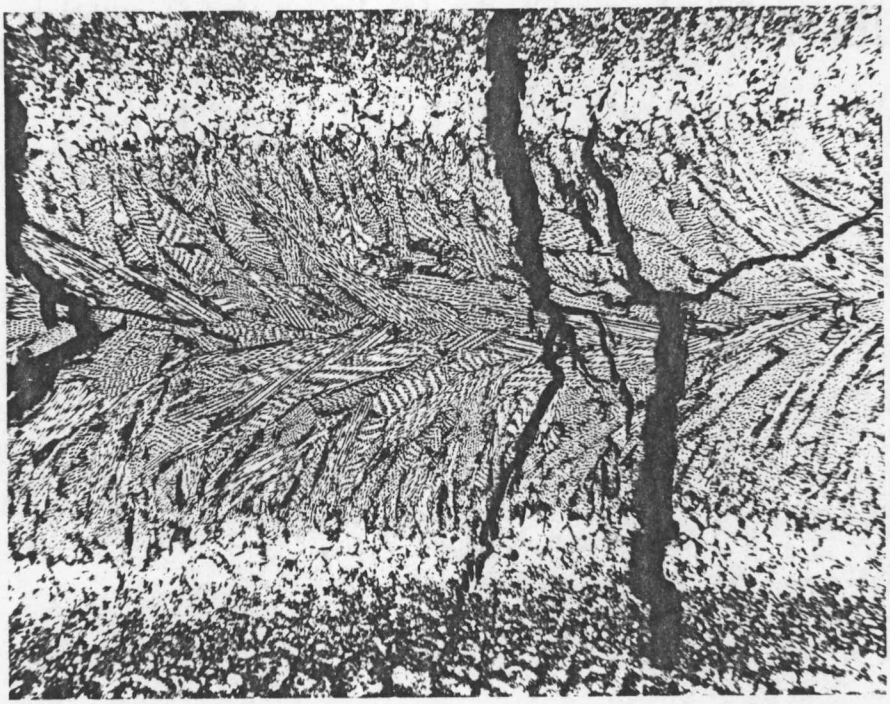


Figure 70. Macrograph of UT-Mod.HST sample from C&N C-Mn-Si steel, C.E. = 0.58. Preheat 75°F. Picral etch, OLM, 20X.

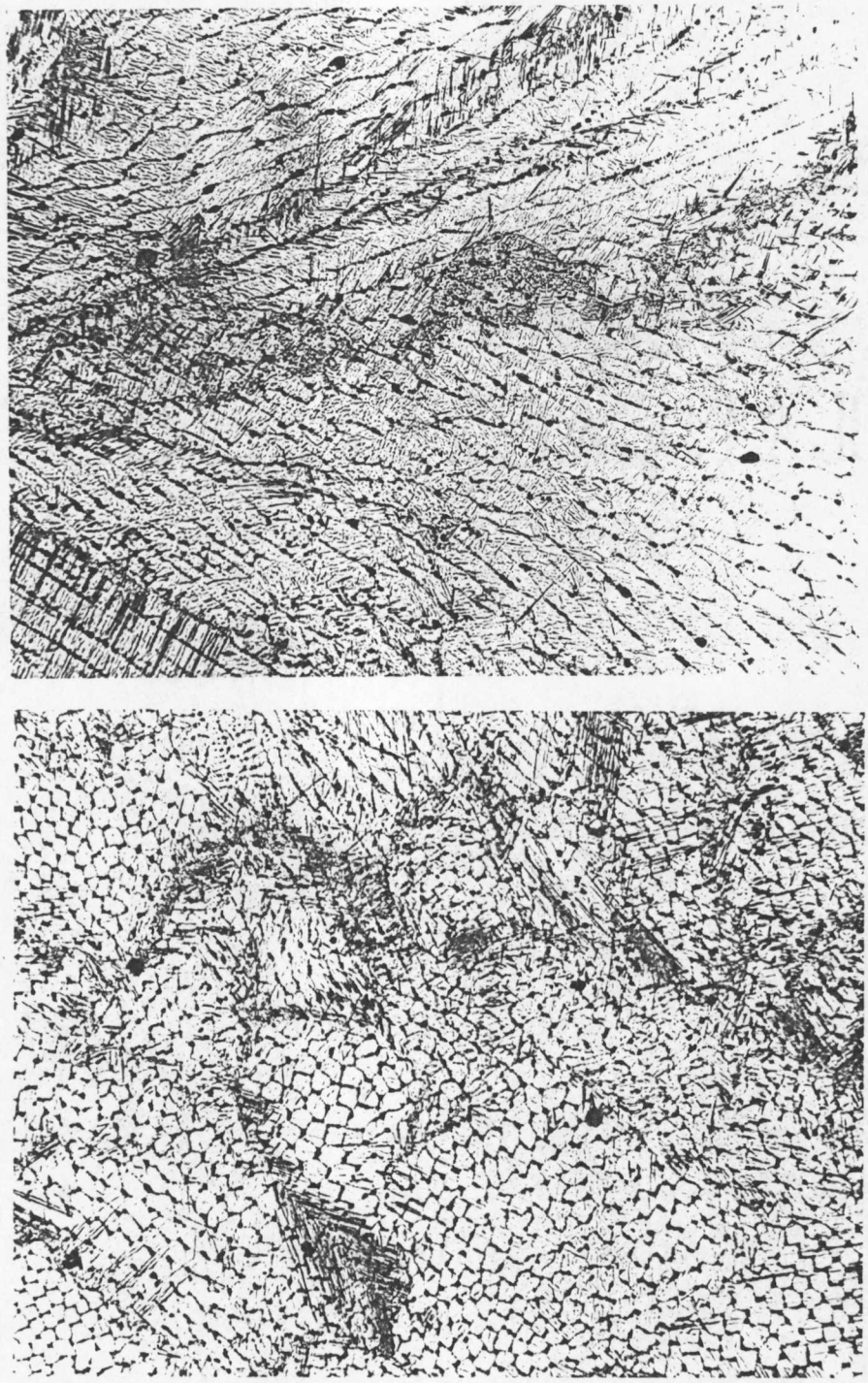


Figure 71. Microstructures of the fusion zone in C&N C-Mn-Si steel, C.E. = 0.58. UT-Mod.HST, preheat 75°F. (See Figure 70.) a) Longitudinal section, b) Transverse section. Picral etch, OLM, 200X.

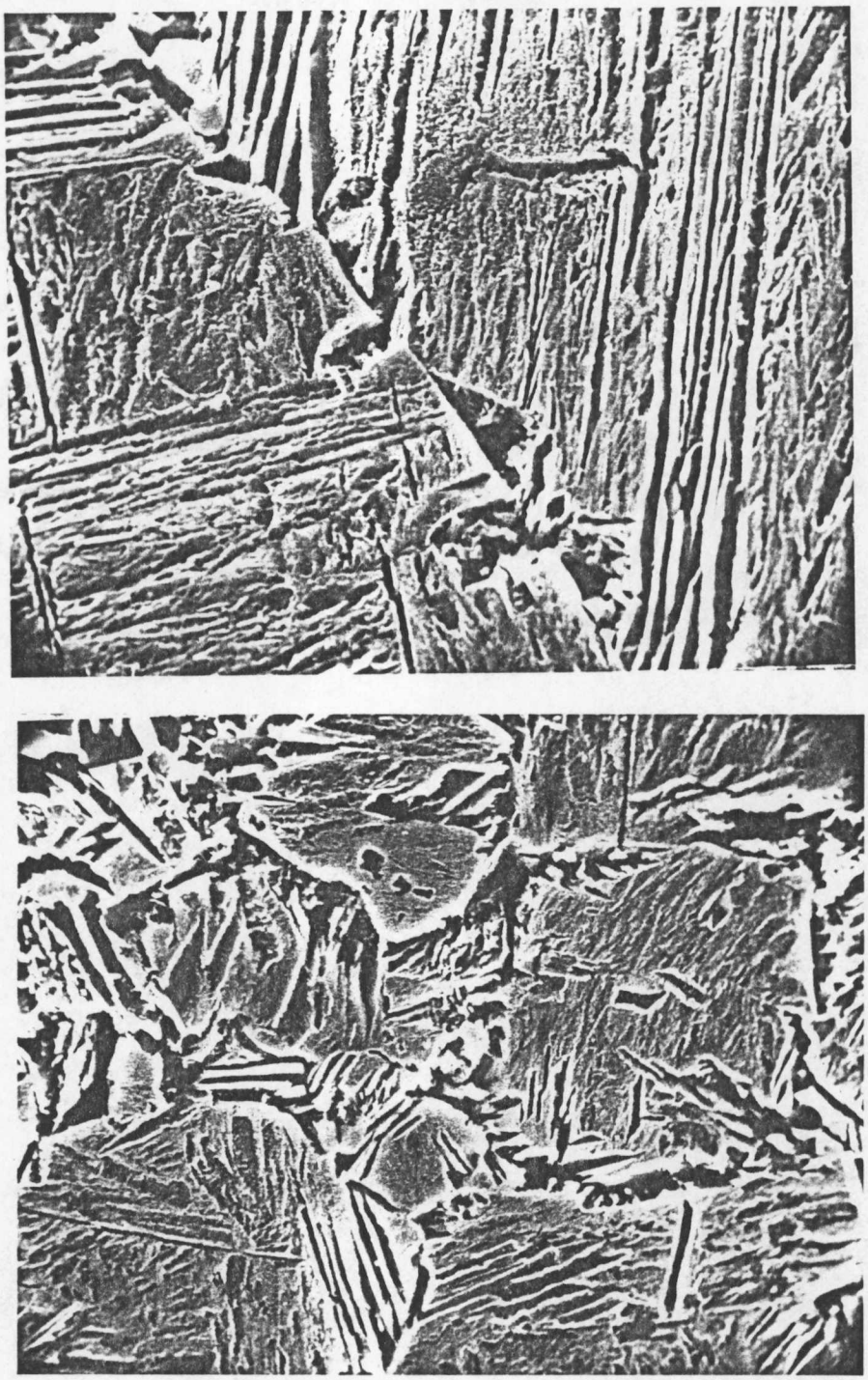


Figure 72. SEM micrographs of the fusion zone in C&N C-Mn-Si steel, C.E. = 0.58. UT-Mod.HST, preheat 75°F. (See Figure 70 and 71) a) Longitudinal section, b) Transverse section. 2% Nital etch, SEM, 5000X.

temperatures to prevent cracking in the UBCT and those required in the UT-Mod.HST is shown in Figure 73. The preheat temperature to eliminate cracking is higher in the UT-Mod.HST and is a result of the severity of the test and the region evaluated. The fusion zone is the region tested in the UT-Mod.HST vs. the "true" HAZ in the UBCT. The advantage of the UT-Mod.HST lies in its ability to quickly rank the HIC susceptibility of steels without the necessity to resort to extensive sample preparation. Further, unlike in the UBCT where hydrogen has to diffuse into the HAZ from the weld metal, the UT-Mod.HST saturates the fusion zone with hydrogen. The strain needed to cause HIC is applied immediately after welding and hence in the presence of a susceptible microstructure in the fusion zone, all the conditions necessary for HIC occur simultaneously. However, the test, in essence, evaluates the "unmixed zone" and therefore does not reveal other factors that may influence HIC susceptibility in the HAZ (such as inclusion morphology/distribution and banding). For this reason, the majority of the testing utilized the UBCT and the implant test, where the "true" HAZ is evaluated for its susceptibility to HIC.

5. Tests on Foundry-Run Cast Steels

It has been mentioned earlier that the residuals elements, as defined by ASTM A216, comprise Cr, Mo, Ni, V and Cu. For the C&N C-Mn-Si steels tested in Phase I, the sum of these elements was restricted to 0.19% maximum. However, since A216 allows a maximum

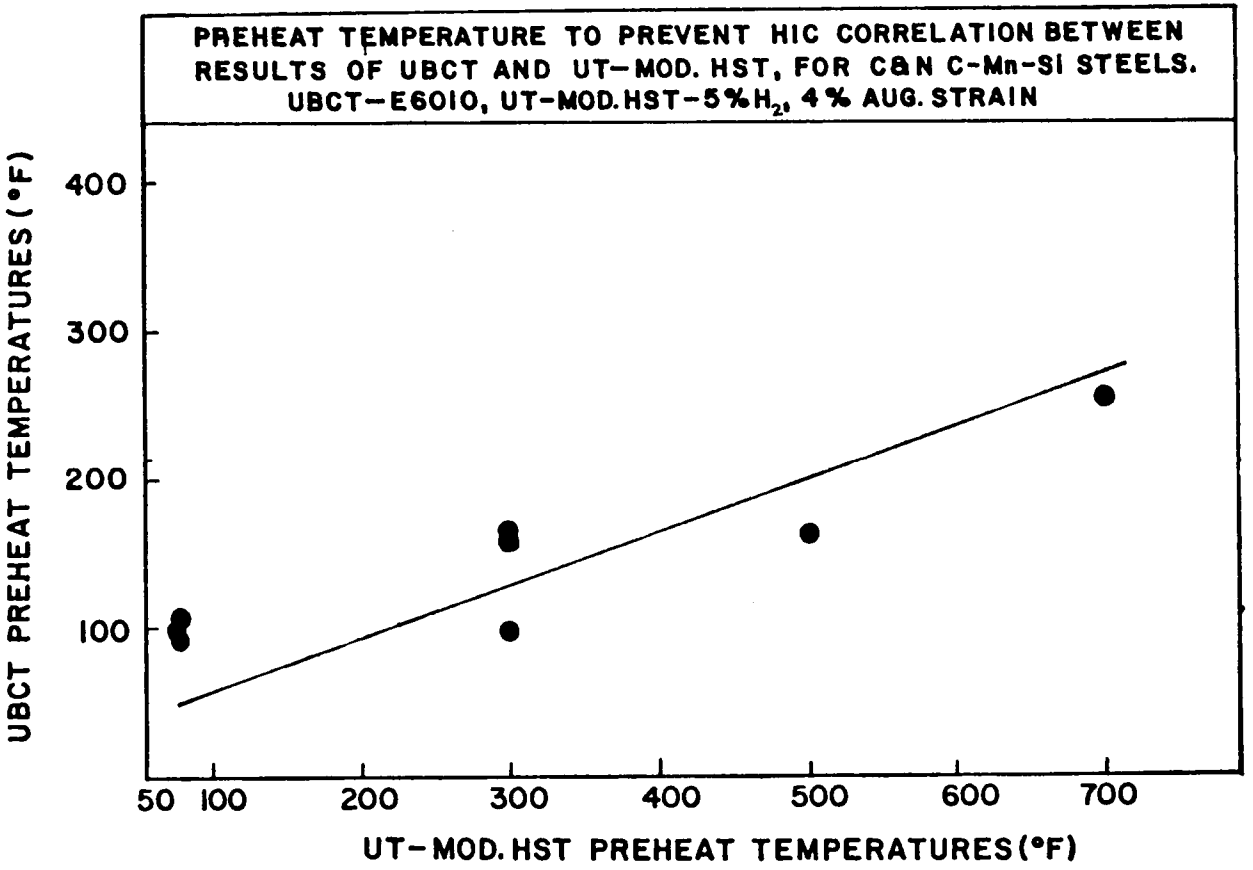


Figure 73. Preheat temperature to prevent HIC correlation between results of the UBCT and the UT-Mod.HST for cast and normalized C-Mn-Si steels.

of 1%, it was necessary to evaluate the HIC susceptibility of cast steels whose residual limits approached those specified in A216. For this purpose, eight grades of cast steels corresponding to the A216 specification were obtained; of these, six were of the A216-WCB type and two were of the A216-WCC type. Of the six A216-WCB steels, four were acid melted and the remaining two were basic melted. Of the two WCC grades, one was acid and one was basic melted. The C.E.'s and the total residual contents are detailed in Table 6 (page 89). The residuals vary from a total of 0.24 to 0.59%, and the C.E.'s range from 0.38 to 0.48. The C.E. values are quite similar to those tested in Phase I, however, the residual content is in the normal range for cast steels with a maximum of 0.59% maximum as compared to the 0.19% maximum for the Phase I materials. The test utilized most extensively in the evaluation of the foundry run steels was the UBCT. For the extent of testing needed, this test provided the information desired using a relatively simple test procedure. As for the Phase I materials, testing was conducted using high-hydrogen electrodes (E6010). Use of high hydrogen electrodes permits a good relative evaluation of the steels, as far as ranking to HIC susceptibility is concerned. The results of the underbead cracking tests are shown as the extent of cracking vs. the preheat temperature, for materials both in the as-cast as well as C&N conditions in Figures 74, 78 and 79. Figure 74 shows the results of the tests on four lots of the acid melted WCB and one lot of the WCC cast materials (BA-1 through BA-4 and CA-1). The results show that in the C&N condition, all of these

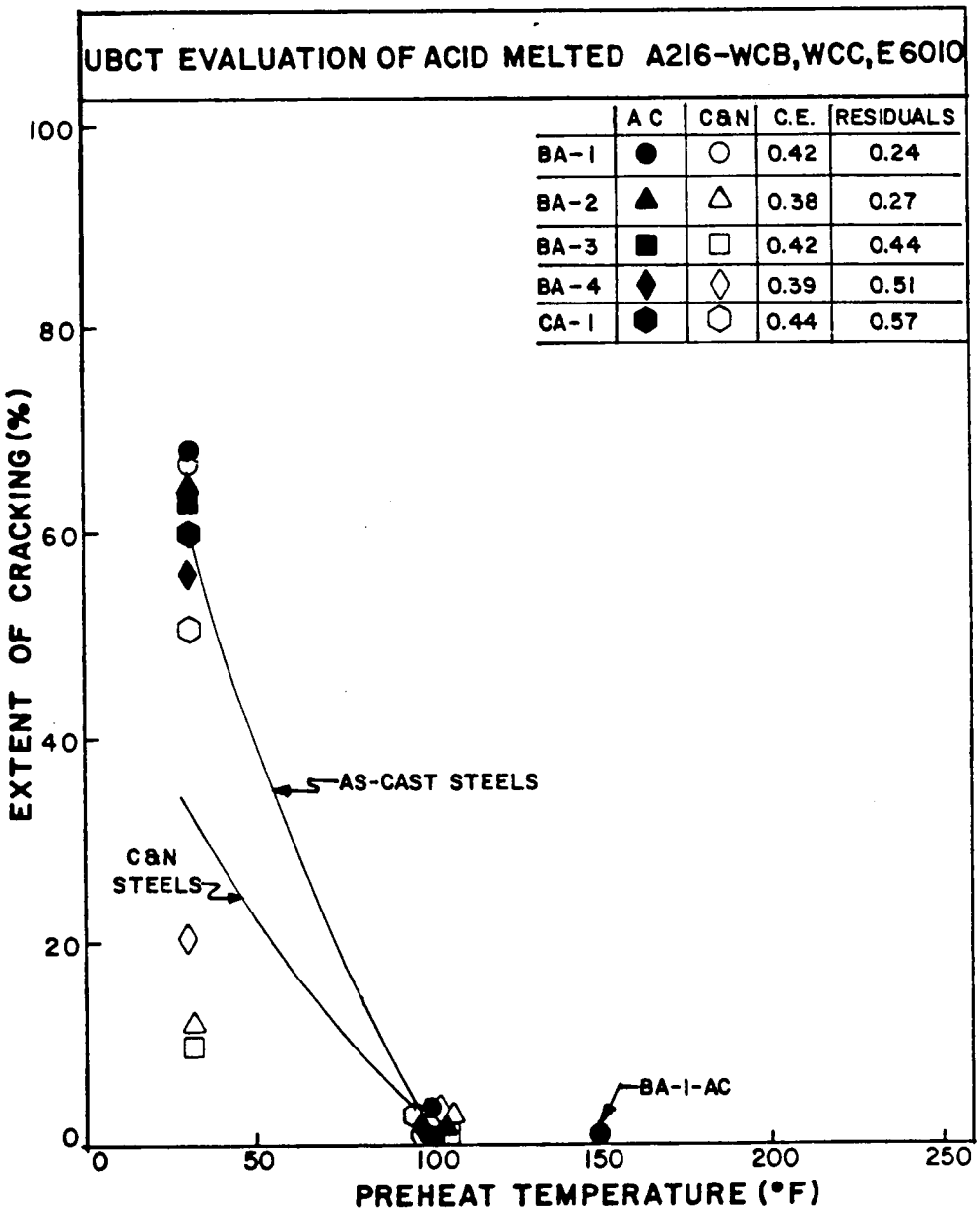


Figure 74. UBCT preheat results for acid-melted A216-WCB and WCC cast steels. As-cast (AC), cast and normalized (C&N). E 6010.

steels required a preheat of only 100°F to remain crack free. These results agree with those obtained in Phase I for C&N steels with C.E.'s up to 0.47. However, these results extend those obtained in Phase I to a total residual content of 0.51%. When tested in the as-cast condition, only BA-1 required an increase in preheat to 150°F to avoid cracking. The increase in preheat for BA-1 is related to a substantial fraction of Type II inclusions (eutectic sulfides) present. Type II sulfides are formed at grain boundaries during primary solidification, and in the HAZ, under a weld thermal cycle, these inclusions pin the prior austenite grain boundaries. Thus hydrogen trapping is enhanced at these grain boundaries due to the presence of the Type II inclusions, leading to intergranular HAZ cracking. Typical Type II inclusions in BA-1 are shown in Figure 75a and the association of cracks with these inclusions is shown in Figure 75b. The deleterious influence of Type II's on HIC is also exemplified in the partially refined regions of the HAZ. In Figure 76, cracks are found in BA-1 associated with inclusions along the grain boundaries in the partially refined region. Inclusions in the other acid melted steels were found to possess essentially Type III morphologies. The inclusions found in BA-3 are typical of the Type III's found, and are shown in Figure 77. In the normalized condition, the location of Type II inclusions is altered with respect to the primary solidification grain boundaries. Further, regions of segregation are modified, such that continuous paths for crack propagation are reduced.

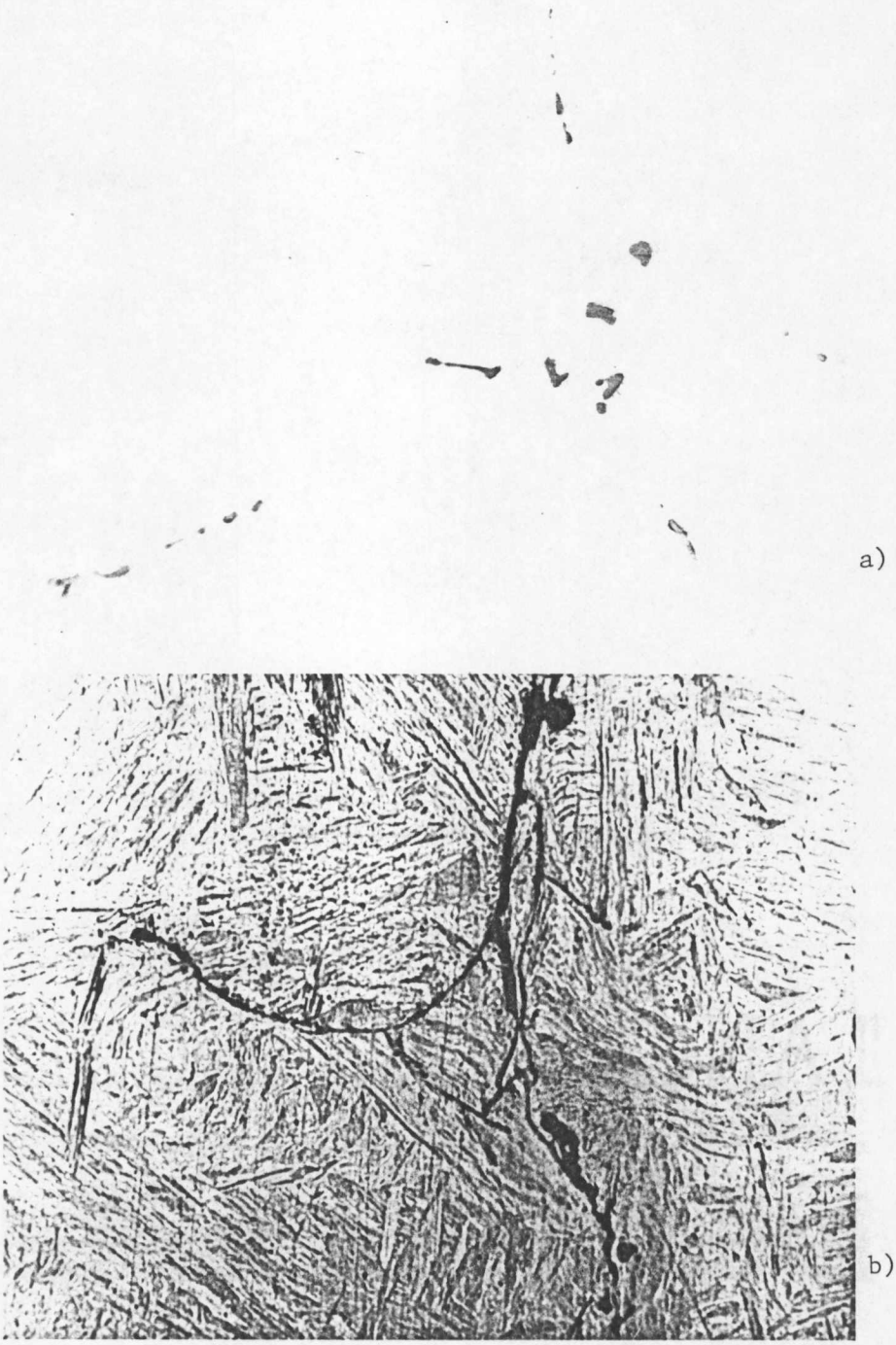


Figure 75. Inclusion morphology and associated HIC in acid-melted as-cast BA-1, A216-WCB, C-Mn-Si steel. C.E. = 0.42, UBCT, preheat 100°F. a) Type II inclusions. Unetched, OLM, 500X. b) Intergranular HIC in coarse grained HAZ. Picral etch, OLM, 1000X.

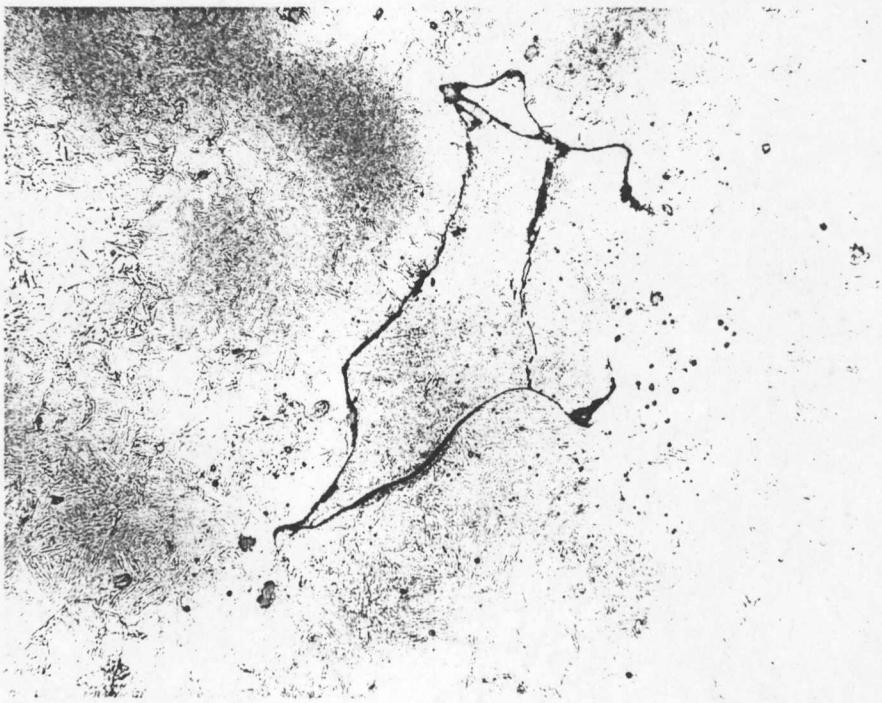


Figure 76. HIC association with Type II inclusions in the partially refined HAZ, as-cast BA-1, acid-melted A216-WCB. C-Mn-Si steel, C.E. = 0.42, UBCT, preheat 150°F. Picral etch, OLM, 200X.

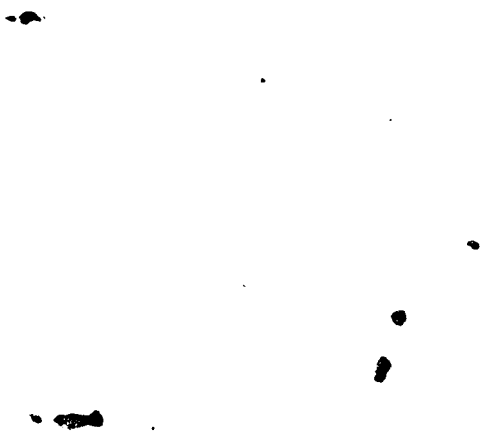


Figure 77. Typical Type III inclusions in acid-melted A216-WCB steel BA-3. Unetched, OLM, 500X.

Trends similar to those obtained for the acid melted steels were obtained for the basic melted A216-WCB and WCC steels. These results are shown in Figure 78. Steels CB-1 and BB-2 having C.E.'s of 0.44 and 0.43 required preheats of 150°F and 100°F respectively to remain crack free in both the AC and C&N conditions. The residuals in BB-2 add up to 0.59%. BB-1, with a carbon content of 0.29% and a C.E. of 0.48 was found to require a preheat of 200°F and 150°F in the AC and C&N conditions to remain crack free. The C.E. of BB-1 exceeds the 0.47 limit beyond which the Phase I materials required preheats greater than 100°F to remain crack free. It is therefore clear that residual contents up to 0.59% did not alter the preheat requirements to prevent cracking in C&N C-Mn-Si steels with C.E.'s up to 0.47.

The results indicate that in case of the C&N steel, BB-1, with a C.E. greater 0.47 (0.29%C, C.E.=0.48), the preheat temperature required to prevent HIC had to be increased to 150°F. This result is in good agreement with those of the UBCT results on C&N C-Mn-Si steels tested in Phase I. For as-cast steels, preheat temperatures to avoid HIC are generally 50°F higher than those required in the C&N condition. The higher preheat temperature requirement for as-cast steels is attributed to both the presence of Type II inclusions on the primary solidification grain boundaries and to the presence of regions of unmodified segregation in the as-cast steels. Both these factors appear to have a synergistic effect on HIC since certain as-cast steels did not indicate any

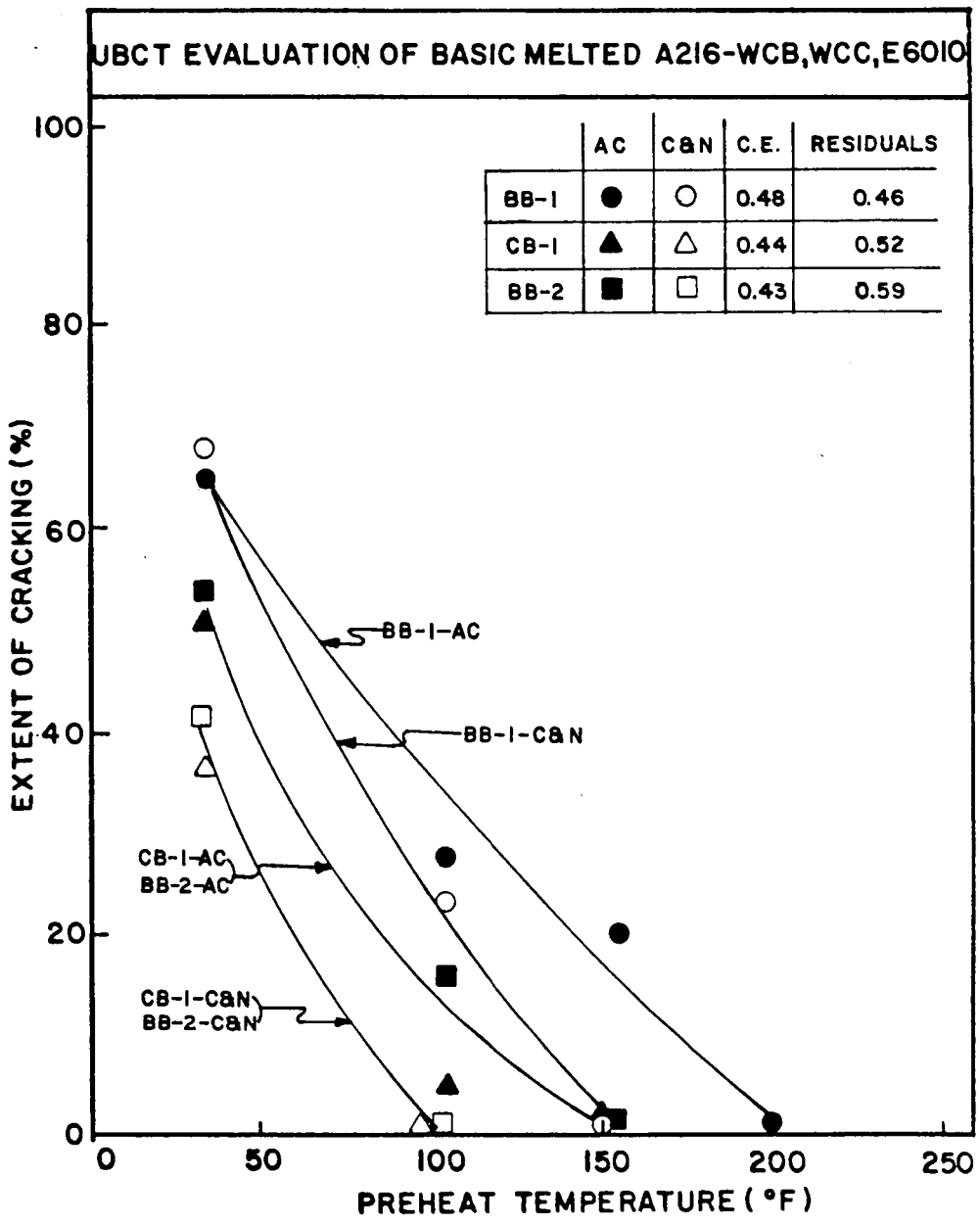


Figure 78. UBCT preheat results for basic melted A216-WCB and WCC cast steels. As-cast (AC), cast and normalized (C&N). E 6010.

enhanced susceptibility to HIC compared to their C&N counterparts. Another conclusion that can be made is that the melting practice (acid or basic) did not have any decipherable effect on the susceptibility to HIC.

Foundry run 8630. The compositions of the cast 8630 steels tested were detailed in Table 7 (page 91). Tests were conducted on the steels in the as-cast as well as C&N conditions. In the as-cast condition, 8630-1 required a preheat of 200°F to remain crack free while in the C&N condition, both steels were crack insensitive at a preheat of 150°F. These results are graphically shown in Figure 79.

Therefore, it is clear that, in general, as-cast materials may require preheat temperatures 50°F higher than those required for the respective C&N grades. The results obtained in Phase I have been verified to be valid with total residual contents of 0.59%. The greater susceptibility of some of the as-cast steels is related to the presence of Type II inclusions at the primary solidification grain boundaries and to the unmodified segregation in the as-cast state. The maximum HAZ hardnesses in the as-cast as well as C&N C-Mn-Si and 8630 steels are shown in Figure 80. The figure indicates that a maximum HAZ hardness criterion does not explain the differences in susceptibility to HIC observed in the UBCT's for some of the as-cast and C&N steels. Therefore, the differences in susceptibility between as-cast and C&N steels are more related to secondary influences (inclusion morphology, segregation)

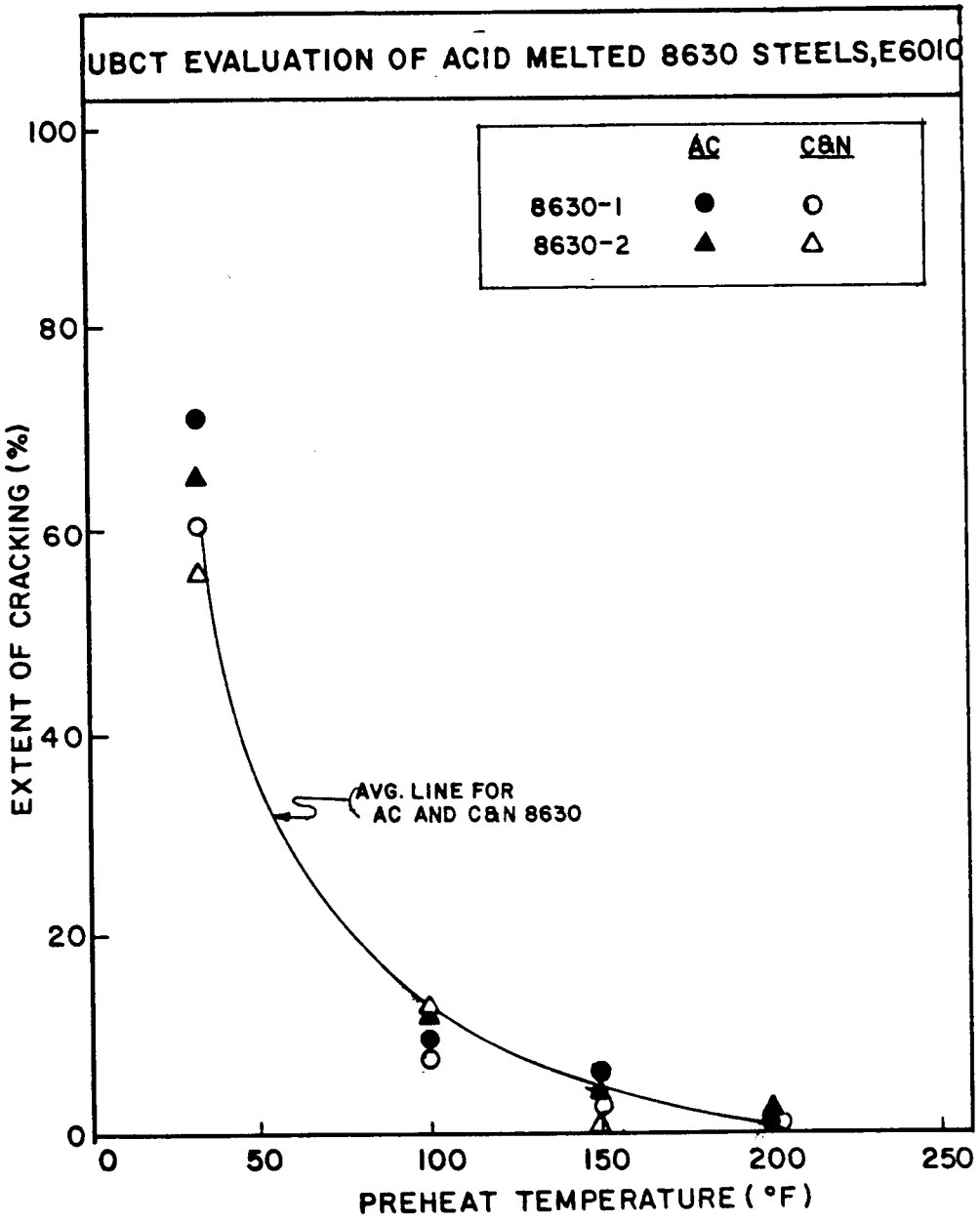


Figure 79. UBCT preheat results for acid melted 8630 steels. As-cast (AC), cast and normalized (C&N). E 6010.

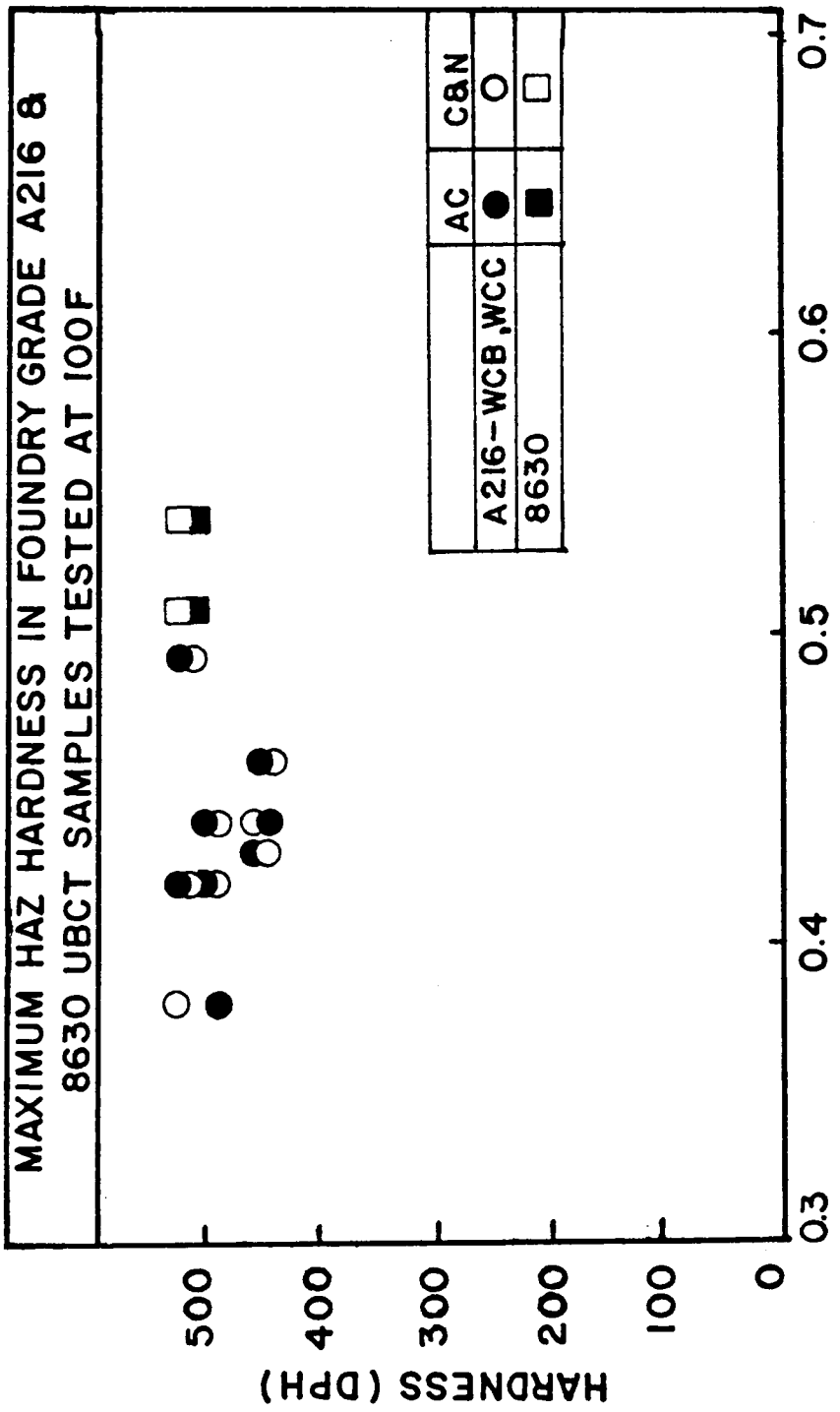


Figure 80. Maximum hardness in the coarse grained HAZ of foundry grade A216 and 8630 cast steels. As-cast (AC), cast and normalized (C&N), UBCT, E 6010.

rather than to the difference in the nature of the microconstituents that result in the coarse grained HAZ due to the weld thermal cycle.

Tests with low hydrogen electrodes. Underbead cracking tests using low-hydrogen electrodes (E7018) were conducted on the cast 8630 steels discussed earlier. The materials were tested in the as-cast condition at room temperature (74°F). No cracking was detected in any of the steels. These results demonstrate the prudence of using low hydrogen procedures. However, tests using high hydrogen electrodes give results that are more conservative, i.e., which may reflect the worst possible shop conditions, and not laboratory controlled conditions. Moreover, the use of high hydrogen electrodes enables the ranking of steels as regards to their inherent underbead cracking sensitivities.

6. Remelted and Recast Wrought Steels

It has been established with tests on the Phase I materials that wrought steels, when welded PRD, are rendered more susceptible to HIC due to the presence of elongated inclusions and also by the presence of banding, than equivalent C&N steels. The results were established for equivalent composition steels, i.e., steels which have similar C.E.'s but not identical compositions. To study directly the effects of inclusion morphology differences between identical composition cast and wrought steels, wrought steels corresponding to A516-70 and 8630 were remelted and cast. The compositions of these remelted steels together with those of the

"parent" wrought steels are given in Table 8 (page 92). The compositions of the remelted steels are seen to closely match that of the wrought steels, excepting for the chromium content for the remelted A516 which has increased in the remelted steel (probably due to contamination from refractories or deoxidizers). UBCT's were conducted on the steels in the as-cast (AC) as well as in the cast and normalized (C&N) conditions and the results compared to that of the "parent" wrought materials (tested both PRD and TTD). The implant test was used as a confirmatory test for both the wrought and remelted A516 steels.

Figure 81 shows the results for the 8630 materials. The results indicate that, i) R8630-AC is more susceptible than the R8630-C&N and, ii) the susceptibility of the W8630 tested TTD is almost identical to that of the R8630-C&N. However, the susceptibility to HIC of the R8630-AC was similar to that of the W8630 welded PRD. The greater susceptibility of the R8630-AC is attributed to its coarse grained as-cast condition (ferrite grain size exceeding ASTM 1) shown in Figure 82. The greater susceptibility of the W8630 tested PRD compared to the R8630-C&N is related to the differences in inclusion morphologies. Figures 83a and b show the difference in morphology. The R8630 essentially has Type III inclusions, which do not act as severe a site for HIC initiation as the elongated stringers in wrought 8630.

The results of the UBCT tests on the R516 (AC and C&N) are compared with its wrought equivalent (tested PRD and TTD) in

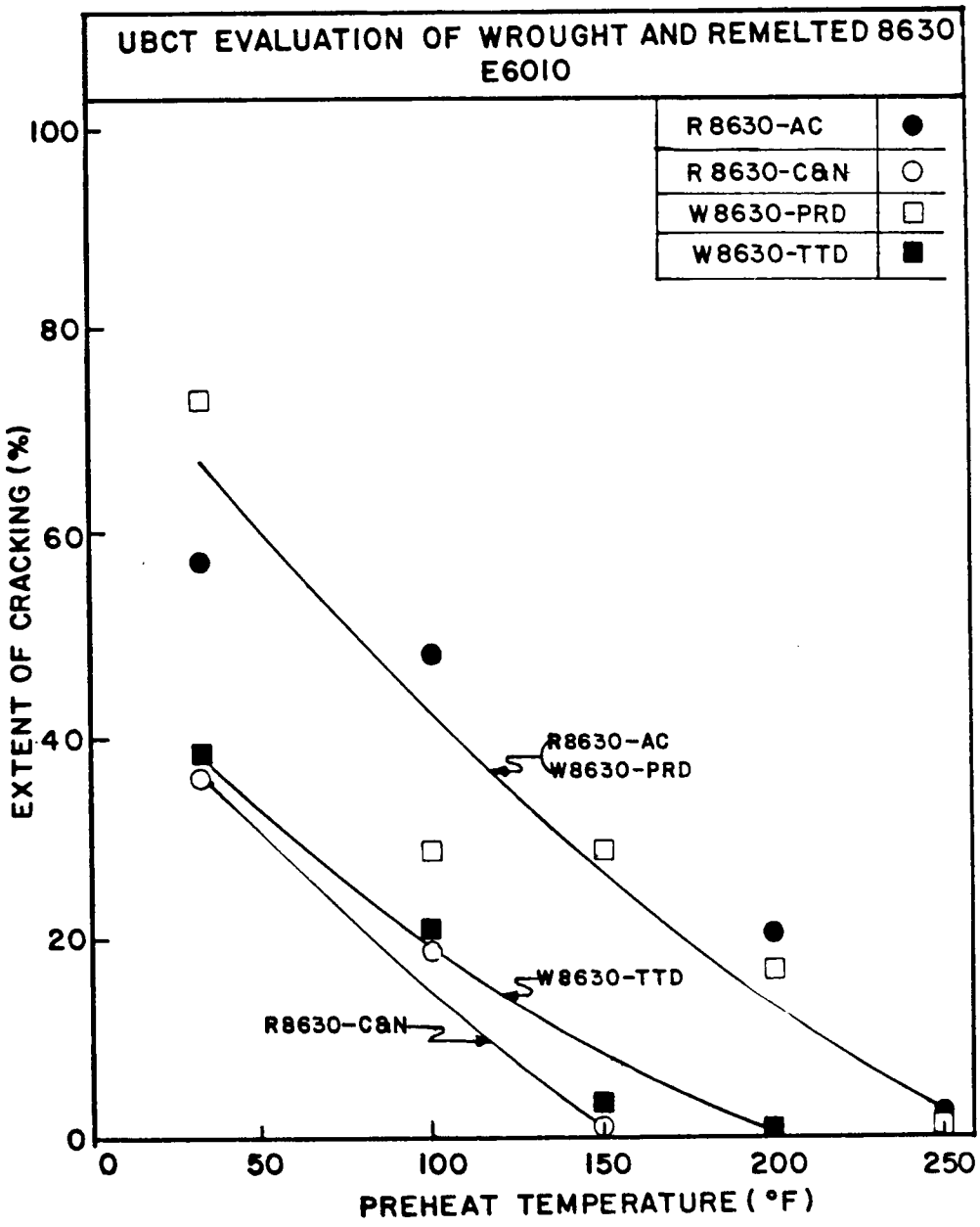


Figure 81. UBCT preheat results for remelted (R) and wrought (W) 8630 steels. As-cast (AC), cast and normalized (C&N). E 6010.

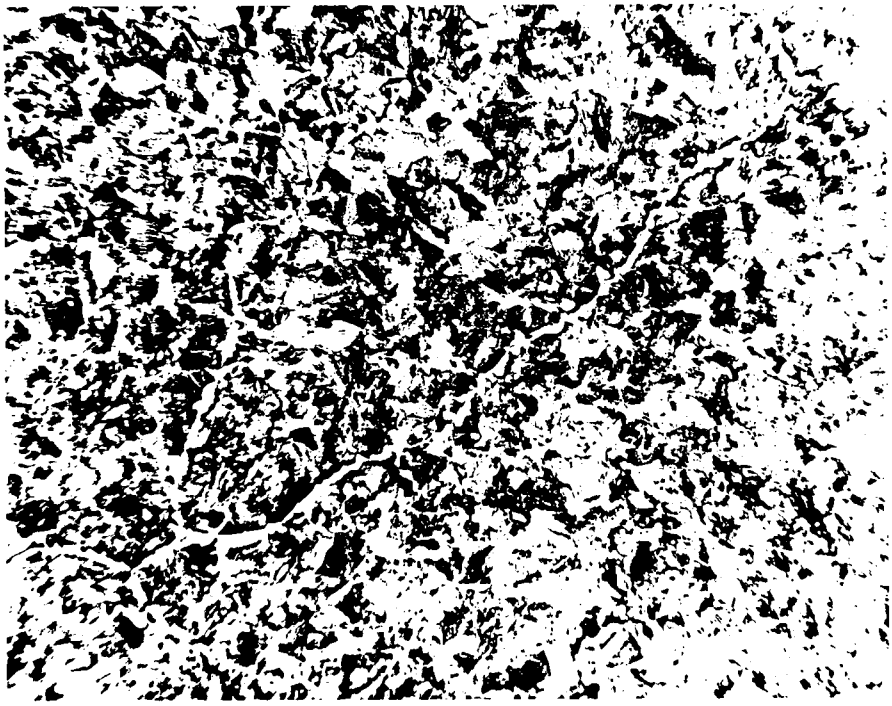


Figure 82. Microstructure of as-cast remelted 8630. 2% Nital etch, OLM, 20X.



Figure 83. Typical inclusions in wrought and remelted 8630. a) Wrought 8630, b) Remelted 8630. Unetched, OLM, 100X.

Figure 84. It is clear that the W516 tested PRD is the most susceptible to HIC. R516-AC as well as R516-C&N required the same preheat (100°F) to be crack free, however, at 32°F the R516-AC cracked to a greater extent than the R516-C&N and both of these were more susceptible than the W516 tested TTD. Metallographic examination revealed that the R516 contained some Type II inclusions located along the primary solidification boundaries. These type of inclusions, because of their location, tend to give rise to intergranular HAZ cracking. Typical examples of such inclusions and the associated cracking are shown in Figures 85a and b respectively. However, as the results indicate, the elongated inclusions present in the wrought A516, control the crack initiation behavior when the welding is performed PRD.

Implant tests were conducted to confirm the results obtained for the wrought and remelted A516 materials. In Figure 86, the results are plotted as applied stress vs. time to rupture. The results indicate the greater susceptibility (lower critical stress) to HIC of the W516 test welded PRD. The R516-AC and C&N steels show equivalent susceptibilities, however, in some unruptured implant samples from the R516-AC steel, intergranular cracking associated with Type II inclusions was noted. This is shown in Figure 87 where HIC is seen to propagate in the transgranular as well as the intergranular mode. In the IG mode, the association of Type II inclusions with the crack is evident. Fractographic evaluations of implant samples from W516 revealed

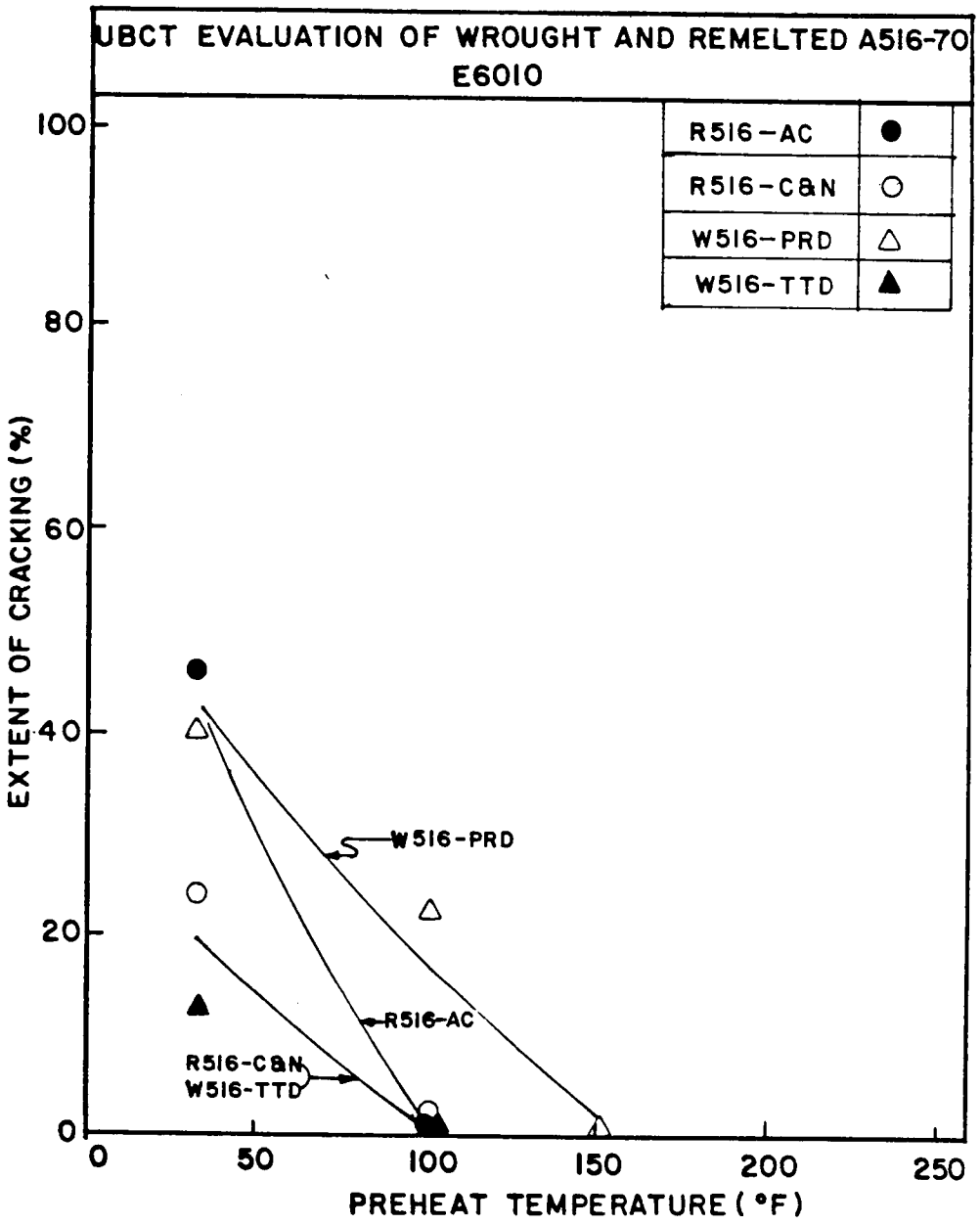


Figure 84. UBCT preheat results for remelted (R) and wrought (W) A516-70 steels. As-cast (AC), cast and normalized (C&N). E 6010.

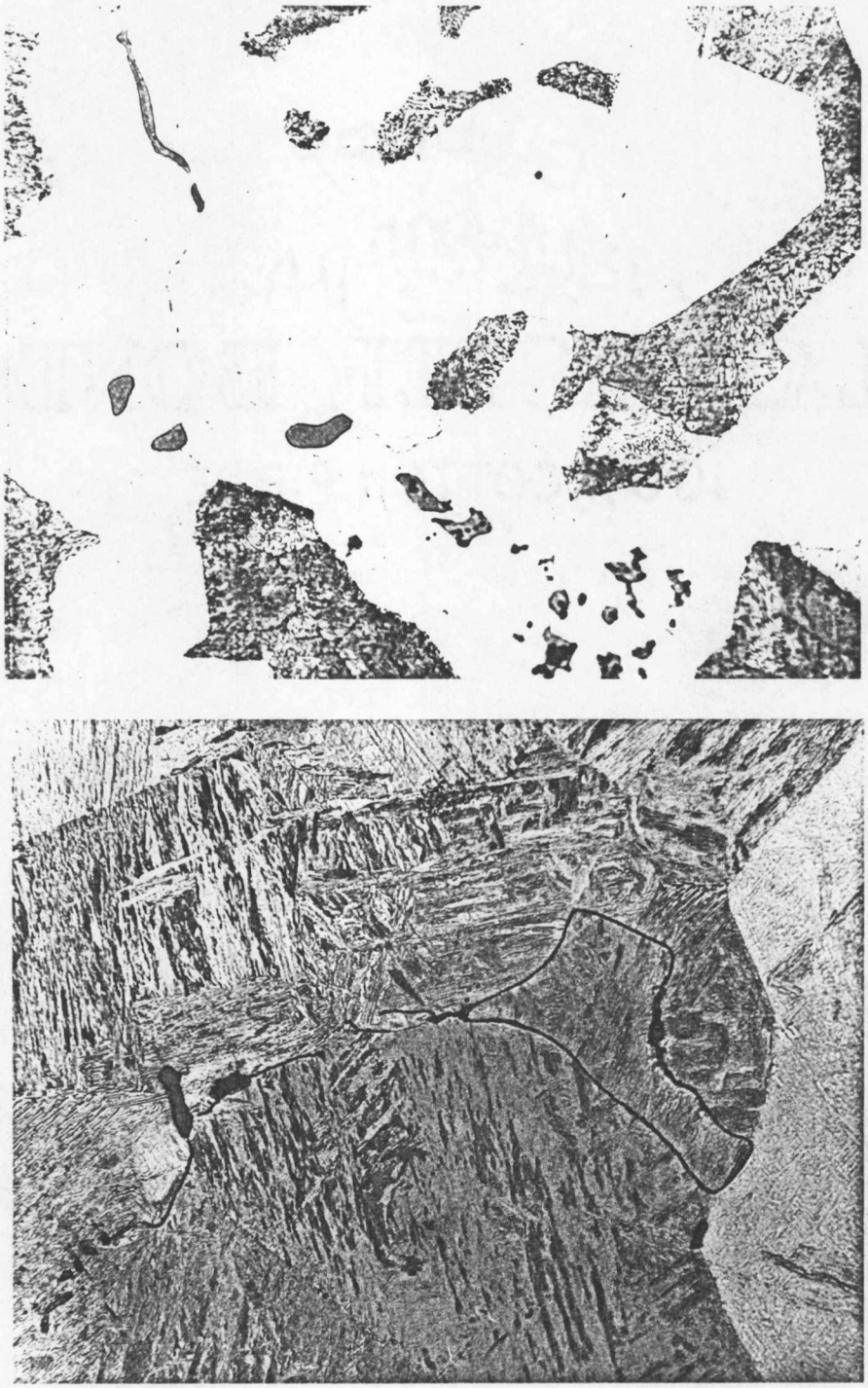


Figure 85. Typical morphology of Type II inclusions in remelted as-cast A516 and associated HIC. a) Type II inclusions. 2% Nital etch, OLM, 500X. b) HIC in coarse grained HAZ, UBCT, preheat 100°F. Picral etch, OLM, 500X.

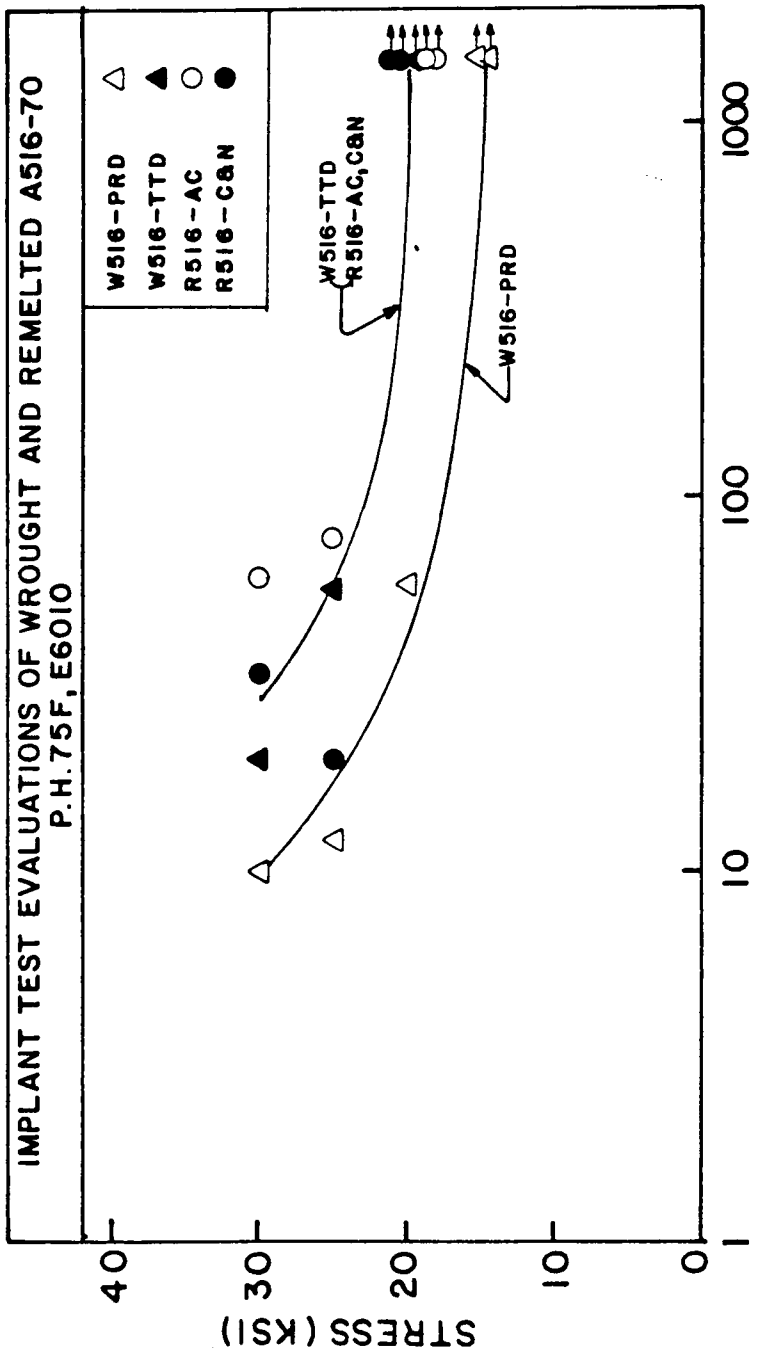


Figure 86. Implant test results for wrought (W) and remelted (R) A516-70. As-cast (AC), cast and normalized (C&N). Preheat 75°F, E 6010.



Figure 87. HIC in coarse grained HAZ of implant tested as-cast remelted A516 showing association of IG cracks with Type II inclusions. Picral etch, OLM, 500X.

several features. In the sample welded PRD shown in Figure 88a, rupture appears to have occurred with little plastic deformation. At higher magnifications in Figures 88b and c, the fracture matrix is seen to possess a "smooth" morphology indicating that failure occurred with no gross plastic deformation. In contrast, the fracture surface of the sample tested TTD (Figure 89a) indicates that in addition to some quasi-cleavage areas, there is also some region of IG cracking. Higher magnification views of the sample shown in Figure 89a indicate that the grain surfaces show a quasi-cleavage fracture morphology (Figures 89b and c). It is therefore clear that the greater susceptibility of the W516-PRD is related to the fact that the inclusions and banding are normal to the direction of the applied load, enabling hydrogen to "decohere" the interface bond between the inclusions and matrix. When the inclusions lie in the direction of the applied load (as in W516-TTD), the inclusion/matrix interfaces are not aligned conducive to the advancing front of hydrogen for accumulation, and further, the inclusion/matrix interfaces may in fact help diffuse the hydrogen in a short circuiting manner away from the HAZ. The results of the implant tests concerning HIC are similar to those obtained in a simple tensile test, where strengths and ductilities in the through-thickness direction are generally found to be lower than those obtained when the tensile tests are carried out with the samples oriented in the rolling direction.

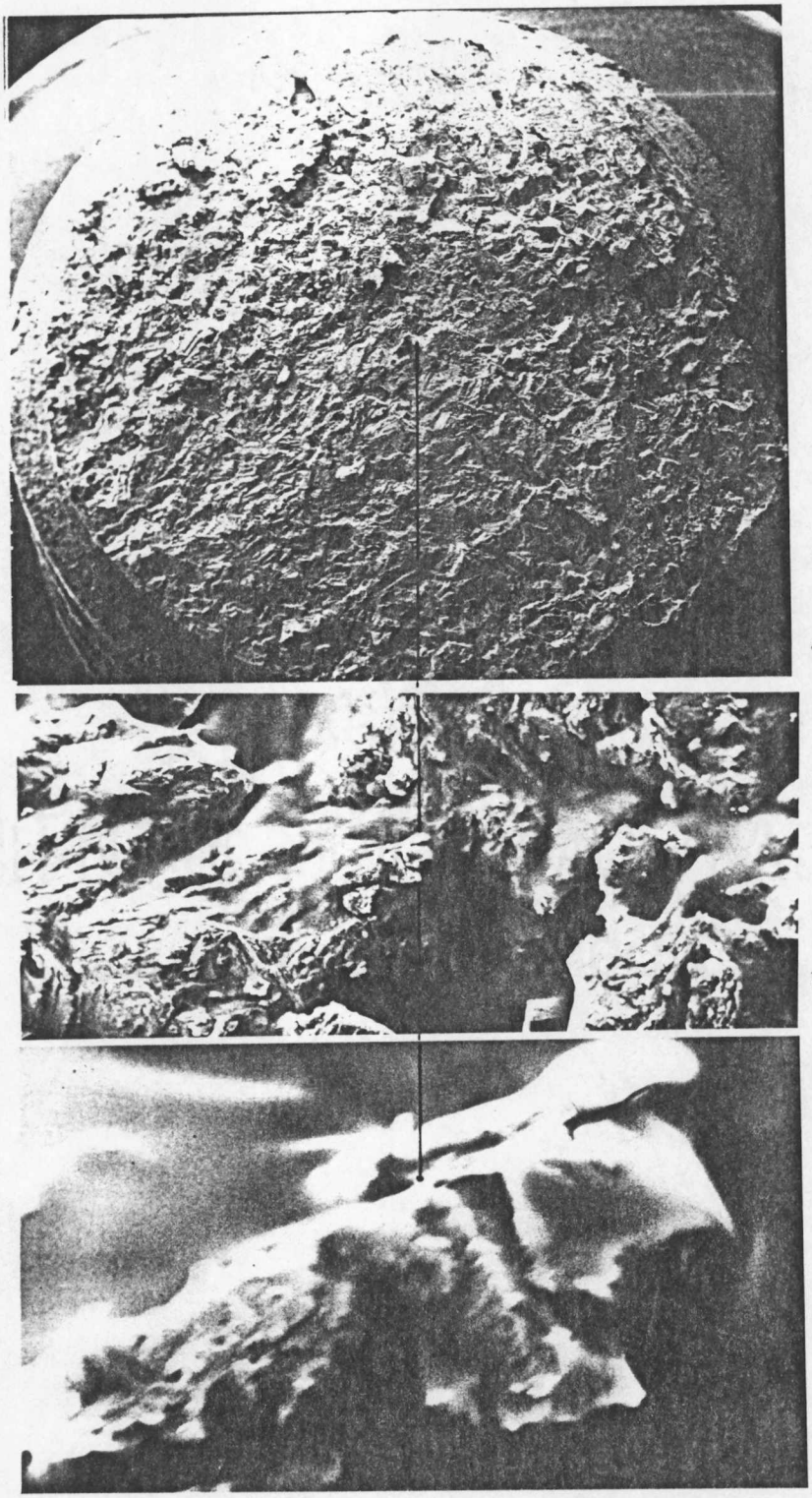


Figure 88. Fracture morphology of implant specimen of W516 tested PRD, C.E. = 0.43. Preheat 75°F, stress 25 Ksi, ruptured in 12 minutes. a) SEM, 20X, b) SEM, 500X, c) SEM, 5000X.

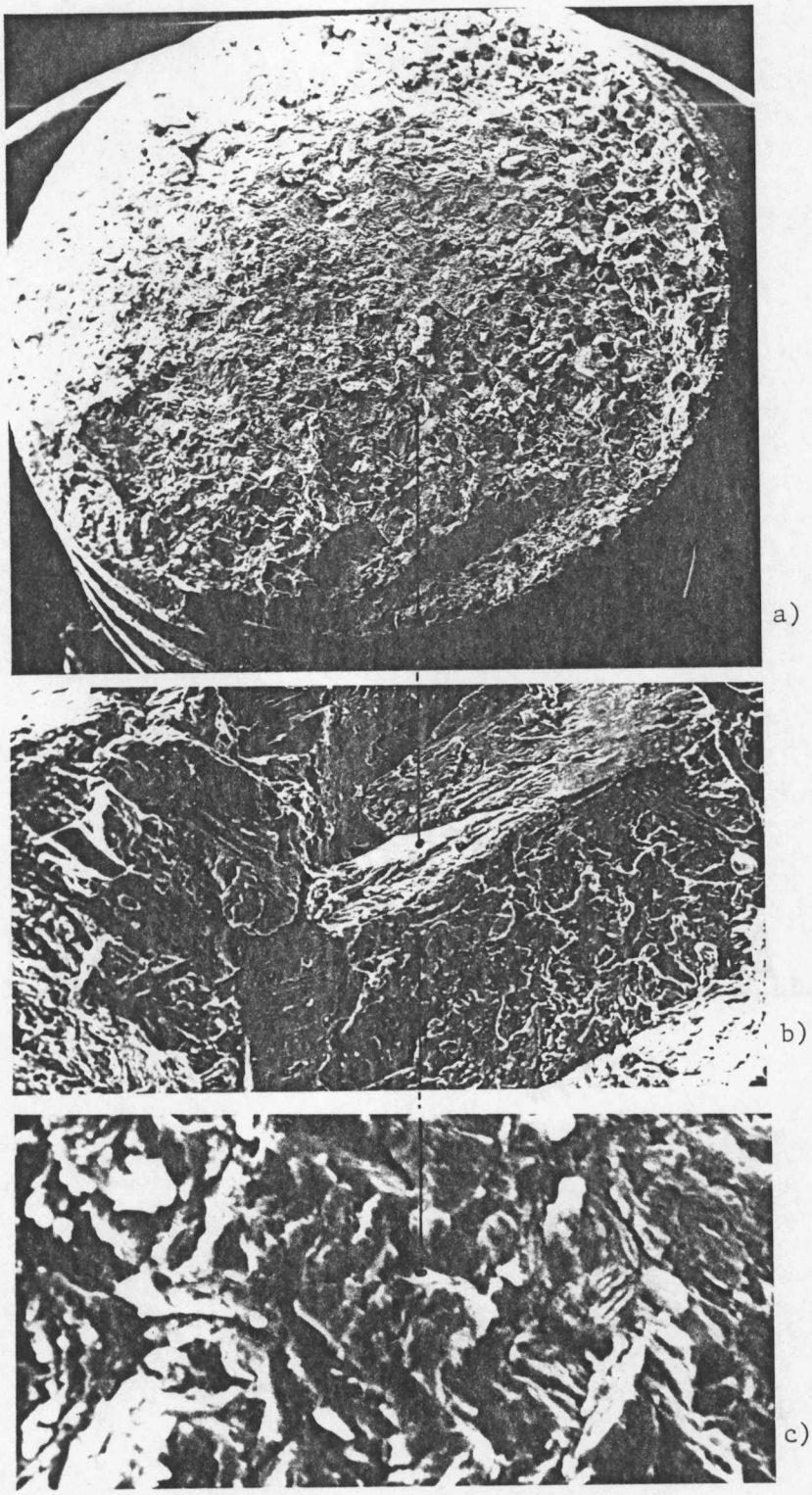


Figure 89. Fracture morphology of implant specimen of W516 tested TTD, C.E. = 0.43. Preheat 75°F, stress 25 Ksi, ruptured in 55 minutes. a) SEM, 20X, b) SEM, 500X, c) SEM, 5000X.

The results of the underbead cracking and the implant tests on the R8630 and the R516 therefore confirm trends obtained in the tests carried out on the Phase I materials. The results of the implant tests generally agree with those of the UBCT's. The additional advantage of the implant test is the ability to examine the fracture morphologies of the hydrogen embrittled HAZ's. This information enables a better understanding of the mechanism of HIC. A detailed discussion regarding the mechanism follows at the end of the chapter.

7. Effect of Inclusion Morphology/Deoxidation Practice

From the results just described, it has been demonstrated that inclusion morphology and distribution and orientation with regard to the weld HAZ and stress state have a significant effect on the HIC susceptibility of steels. In the wrought steels, elongated inclusions provide initiation sites for HIC whereas in cast steels, the presence of Type II inclusions (eutectic sulfides) at the primary solidification grain boundaries aggravates the problem of HIC. The importance of inclusion morphology as directly affected by deoxidation practice is of greater significance for the cast steels, since the inclusions in the cast steels are not altered by any thermo-mechanical treatments after casting and solidification. Sulfides comprise a majority of the inclusions in steels, and the types of sulfides that exist in cast steels and the conditions under which they are formed are important to HIC behavior and are briefly described.[94] Sulfides of Type I are

found in rimming or semi-killed steel where the oxygen content of the steel is high and thus the sulfur solubility is low. This results in precipitation of sulfides at a comparatively high temperature, giving rise to spherical Type I sulfides. Type II sulfides are found in steels where the extent of deoxidation is just enough to neutralize all the oxygen content. This increases the solubility of sulfur in the liquid steel leading to the precipitation of the sulfides in the last portions of the ingot to solidify. The sulfide morphology is dendritic from a eutectic reaction. A third type of sulfide, Type III, is found in cast steels deoxidized with an excess of aluminum. The oxygen content of the steel is low, however the sulfur solubility is also low because aluminum in solid solution reduces sulfur solubility. Type III sulfides are presumed to be precipitated at higher temperatures than Type II sulfides but at lower temperatures than Type I. Type III inclusions are monophase (no oxides due to low oxygen content of the steel) and generally possess an angular morphology.

In Chapter III, Table 9 (page 93), the steels utilized for the deoxidation practice/inclusion morphology were described. DEOX-1, DEOX-2 and DEOX-3 were intended to have exclusively Type I, Type II and Type III inclusions. However, metallographic examination of the DEOX-1 cast plate showed that in addition to Type I inclusions (Figure 90), the cast steel also contained a substantial fraction of Type II inclusions. Typical examples are shown in Figures 91a and b. The DEOX-2 lot was found to contain a mixture



Figure 90. Typical Type I inclusions in DEOX-1 cast A216-WCB steel. Acid sol. Al = 0.007%, Total Al = 0.015%. Unetched, OLM, 500X.



Figure 91. Typical Type II inclusions in DEOX-1 cast A216-WCB steel. Acid sol. Al = 0.007%, Total Al = 0.015%. a) Unetched, OLM, 100X, b) Unetched, OLM, 500X.

of Type II and Type III inclusions (Figure 92) whereas the DEOX-3 lot had exclusively Type III inclusions (Figure 93). Metallographic examination revealed that it was apparently extremely difficult to control deoxidation to highly critical levels to achieve Type I or Type II inclusions. However, achieving exclusively Type III inclusions is not difficult, since excessive aluminum deoxidation does not require any extraordinary control. In Table 9 (page 93), the oxygen contents given are total oxygen; the greatest oxygen level is in the DEOX-3 steel which probably indicates that most of the oxygen tied up as oxides (Al_2O_3). The total nitrogen content indicates the extent of nitride formation in the steels. The acid-soluble and the total aluminum contents are in the right order with the DEOX-3 having a maximum total aluminum content of 0.071%. Since the C.E.'s of the steels are quite similar, the results of the HIC tests may be correlated with the acid soluble and total aluminum content as well as to the inclusion morphology/distribution. In the Literature Review, it was mentioned that HIC susceptibility as well as HAZ impact toughnesses have been related to the aluminum content in wrought steels. Hence, in addition to underbead cracking and implant tests, simulated HAZ charpy samples were tested.

Underbead cracking tests were conducted on the three deoxidized level steels in the as-cast (AC) as well as in the cast and normalized (C&N) conditions. For the as-cast condition, the results are shown in Figure 94. DEOX-1-AC is seen as the most susceptible to HIC requiring a preheat temperature of 250°F to avoid cracking.

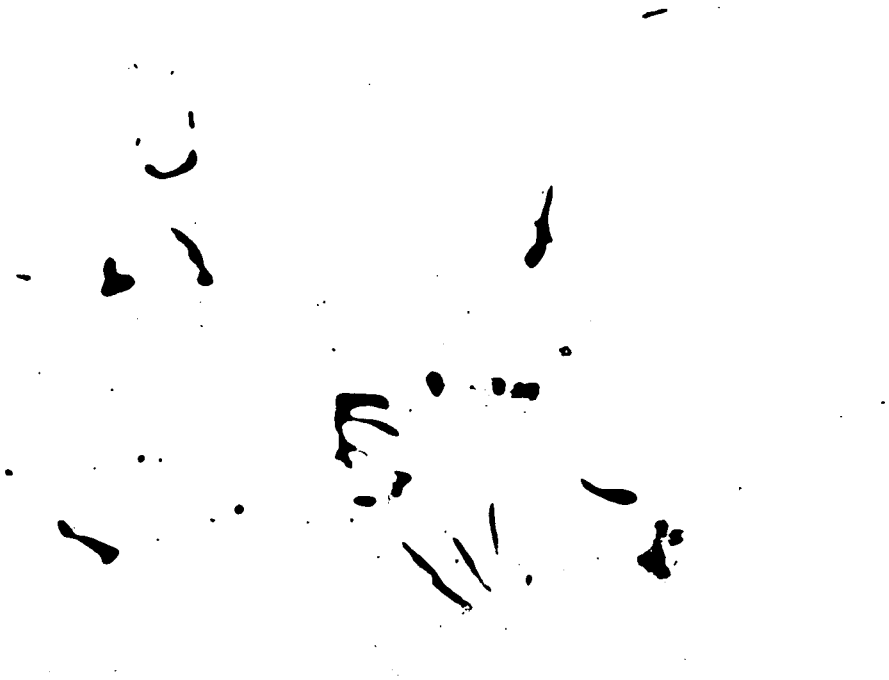


Figure 92. Typical Type II and Type III inclusions in DEOX-2 cast A216-WCB steel. Acid sol. Al = 0.019%, Total Al = 0.030%. Unetched, OLM, 500X.



Figure 93. Typical Type III inclusions in DEOX-3 cast A216-WCB steel. Acid sol. Al = 0.064%, Total Al = 0.071%. Unetched, OLM, 500X.

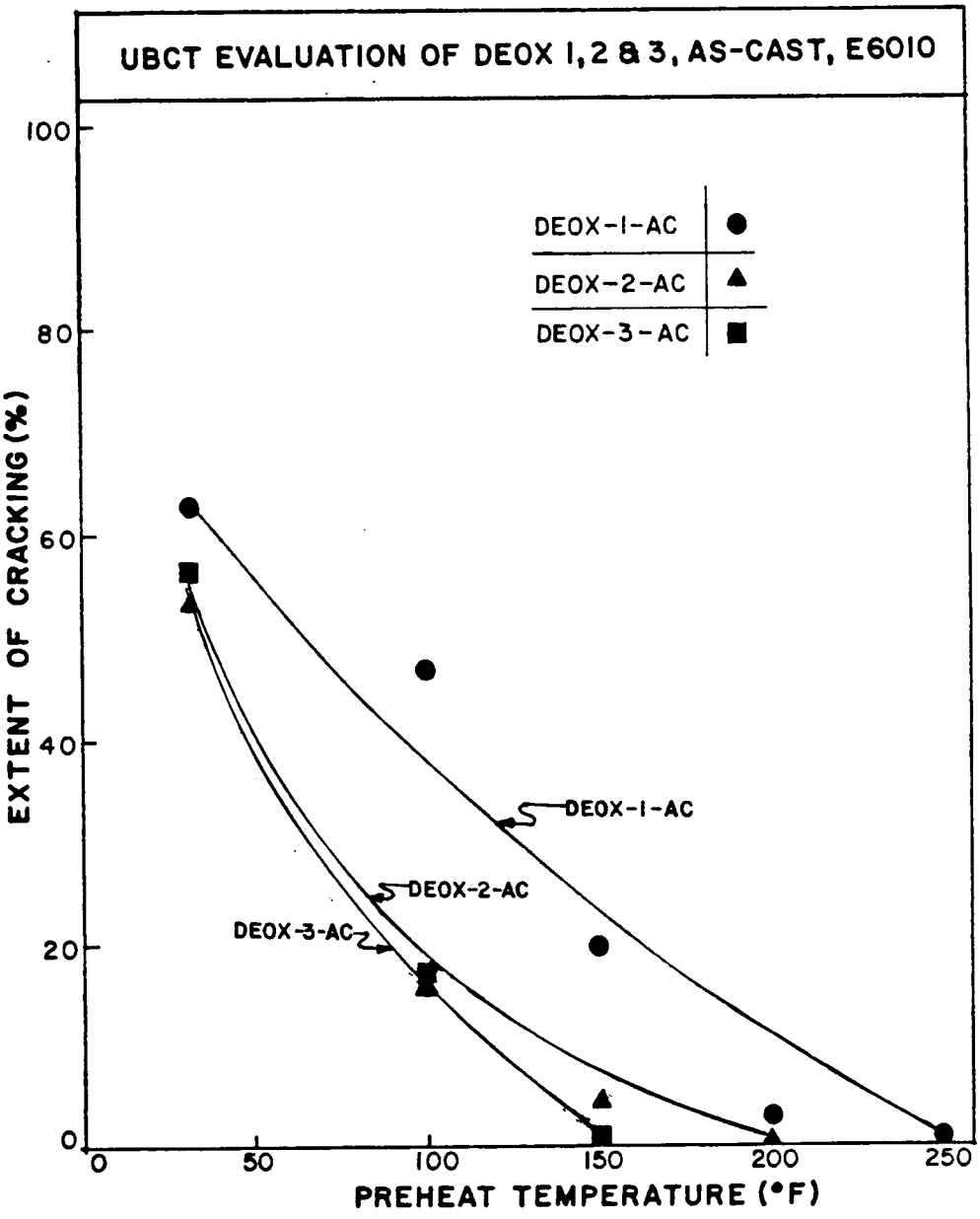


Figure 94. UBCT preheat results for DEOX-1,2,3 tested in the as-cast (AC) condition. E 6010.

DEOX-2-AC and DEOX-3-AC follow in the order of decreasing susceptibility. A similar trend is observed for the testing conducted in the C&N condition (Figure 95). However, the preheat temperatures required to prevent cracking for each of the steels was 50°F lower than when the steels were tested in the as-cast condition. Microhardness surveys carried out in the HAZ's of UBCT samples show a higher hardness is retained at greater distances from the fusion line for DEOX-1 as compared to DEOX-2 or DEOX-3, in both the as-cast and C&N conditions. The microhardness surveys for samples in the AC and C&N conditions are shown in Figures 96 and 97 respectively. The greater HIC susceptibility of DEOX-1 can be attributed to both the presence of Type II inclusions and to its higher hardenability (as indicated by the microhardness survey). These HIC results corroborate those of Sims[64] and Hasebe[66], who have reported decreasing susceptibilities to HIC with increasing residual aluminum contents in wrought steels. The results obtained indicate a difference in HIC susceptibility for cast steels depending on the extent of deoxidation. The susceptibility to HIC is governed by the total/residual aluminum content and the inclusion morphology/distribution obtained. Type II inclusions render cast steels more susceptible to HIC whereas the aluminum content apparently has an effect on the microstructure resulting in the coarse grained HAZ.

Implant tests conducted on the steels in the AC condition confirm the results obtained in the underbead cracking tests.

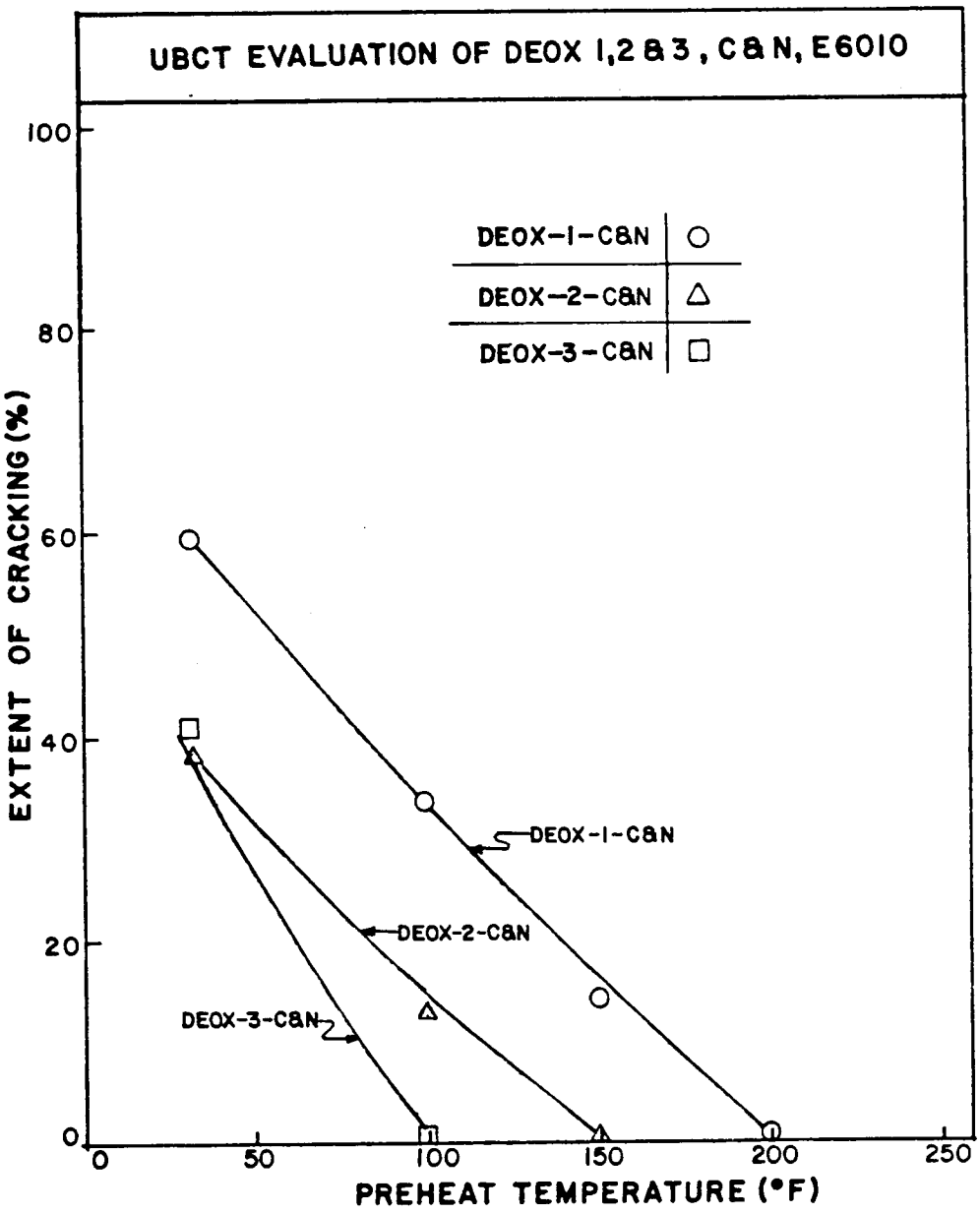


Figure 95. UBCT preheat results for DEOX-1,2,3 tested in the cast and normalized (C&N) condition. E 6010.

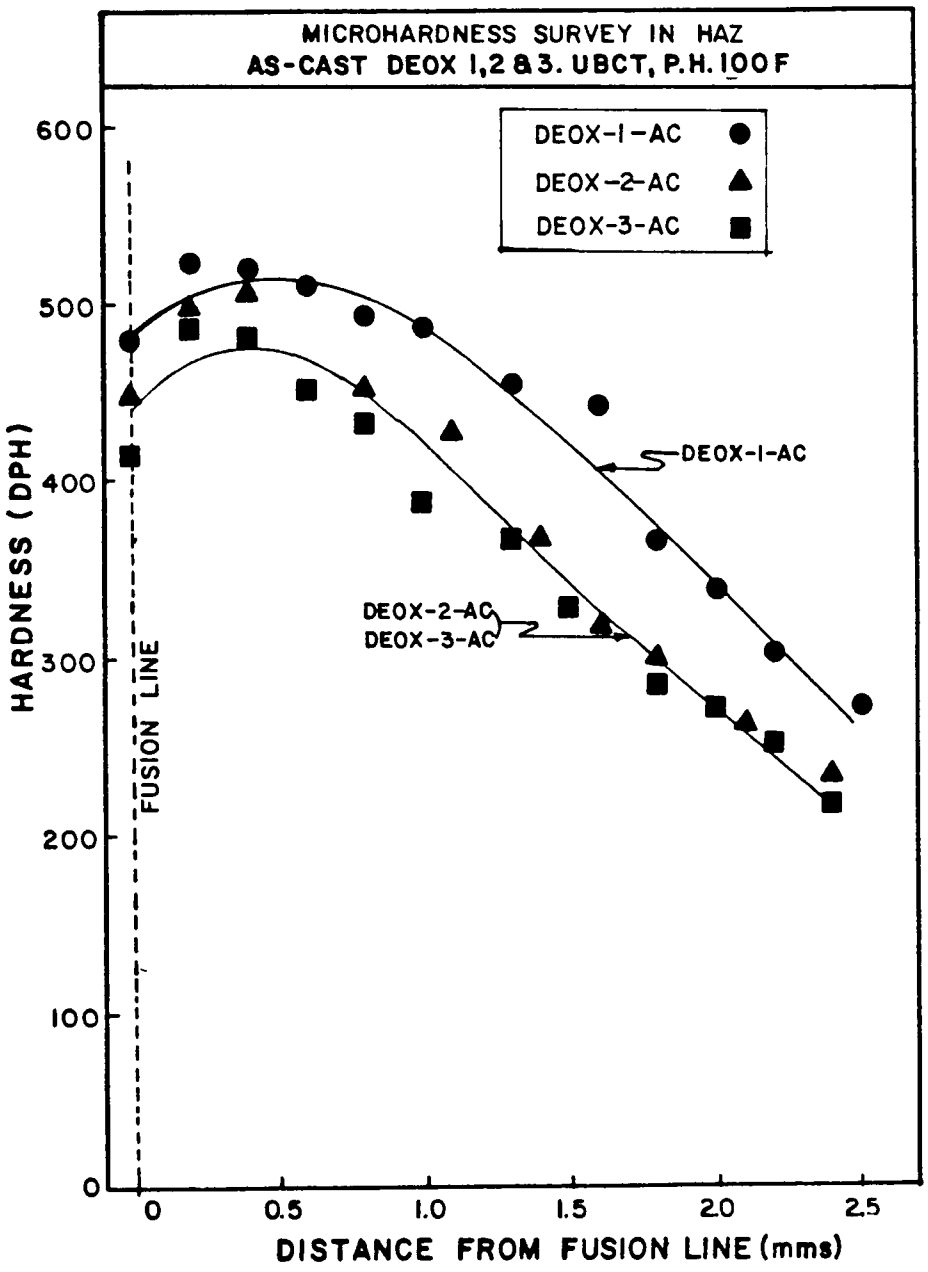


Figure 96. Microhardness distribution in the HAZ of DEOX-1,2,3 UBCT samples tested in the as-cast (AC) condition.

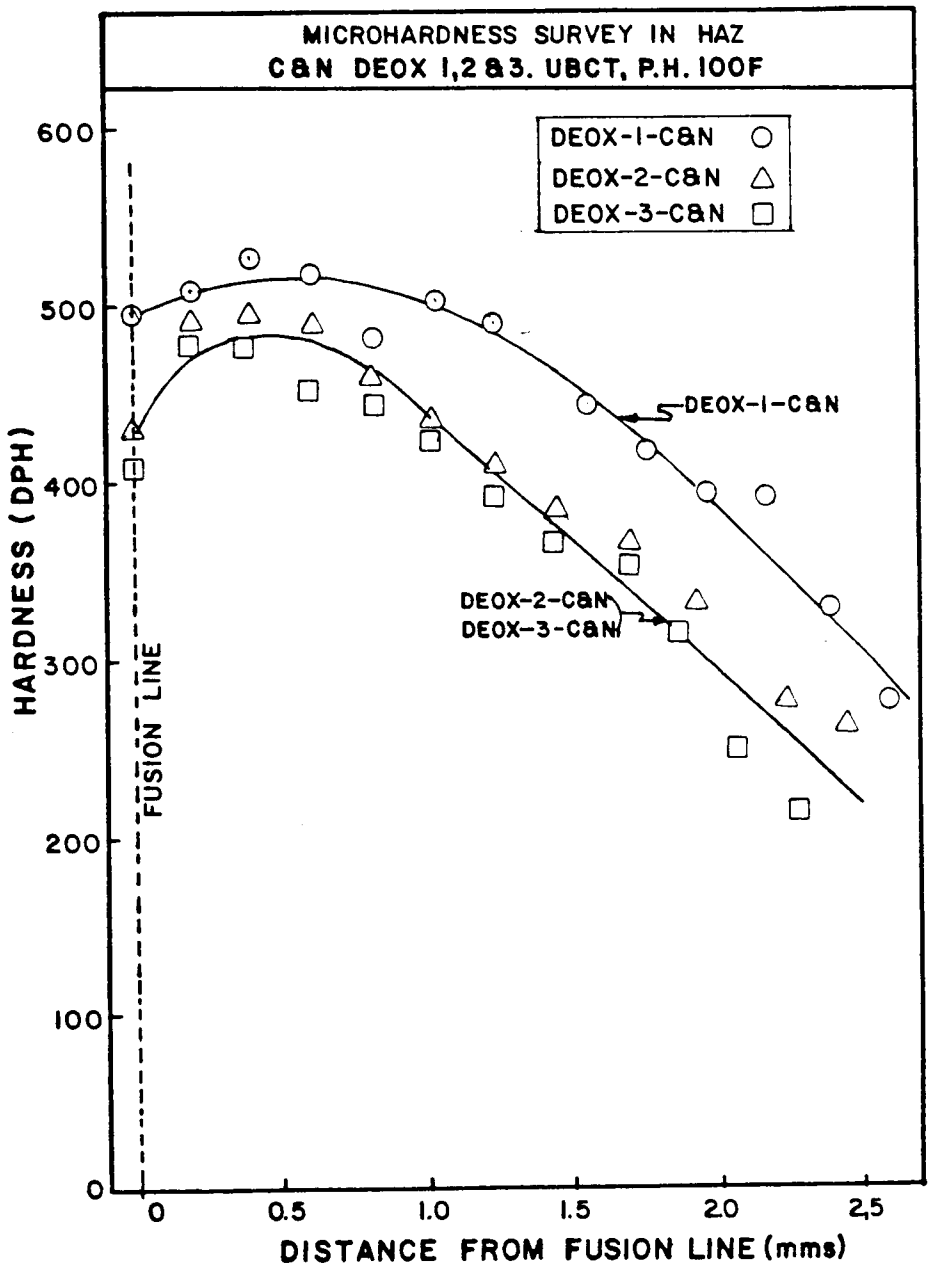


Figure 97. Microhardness distribution in the HAZ of DEOX-1,2,3 UBCT samples tested in the cast and normalized (C&N) condition.

The results of these tests are presented in Figure 98 as the stress applied vs. time to rupture. The results shown indicate that DEOX-1-AC has a lower critical stress (greater susceptibility to HIC) than DEOX-2-AC or DEOX-3-AC. Moreover, at equivalent applied stress levels, DEOX-1-AC failed at shorter times than either DEOX-2-AC or DEOX-3-AC. Microhardness traverses in the HAZ's of the implant samples further give credence to these results. In Figure 99, higher hardnesses are retained for a greater distance from the fusion line for DEOX-1-AC when compared to DEOX-2-AC or DEOX-3-AC. Metallographic examination of a ruptured specimen from DEOX-1-AC (Figure 100a) shows secondary cracks in the HAZ and at a higher magnification (Figure 100b), the intergranular nature of some of the cracks is revealed clearly. The intergranular nature of the cracks indicates that Type II inclusions play a part in both crack initiation and propagation. Figure 101 shows a section for an implant sample from DEOX-2-AC where the secondary cracks are seen emanating from inclusions/matrix interfaces and propagating in both the intergranular and transgranular modes.

The results of the underbead cracking and implant tests indicate that the difference in susceptibilities to HIC between the three lots of cast steels deoxidized to different levels is related to the inclusion morphology as well as to a difference in the type of transformation products in the HAZ resulting from the weld thermal cycle. The microhardness tests clearly indicate the difference in the type of transformation products. However, due

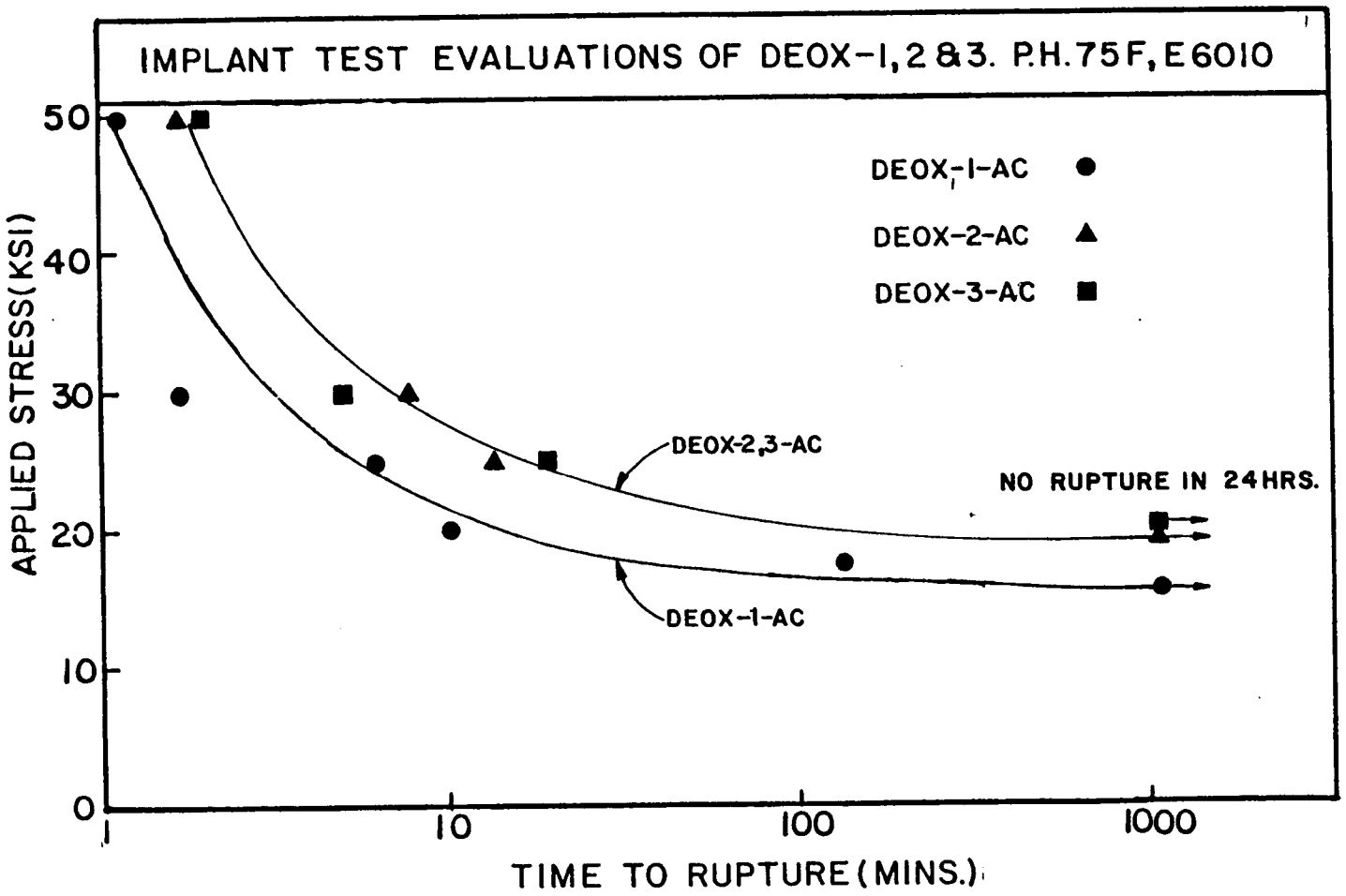


Figure 98. Implant test results for steels DEOX-1,2,3 tested in the as-cast (AC) condition. Preheat 75°F, E 6010.

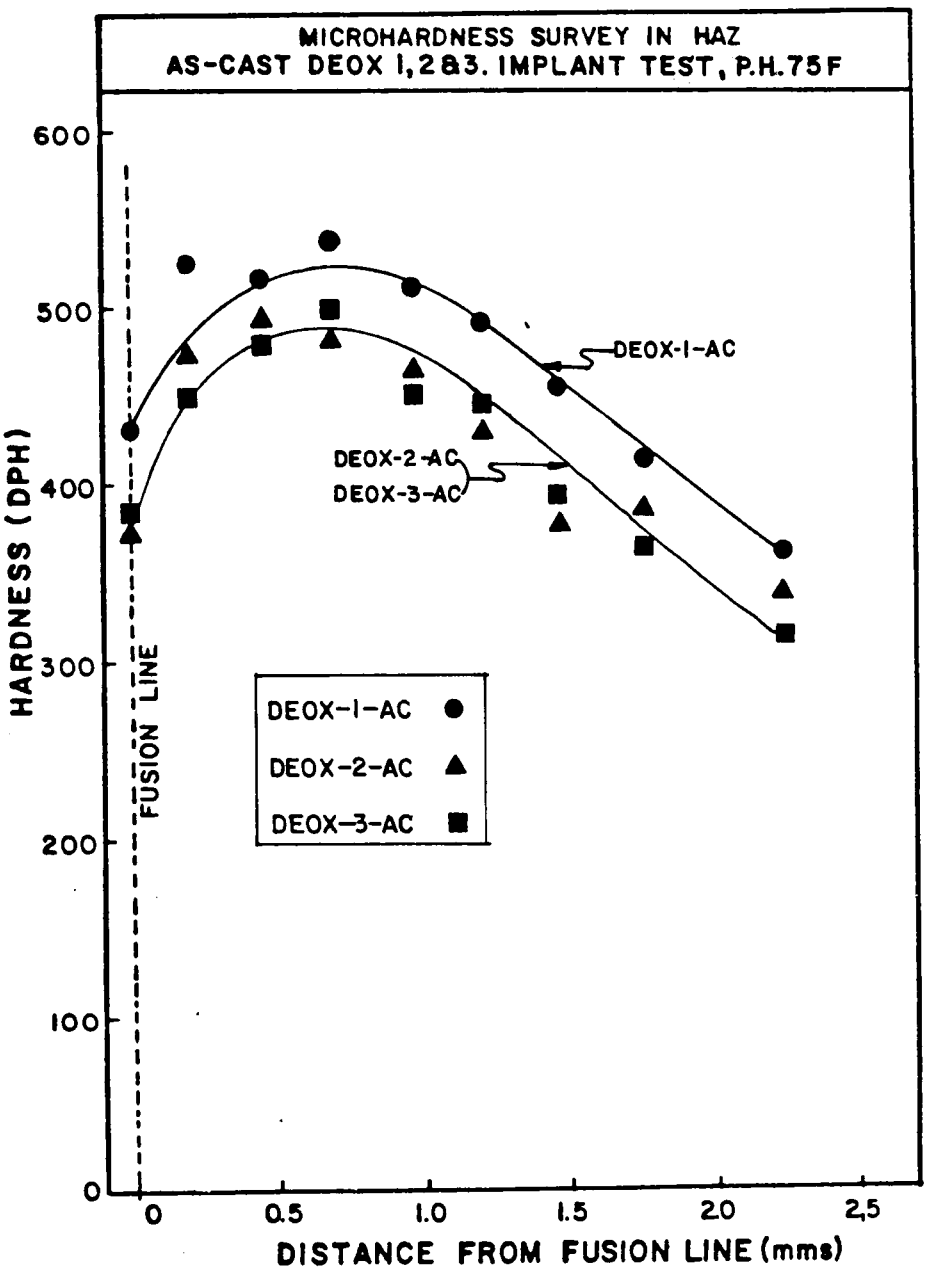


Figure 99. Microhardness distribution in the HAZ of steels DEOX-1,2,3 implant tested in the as-cast (AC) condition.

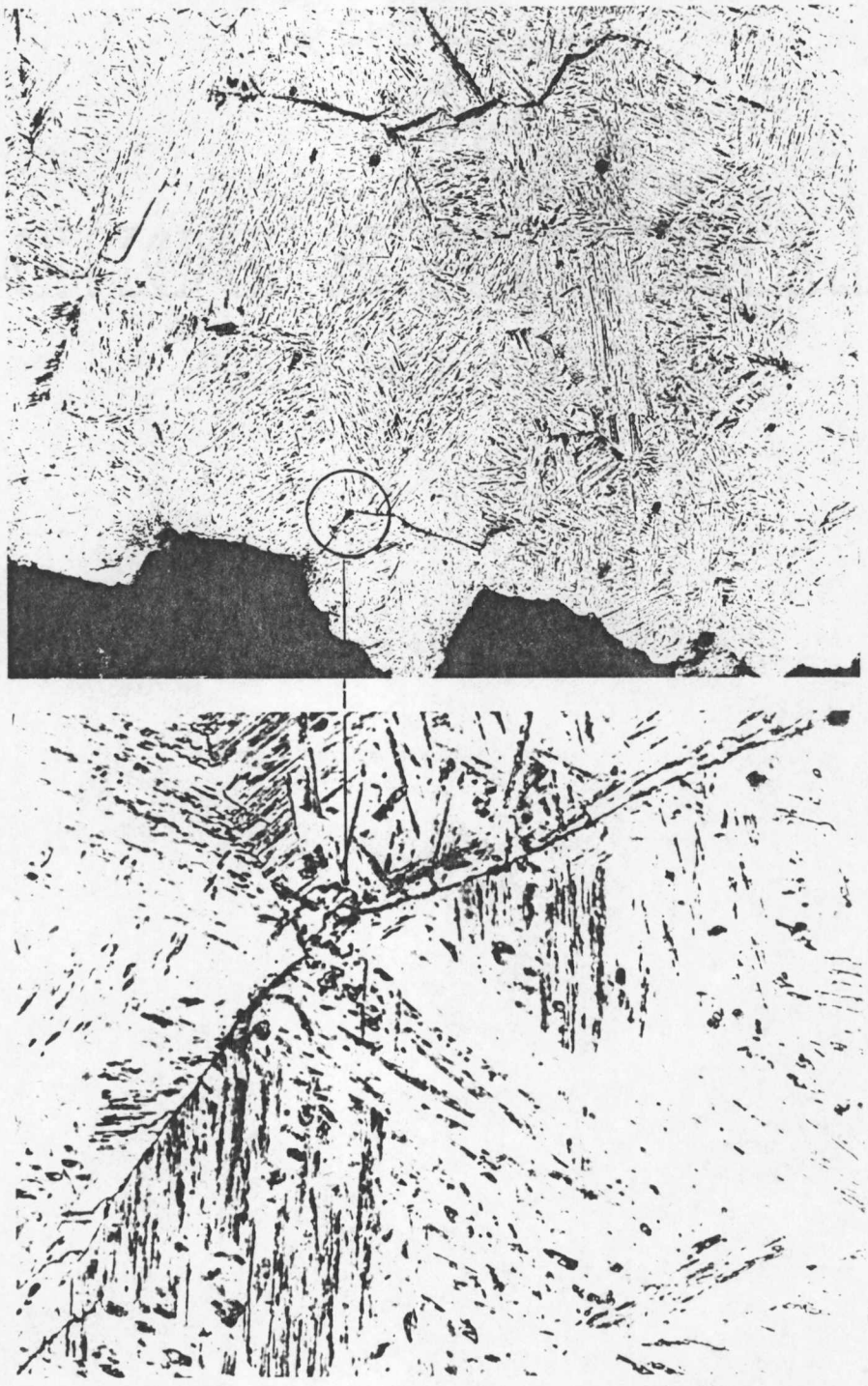


Figure 100. Microstructure at fracture interface in implant specimen of DEOX-1-AC, C.E. = 0.45. Preheat 75°F, stress 25 Ksi, ruptured in 8 minutes. a) Secondary HIC. Vilella's etch, OLM, 20X, b) Intergranular HIC. Vilella's etch, OLM, 500X.

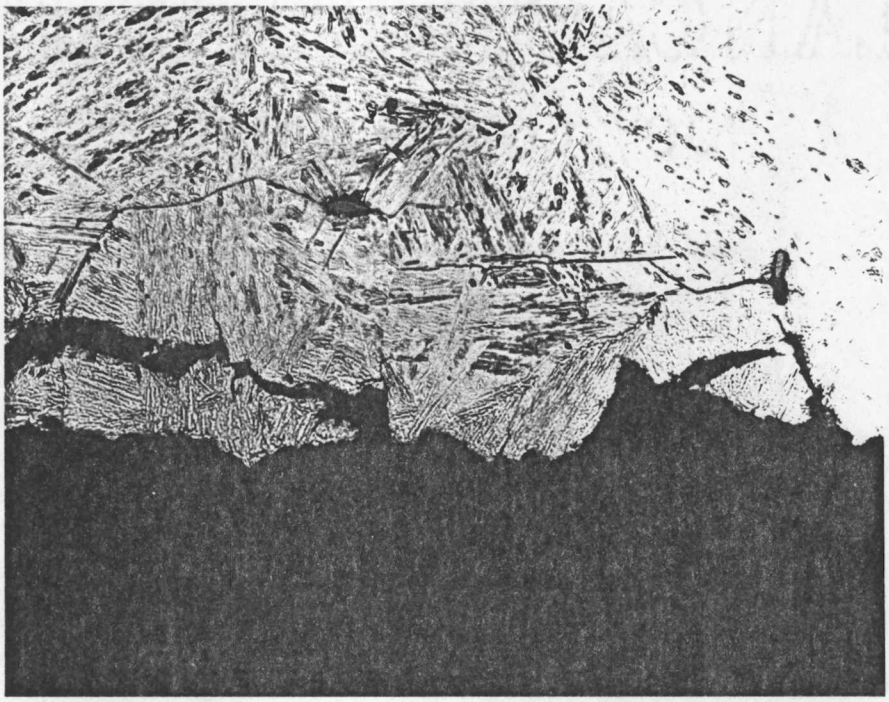


Figure 101. Microstructure at fracture interface in implant specimen of DEOX-2-AC, C.E. = 0.42. Preheat 75°F, stress 25 Ksi, ruptured in 20 minutes. Vilella's etch, OLM, 200X.

to the nearly identical composition of the steels, these differences could not easily be deciphered in the microstructure in the HAZ. Coarse grained HAZ's were therefore simulated in these steels in charpy blanks, so that the impact toughness of such regions could be compared between the three deoxidized steels in the as-thermal cycled as well as PWHT condition. Further, the transformation products resulting from a known thermal cycle in a large area of the coarse grained HAZ could be examined. Simulated coarse grained HAZ impact studies were conducted on the materials only in the as-cast condition and it was presumed that a similar trend of results would be obtained for the materials tested in the C&N condition. The thermal cycle utilized was one corresponding to a heat input of 50 KJ/in with a 2400°F peak temperature in a 1" thick steel plate. Two samples from each of the steels were impact tested in the as-cast as well in the as-thermal cycled condition at temperatures of 100°F, 212°F and 400°F. The higher-than-ambient test temperatures were used to determine if there was a correlation between the preheat temperatures used in the UBCT's to prevent cracking and the impact toughnesses at these test temperatures. Figure 102 shows the results of the impact tests. In the as-thermal cycled condition (T), DEOX-3 exhibits a higher impact toughness than DEOX-1 or DEOX-2 at all three test temperatures. In the AC condition, there is considerable scatter in the impact data since the as-cast steel is prone to have grain size and segregation differences. DEOX-3 also exhibited a higher toughness

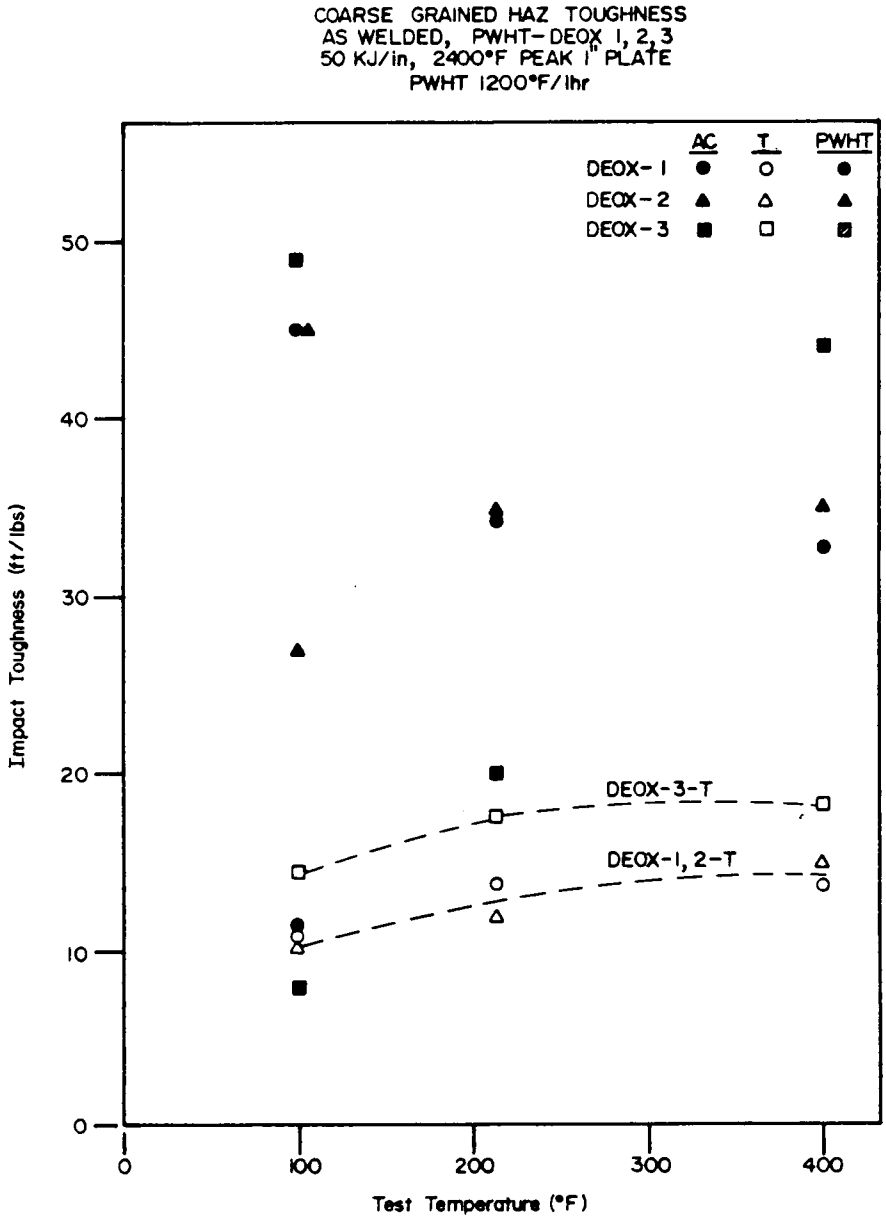


Figure 102. Impact test results for DEOX-1,2,3 in the as-cast (AC), as-welded (T) and PWHT conditions. 50 KJ/in, 2400°F, 1" plate, PWHT 1200°F/1 hr.

after PWHT than DEOX-1 and DEOX-2. Hardness testing clearly showed that both in the as-thermal cycled and in the PWHT conditions. the hardness is highest for the DEOX-1, followed by DEOX-2 and DEOX-3 (Table 12). The hardness data correlates well with the impact test results. The data demonstrates that for identical thermal cycles, the transformation products (or their volume fractions) that result in the coarse grained HAZ are different for the three steels. Figures 103a, b and c show typical microstructures obtained in the coarse grained HAZ's of charpy samples from DEOX-1, 2 and 3 respectively. The microstructures are essentially composed of martensite within the grains and bainite and Widmanstätten ferrite at the grain boundaries. The microhardness within the grains was found to be HRC 45 which corresponds to over 95% martensite in a steel having a carbon content of 0.25%. The volume fraction of Widmanstatten ferrite increases from DEOX-1 to DEOX-3 and this is reflected in the drop in the overall hardness of the microstructure from 427 to 387 DPH (Table 12). In the thermal cycled and PWHT condition, a very similar trend is seen in Figures 104a, b and c. DEOX-3 again has the largest amount of upper temperature transformation products reflected in its hardness of 210 DPH compared to the 300 DPH for DEOX-1.

The results of the impact tests and associated metallographic analysis clearly indicate that in addition to inclusion morphology differences, the relative volume fraction of transformation products resulting from an identical weld thermal cycle is different

Table 12. Hardnesses (DPH) of charpy samples from DEOX-1, 2 and 3--as-thermal cycled and PWHT.

Steel	Thermal Cycled	Thermal Cycled and PWHT
DEOX-1	427	300
DEOX-2	400	240
DEOX-3	387	210

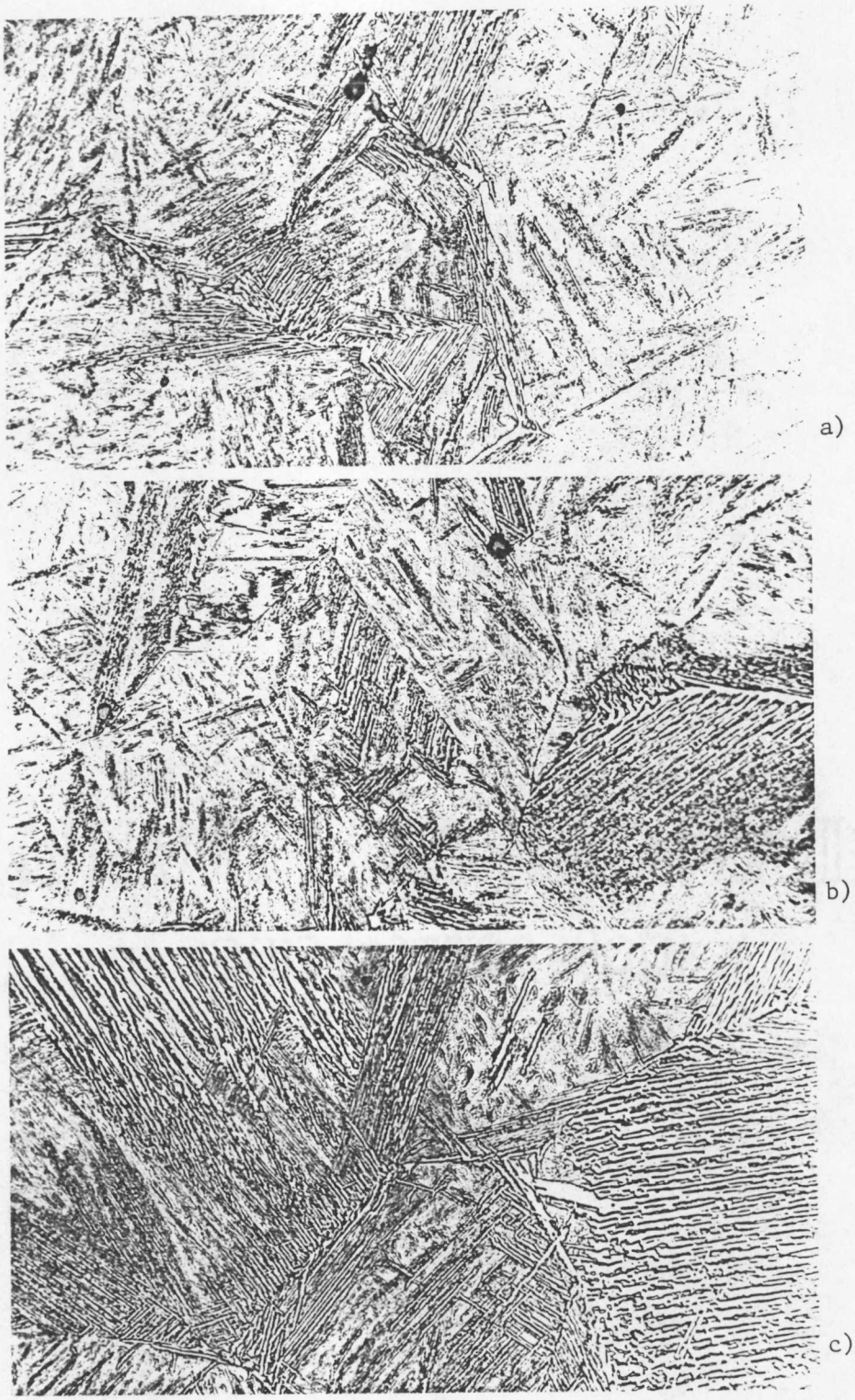


Figure 103. Microstructures in simulated coarse grained HAZ's of charpy specimens from DEOX-1, DEOX-2 and DEOX-3. 50 KJ/in, 1" plate, 2400°F peak. a) DEOX-1, b) DEOX-2, c) DEOX-3. Picral etch, OLM, 500X.

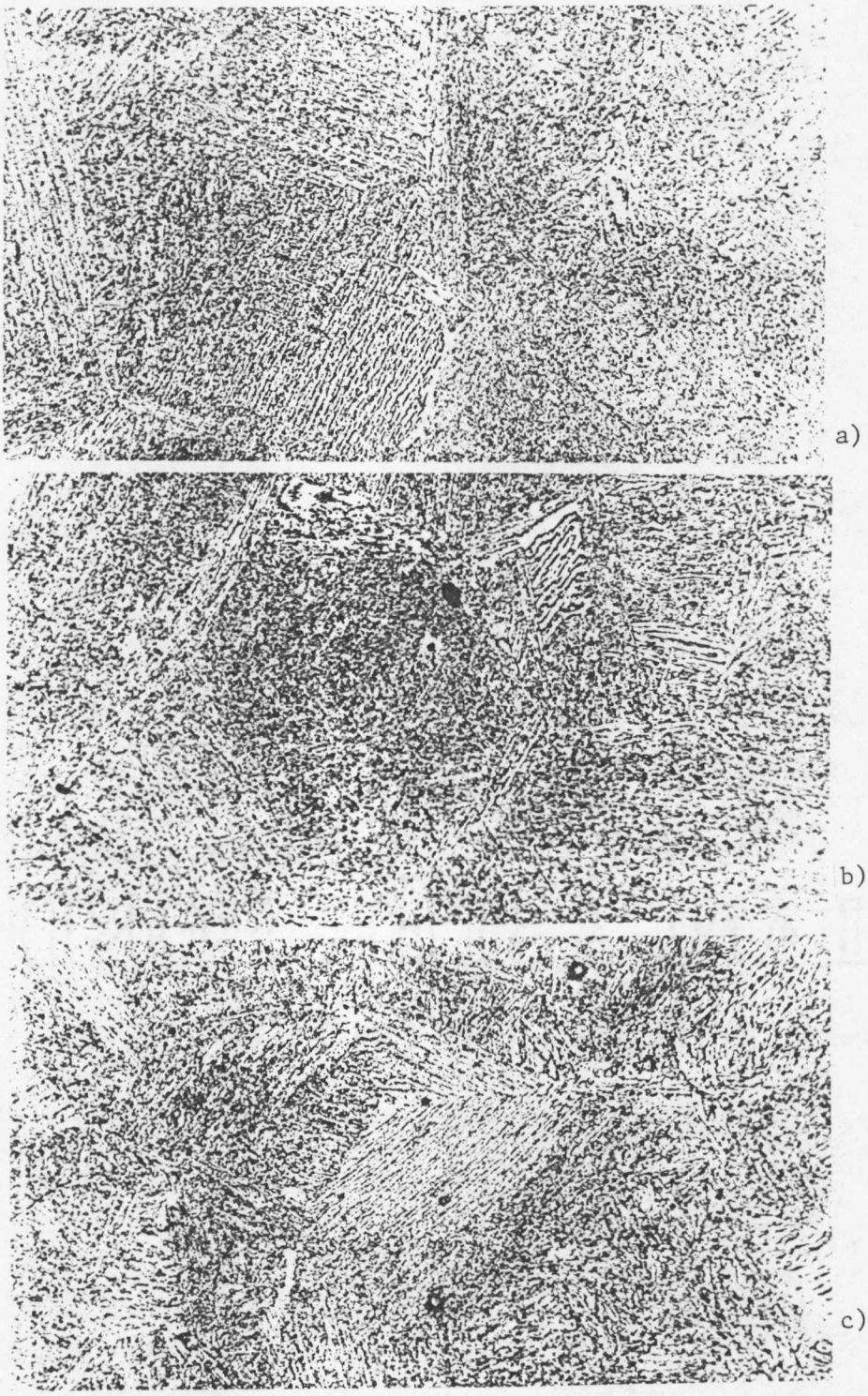


Figure 104. Microstructures in simulated post weld heat treated coarse grained HAZ's of charpy specimens from DEOX-1, DEOX-2 and DEOX-3. 50 KJ/in, 1" plate, 2400°F peak, PWHT 1200°F/1 hr. a) DEOX-1, b) DEOX-2, c) DEOX-3. Picral etch, OLM, 500X.

among the three steels. Considering the fact that the composition of the steels is almost identical, the effects of the differences in acid-soluble and total aluminum contents on the transformational characteristics has to be taken into account. As stated earlier, the trend of the cast steel results obtained in this work not only agrees with HIC behavior noted for wrought steels by other researchers,[64,66] but are also in agreement with Japanese work[67] on HAZ toughnesses. Among other compositional differences, Table 9 (page 93) also shows the nitrogen content of DEOX-2 and DEOX-3 to be higher than that of DEOX-1. This could imply that the presence of a higher volume fraction of AlN in DEOX-3. AlN has been reported[68] to provide effective resistance to grain coarsening. However, no significant differences in grain sizes were observed between the three steels in the simulated coarse grained HAZ. In addition, AlN can also act as a nucleant for upper temperature transformation products and this hypothesis is consistent with the metallographic analysis and hardness data presented earlier. Fractured charpy samples from DEOX-1, 2 and 3 (Figures 105a, b and c) did not reveal the presence of AlN. The location and identification of AlN inclusions has been reported[95] to be an extremely difficult task, especially in fast cooled ingots. The definition of AlN was not pursued further in this study.

In summary, the greater the extent of deoxidation in aluminum killed cast steels, the better is the resistance to HIC. An added benefit is improved toughness, both in the as-welded and PWHT

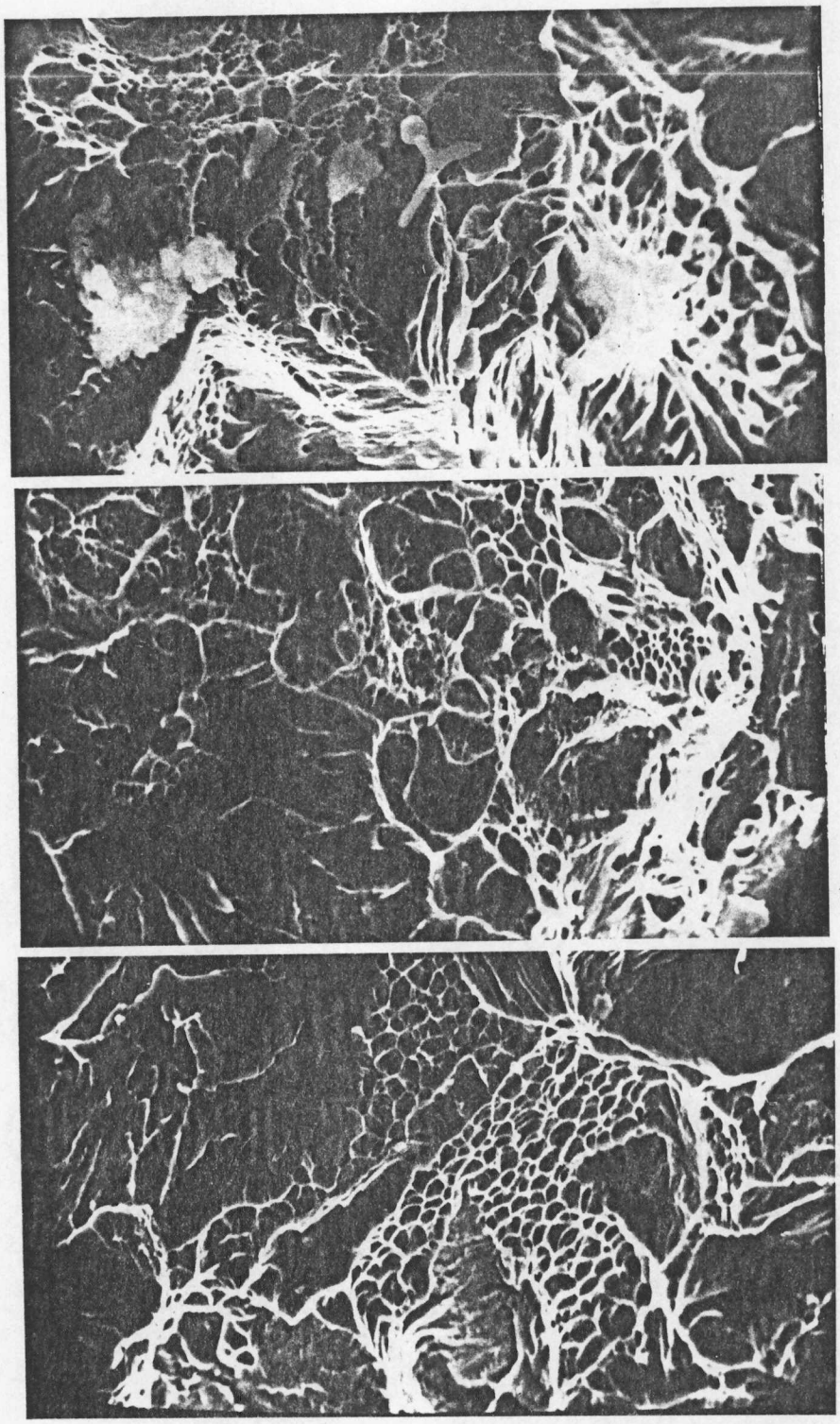


Figure 105. Fracture morphology of charpy samples of DEOX-1, DEOX-2 and DEOX-3, AC, impact tested at 100°F. a) DEOX-1, b) DEOX-2, c) DEOX-3. SEM, 2000X.

conditions. However, the above data has to be used in conjunction with the realization that excessive aluminum deoxidation, especially in large castings (which cool slowly), can give rise to the problem of intergranular AlN embrittlement. The better weldability characteristics of DEOX-3 can be related to the presence of Type III inclusions in preference to Type II's. Type II inclusions render cast steels more susceptible to intergranular HIC. In addition, higher total/residual aluminum contents aid the formation of a softer, and hence less susceptible microstructure in the coarse grained HAZ.

8. Tests on Low Sulfur Steels

The HIC susceptibility of cast and wrought steels is a function of the microstructure in the HAZ, and the inclusion morphology as affected by the deoxidation practice and thermo-mechanical treatments. The HIC susceptibility of cast steels is exacerbated by the presence of Type II inclusions, whereas for the wrought steels, cracking is aggravated by the presence of elongated sulfide inclusions. In addition, in wrought steels, laminations of sulfides reduce the through-thickness strength and during welding can give rise to the problem of lamellar tearing, especially in the high restraint welds. One of the ways to alleviate the problem of lamellar tearing is by reducing the sulfur content to a low level so that a large volume fraction of inclusions are not present to reduce the through thickness strength of the steel. However, as reported in the Literature Review, low sulfur (0.01%) wrought steels have been noted[23,47] to occasionally be extraordinarily

susceptible to HIC. In this research program, four grades of A537 steel (Table 10, page 95) with sulfur contents ranging from 0.001% to 0.012% were tested for HIC susceptibility, using both the UBCT (PRD) and the implant test (TTD). In addition, steels A537-1 and A537-8 were also implant tested PRD, since sufficiently thick plates were available in this material to machine through-thickness implant specimens. Also, a low sulfur cast steel was tested for a comparative evaluation.

The results of the underbead cracking tests are shown in Figure 106. A537-7 is the least susceptible to HIC requiring a preheat temperature of only 100°F to remain crack free. A537-12 required a preheat of 150°F whereas both A537-1 and A537-8 required preheats of 300°F to avoid underbead cracking. The results can be essentially divided into two levels based on the C.E.'s of the steels. Steels A537-7 and A537-12 have C.E.'s of 0.47 and 0.46 respectively and steels A537-1 and A537-8 possess C.E.'s of 0.51 and 0.49 respectively. At the lower C.E. level, the higher sulfur content steel (A537-12) was more susceptible to HIC than the lower sulfur content steel (A537-7). Metallographic examination revealed A537-12 to have a considerably larger fraction of elongated sulfides than the A537-7 (Figures 107a and b). The underbead cracks in A537-12 were mostly associated with these elongated sulfide inclusions, and therefore its greater susceptibility to HIC can be attributed to the larger volume fraction of sulfides. At the higher C.E. level, steels A537-1 and A537-8 were

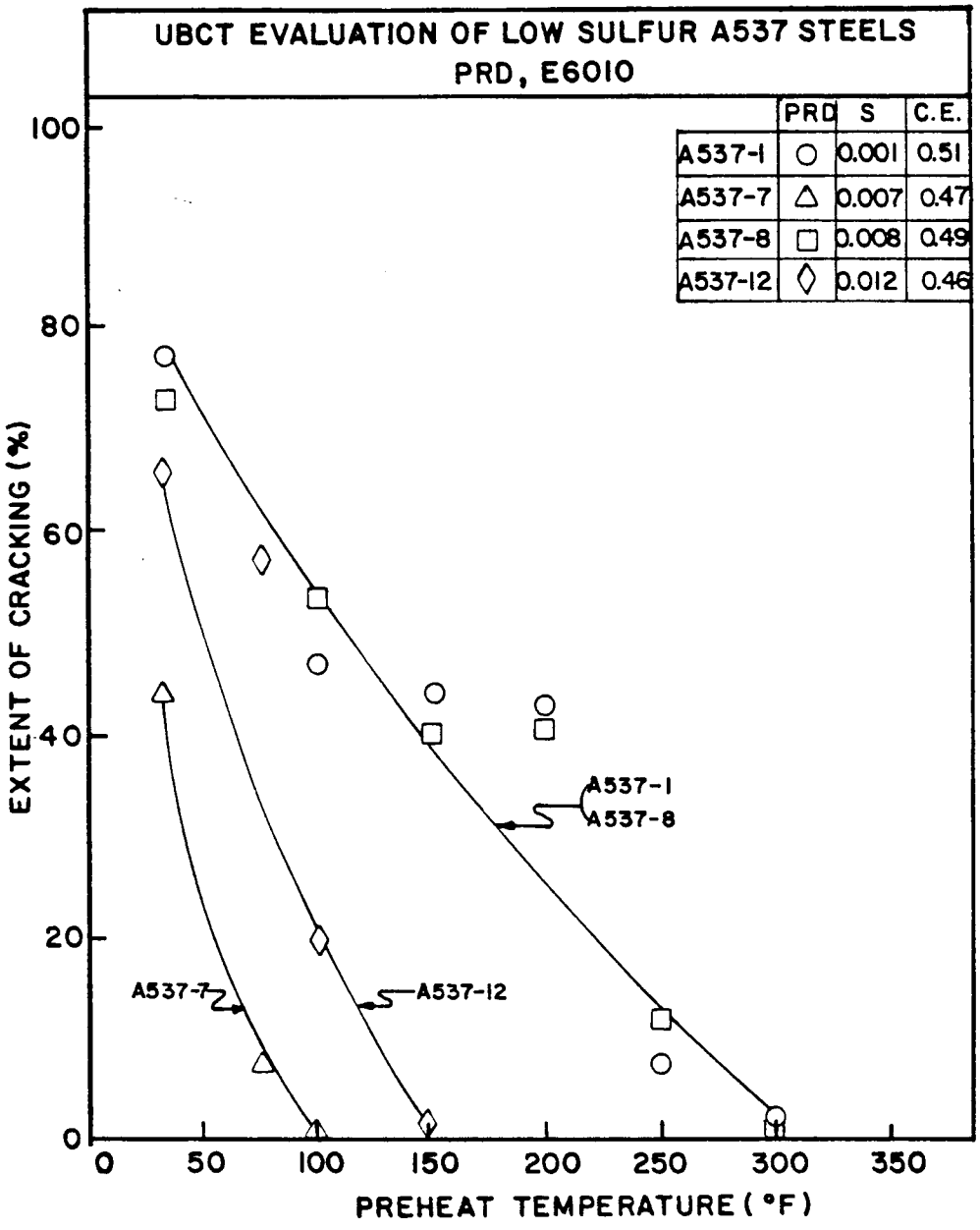


Figure 106. UBCT preheat results for low sulfur A537 wrought steels tested PRD. E 6010.

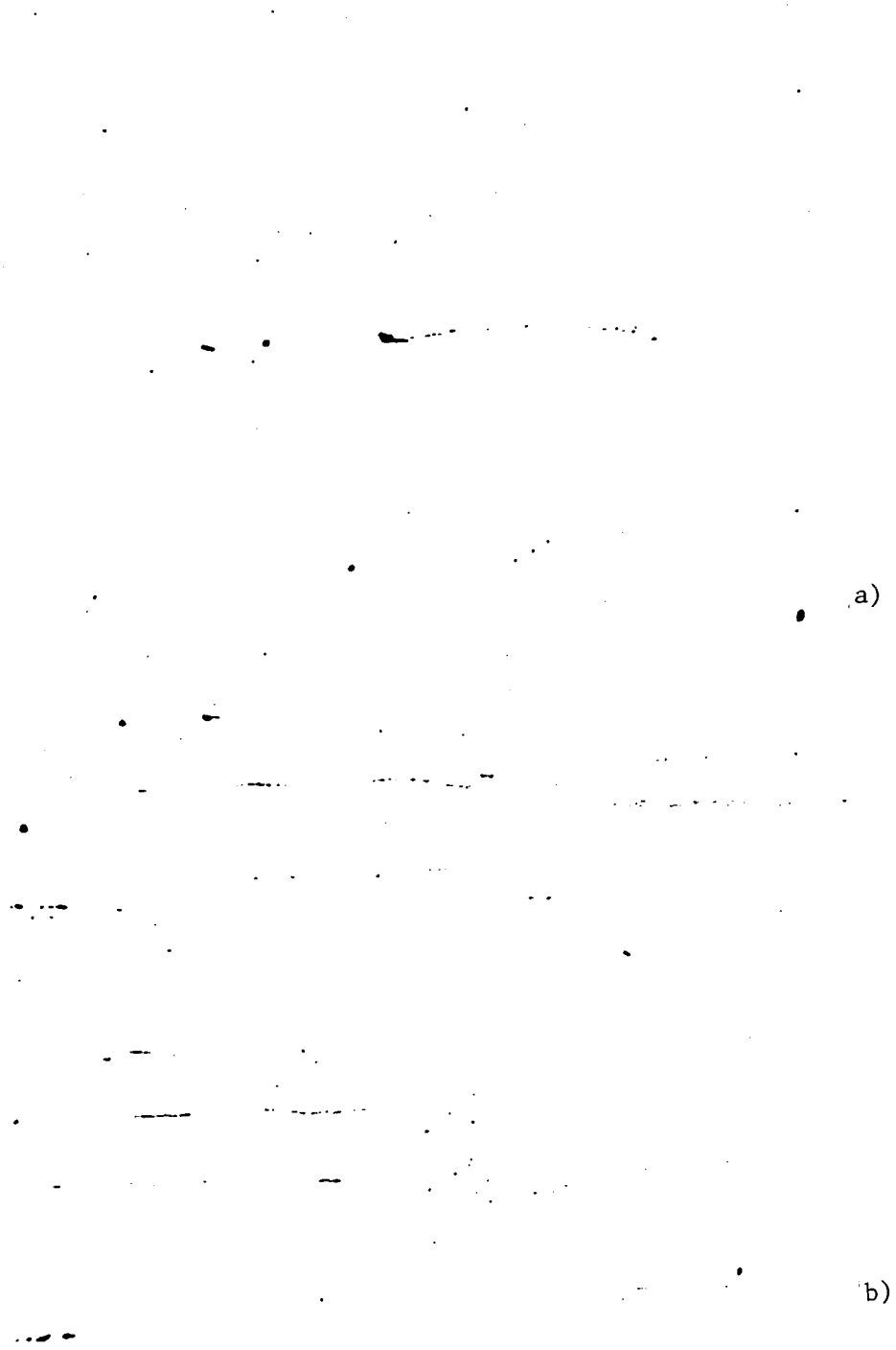


Figure 107. Inclusion morphology in A537-7 and A537-12 steels. a) A537-7, b) A537-12. Unetched, OLM, 100X.

more susceptible to HIC than the lower C.E. steels A537-7 and A537-12. Typical inclusion morphologies in A537-1 and A537-8 are shown in Figures 108a and b respectively. The greater susceptibility of the higher C.E. steels A537-1 and A537-8 can be attributed to a compositional effect as well as to the fact that these steels possess banded base metal microstructures (Figures 109a and b) when compared to the quenched and tempered base metal microstructures of steels A537-7 and A537-12 (Figures 110a and b). It had been established previously that banding leads to an increased susceptibility to HIC. For the wrought A537 steels welded in the rolling direction (PRD) in the UBCT, the susceptibility to HIC (underbead cracking) is strongly influenced by chemical banding and inclusion morphology. Underbead cracking tests were not conducted TTD since adequately sized material was not available to extract samples to be tested in the TTD. However, in the implant test, the higher C.E. materials (A537-1 and A537-8) were tested both PRD and TTD, whereas the lower C.E. steels were tested TTD.

Figure 111 shows the implant test results for the steels tested in the TTD. The results show a trend indicating that the lowest sulfur steel, A537-1, has the greatest susceptibility to HIC (lowest critical stress of 12.5 Ksi). The three steels with higher sulfur contents had critical stress of 15Ksi. The times to rupture were, in general, greater for the higher sulfur steels than for the A537-1. The reasons for the lower susceptibility



Figure 108. Inclusion morphology in A537-1 and A537-8 steels.
a) A537-1, b) A537-8. Unetched, OLM, 100X.

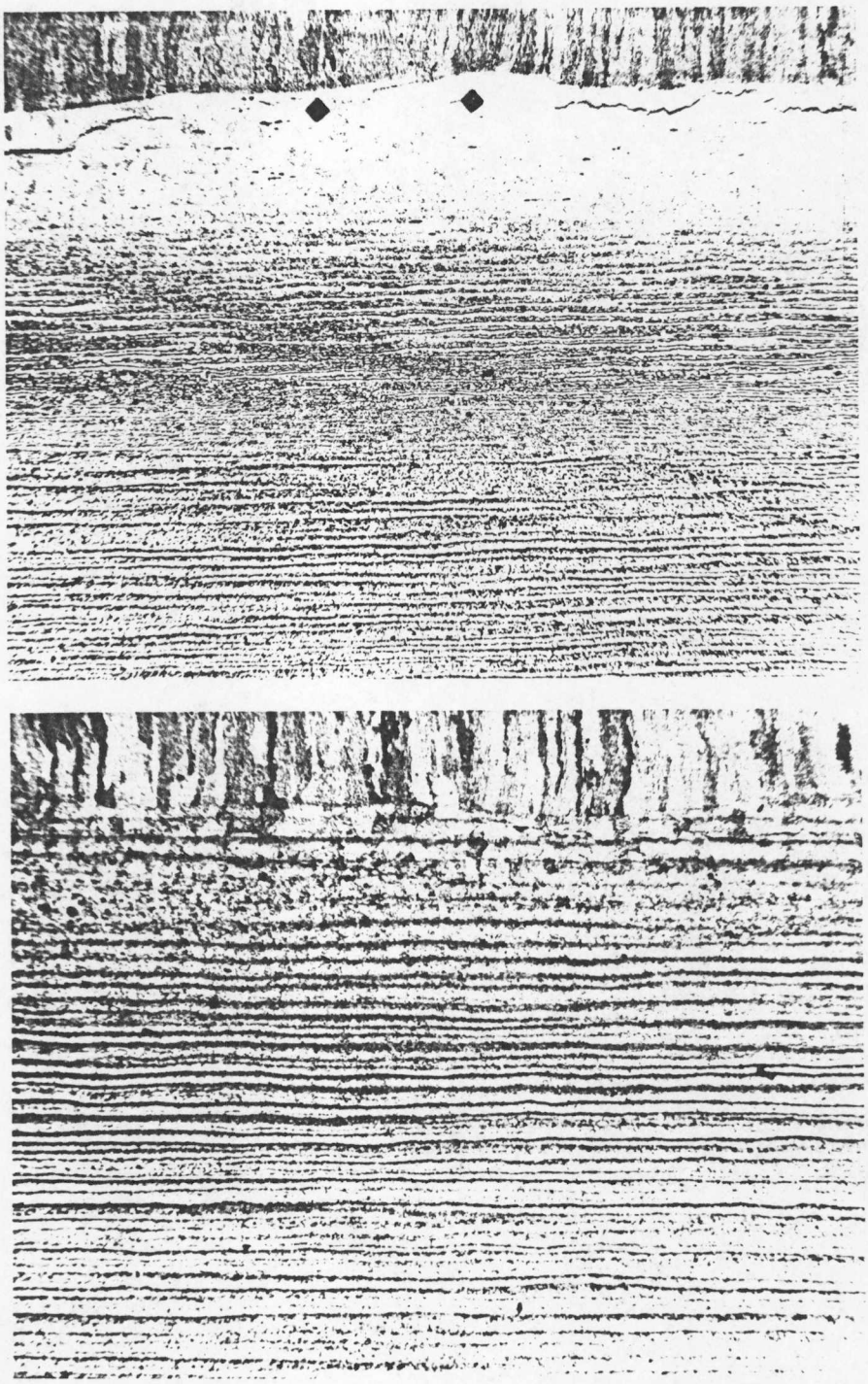


Figure 109. Macrographs of UBCT samples of A537-1 and A537-8 showing HIC in the coarse grained HAZ and banding in base metal. PRD, preheat 100°F. a) A537-1, b) A537-8. Picral etch, OLM, 20X.

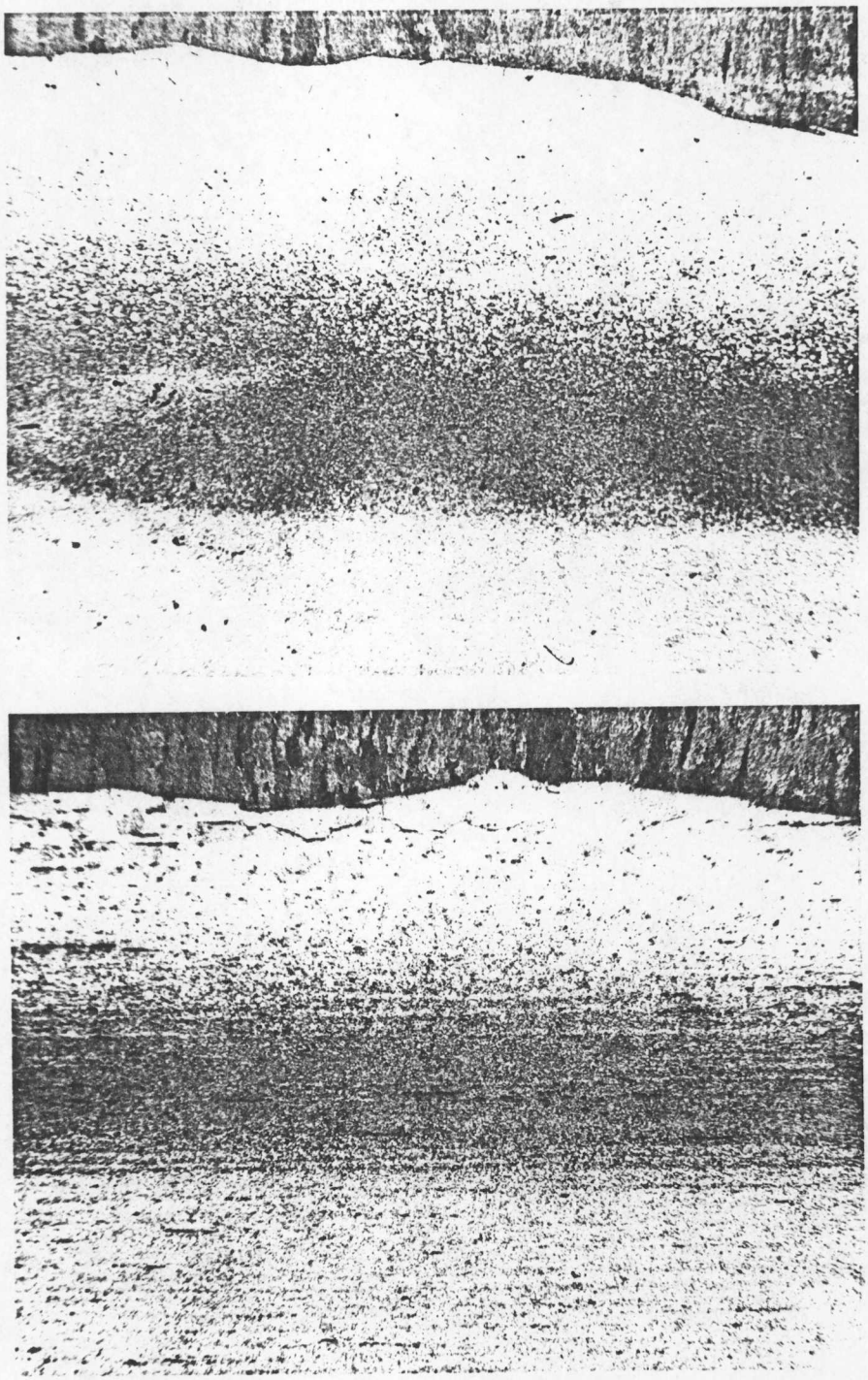


Figure 110. Macrographs of UBCT samples of A537-7 and A537-12 showing quenched and tempered base metal and HIC in coarse grained HAZ of A537-12. PRD, preheat 100°F, a) A537-7, b) A537-12. Picral etch, OLM, 20X.

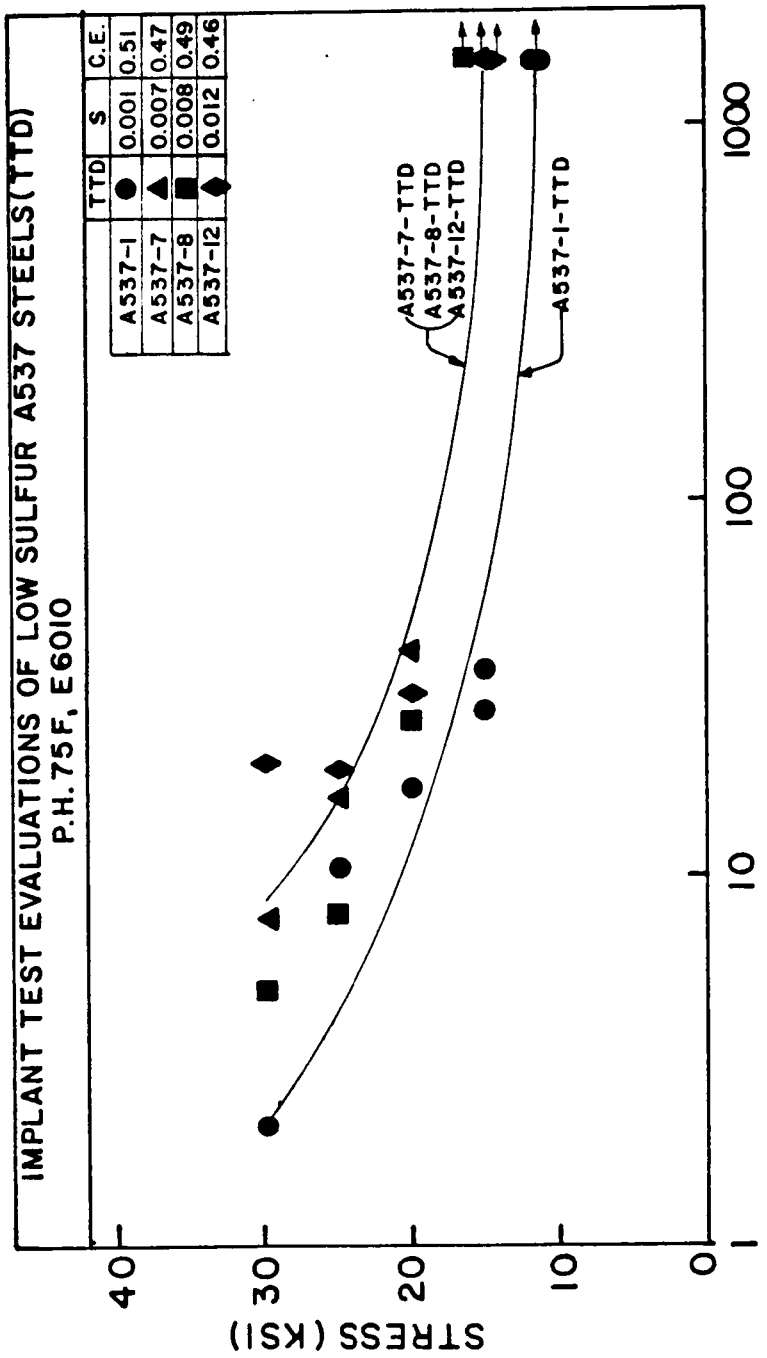


Figure 111. Implant test results for low sulfur steels A537-1,7,8,12 tested TTD. Preheat 75°F, E 6010.

to HIC of the higher sulfur steels may be linked to the lower C.E. of these steels and to the fact that when the implant specimens are welded TTD, a greater volume fraction of inclusions in the higher sulfur steels are aligned perpendicular to the probable plane of cracking than in the lower sulfur steels. This probable plane of cracking will be perpendicular to the alignment of inclusions since in the implant test a tensile load is applied to the HAZ. It is conceivable that inclusions lying perpendicular to the plane of a propagating crack can inhibit the propagation of the crack. Fractographic evidence points to this and is detailed below. A decrease in susceptibility to HIC when implant tests are conducted in the TTD has also been reported by Evans et al.[48] in tests conducted by them both in the PRD and TTD. Another factor that reduces the susceptibility to HIC in implant samples welded in the TTD is that hydrogen diffusion occurring along inclusion/matrix interfaces in a short-circuiting manner leads it away from the susceptible coarse grained HAZ to regions which are less susceptible to HIC. The general trend of results is therefore similar to that for wrought steels tested by the UBCT in Phase I.

With implant tests conducted on A537-1 and A537-8 PRD, the critical stress for the A537-1 remained at 12.5 Ksi, however, for the A537-8 the critical stress fell from 15 to 12.5 Ksi (Figure 112). The increase in susceptibility to HIC of the A537-8 steel when tested PRD demonstrates the influence of orientation of inclusions and banding normal to the applied stress. In such a

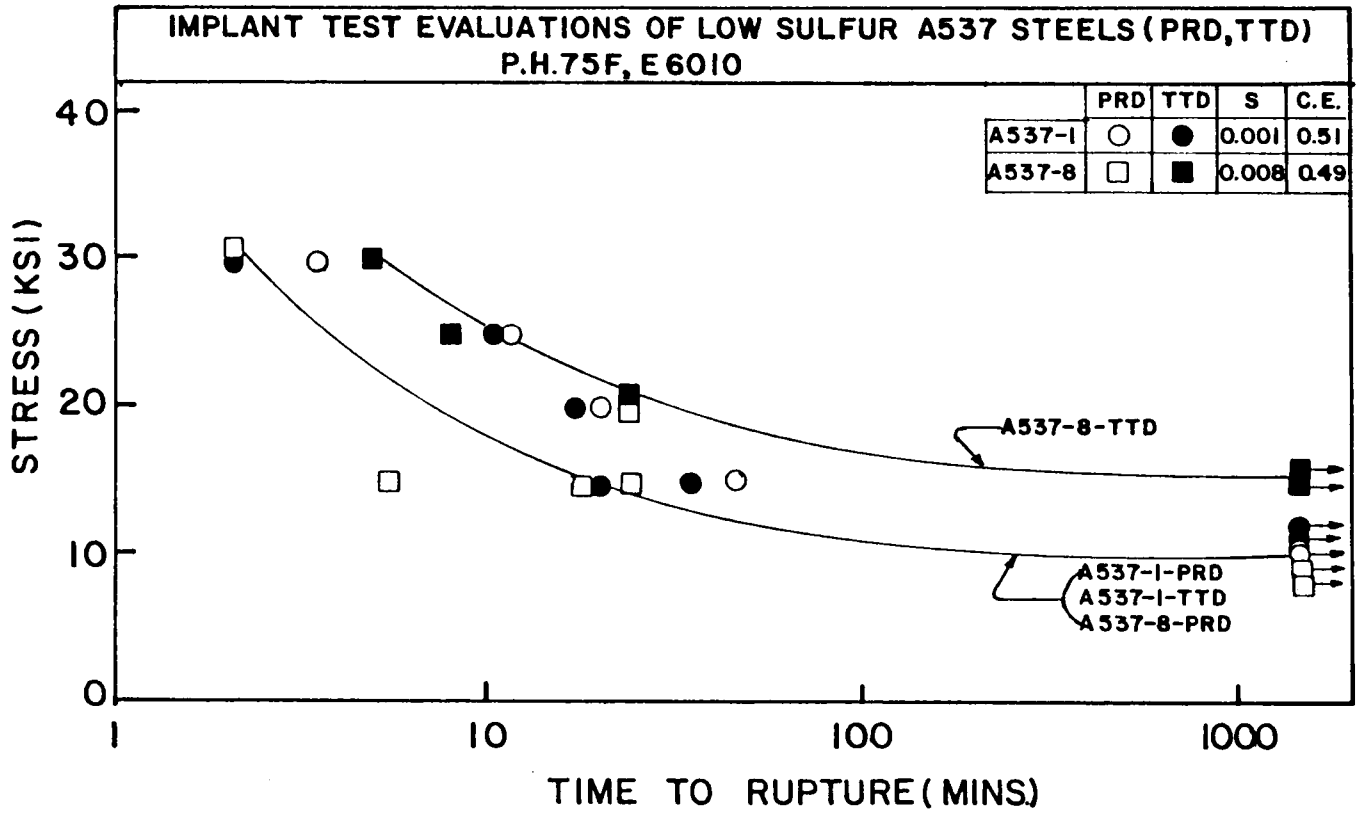


Figure 112. Implant test results for low sulfur steels A537-1 and A537-8, tested PRD and TTD. Preheat 75°F, E 6010.

situation, the inclusion matrix interfaces would tend to decohere, and further, banding also lying normal to the applied stress can present a continuous path for crack propagation. In addition, short circuit hydrogen diffusion along inclusion/matrix interfaces would lead to hydrogen accumulation in regions within the coarse grained HAZ, thus enhancing the probability for crack initiation.

In order to understand the mechanism of failure in the steels tested, extensive metallographic and fractographic examination was carried out. The characteristics and features evaluated include microstructure, microhardness and the morphology of cracking. Typical implant samples from the four steels tested TTD are shown in Figures 113a through d. The implant samples show three modes of fracture--intergranular (IG), quasi-cleavage (QC) and microvoid coalescence (MVC). These basic features are visible on each of the fractures, however, the extent of each mode is significantly different. Critical examination indicates that the lowest sulfur (A537-1) shows the maximum amount of IG cracking. Transverse cross sections of the implant assemblies shown in Figures 114a through d indicate similar results with the A537-1 displaying a predominantly IG mode of cracking in the coarse grained HAZ. Examination of the A537-1 sample shown in Figure 113a at higher magnifications (Figures 115a and b), reveals that in the IG mode of cracking, some grain boundaries show no ductility while other grain boundaries possess QC (semi-ductile) features. Similar observations are evident in

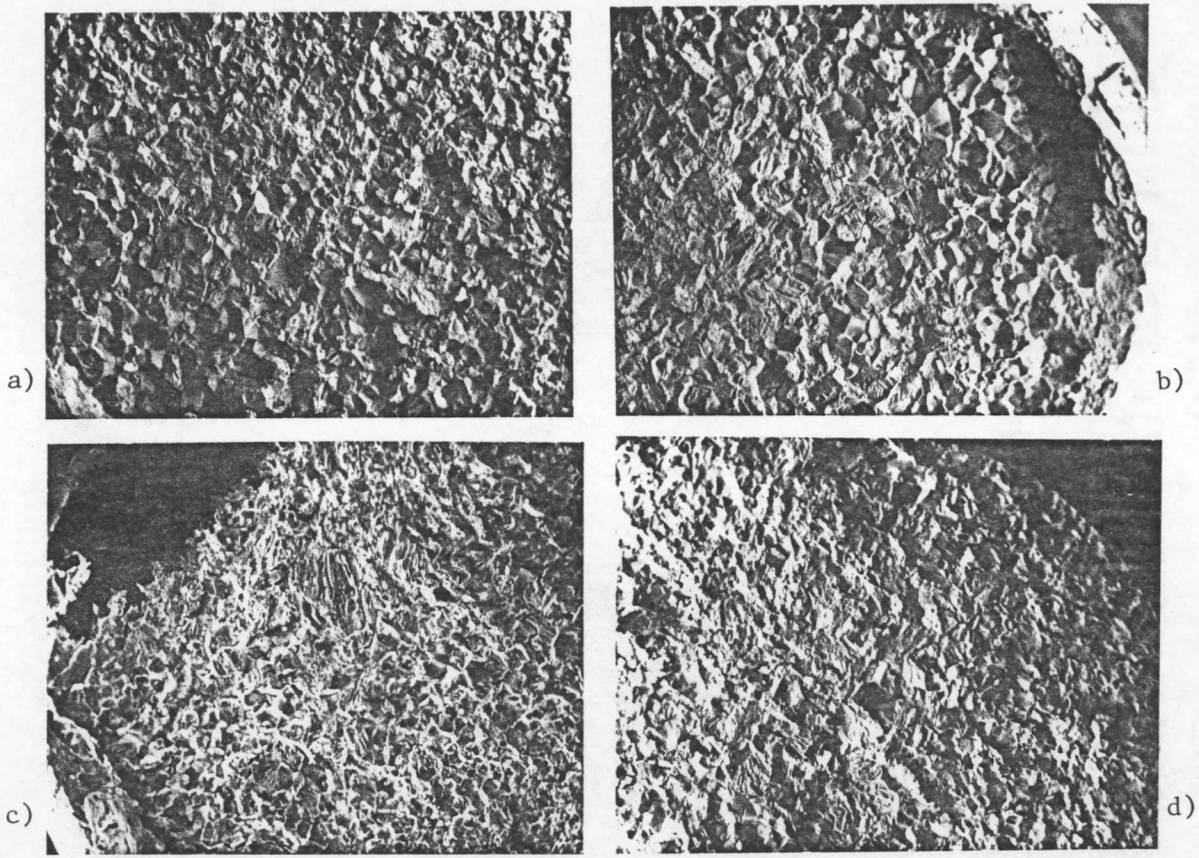


Figure 113. Fracture morphologies in implant specimens of A537 low sulfur steels tested TTD. Stress 20 Ksi, preheat 75°F. a) A537-1, b) A537-7, c) A537-8, d) A537-12. SEM, 20X.

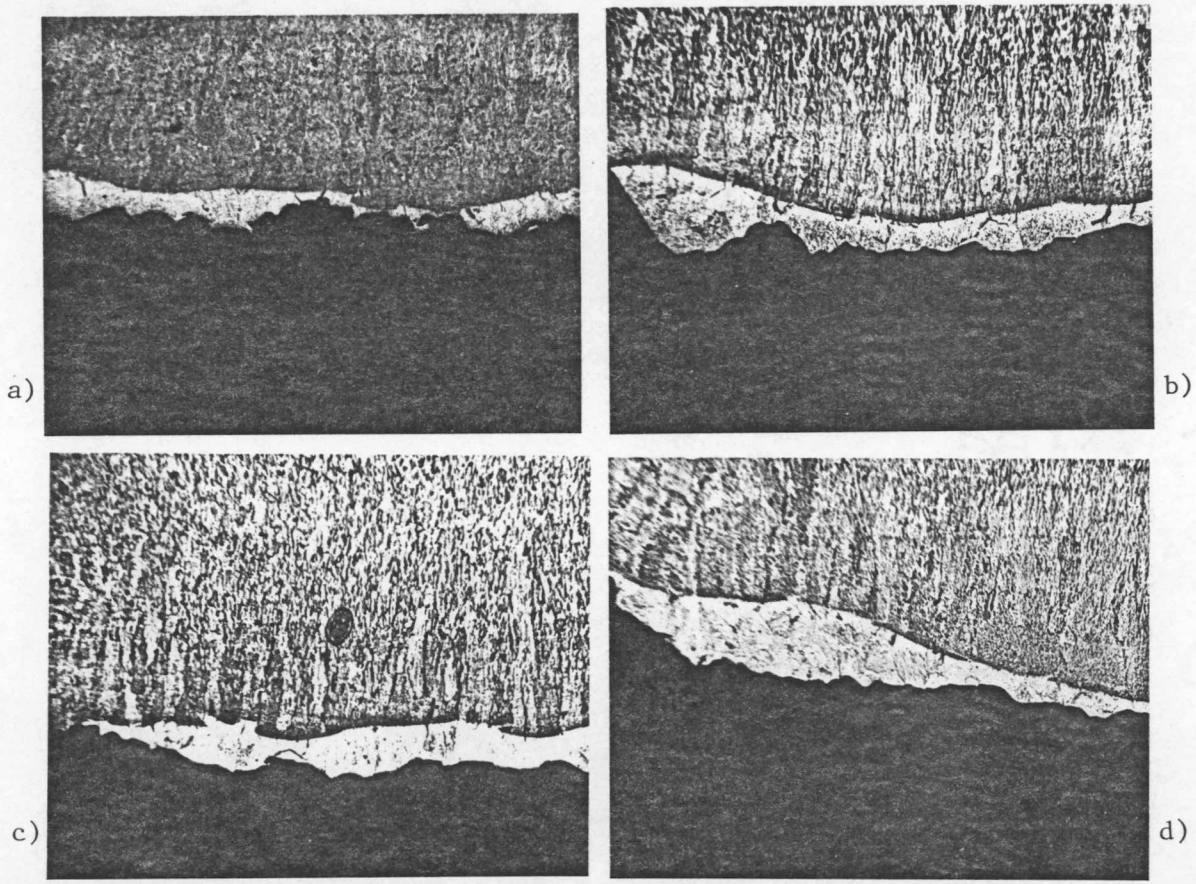
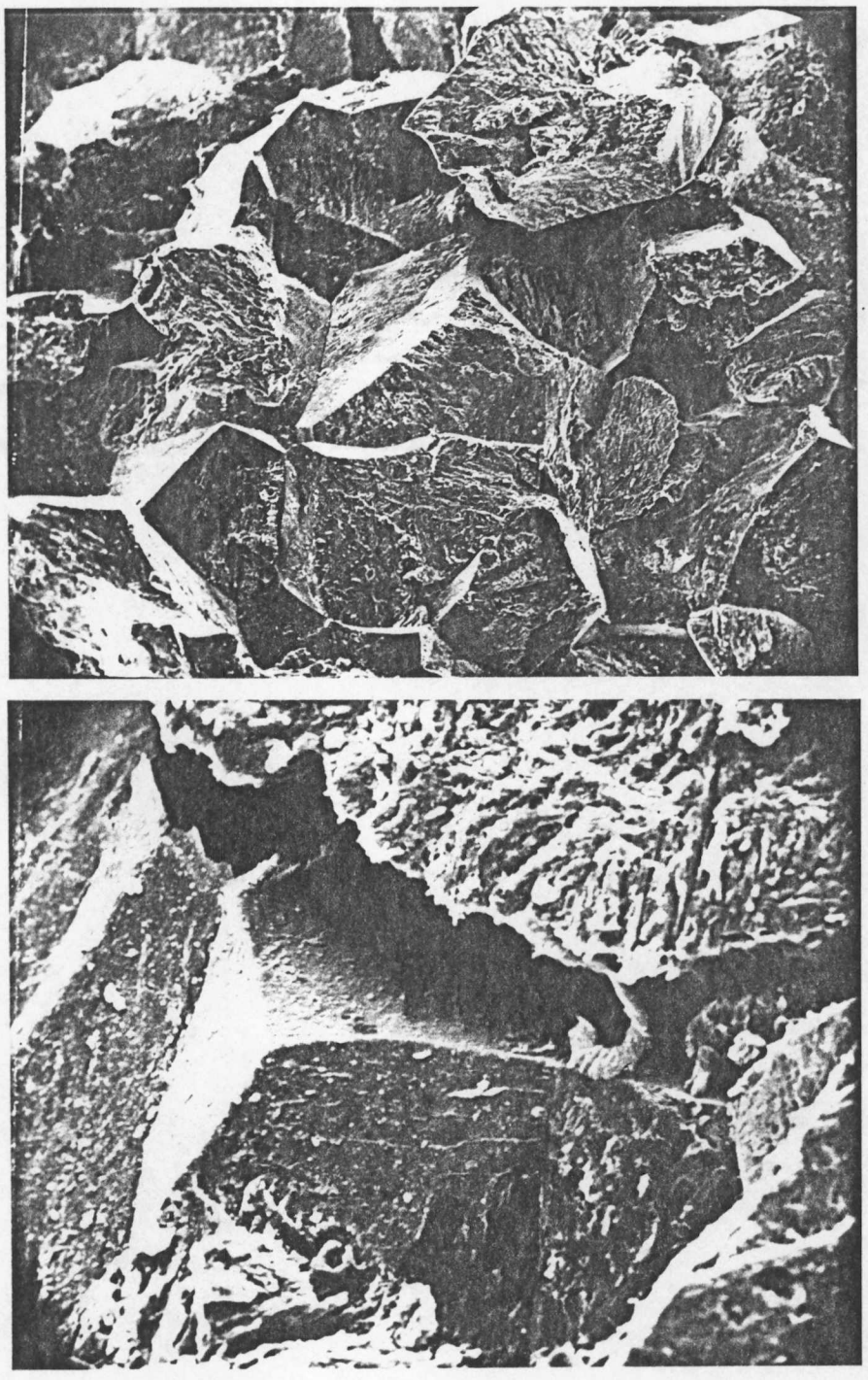


Figure 114. Typical fracture interface sections of implant specimens of A537 low sulfur steels tested TTD. Stress 20 Ksi, preheat 75°F. a) A537-1, b) A537-7, c) A537-8, d) A537-12. Picral etch, OLM, 20X.

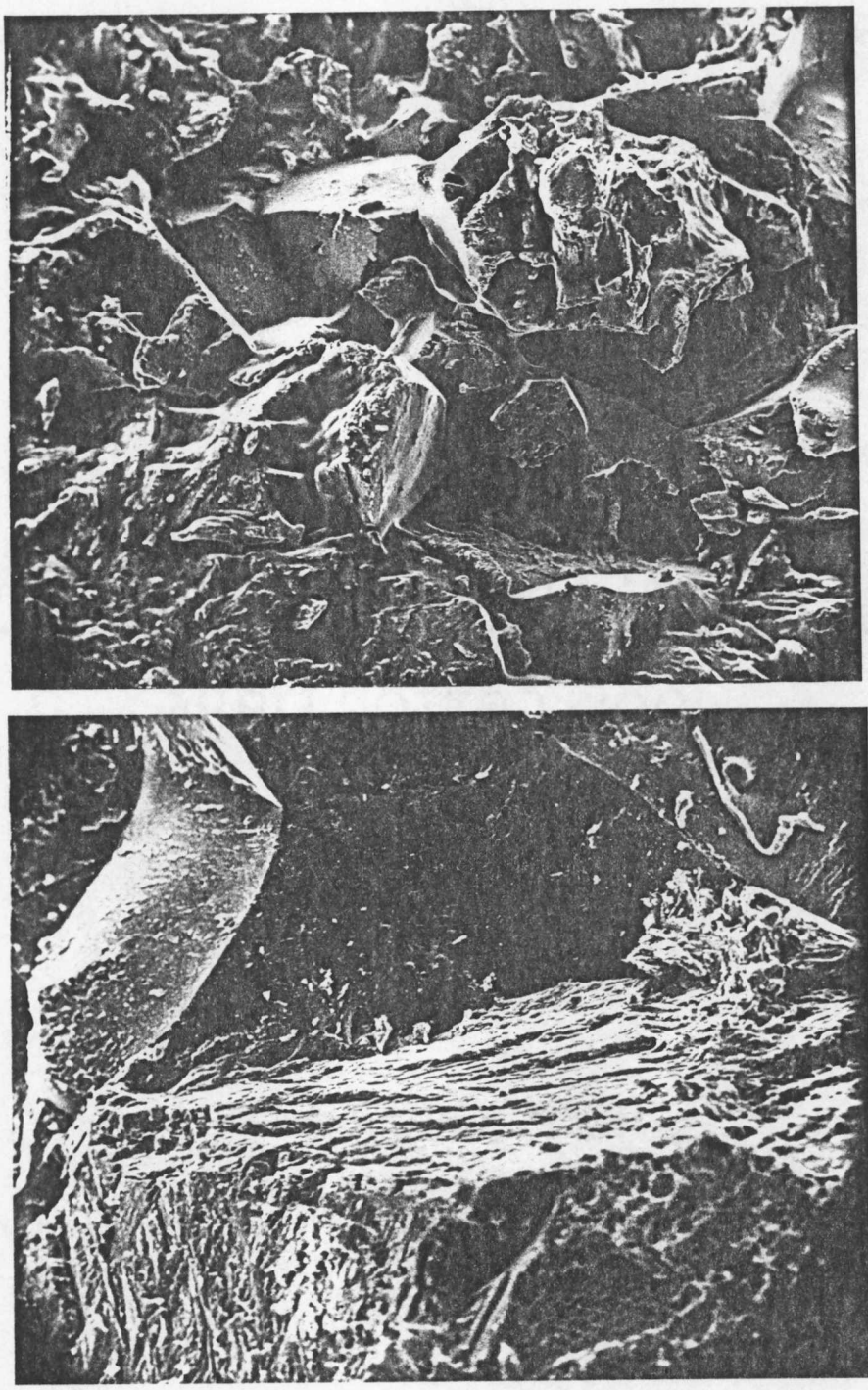


a)

b)

Figure 115. Fracture morphology of implant specimen of A537-1. (See Figure 113a) TTD, Stress 20 Ksi, ruptured in 17 minutes. a) SEM, 200X, b) SEM, 2000X.

the A537-8 sample (Figure 116a and b). It is clear that considerably greater extent of quasi-cleavage exists in the A537-8 sample, however, the general topology is the same as for the A537-1, with some grain faces exhibiting no ductility, whereas others exhibit "roughening," indicative of a QC mode of fracture. When the A537-1 and A537-8 were implant tested PRD, there was a significant change in fracture morphology. Figures 117a through d show the fracture cross-section in the A537-1 material tested PRD. It is clear that compared to the A537-1 material tested in the TTD, the extent of IG cracking is less. The IG fracture is confined to areas adjacent to the notch. At a higher magnification in Figure 117b, some grain boundary decohesion and grain faces exhibiting little or not ductility are evident. The central region of the sample has QC features (Figure 117c) and at 5000X (Figure 117d), the QC morphology is clearly revealed. A fracture face from A537-8 tested PRD is shown in Figure 118. No IG cracking is seen on the fracture surface. The fracture is a 50/50 mix of QC and QC+MVC. In Figure 118b, at a magnification of 500X, the fine facet size of the MVC is visible, and in Figure 118c, at a higher magnification of 5000X, the association of MVC with inclusions in the A537-8 steel is noted. A larger region of ductile tearing exists in the A537-8 steel tested PRD than in the A537-1 steel because of a difference in their sulfur contents. The greater extent IG and QC in the lower sulfur steel, A537-1, is apparently due to the paucity of a sufficient volume fraction of inclusions in this low sulfur steel that can



a)

b)

Figure 116. Fracture morphology of implant specimen of A537-7. (See Figure 113b.) TTD, Stress 20 Ksi, ruptured in 40 minutes. a) SEM, 200X, b) SEM, 2000X.

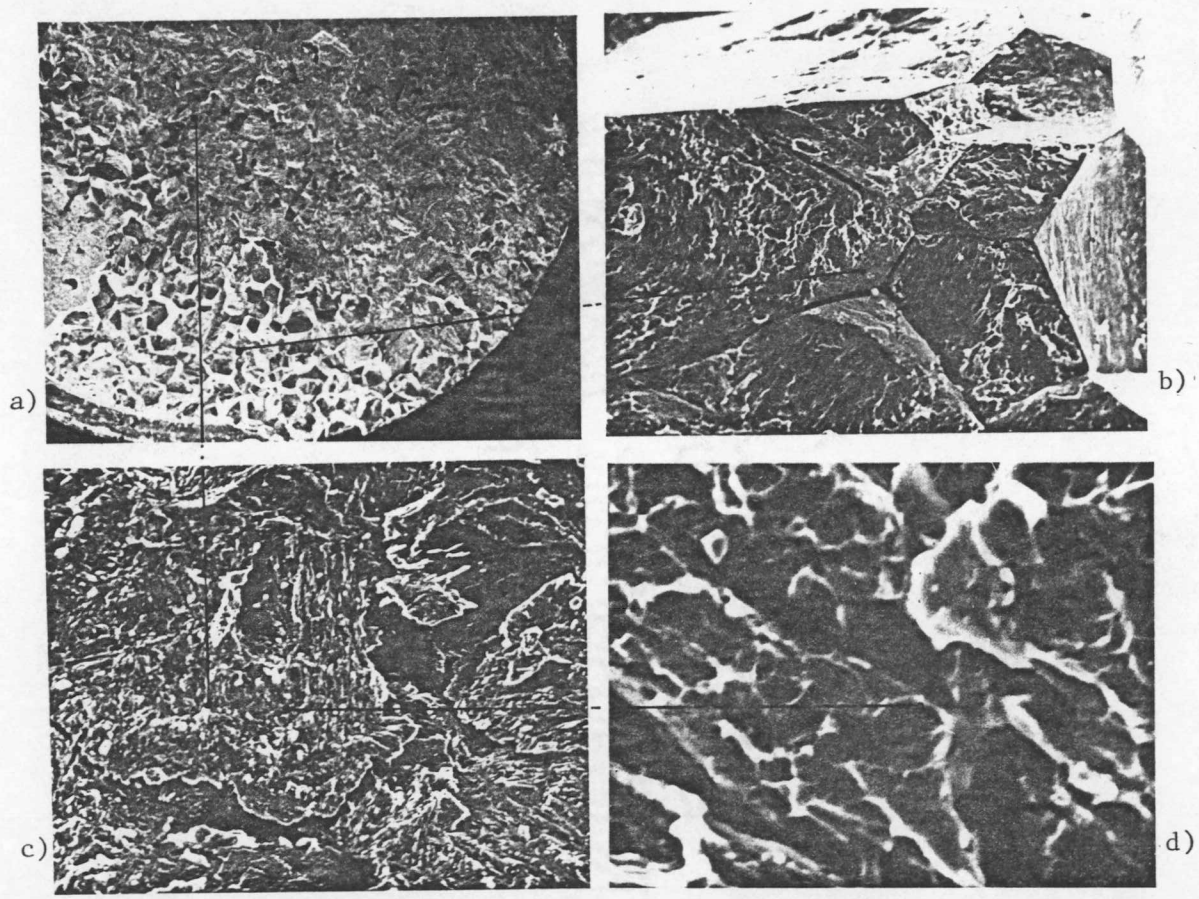


Figure 117. Fracture morphology of A537-1 implant specimen tested PRD. Stress 15 Ksi, ruptured in 46 minutes. SEM, a) 20X, b) 500X, c) 500X, d) 5000X.

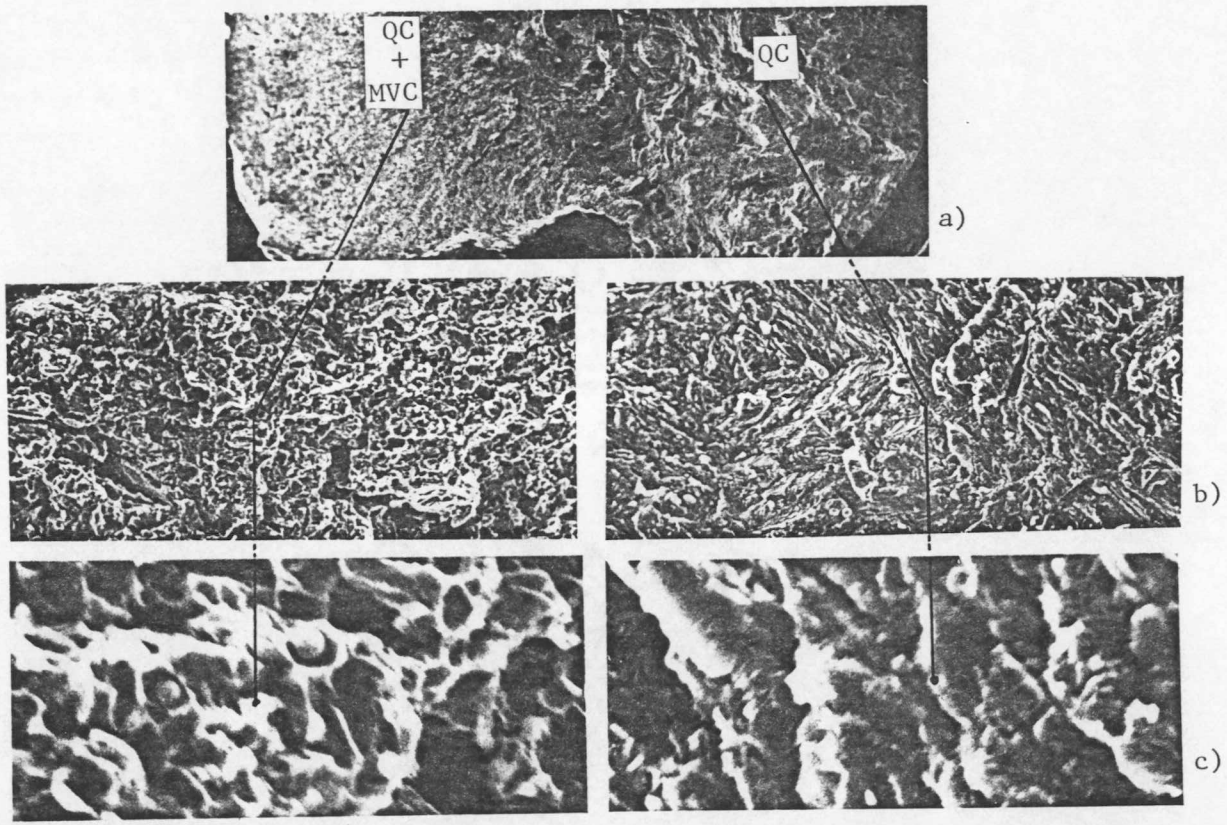


Figure 118. Fracture morphology of A537-8 implant specimen tested PRD. Stress 15 Ksi, ruptured in 5.5 minutes. SEM, a) 20X, b) 500X, c) 5000X.

act as initiation sites for MVC. The importance of inclusions acting as sites for MVC during HIC was further established in tests on the low sulfur cast steel (LSC in Table 10, page 95). Implant tests with high-hydrogen electrodes (E 6010) at a stress of 30 Ksi did no cause fracture. When the stress was raised to 40 Ksi, fracture occurred in about 30 minutes but in the weld metal and not in the HAZ. Use of higher strength electrodes (E 8010) resulted in an increase in rupture time to about 50 minutes for a stress of 40 Ksi, however, rupture again occurred in the weld metal and not in the HAZ. Metallographic and fractographic examinations were carried out to determine the reasons for this behavior. Figure 119 shows a typical coarse grained HAZ microstructure in the low sulfur cast steel. The microstructure is essentially bainitic with some auto-tempered martensite. The maximum hardness of the composite microstructure was found to be about 320 DPH, which is below the 350 DPH level which some investigators[13] have suggested as a threshold hardness for HIC problems. A typical cross section for a fractured implant assembly and the implant sample as seen in optical and SEM micrographs are shown in Figures 120a and b respectively. A higher magnification of the sample in Figure 120b is shown in Figure 121 which indicates the fracture mode in the weld metal to be MVC, with initiation at inclusions in the weld metal. It can therefore be argued that in the absence of a susceptible martensitic microstructure in the HAZ, HIC occurred in the weld metal where the presence of a larger volume of inclusions aided



Figure 119. Microstructure in coarse grained HAZ of implant sample of low sulfur cast steel (LSC). Preheat 75°F. Picral etch, OLM, 500X.

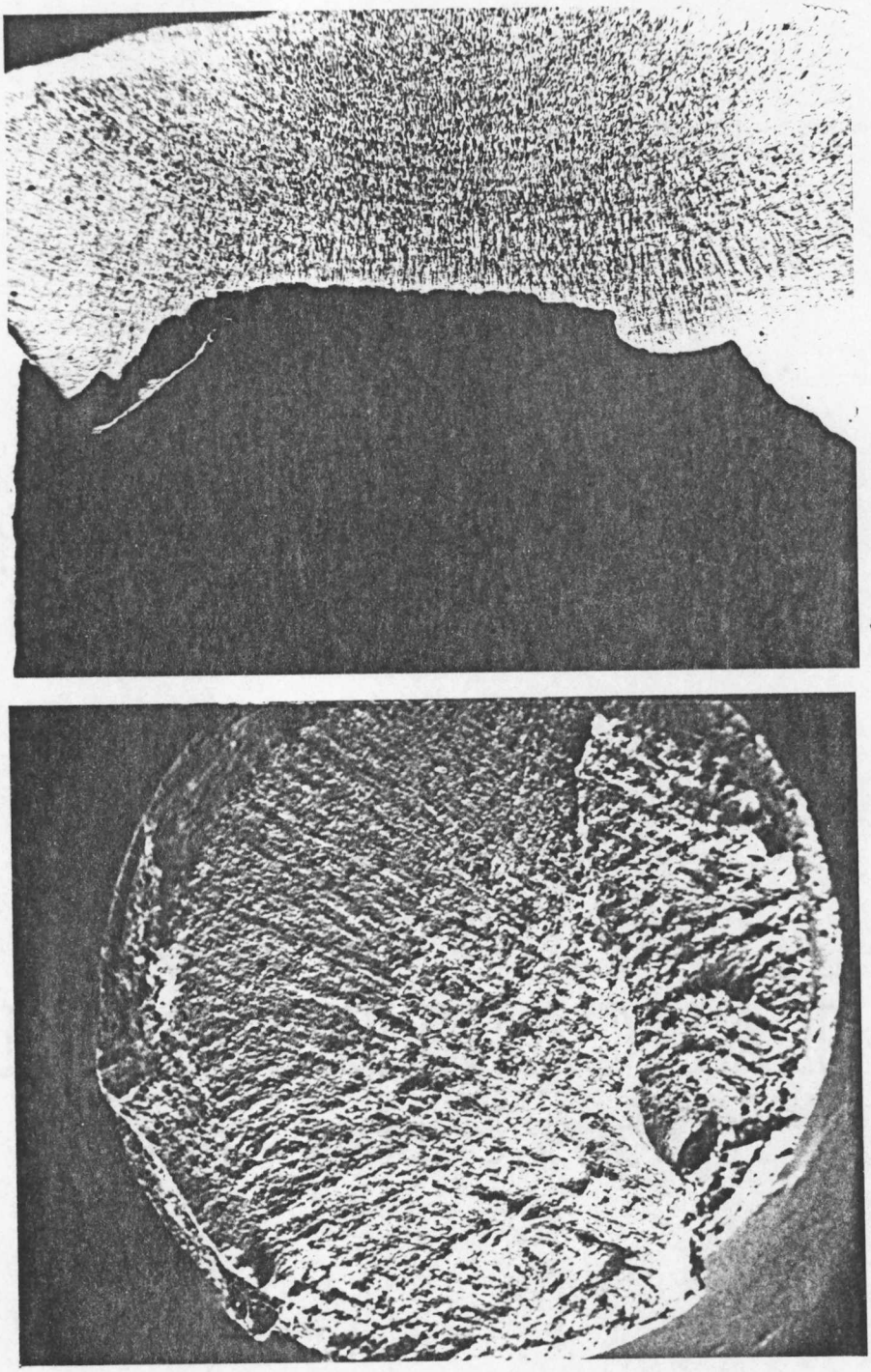


Figure 120. Ruptured cross-section of implant sample of low sulfur cast steel (LSC). Preheat 75°F, Stress 40 Ksi, time to rupture 30 minutes. a) Rupture in weld metal (E 6010). Picral etch, OLM, 20X. b) Fracture face of E 6010 weld metal. SEM, 20X.

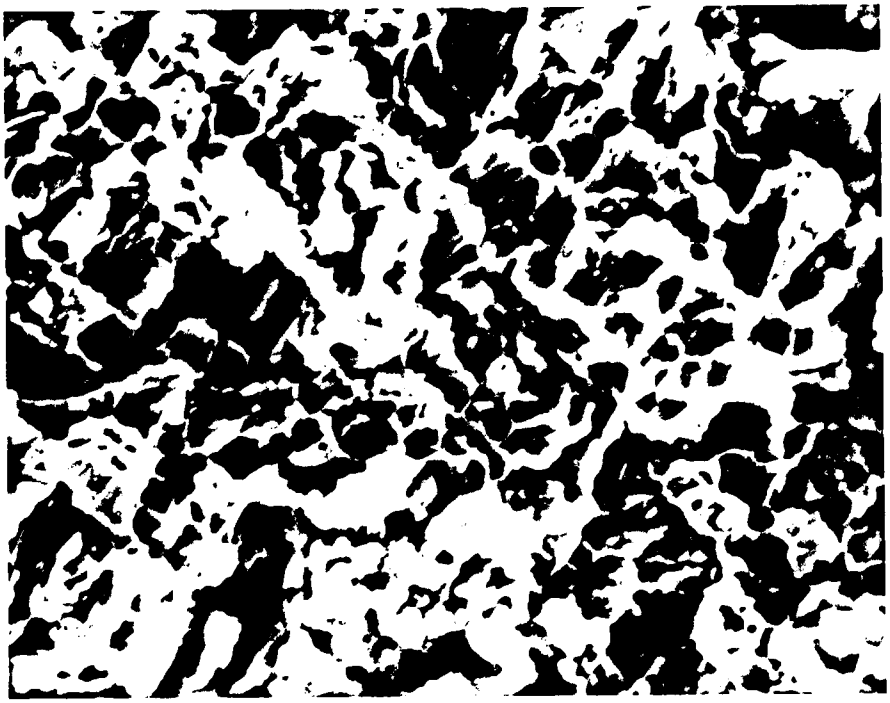


Figure 121. Fracture morphology of rupture in E 6010 weld metal in implant tested low sulfur cast steel (LSC) (See Figure 120b). Preheat 75°F, Stress 40 Ksi, time to rupture 50 minutes. SEM, 5000X.

MVC. The results therefore indicate that the susceptibility to HIC cannot be related solely to a single factor such as sulfur content; it is related to factors such as the microstructure in the HAZ, inclusion morphology, banding and segregation. This implies that, provided a microstructure susceptible to HIC is present in the HAZ, inclusion morphology, banding and segregation have secondary effects on HIC. However, the sulfur content does affect the volume fraction of inclusions that will exist in the steel and therefore dictate the fracture modes that will prevail during HIC. The ramifications of these different fracture modes are discussed in detail in a later section on the mechanism of HIC.

9. Two Pass Implant Tests

In a practical welding situation, the thickness of joints usually requires the deposition of a multitude of passes to complete the joint. This procedure results in the creation of a tempered HAZ adjacent to every subsequent pass. To simulate the above situation, two pass implant tests were conducted in the TTD on the A537-1 steel utilizing high hydrogen as well as low hydrogen electrodes. In the first case, both passes were made using E 6010 (high hydrogen) electrodes whereas in the second case, the first pass was deposited using low hydrogen (E 7018) electrodes and the subsequent pass with high hydrogen (E 6010) electrodes, so that a tempered HAZ (created in the HAZ of the first pass by the second pass) could be subject to HIC conditions. These tests were carried out on the A537-1 material since this steel had the greatest

susceptibility to HIC (among the low sulfur steels) when tested TTD in the implant test. The tests were carried out at a stress level of 20 Ksi so that a comparative evaluation of the low and high hydrogen conditions could be made. The implant sample with two passes of E6010 failed in ten minutes after loading and the fracture details are shown in Figure 122a through d. The fracture morphology in the implant sample is seen to have two distinct areas--one coarse grained and the other relatively fine grained. The coarse grained HAZ corresponds to that created by the second pass, whereas the fine grained HAZ is the refined area in the first pass due to the deposition of the second pass. The boundary region separating the two microstructures is shown in Figure 122b. It is evident that the IG mode of fracture dominates in both regions. However, at higher magnifications, in the coarse grained HAZ (Figure 122d), the IG mode is seen to be comprised of cleavage and MVC on the grain faces. In the fine grained HAZ (Figure 122c), the IG mode of fracture comprises mainly of QC features on the grain faces. These observations suggest that under high-hydrogen conditions, tempered HAZ's in low sulfur steels are susceptible to intergranular HIC. This general morphology of cracking is accompanied by localized regions of pure cleavage, QC and MVC. It may be recalled that an IG mode of HIC was also prevalent in the single pass implant tests on the low sulfur steel A537-1. The results therefore point to a characteristic nature of HIC in low sulfur A537 steels. The reasons for the occurrence of this characteristic morphology are expanded in a later section.

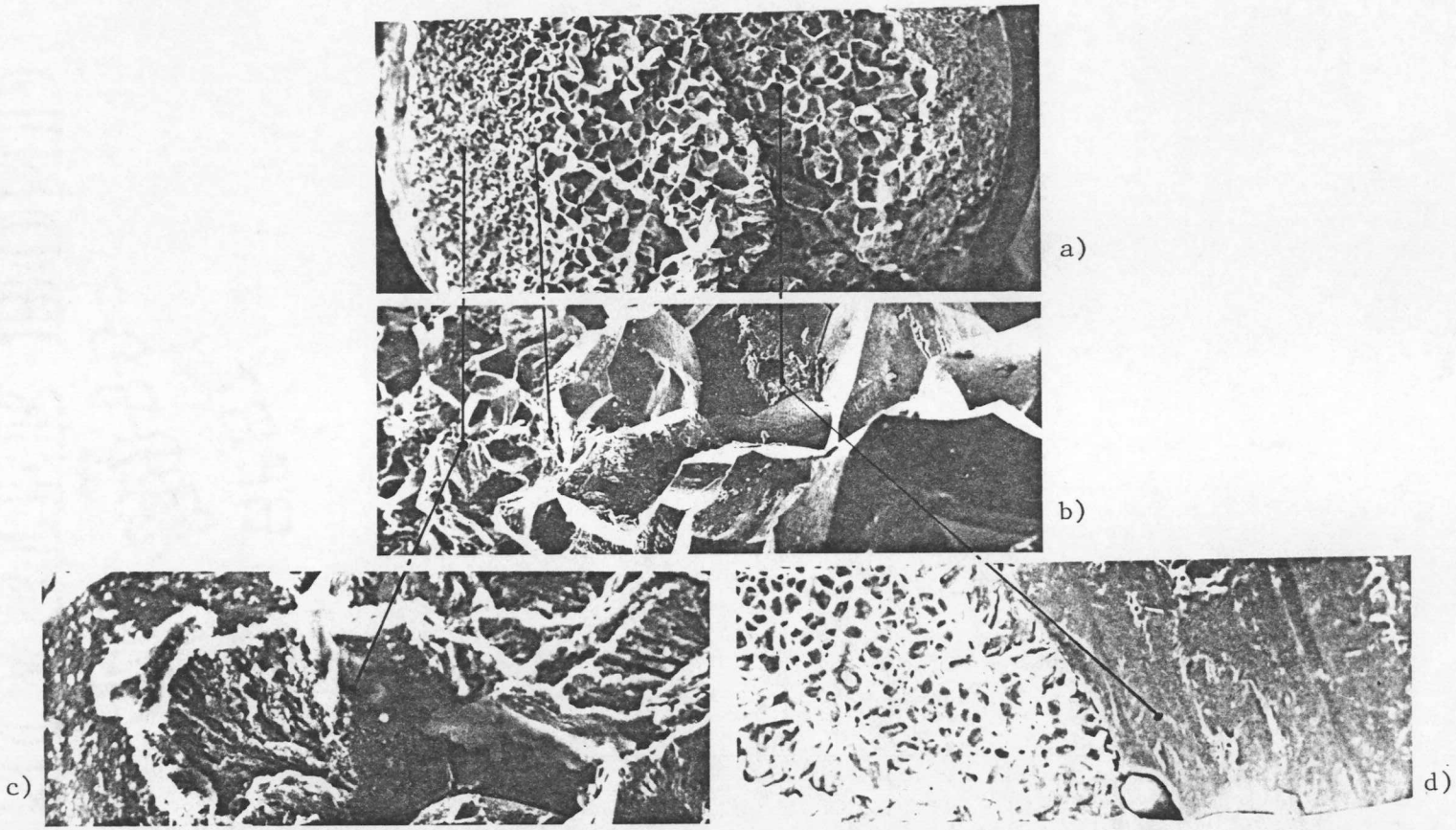


Figure 122. Fracture morphology of HIC in two pass implant sample (E 6010 + E 6010) of A537-1, TTD, preheat 75°F, stress 20 Ksi, time to rupture 11 minutes. a) SEM, 20X, b) SEM, 200X, c) SEM, 2000X, d) SEM, 2000X.

In the second case of the two-pass implant study, an E7018 (low-hydrogen) pass was first deposited, and the second pass was made using E6010 electrodes. A stress of 20 Ksi did not cause any rupture of the implant tested TTD. Metallographic examination of the cross-section of the implant assembly (Figure 123), revealed that the cracking had occurred and was confined to the coarse grained HAZ created by the second (E6010) pass. A composite micrograph of the crack shown in Figure 124a indicates that the propagation of the crack was arrested by the tempered martensite created in the HAZ of the first (E7018) pass. A higher magnification view of the crack shown in Figure 124b indicates that the crack is essentially IG in nature. A few secondary cracks emanate in a transgranular mode from the primary crack. Thus, under low hydrogen conditions, tempered HAZ's in high hardenability steels such as A537 can prevent the propagation of HIC. Under high hydrogen condition, the tempered HAZ's themselves may be subjected to HIC. In addition to these results, another important observation that was made in the two-pass implant tests is that under both low and high hydrogen conditions, the IG mode of HIC is favored in low sulfur steels. This observation is consistent with those reported for the single pass implant tests. The reasons for and the significance of this fractographic observations are discussed in detail in a later section on the mechanism of HIC.

10. Serviceability Requirements--Response to PWHT

Post weld heat treatments (PWHT), as opposed to post weld holds, are conducted at temperatures below the lower critical

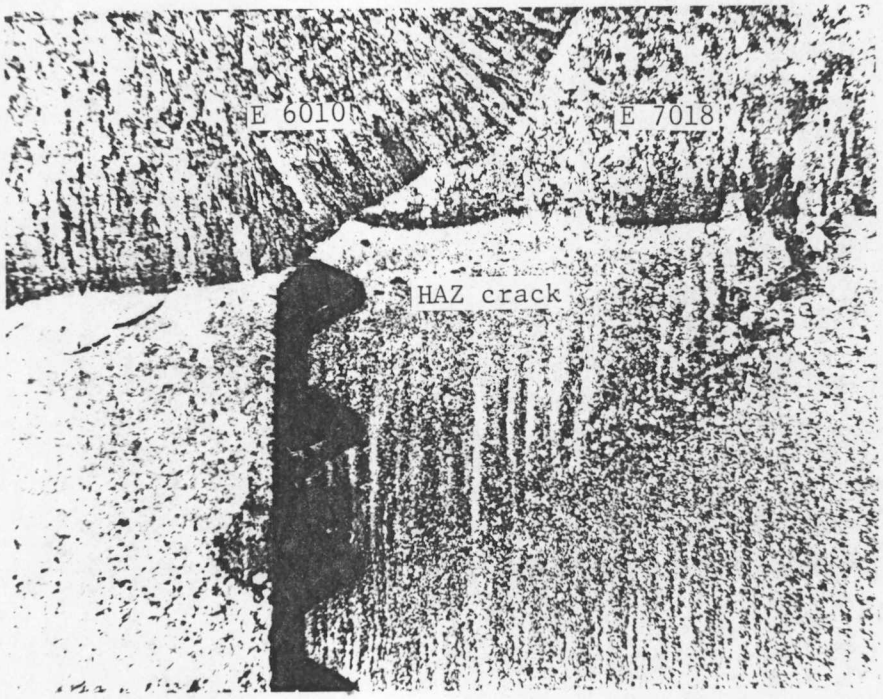


Figure 123. Cross-section of two-pass (E 7018 + E 6010) implant sample of A537-1. TTD, preheat 75°F, Stress 20 Ksi, no rupture in 24 hours. Vilella's etch, OLM, 20X.

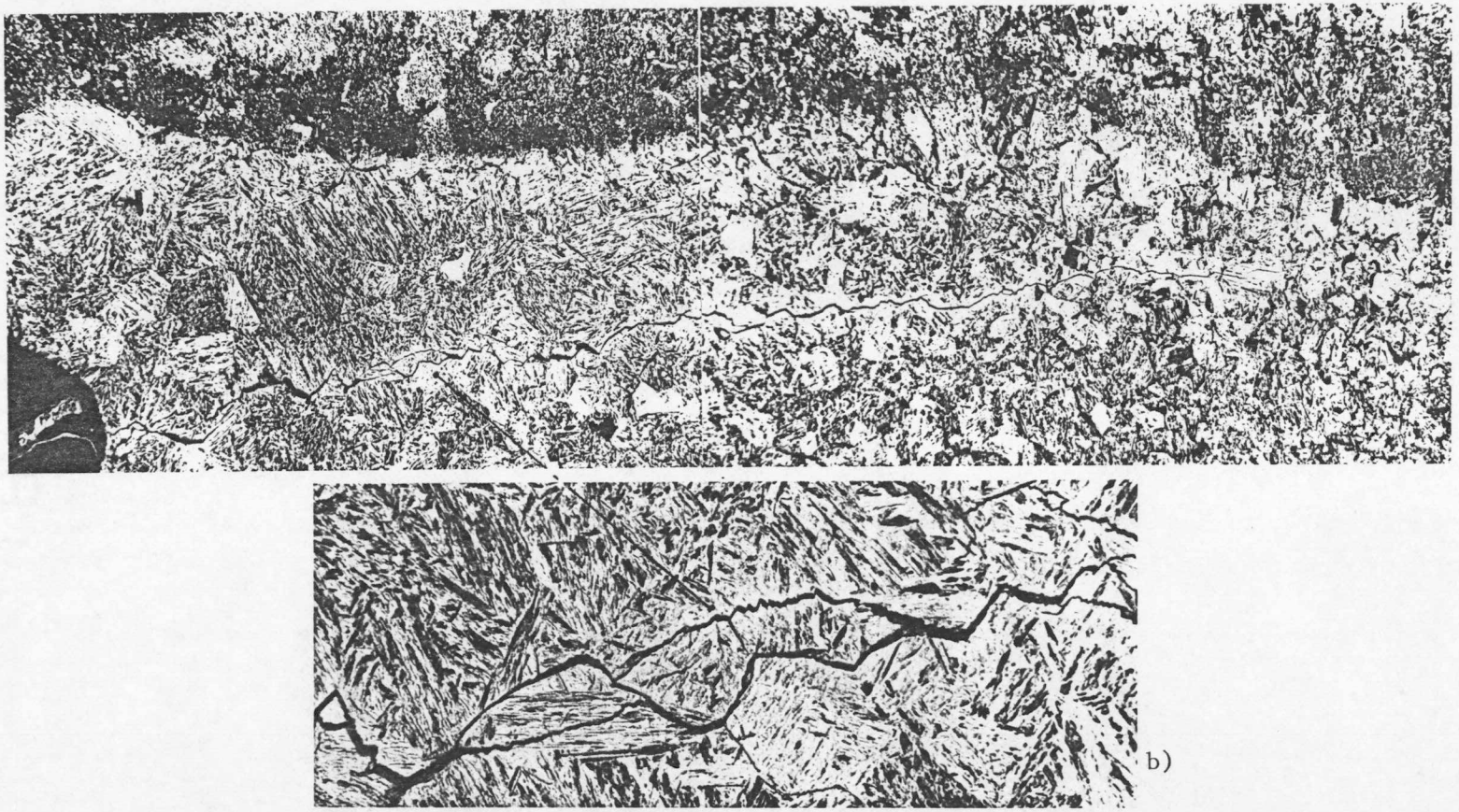


Figure 124. Microstructural details of crack shown in Figure 123. Two pass (E 7018 + E 6010) implant sample of A537-1. TTD, preheat 75°F, Stress 20 Ksi, no rupture in 24 hours. a) Vilella's etch, OLM, 100X, b) Vilella's etch, OLM, 500X.

temperature to temper the hard structures formed in the coarse grained HAZ and thus to improve the impact properties of the HAZ. It is obvious that if PWHT's are carried out immediately after welding, they can also serve as high temperature post weld holds (to diffuse very effectively hydrogen from the weldment).

The impact toughness of a tempered HAZ will be governed by the quenched structures that will result from the weld thermal cycle and the PWHT schedule. For a particular heat input, these quenched structures will depend upon the composition and hence the hardenability of the steel. The well documented control composition steels obtained for weldability studies in Phase I (Table 4, page 87) were chosen for a PWHT effect study. The details of the testing procedure are given in Chapter III. Briefly, charpy samples were thermal cycled in the Gleeble under heat input conditions of 50 KJ/in, 2400°F peak temperature in a 1" steel plate welded at 80°F to provide simulated coarse grained HAZ regions. The samples were PWHT at 1200°F for 1 hour. Impact testing was conducted at room temperature (75°F) and at -25°F. The results of the tests at 75°F are shown in Figure 125. From the bar graph, it is clear that excepting for C&N C-Mn-Si steels with C.E.'s of 0.37 and 0.45, impact toughnesses after thermal cycling and PWHT are equal to or better than those for the C&N condition. The results of the tests at -25°F on the same materials show a trend similar to that observed at 75°F (Figure 126). Examination of the cooling curves for two of the C&N steels (C.E.=0.37 and 0.45) revealed a thermal

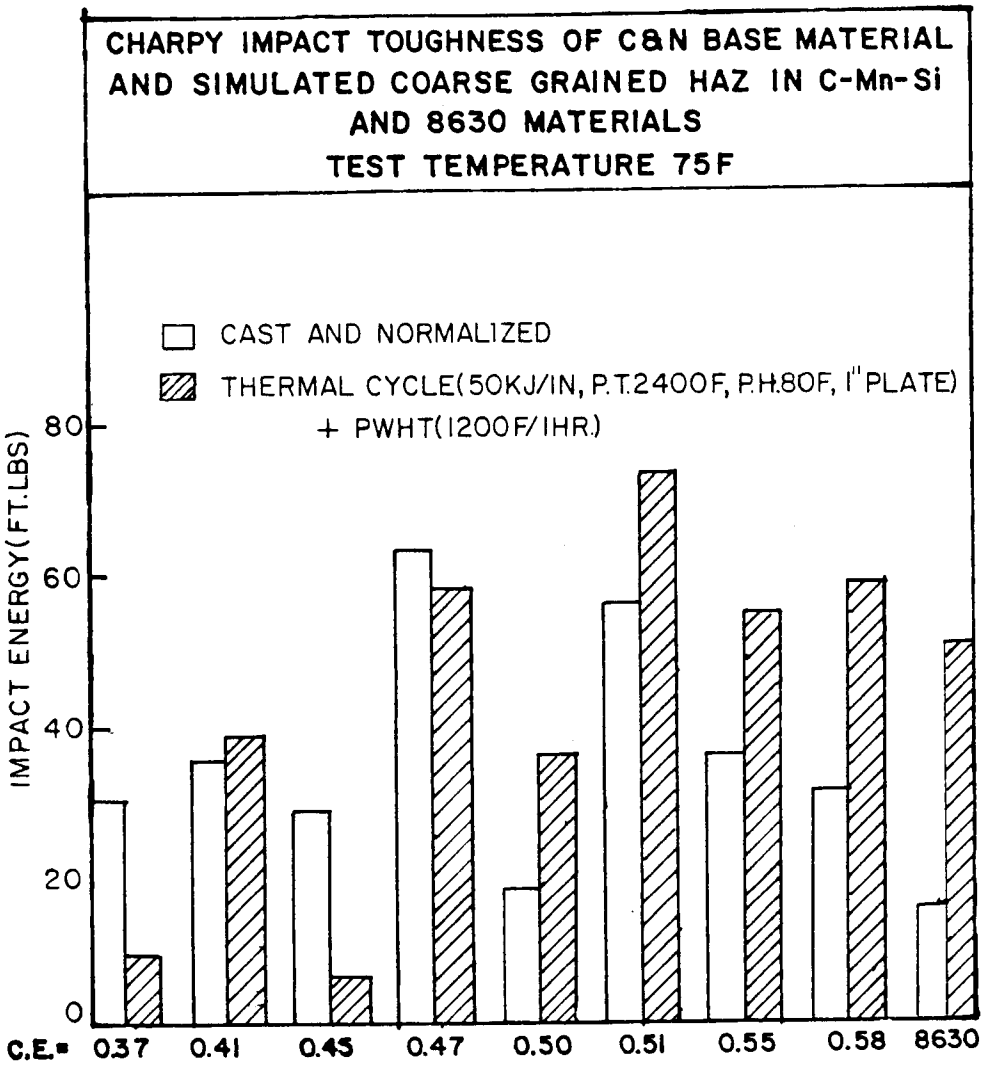


Figure 125. Impact toughness at room temperature (75°F) of simulated coarse grained HAZ's in cast and normalized and 8630 steels.

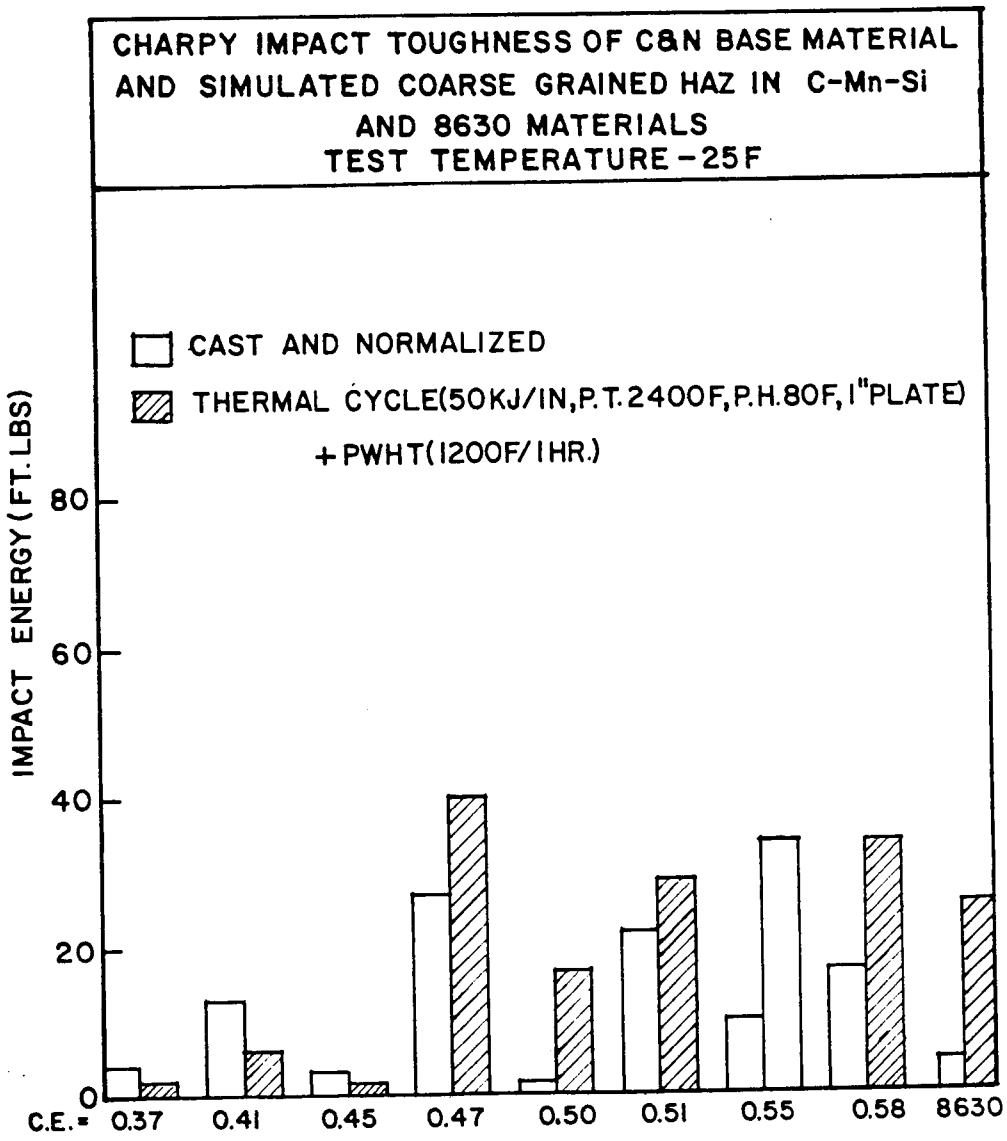


Figure 126. Impact toughness at -25°F of simulated coarse grained HAZ's in cast and normalized C-Mn-Si and 8630 steels.

arrest at approximately 1140-1150°F, implying that transformation during cooling produced upper temperature constituents. In Figure 127, the microstructures obtained in the C&N steel (C.E.= 0.37) after thermal cycling as well as after thermal cycling and PWHT are shown. The presence of extensive amounts of pro-eutectoid and Widmanstätten ferrite at the grain boundaries in the untempered as well as tempered condition explains the lower toughness obtained in the room temperature tests. The microstructural evidence and thermal recalescence are corroborative evidence of upper temperature transformations. The microstructures of the C&N steel with a C.E. of 0.47 (Figures 128a and b) are untempered martensitic/bainitic as thermal cycled and tempered martensitic/bainitic after PWHT. A significant improvement in toughness is observed after PWHT (11 ft-lbs to 58 ft-lbs). For the C&N C-Mn-Si steel with a C.E. of 0.58, the microstructure in the as-thermal cycled condition (Figure 129a) is essentially fully martensitic with a toughness of 3 ft-lbs. However, in the PWHT condition, the microstructure is tempered martensite (Figure 129b) with an impact toughness of 59 ft-lbs. The results of the impact tests and the microstructural analysis clearly indicate that upper temperature microconstituents located along prior austenite grain boundaries deteriorate the toughness with or without PWHT. The results also demonstrate that the lower C.E. C&N C-Mn-Si steels (which are less susceptible to HIC) may not achieve suitable toughness after post weld heat treatment for a particular service requirement. A higher PWHT toughness can be obtained if low heat inputs are used resulting

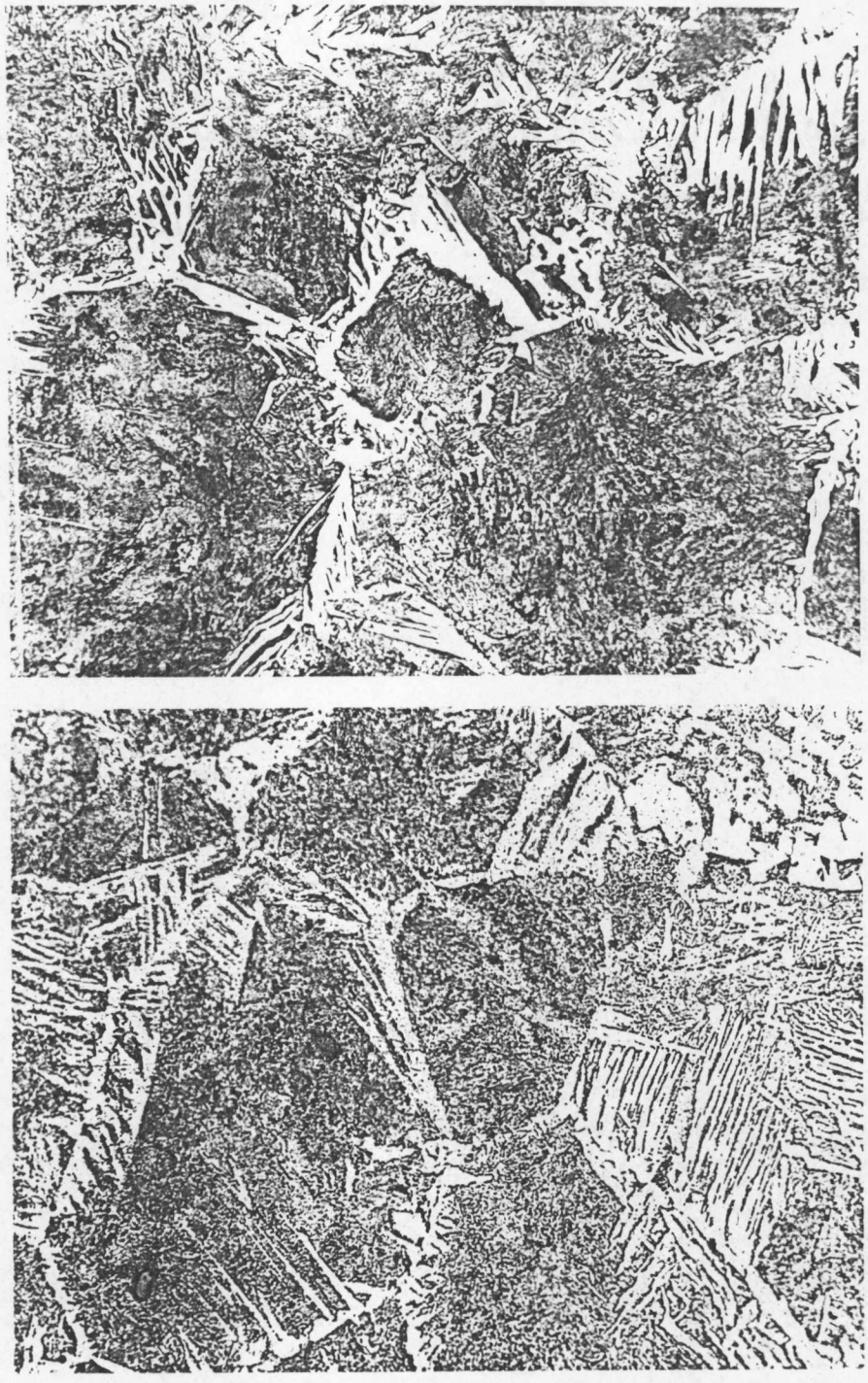


Figure 127. Microstructures of simulated coarse grained HAZ charpy samples of C&N C-Mn-Si steel, C.E. = 0.37. 50 KJ/in, 2400°F peak, 1" plate. a) As thermal cycled, b) PWHT. Picral etch, OLM, 500X.

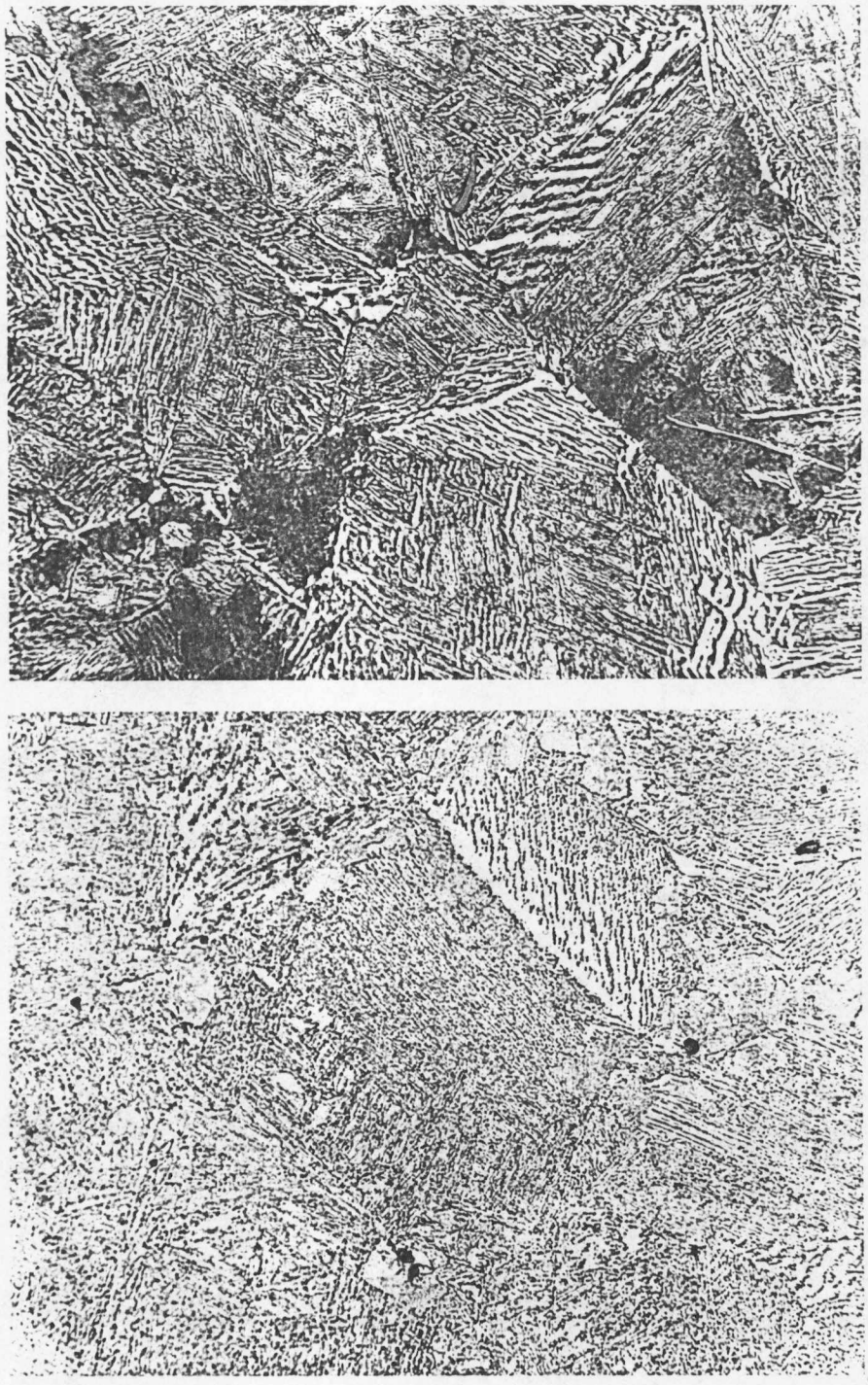


Figure 128. Microstructures of simulated coarse grained HAZ charpy samples of C&N C-Mn-Si steel, C.E. = 0.47. 50 KJ/in, 2400°F peak, 1" plate. a) As-thermal cycled, b) PWHT. Picral etch, OLM, 500X.

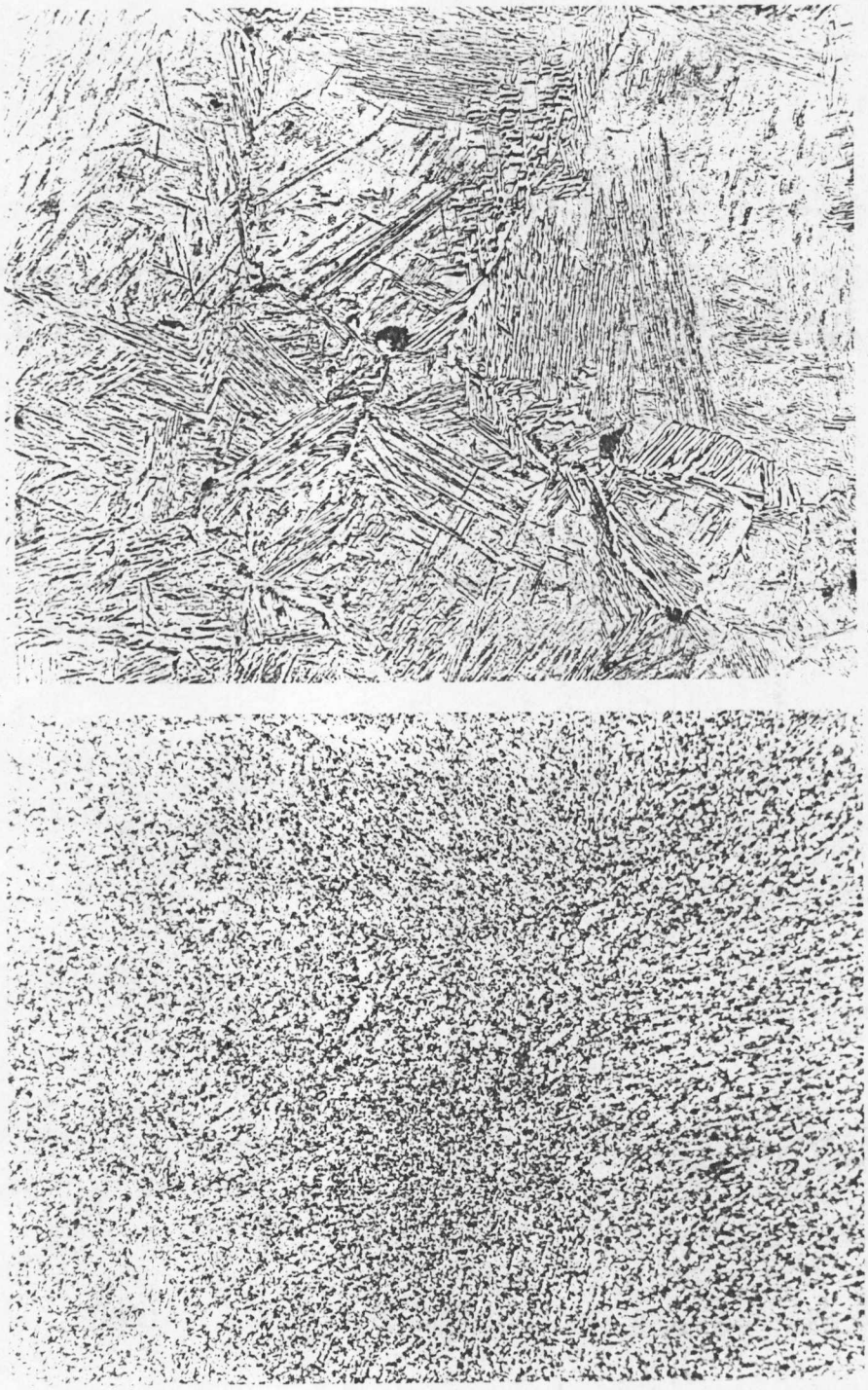


Figure 129. Microstructures of simulated coarse grained HAZ charpy samples of C&N C-Mn-Si steel, C.E. = 0.58. 50 KJ/in, 2400°F peak, 1" plate. a) As-thermal cycled, b) PWHT. Picral etch, OLM, 500X.

in cooling rates which avoid the formation of upper temperature transformation products predisposed at prior austenite grain boundaries. The use of continuous cooling transformation diagrams based on welding conditions which govern the cooling rate in the coarse grained HAZ will help in the selection of correct heat inputs. A lower heat input gives rise to a faster cooling rate in the HAZ, and therefore to achieve good PWHT toughness in the HAZ, the heat input chosen should decide a cooling rate which avoids the formation of upper temperature transformation products which form on prior austenite grain boundaries. For the heat input utilized in this study, the conclusion that can be made is that C&N steels having C.E.'s greater than 0.47 gave rise to adequate PWHT toughnesses in the HAZ. It may be recalled that it was precisely beyond this C.E. level that the susceptibility to HIC showed a sudden increase in the group of C&N C-Mn-Si steels tested. The results demonstrate that microstructures which are not susceptible to HIC may not necessarily possess good as-welded or PWHT toughnesses. The presence of upper temperature transformation products on prior austenite grain boundaries is especially detrimental to the impact properties of the HAZ. In contrast, the susceptibility to HIC is not governed by the location of the constituents in the microstructure. It is governed by the type and volume fraction of constituents in the microstructure. The influence of microstructure and other factors relevant to HIC are discussed in detail in the next section.

11. Suggested Mechanism of HIC

The series of tests and results that have been presented concerning the HIC susceptibility of cast and wrought steels suggests that HIC is a very complex phenomenon, and is dependent on a number of variables. Inherent in the steel, these variables include composition, deoxidation practice, heat treatment and thermo-mechanical treatment. Variables concerning the particular welding situation are the state of stress (restraint or applied) and the hydrogen potential of the welding process. The material variables control the microstructural features that will affect HIC (martensite, inclusions) whereas the welding process variables will influence the other prerequisites for HIC which are; the state of stress and the hydrogen content. A brief summary of the current knowledge regarding HIC is given below following which a consolidated mechanism of HIC is presented to explain the results obtained in this program.

Current assessment of HIC. As has been indicated in the literature review, despite the extensive amount of research conducted by numerous investigators, no single theory has been advanced to clarify all of the experimental observations concerning HIC. The common denominators are that HIC is a form of hydrogen embrittlement which is most potent at temperatures near ambient and at low strain rates (as in a tensile test compared to those in an impact test). These phenomena indicate that HIC is dependent on the diffusion of hydrogen. The theories of hydrogen embrittlement put forth by Troiano[39] and

Oriani[40] fully recognize this factor and postulate that a critical combination of stress state and hydrogen concentration is necessary to cause HIC; the critical concentration of hydrogen being achieved by the diffusion of hydrogen to regions of high tri-axial stress. These regions are postulated to be imperfections such as voids, inclusion/matrix interfaces (macroscopic) or grain boundaries and dislocations (microscopic). Bastien and Azou[36] have indicated that such areas possess high free energy where hydrogen tends to accumulate and increase in concentration. Using current terminology, this "trapping" of hydrogen has been suggested[101,102,103] to take place at both microscopic and macroscopic discontinuities in the matrix. Trapping occurs due to[101,102] attractive interactions between dissolved hydrogen atoms and the structural imperfections and results in the reduction of the total free energy. Pumphrey[98] and Pressouyre[102] have further indicated that short-circuit diffusion of hydrogen can occur along trap interfaces e.g., diffusion of hydrogen along inclusion/matrix interfaces. Almost all current theories agree that HIC occurs when a critical combination of stress state and hydrogen concentration is achieved. A more recent approach to the problem given by Beachem aids in the prediction of the fracture modes developed during HIC if the hydrogen concentration and the stress intensity are known. In the consolidated mechanism of HIC presented, the theories indicated above have been adapted to the case of hydrogen diffusing into the coarse grained HAZ consisting of a susceptible (martensitic) microstructure. The

consolidated mechanism explains the behavior of cast vs. wrought steels as far as their relative susceptibilities to HIC are concerned. Further, the mechanism also aids in the understanding of the fracture morphologies observed in the hydrogen embrittled HAZ's.

Consolidated mechanism of HIC. The most important variable with respect to the occurrence of HIC is the microstructure in the coarse grained HAZ. Among the different micro-constituents that can result in the HAZ due to a weld thermal cycle, martensite has been reported to be the most susceptible to HIC.[26,27] The carbon content is therefore the most important compositional variable since it has the greatest contribution to the hardenability of the steel as well as governs the hardness of the martensite. Higher carbon martensites have been reported[26] to be more susceptible to HIC than lower carbon martensites, with twinned martensitic structures having the greatest susceptibility. The Phase I results on the cast and normalized C-Mn-Si steels had clearly indicated the increasing susceptibility to HIC with decreasing amounts of non-martensitic constituents in the microstructure. This increased susceptibility of as-quenched martensite to HIC can be attributed to a limited capacity for plastic deformation and a low fracture toughness. Further, the dislocation density in martensite is of the order of 10^{11} to 10^{12} per sq. cm. compared to 10^{6} to 10^{8} per sq. cm. for upper and lower bainite in steels of identical composition.[96] This high dislocation density

implies that martensite provides a high hydrogen trapping capacity. Cracking in martensite is known to occur in both an intergranular and transgranular manner, further, it can occur translath, interlath or intercolony (Figure 130). These morphologies of cracking have been observed in the UBCT's as well as in the implant samples tested in this research program. To explain these modes of cracking, one has to consider the role of hydrogen. In a typical welding situation using high hydrogen electrodes (E 6010), approximately 25-30 cc of hydrogen per 100 grams of weld metal were determined in the RPI silicone oil test. This is above the equilibrium solubility of hydrogen in liquid iron (Figure 4a, page 14) and hence the weld metal in the liquid state is saturated with hydrogen. However, as the weld metal solidifies, the solubility of hydrogen decreases sharply to approximately half the value in liquid iron. Hydrogen is therefore rejected out of the weld metal into the atmosphere as well as into the HAZ. Further rejection of hydrogen into the HAZ is aided, as the austenite, under the fast cooling rates experienced in the HAZ, transforms to martensite. The diffusivity of hydrogen in the BCT martensite is higher than in the austenite and hence it is able to diffuse easily through the lattice as well via the grain boundaries. Hydrogen atoms close to the metal surface will be able to diffuse out in a short period of time ($t=x^2/D$, where "x" is the diffusion distance and "D" the diffusivity of hydrogen). For hydrogen diffusing into the HAZ, trapping takes place at areas of high dislocation density (martensite, grain boundaries) or at

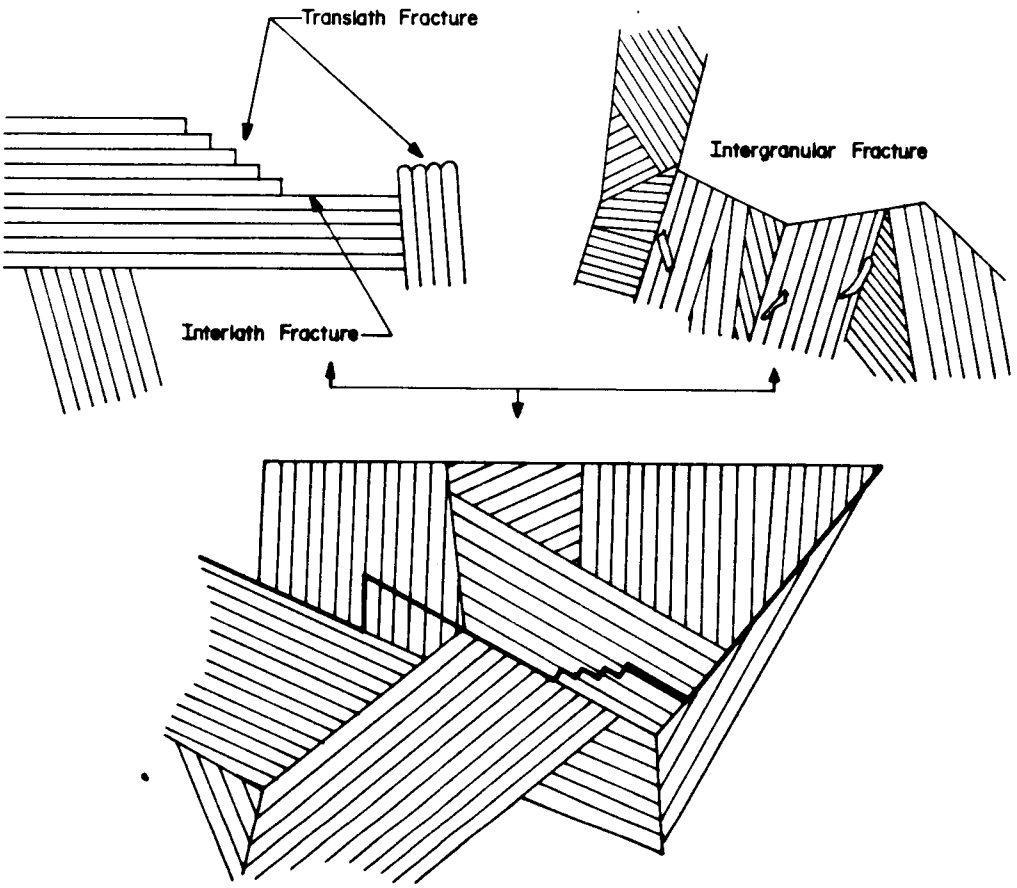


Figure 130. Schematic representation of fracture modes in martensite during HIC.

Source: Kikuta, Y., Araki, T., and Kunada, T., "Analysis of Fracture Morphology of Hydrogen-Assisted Cracking in Steel and Its Welds," Fractography in Failure Analysis, ASTM STP 645, 107-127 (1978).

macroscopic areas such as inclusion/matrix interfaces and voids. Though the specific nature of traps has not been defined, the term "trap" includes any discontinuity in the microstructure such as grain broundaries, precipitates, voids, dislocations and solid/solid interfaces.[99] Trapping has been suggested[100,101] to be due to the attractive interactions between the dissolved hydrogen atoms and structural imperfections. For hydrogen diffusing into the HAZ, as-quenched martensite offers a region of high dislocation density composed of dislocation tangles and a large concentration of low angle boundaries.[99] As-quenched martensite has been indicated[99] to be the microstructure most susceptible to hydrogen embrittlement having the highest concentration of trapped hydrogen for any metallurgical structure. In addition to martensite, Oriani[100] has shown that solid/solid interfaces (as opposed to solid/vapor interfaces) represent the predominant trapping sites for hydrogen in steels that have not been cold worked. In a typical situation for cast steels, depicted in Figure 131, in addition to areas of high dislocation density, inclusion matrix/ interfaces (Type I, II and III) can also be expected to be areas of high hydrogen concentration. However, Type II inclusions can be expected to be more effective in trapping hydrogen than Type I or III since Type II inclusions have a larger inclusion/matrix area than the Type I or III inclusions which are "rounded" in nature. Moreover, Type II inclusions are situated at the primary solidification grain boundaries which further aids hydrogen trapping. Crack initiation occurs when the hydrogen concentration reaches a critical value;

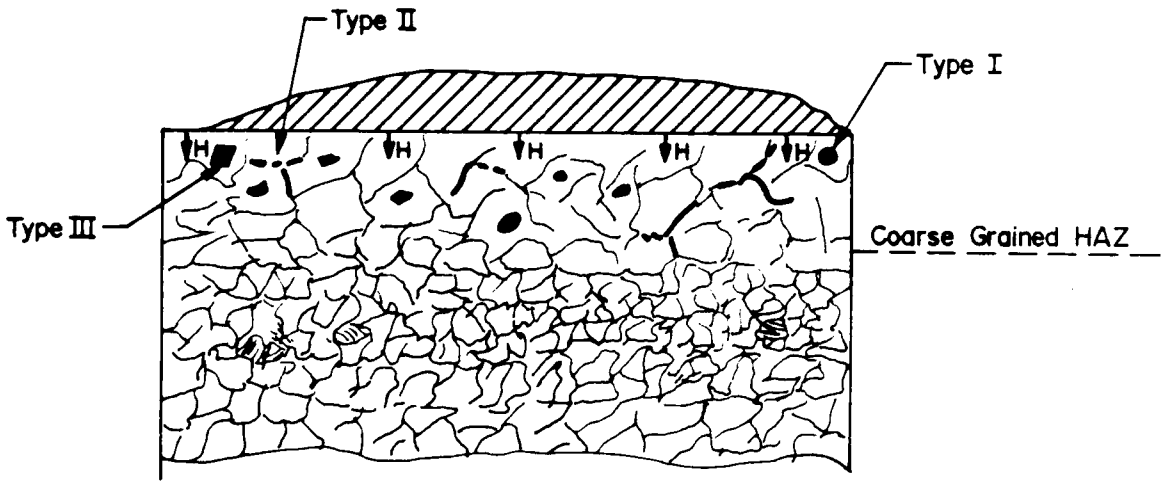


Figure 131. Schematic representation of HAZ in cast steels illustrating location of microstructure and inclusions with respect to diffusing hydrogen front (from the weld metal into the HAZ).

the higher the stress present, the lower the critical amount of hydrogen required, and conversely the higher the amount of hydrogen, the lower is the stress required to initiate cracking. Type II inclusions can therefore be expected to render cast steels more susceptible to HIC than Type I or Type III's. The greater susceptibility of high carbon martensites can be understood on the basis of the high trapping potential for hydrogen and the high internal stress that exists within such microstructures. Crack propagation occurs until the concentration of hydrogen at the crack tip falls below the critical value. At this stage, the crack is arrested. Based on the above reasoning, the beneficial effect of preheating and post weld holds can be rationalized. Preheating causes the temperature of the weldment to remain higher for a longer time causing the hydrogen to diffuse ahead of the arrested crack front. The hydrogen is eventually diffused out of the weldment, thus keeping the hydrogen concentration below that required for crack initiation or propagation.

In the case of the wrought plate steels, two unique situations can be effective in altering the influence of hydrogen. When the weld is made parallel to the rolling direction in the plane of the plate, the elongated sulfide inclusions as well as banding (if present) are aligned parallel to the fusion line and perpendicular to the path of the hydrogen diffusing into the HAZ (Figure 132a). The inclusion matrix interfaces hence lie in the correct aspect ratio to provide large interface regions for hydrogen trapping.

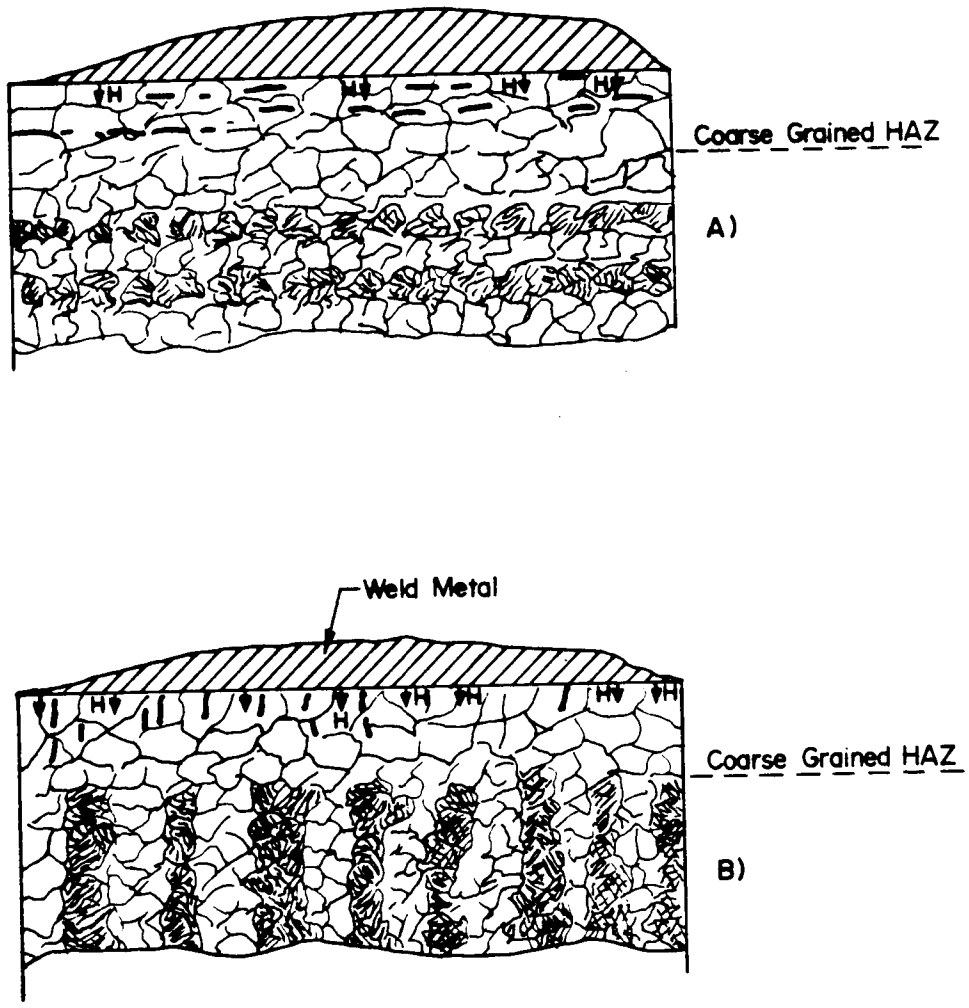


Figure 132. Schematic representation of HAZ in wrought steels showing location of microstructure and inclusions with respect to diffusing hydrogen front.
a) welded PRD, b) welded TTD.

Further, inclusion asperites form ideal stress concentrators and this enables hydrogen concentrations to be easily built up to the critical value for crack initiation. Cracking proceeds so long as the hydrogen concentration is above the critical level. In addition, chemical banding (which is not erased during a weld thermal cycle), provides a region of continuous crack propagation. The state of stress in the UBCT sample shown in Figure 59 (page 156) indicates that tensile stresses act in the coarse grained HAZ in the longitudinal, transverse and short-transverse directions. Thus for a crack propagating in a ferrite band (Figure 54, page 149), there is no microstructural "obstruction" to its propagation. The association of HIC in the HAZ with inclusions in the ferrite bands can be related to the fact that initial precipitation of the inclusions takes place in the ferrite phase during ingot solidification and during subsequent hot working these inclusions are rolled out in the ferrite.

When the welds in the wrought steels are made in the through thickness direction (TTD), the inclusions and banding are aligned perpendicular to the fusion line, traversing from hard martensitic regions in the coarse grained HAZ to softer non-martensitic regions. Hydrogen can diffuse out of the coarse grained HAZ along inclusion matrix interfaces in a short circuiting manner.[98] Also, chemical banding does not provide a continuous easy path for crack propagation. This is because the residual stresses in the UBCT sample as well as the applied stress in the implant test now act parallel to

the plane of inclusions and banding. Evans et al.[48] have also reported lower susceptibilities in wrought steels tested TTD in implant tests. The results of the underbead cracking and the implant tests conducted in this research program agree with their results.

The mechanism of HIC presented above is based on an assumption that some critical concentration of hydrogen has to be reached at potential sites for crack initiation. The critical concentration depends on the nature of the potential crack site that is a hydrogen trap, its shape and location in the lattice and the state of stress at the site.[102] Pressouyre's studies[102] have shown that elongated manganese sulfide inclusions initiate cracks at lower hydrogen concentrations than rounded ones and that the effect is more pronounced in bainitic-martensitic microstructures than in ferritic-pearlitic structures. The results of the HIC tests conducted in this research program fully corroborate Pressouyre's conclusions.

The fracture morphologies evidenced in the implant tests and the underbead cracking tests can be explained using Beachem's model of hydrogen-assisted cracking. The model proposes that hydrogen diffuses into the lattice just ahead of the crack tip and aids whatever deformation processes the material will allow. The deformation processes that can exist are governed by the stress intensity at the crack tip. In the implant test, for a particular applied stress, the stress intensity just prior to crack initiation is the lowest and gradually increases after the crack initiates

and propagates. At the relatively low stress intensity achieved at the beginning of the implant test, Beachem's model predicts that large amounts of hydrogen are required to cause plastic flow at the notch and thus cause crack initiation. The volume of metal plastically deformed is small and hence a "low energy" plastic deformation process of IG fracture occurs. This reasoning explains the IG initiation of cracking in the implant test. As the crack propagates, the stress intensity increases (constant load applied in the implant test) and hence a larger volume of metal at the crack tip deforms plastically causing the fracture mode to change from a low energy IG mode to a higher energy (more plastic deformation) QC mode. With further increase in the stress intensity, larger volumes of plastic deformation results ahead of the crack encompassing numerous inclusions and now MVC is the preferred mode of cracking. The above reasoning can explain the fracture morphology found in the low sulfur steels. In these steels, the majority of the hydrogen in the HAZ can be considered to be predisposed at the grain boundaries due to the fact that fewer inclusions are present to act as trapping sites for the hydrogen. This implies that cracking more easily initiates in the IG mode (which is also preferred mode at the beginning of an implant test). As the crack propagates, the stress intensity increases, however, the occurrence of extensive MVC is not feasible since a sufficient volume fraction of inclusions are not present to act as sites for MVC. This implies that the extent of IG cracking in the low sulfur steels should be

greater than in the higher sulfur steels, which is exactly what is observed. As the sulfur and hence the inclusion content increases, the plastic zone envelops more inclusions and hence QC and MVC are the preferred modes for crack propagation. The grain surfaces of some of the IG cracks show "perfect" cleavage ruptures thus implying that hydrogen has induced failure without causing any gross plastic deformation. This observation is representative of Oriani's[40] theory of hydrogen embrittlement where hydrogen is hypothesized to lower the cohesive strength of the lattice causing "lattice-decohesion." A practical implication of this is that low sulfur steels may be susceptible to a more "brittle" (low energy) type of HIC compared to higher sulfur steels of identical composition.

The situation described above holds good for the case when the steels were TTD. However, when tested PRD, the higher sulfur steels showed a greater susceptibility to HIC. The state of stress now involves a tensile stress acting in a plane perpendicular to that of the inclusions and banding thus aiding crack initiation and propagation. Crack initiation is aided because hydrogen can diffuse along inclusion/matrix interfaces in the coarse grained HAZ and attain the critical concentration. The results of the implant tests are very similar to those of the underbead cracking tests where samples tested PRD were found to be more susceptible to HIC than those tested in the TTD.

The definition of the fracture morphologies in the UBCT samples presented a more complicated task than the evaluation of the implant

test samples. This is because, firstly, the location of the crack had to be determined without using any etching procedures so as to prevent the crack surfaces from corroding, and secondly, because the cracked region had to be extracted without causing any distortion or "rubbing" of the crack surfaces. Hence, fractographic examination of HIC in UBCT samples was limited to some typical cases in the cast and wrought steels. In both these types of materials the fracture morphology was essentially found to be QC. This observation can be rationalized using Beachem's model in the following manner. In contrast to the implant test where an external restraint is applied, the stress developed in the UBCT sample is that due to the self restraint of the sample and the transformation stresses. Hence, the stress intensity is the highest at crack initiation and then decreases as crack propagation occurs. The QC fracture mode indicates that the stress intensity is not high enough to cause MVC and the restraint is probably released by crack propagation in a "burst-arrest" type of phenomenon leading to a majority of the fracture to be QC. The proposition of a "burst-arrest" phenomenon is rational since residual stresses get relieved as soon as they have reached a magnitude equal to the yield strength of the microstructure (martensite) they exist in. For martensite, the yield to tensile strength ratio is very nearly unity, and hence it can be presumed that all the residual stresses get relieved as soon as crack initiation and propagation have occurred.

In summary, a unified mechanism of HIC has been proposed for cast and wrought steels. It involves the concept of hydrogen accumulation of critical levels at microscopic and macroscopic sites in the HAZ causing initiation and the propagation of cracks. The fracture modes and morphologies can be explained using Beachem's model of hydrogen-assisted cracking. In addition, the presence of "perfect" IG fracture (plane grain faces) on grain boundaries observed in the IG mode of cracking indicates that hydrogen adsorption may be causing a low energy mode of cracking. These features were found to be more prevalent in the low sulfur steel (0.001%) in the implant test.

12. Fundamental Significance of this Work

The fundamental significance of this work is:

1. Inclusion/matrix interfaces form the primary trapping sites for hydrogen in the HAZ. Grain boundaries and dislocations, in the order of decreasing incoherency, form the next logical sites for hydrogen trapping.
2. Short-circuit diffusion of hydrogen along inclusion/matrix interfaces (as has been suggested by other investigators) is a viable mode for hydrogen transport.
3. The increase in susceptibility of wrought steels to HIC when welded parallel to the rolling direction compared to that when welded perpendicular to the rolling direction is convincing proof of the first and second propositions above.

4. The deleterious influence of Type II inclusions on the HIC susceptibility of cast steels further confirms the trapping mechanism suggested in "1" above.
5. The greater extent of grain boundary embrittlement in the low sulfur wrought steels is further evidence of the trapping of hydrogen at grain boundaries in the absence of a sufficient inclusion/matrix area for hydrogen trapping. This hypothesis explains the apparent anomalies reported in literature regarding the HIC susceptibility of low sulfur steels.
6. Beachem's model of HIC has been found to be valid for the observations in the tests carried out. Fracture morphologies of the hydrogen embrittled HAZ's have been found to correlate well with those predicted by the Beachem model. In particular, the model also predicts an increasing extent of intergranular HIC for low sulfur steels.

13. Engineering Significance of this Work

The engineering significance of this work is:

1. The weldability of cast steels with regard to their susceptibility to hydrogen-induced HAZ cracking is as good or better than that of comparable wrought steels. Preheat temperatures required to prevent HIC in cast steels are well within those established for equivalent wrought steels, e.g., A216-WCB steels with carbon equivalents up to 0.47

and residuals up to 0.59% can be welded with a preheat of only 100°F to avoid HIC under high hydrogen conditions.

2. The susceptibility to HIC of wrought steels is dependent upon orientation effects e.g., HAZ's in welds made parallel to the rolling direction are more susceptible to HIC than those in welds made perpendicular to the rolling direction. In practical terms, this conclusion has a significant impact on the orientation of welds in wrought steels.
3. The susceptibility to HIC of cast steels is not orientation dependent, however, it is dependent on the inclusion morphology resulting from the deoxidation practice. The presence of Type II inclusions exacerbates the susceptibility to HIC.
4. As-cast steels may, in general, require a higher preheat to prevent HIC than cast and normalized steels.
5. The melting practice, acid or basic, did not have any decipherable influence on the HIC susceptibility of cast steels.
6. The relative susceptibility to HIC of a comparable group of cast C-Mn-Si steels can be predicted by a simple relative comparison of their Jominy hardenabilities.
7. Post weld holds are a convenient way to prevent HIC at the expense of higher preheat temperatures.
8. For cast steels, increasing the extent of deoxidation reduces the susceptibility to HIC. This arises from the

fact that increasing extents of deoxidation lead to the formation of Type III inclusions in preference to Type II inclusions. An added benefit obtained is that, a greater impact toughness is obtained in the coarse grained HAZ (as-welded as well as PWHT) as the residual/total aluminum content is increased. However, intergranular aluminum nitride embrittlement may become a problem at excessively high aluminum contents.

9. Low sulfur (0.001%S) wrought steels were found to be susceptible to intergranular HIC. Thus, while clean steel may have significant advantages as far as their mechanical properties are concerned, the potential for an increased susceptibility to HIC should be accounted for during design and subsequent fabrication.
10. The as-welded impact toughness of the HAZ and its resistance to HIC should be treated as two separate entities, for one may not predict the other.

14. Future Work

In light of the extensive weldability testing carried out and the results consequently obtained, the following future work is suggested:

1. Use of a severe restraint test such as the Y-groove test to complement the results of the underbead cracking tests.
2. The development of CCT diagrams relevant to welding conditions for typical A216-WCB and WCC steels. This task

will enable the prediction of the coarse grained HAZ microstructure for known welding heat input and preheat conditions.

3. A more thorough investigation of the HAZ toughness (both as-welded and PWHT) spanning the range of peak temperatures from the coarse grained HAZ to the unaffected base material.
4. An investigation of the role of aluminum content (acid soluble/total) on the HAZ properties in cast steels. A complementary investigation would be to study the role of nitrogen and nitride forming elements (Ti, V, Cb, W) with regard to their effect on the grain coarsening and transformation characteristics of the HAZ.
5. A detailed investigation into the effect of very low sulfur contents (0.001%S) as to the affect on the HIC susceptibility of cast steels of C.E. 0.50 and greater.

It is believed that these added investigations will enhance the information gained in the current work on the weldability of cast steels.

CHAPTER V

CONCLUSIONS

In light of the extensive weldability testing that has been conducted to understand the HIC susceptibility of cast and wrought steels, the following conclusions were derived.

A. Cast C-Mn-Si and 8630

1. The relative susceptibility to HIC of cast C-Mn-Si steels can be evaluated using a simple self restraint test such as the (Battelle) Underbead Cracking Test (UBCT).
2. The susceptibility to HIC is largely governed by the composition of the cast steels represented with a carbon equivalent,

$$C.E. = \%C + \%Mn/6 + \%Si/24 + \%Cr/12 + \%Mo/10 + \%Ni/40.$$

The above formula is a modified version of Kihara's and enables better correlation between the HIC susceptibilities of C-Mn-Si and 8630 steels.

3. Under high hydrogen welding conditions, C&N steels with C.E. values up to 0.47 and residuals (%Cr + %Mo + %Ni + %V + %Cu) up to 0.59% require a preheat of only 100°F to avoid HIC. For C.E. values up to 0.55, a preheat temperature of 150°F is required, whereas for C.E. values of 0.58, a preheat temperature of 250°F is required to prevent HIC.

4. As-cast steels may, in general, require a preheat 50°F higher than those described above for C&N steels, to avoid cracking under high hydrogen conditions.
5. Type II sulfides render cast steels more susceptible to HIC because of their morphology (eutectic films) and their location on the primary solidification grain boundaries.
6. The type of melting practice used, acid or basic, did not have any decipherable influence on HIC.
7. The use of post weld holds is beneficial in reducing the risks of HIC and in lowering the preheat temperatures required to prevent HIC.
8. The susceptibility to HIC for a group of C&N steels with comparable melting and deoxidation practices can be related to the hardenability of the steels.
9. Under low hydrogen welding conditions, HIC was found to be absent in all of the cast steels tested. The use of low hydrogen electrodes is therefore recommended.
10. The UT-Mod.HST ranks the C&N C-Mn-Si steels in the same order as predicted by the C.E. and the UBCT.

B. Wrought C-Mn-Si and 8630

1. Under high hydrogen conditions similar to those used for cast steels, wrought steels tested in the rolling direction (PRD) were more susceptible to HIC than comparable C.E. cast steels. When tested normal to the rolling direction (TTD),

such that inclusions and banding are oriented perpendicular to the fusion line, the susceptibility is comparable to that of cast steels. The greater susceptibility of the wrought steels when tested PRD is attributed to the presence of elongated sulfide inclusions in the coarse grained HAZ which act as sites for hydrogen accumulation and crack initiation. In addition, banding, when present, provides regions of continuous crack propagation. When tested TTD, the elongated inclusions in wrought steels are oriented away from the coarse grained HAZ and act as short circuit diffusion paths for hydrogen, leading it away from the HAZ. Further, banding does not allow a continuous path for crack propagation in the coarse grained HAZ. The results therefore indicate that generally, cast steels are more resistant to HIC than comparable wrought steels.

2. The UT-Mod.HST did not reveal differences in HIC susceptibility between cast and wrought steels. This is due to the fact that the fusion zone and not the HAZ is the region of evaluation in this test method and hence inclusion morphology and banding in the base material do not affect the results of this test.

3. The use of post weld holds also reduced the extents of cracking for wrought steels, however, post weld hold schedules sufficient to prevent cracking in cast steels were not able to do so in comparable C.E. wrought steels welded PRD.

C. Remelted and Recast Steels

1. Direct comparison of the HIC susceptibilities of remelted and recast wrought steels with those of "parent" steels confirms that cast steels are less susceptible to HIC than equivalent wrought steels. When the wrought steels are tested TTD (in the underbead cracking as well as in the implant test), the susceptibilities of the cast and wrought steels was found to be similar. The results of the HIC tests on the remelted wrought steels confirm results of the earlier portions of this work which indicated that elongated inclusion morphology and banding in wrought steels which results from thermo-mechanical treatments on the cast ingot, are primarily responsible for the greater HIC susceptibility of wrought steels compared to that of equivalent composition cast steels.

D. Inclusion Morphology/Deoxidation Practice

1. Under high hydrogen conditions, the susceptibility to HIC decreases as the extent of deoxidation is increased.
2. The decrease in susceptibility to HIC with an increase in the extent of deoxidation is attributed to a change in inclusion morphology from largely Type II (eutectic sulfides) to Type III (angular sulfides) and also to the contribution of aluminum. Aluminum, as aluminum nitrides, promotes the formation of softer, high temperature transformation products

and hence a microstructure less susceptible to HIC in the coarse grained HAZ.

3. Results of microhardness traverses in the coarse grained HAZ's confirm the trends observed in the underbead cracking as well as in the implant tests, in that steels having greater susceptibility to HIC showed greater hardenability in the HAZ.
4. Increasing the extent of deoxidation results in improved weld HAZ toughness, both in the as-thermal cycled (as-welded) and in the PWHT condition.

E. Low Sulfur Steels

1. The relative susceptibility of similar composition steels to HIC cannot be predicted solely on the basis of their sulfur contents.
2. When tested PRD, the susceptibility of wrought steels of comparable C.E. is governed by the sulfur content; elongated inclusion morphologies in the higher sulfur steels rendering them more susceptible to HIC. In addition, banding when present, can exacerbate the susceptibility to HIC by providing continuous paths for crack propagation.
3. When tested TTD, higher sulfur steels are less susceptible to HIC compared to lower sulfur steels of equivalent composition.
4. The high sulfur (0.012%) steels showed predominantly transgranular cracking possessing a quasi-cleavage (QC) fracture

morphology, whereas the lower sulfur (0.001%S) steels showed a significant amount of intergranular (IG) fracture (IG cracking being a relatively "low energy" mode of fracture). A lower critical stress (greater susceptibility to HIC) was exhibited by the low sulfur steels as compared to that exhibited by the high sulfur steels in the implant test. The results indicate that, when a hardened (primarily martensitic) microstructure susceptible to HIC exists in the HAZ, steels with very low sulfur contents (0.001%S) can exhibit cracking in the IG mode at lower stresses than the higher sulfur materials.

5. The fact that sulfur content alone cannot be used to predict HIC, susceptibility was demonstrated in implant tests on a single lot of cast steel (0.001%S) where HIC occurred by microvoid coalescence in the weld metal rather than in the HAZ. The coarse grained HAZ in this steel exhibited a soft matrix microstructure as a result of the low C.E. (0.38) of this steel, which is not susceptible to HIC.

F. Hydrogen-Induced Cracking Tests

1. The underbead cracking test (UBCT) was again revealed to be a simple viable test for evaluating the relative HIC susceptibilities of C-Mn-Si and low alloy steels. Preheat temperatures required to prevent HIC obtained from this test are quite representative of those utilized in practice with high hydrogen conditions.

2. The results of the implant tests were found to correlate well with those of the UBCT as far as ranking of the steels to HIC susceptibility is concerned.
3. Applied restraint tests such as the implant test can provide results which are more representative of actual welding conditions. Such tests can better simulate "long range" stresses present in welded structures and vessels as well as duplicating welding conditions and attendant HAZ microstructures.
4. The UT-Mod.HST is a quick and simple test to evaluate the relative HIC susceptibilities of steels. However, effects of factors such as inclusion morphology and banding cannot be studies since the region evaluated is the fusion zone and not the HAZ.

G. Response to PWHT

1. The toughness of the PWHT coarse grained region of the HAZ in C&N steels with a C.E. above 0.47 was greater than for the starting C&N base metal (i.e. toughness was improved by welding and PWHT).
2. The toughness deterioration in the PWHT HAZ of C&N steels with C.E.'s less than 0.47 is attributed to the presence of a continuous network of upper temperature transformation products (pro-eutectoid ferrite, Widmanstätten ferrite) on the prior austenite grain boundaries.

3. The average as-welded toughness at room temperature of C&N C-Mn-Si steels with C.E.'s of 0.37, 0.47 and 0.58 was found to be 7.5, 11.5 and 4.5 ft-lbs, respectively. The as-welded toughness of the C&N C-Mn-Si steel with a C.E. = 0.37 resulted from the presence of a continuous network of pro-eutectoid ferrite and Widmanstätten ferrite along the prior-austenite grain boundaries. The as-welded microstructure in the steel with a C.E. of 0.47 showed the presence of discontinuous bainite along the prior-austenite grain boundaries and a martensite matrix whereas for the C&N steel with the highest C.E. of 0.58, the as-welded microstructure was fully martensitic. The highest as-welded toughness was exhibited by the steel with the intermediate C.E. (0.47) and this indicates that the as-welded impact toughness of the coarse grain HAZ is related in a complex manner to the location and extent of microconstituents. The lowest susceptibility to HIC was exhibited by the C&N steel with the lowest C.E. (0.37), showing that as-welded toughness may not necessarily indicate relative resistance to HIC. Hence, fabricability (resistance to HIC) and serviceability (HAZ toughness) are properties that should be considered separately.

H. Mechanism of HIC

1. HIC is proposed to be caused by the accumulation of a critical amount of hydrogen at regions of high triaxial

stresses (such as martensitic areas) or at macroscopic areas such as inclusion/matrix interfaces. Inclusion/matrix interfaces are proposed to have the maximum potential for hydrogen accumulation. Cracks initiate and then propagate until the amount of hydrogen at the crack tip falls below the critical amount, and propagation resumes when the hydrogen level reattains the critical value. This hypothesis is in agreement with the work of many investigators.

2. In cast steels, Type II inclusions offer the largest macroscopic areas for hydrogen to accumulate and hence render the steel more susceptible to HIC.
3. In wrought steels, elongated inclusions lying in the coarse grained HAZ normal to the path of the diffusing hydrogen (welded PRD) offer large inclusion/matrix interfaces for hydrogen accumulation and hence increase the susceptibility to HIC. When inclusions lie in the direction of the diffusion of hydrogen (welded TTD), the inclusion matrix areas act as short circuit diffusion paths for hydrogen, leading it away from the HAZ, thus reducing the susceptibility to HIC.
4. Fracture morphologies observed in the underbead cracking and the implant tests can be explained using Beachem's model of hydrogen-assisted cracking. The quasi-cleavage (QC) mode of fracture found in the UBCT samples indicates

that stress intensities developed are between those required for IG and MVC fracture morphologies. The greater amount of IG fracture in the low sulfur steels is related to a reduced volume fraction of inclusions available for hydrogen accumulation, thus predisposing the hydrogen at the grain boundaries. Beachem's model also predicts that the extent of IG fracture will be extended in the absence of sufficient volume fraction of inclusions in the plastic zone ahead of the crack tip, to act as nuclei for MVC.

5. The fracture morphology of HIC in low sulfur steels also indicated "perfect" IG fracture (plane grain faces) in that no evidence of any ductility was noted up to magnifications of 5000X in the SEM. This suggests that the lattice decohesion model of hydrogen embrittlement may also be operational.

LIST OF REFERENCES

LIST OF REFERENCES

1. Williams, R.D., Roach, D.B., Martin, D.C., and Voldrich, C.B., "The Weldability of Carbon-Manganese Steels," Welding J., 28 (7), 311s-325s (1949).

2. Short, J.M.: In Discussion on Papers 1-2 Proc. B.S.C.R.A. One-Day Conference, Design, Application and Quality Control of Steel Castings (1965).

3. Granjon, H.: Rapporteur, IIW Report on the Use of the Controlled Thermal Severity (CTS) Test in Different Laboratories, British Welding J., 10 (1), 3-9 (1963).

4. Luther, G.G., Jackson, C.E., and Hartbower, C.E., "A Review and Summary of Weldability Tests of Carbon and Low Alloy Steels," Welding J., 25 (7), 376s-396s (1946).

5. Herres, S.A., "Weldability--Hot Rolled vs. Quenched and Tempered Constructional Steels," Welding J., 24 (3), 129s-152s (1945).

6. Reeve, L., "Factors Controlling the Weldability of Steels," British Welding J., 12 (12), 521-530 (1944).

7. Kinzel, A.B., "The Specification of the Weldability of Steels," Welding J., 20 (10), 483s-491s (1941).

8. Ridal, E.J., "Metallurgical Factors Involved in Welding Carbon and Low Alloy Steel Castings," AFS International Cast Metals J., 2 (2), 47-56 (1977).

9. Coe, F.R., "The Avoidance of Hydrogen Cracking in Welding," The Welding Institute (1973).

10. Coe, F.R., "Welding Steels Without Hydrogen Cracking," The Welding Institute (1973).

11. Linnert, G.E., "Welding Metallurgy," Vol. 2, AWS (1967).

12. Granjon, H., "Cold Cracking in the Welding of Steels," Welding in the World, 9 (11/12), 66-72 (1971).

13. Stout, R.D., "Hardness as an Index of the Weldability and Service Performance of Steel Weldments," WRC Bulletin 189, Nov. (1973).

14. Winterton, K., "Weldability Prediction from Steel Composition to Avoid Heat Affected Zone Cracking," Welding J., 40 (6), 253s-258s (1961).

15. Edson, A., "Weld Hardening and Steel Composition," Metals and Alloys, June, 966-971 (1942).

16. Cottrell, C.L.M., "Hydrogen--Barrier to Welding Progress," British Welding J., 1 (4), 167-176 (1954).

17. Ito, Y., and Bessyo, K., "Weldability Formula of High Strength Steels," I.I.W. Document IX-576-68 (1954).

18. Bradstreet, B.J., "Arc Welding Low Alloy Steels," British Welding Research Association, August (1956).

19. Rothwell, A.B., "Weldability of HSLA Structural Steels," Metal Progress, June, 43-50 (1977).

20. Wade, J.B., "The Concept of Weldability," Australian Welding J., Sept., 67-75 (1967).

21. Luther, G.G., Laxar, F.H., and Jackson, C.E., "Weldability of Manganese-Silicon High Tensile Steels," Welding J., 24 (4), 245s-254s (1945).

22. Jackson, C.E., Luther, G.G., and Fritz, K.E., "Weldability Tests on Silicon Manganese Steels," Welding J., 23 (1), 33s-43s (1944).

23. Hewitt, J., and Murray, J.D., "Effect of Sulphur on the Production and Fabrication of Carbon-Manganese Steel Forgings," Metal Construction and British Welding J., Feb., 24-31 (1969).

24. Doan, G.E., Stout, R.D., and Frye, J.H., "A Tentative System for Preserving Ductility in Weldments--Part I," Welding J., 22 (7), 278s-299s (1943).

25. Watkinson, F., Baker, R.G., and Tremlett, H.F., "Hydrogen Embrittlement in Relation to the Heat Affected Zone Microstructure of Steels," British Welding J., Feb., 54-62 (1963).

26. Bonizewski, T., Watkinson, F., Baker, R.G., and Tremlett, H.F., "Hydrogen Embrittlement and Heat Affected Zone Cracking in Low Carbon Alloy Steels with Acicular Microstructures," British Welding J., Jan., 14-36 (1965).

27. Bonizewski, T., and Baker, R.G., "Hydrogen Embrittlement in Low Carbon Nickel and Manganese Steels," British Welding J., July, 349-362 (1965).

28. Hoyt, S.L., Sims, C.E., and Banta, H.M., "Metallurgical Factors of Underbead Cracking," Welding J., 24 (9), 433s-445s (1945).

29. Voldrich, C.B., "Cold Cracking in the Heat Affected Zone," Welding J., 26 (3), 153s-169s (1947).

30. Tsoriev, S.O., "The Effect of Initial Structure of a High Strength Steel on the Resistance of the Weld Zone to Cold Cracking," Welding Research Abroad, 24 (4), 31-34 (1980).

31. Caplan, J.S., and Landerman, E., "Preventing Hydrogen Induced Cracking After Welding of Pressure Vessel Steels by Use of Low Temperature Post Weld Heat Treatment," Welding Research Council Bulletin 216, June (1976).

32. Mnushkin, O.S., and Petrov, V.P., "The Effect of Hydrogen on the Properties of the Heat Affected Zone in Low and Medium Alloy Steels," Welding Research Abroad, 25 (1), 20-22 (1979).

33. Mallett, M.W., and Rieppel, P.J., "Arc Atmospheres and Underbead Cracking," Welding J., 25 (1) 748s-759s (1946).

34. Zappfe, C.A., and Sims, C.E., "Hydrogen Embrittlement, Internal Stress and Defects in Steels," Trans. AIME, Vol. 145, 225-237 (1941).

35. deKazinczy, F., "A Theory of Hydrogen Embrittlement," J. of the Iron and Steel Inst., Vol. 177, 85-92 (1954).

36. Bastien, P., and Azou, P., "Influence of Hydrogen on the Deformation Characteristics and Tensile Test Results for Iron and Steel," Rev. Mét., Vol. 49, 837-848 (1952).

37. Smialowski, M., "Hydrogen in Steels," Pergamon Press (1962).

38. Petch, N.J., and Stables, P., "Delayed Fracture of Metals under Static Load," Nature, Vol. 169, 842-843 (1952).

39. Troiano, A.R., "The Role of Hydrogen and Other Interstitials in the Mechanical Behavior of Metals," Trans. ASM, Vol. 52, 54-80 (1960).

40. Oriani, R.A., "A Mechanistic Theory of Hydrogen Embrittlement of Steels," Berichte der Bunsen--Gessellschaft für Physikalische Chemie, Vol. 76, (1972).

41. Beachem, C.D., "A New Model for Hydrogen-Assisted Cracking (Hydrogen "Embrittlement")," Met. Trans., 3 (2), 437-451 (1972).

42. Vasudevan, R., Stout, R.D., and Pense, A.W., "Hydrogen-Assisted Cracking in HSLA Pipeline Steels," Welding J., 60 (9), 155s-168s (1981).

43. Hess, W.F., Merrill, L.L., Nippes, E.F., and Bunk, A.P., "The Measurement of Cooling Rates Associated with Arc Welding and Their Application to the Selection of Optimum Welding Conditions," Welding J., 22 (9), 372s-422s (1943).

44. Flanigan, A.E., and Lee, E.U., "On the Escape of Dissolved Hydrogen from Weld Metal," Welding J., 45 (10), 477s-480s (1966).

45. Graville, B.A., "Effect of Hydrogen Concentration on Hydrogen Embrittlement," British Welding J., 15 (4), 191-195 (1968).

46. Kyte, W.S., and Chew, B., "Postweld Heat Treatment for Hydrogen Removal," Welding J., 58 (2), 54s-58s (1979).

47. Smith, N., and Bagnall, B.I., "The Influence of Sulphur on Heat Affected Zone Cracking of Carbon Manganese Steel Welds," Metal Construction and British Welding J., 15 (2), 17-23 (1969).

48. Evans, G.M., Wintermark, C., and Christensen, N., "Effect of Sulfur on the Weldability of Rolled C-Mn Steels," Scand. J. of Metallurgy, Vol. 2, 228-232 (1973).

49. Hart, P.H.M., and Brooks, T.L., "The Effects of Sulphur on HAZ Hydrogen Cracking in C-Mn Steels," The Welding Institute, Report 43/1977/M (1977).

50. Gondoh, H., and Nakasagi, H., "Welding of Extremely Low Sulfur Steels for Large Diameter Pipe," Nippon Steel Corporation Report.

51. Hirai, Y., Minakawa, S., and Tsuboi, J., "Effects of Sulfur on Hydrogen-Assisted HAZ Cracking in Al-rolled Plates," I.I.W. Doc. IX-1160-80 (1980).

52. Sykes, C., Burton, H.H., and Gegg, C.C., "Hydrogen in Steel Manufacture," J. of the Iron and Steel Inst., June, 155-180 (1947).

53. Coe, F.R., and Moreton, J., "Estimation of Diffusion Coefficients for Hydrogen in Ferrous Materials," British Welding J., June, 313-320 (1967).

54. Bonizewski, T., and Moreton, J., "Effect of Microvoids and MnS Inclusions in Steel on Hydrogen Evolution and Embrittlement," British Welding J., June, 321-333 (1967).

55. Brooksbank, D., and Andrews, K.W., "Thermal Expansion of Some Inclusions Found in Steels and Relation to Tessellated Stresses," J. of the Iron and Steel Inst., June, 595-599 (1968).

56. Evans, G.M., and Rollason, E.C., "Influence of Non-metallic Inclusions on the Apparent Diffusion of Hydrogen in Ferrous Materials," J. of the Iron and Steel Inst., Nov., 1484-1490 (1969).

57. Evans, G.M., and Rollason, E.C., "Influence of Microvoids on the Apparent Diffusion of Hydrogen," J. of the Iron and Steel Inst., Dec., 1591-1598 (1969).

58. Chew, B., and Fabling, F.T., "Hydrogen Diffusion in 2 1/4Cr-1Mo Steels with Various Sulfur Contents," Metal Construction and British Welding J., April, 132-134 (1972).

59. Steel, A.C., "The Effects of Sulphur and Phosphorus on the Toughness of Mild Steel Weld Metal," Welding Institute Report M/64/71 (1971).

60. Abson, D.J., Dolby, R.E., and Hart, P.H.M., "Investigation into the Role of Non-metallic Inclusions on Ferrite Nucleation in Carbon Steel Weld Metals," Welding Institute Report 67/1978/M (1978).

61. Baillie, J.G., "Underbead and Toe Cracks," British Welding J., 14 (2), 51-61 (1967).

62. Savage, W.F., Nippes, E.F., and Szekeres, E.W., "Hydrogen Induced Cold Cracking in a Low Alloy Steel," Welding J., 50 (1), 42s-60s (1971).

63. Suzuki, H., "Weldability of Modern Structural Steels," IIW Houdremont Lecture, (1982).

64. Sims, C.E., and Banta, H.M., "Development of Weldable High Strength Steels," Welding J., 28 (4), 178s-192s (1949).

65. Campbell, W.P., "Effect of Aluminum on HAZ Cold Cracking in C-Mn Steels," Welding J., 54 (5), 154s-161s (1975).

66. Hasebe, S., "Effect of Aluminum on the Weldability of Structural Steel," I.I.W. Document No. IX-689-70 (1970).

67. NKK Technical Report," Newly Developed Steel Suitable for High Heat Input Welding--"NK-HIWEL"."

68. Ship Structure Committee Report, "Investigation of Steels for Improved Weldability in Ship Construction--Phase I," SSC-298 (1980).

69. Dolby, R.E., and Saunders, G.G., "Sub-Critical HAZ Fracture Toughness of C:Mn Steels," Metal Construction and British Welding J., May, 185-190 (1972).

70. Bolton, J.W., and Smith, A.J., "Welded Structures of Some Cast and Wrought Steels," Welding J., 18 (11), 398s-417s (1939).

71. Smith, A.J., and Bolton, J.W., "The Effect of Welding on the Structures of Some Cast and Wrought Steels," Trans. AFS, 47 (1), 31-65 (1940).

72. Mueller, S.E., Smith, A.B., and Oersterle, J.F., "Welding of Medium Carbon Steel Castings by the Metal Arc Process," Trans. AFS, Vol. 50, 995-1031 (1942).

73. Bland, J., Parrish, C.B., and Wheeler, R.C., "Casting Weldments in a Petroleum Refinery," Welding J., 37 (8), 789-798 (1958).

74. Chapin, N.A., Soldan, C.H., and Songer, L.W., "Welding Low Alloy Steels for High Pressure and High Temperature," Welding J., 37 (10), 979-987 (1958).

75. Ridal, E.J., "Welding and Fabrication of Steel Castings," Proceedings BSCRA, Paper 10:1 (1965).

76. Hipkins, M.G., "Metallurgical Control of Steel Castings," Proceedings of BSCRA Conference on Welding in Steel Foundries, 25-28 (1962).

77. Bower, C.W., "Fabrication of Dragline Buckets for Earth Moving Equipment," Proceedings SCRATA, Paper 3:1-3:19 (1968).

78. Kenyon, D., and Minard, L.D., "Weldability of New High Strength Low Alloy Cast Steel," Welding J., 55 (1), 28s-31s (1976).

79. Whitley, G.H., "Steel Castings for use in the Power Generating Industry," Proceedings of Annual SCRATA Conference, Paper 10:1-10:7 (1974).

80. Wallett, J.K., "Cast Weld Assemblies," Welding Institute Conference on the Welding of Castings, Paper 4, 11-23 (1976).

81. Wu, K.C., "A Study of the Weld HAZ of Centrifugally Cast 5% Cr Steel," Welding J., 42 (9), 392s-396s (1963).

82. Mellili, A.S., and Biron, R.H., "Preparation, Preheat and Postheat Considerations for the Welding of Steel Castings," Trans. AFS, 429-436 (1975).

83. Gross, A.F., "Why a Qualified Welding Procedure," Trans. AFS, 321-324 (1975).

84. Ridal, E.J., "Influence of Sulfur on the Weldability of Cast Carbon Manganese Steels," Metal Construction and British Welding J., Nov., 413-417 (1972).

85. Aymard, J.P., and Nectoux, G., "Characteristics de Soudabilite des Aciers Moule," Founderie, May, 165-178 (1979).

86. AWS Handbook, Vol. 1, Seventh Edition (1976).

87. Inagaki, M., and Sekiguchi, H., "Continuous Cooling Transformation Diagrams of Steels for Welding and Their Applications," Trans. of the National Research Institute for Metals (Japan), 2 (2), 102-125 (1960).

88. "Hydrogen Induced Cracking in HY-80 Steel Weldments," Welding J., 55 (11), 368s-376s (1976).

89. Patriarca, C.R., and Lundin, C.D., "Weldability of 9Cr-1Mo Steel," UT Progress Report to ORNL, (1979).

90. Lundin, C.D., Kruse, B.J., and Menon, R., "Weldability and Transformational Characteristics of 9Cr-1Mo Steel," AR&TD Progress Report for period ending September 30, 1981, ORNL/FMP-81/4.

91. Granjon, H., "The 'Implants' Method for Studying the Weldability of High Strength Steels," Metal Construction, Nov., 501-515 (1969).

92. Sawhill, J.M., Dik, A.W., and Savage, W.F., "Modified Implant Test for Studying Delayed Cracking," Welding J., 53 (12), 554s-559s (1974).

93. Ball, D.J., Gestal, W.J., Jr., and Nippes, E.F., "Determination of Diffusible Hydrogen in Weldments by the RPI Silicone-Oil Extraction Method," Welding J., 60 (3), 50s-560 (1981).

94. Kiessling, R., and Large, Nils., "Non-Metallic Inclusions in Steel," The Metals Society, London (1978).

95. Case, S.L., and Van Horn, K.R., "Aluminum in Iron and Steel," John Wiley and Sons (1953).

96. Honeycombe, R.W.K., "Steel-Microstructure and Properties," Edward Arnold Publishers (1981).

97. Kikuta, Y., Araki, T., and Kuroda, T., "Analysis of Fracture Morphology of Hydrogen-Assisted Cracking in Steel and Its Welds," Fractography in Failure Analysis, ASTM STP 645, 107-127 (1978).

98. Pumphrey, P.H., "Effect of Sulphide Inclusions on Hydrogen Diffusion in Steels," Metal Science, Vol. 16, 41-47 (1982).

99. Craig, B.D., "On the Elastic of Hydrogen with Precipitates in Lath Martensite," Acta. Met., 25, 1027-1030 (1977).

100. Oriani, R.A., "The Diffusion and Trapping of Hydrogen in Steel," Acta. Met., 18, 147-157 (1970).

101. Kummick, A.J., and Johnson, H.H., "Deep Trapping Sites for Hydrogen in Deformed Iron," Acta. Met., 28, 33-39 (1980).

102. Pressouyre, G.M., "Trap Theory of Hydrogen Embrittlement," Acta. Met., 28, 89s-91s (1980).

103. Private Communication, Ed Rybicki, Dec. 1983.

VITA

Ravindra Menon was born in Cochin, India on August 7, 1954. He attended elementary and high schools in Akola, India and graduated from the Holy Cross High School in June 1968. After pursuing two years of pre-university studies, he entered the Indian Institute of Technology (I.I.T.), Madras, India and received a Bachelor of Technology degree in Metallurgy in June 1975. He continued on at I.I.T. Madras for a Master of Technology degree in Metallurgy which he received in June 1977. From August 1977 to July 1978 he worked for Richardson and Cruddas Ltd, Madras as a welding engineer and from August 1978 to July 1979 he was employed as a welding metallurgist by M.N. Dastur and Co. (P) Ltd, Madras. In the fall of 1979 he was admitted into the Ph.D. program in Metallurgical Engineering at The University of Tennessee, Knoxville. This degree was awarded June 1984.

The author is a member of the American Society for Metals, American Welding Society and the National Association of Corrosion Engineers. He will continue his stay at The University of Tennessee as a research associate in Metallurgical Engineering.